Targeting ERAPs in autoimmune uveitis

The function and regulation of ERAP2 in birdshot uveitis

Wouter Venema

Targeting ERAPs in autoimmune uveitis

The function and regulation of ERAP2 in birdshot uveitis

Wouter Venema

The research described in this thesis was financially supported by UitZicht and Stichting Lijf & Leven.
Publication of this thesis was financially supported by J. Venema BV, Landelijke Stichting voor Blinden en Slechtzienden and Infection & Immunity Utrecht.

ISBN 978-94-6469-659-2
Cover image by Wouter Venema: The Helix Nebula (also known as The Eye of God) is a planetary nebula, an expanding shell of gas around a dying star located ~650 light-years away from Earth. In the summer of 2022 I spend a week in the Cévennes National Park (France) to collect the data for this cover image by using a telescope and dedicated astrophotography camera.
Layout by ProefschriftMaken
Printed by ProefschriftMaken

Targeting ERAPs in autoimmune uveitis

The function and regulation of ERAP2 in birdshot uveitis

Richten op ERAPs in auto-immuun uveitis
De functie en regulatie van ERAP2 in birdshot uveitis
(met een samenvatting in het Nederlands)

Proefschrift

ter verkrijging van de graad van doctor aan de
Universiteit Utrecht
op gezag van de
rector magnificus, prof.dr. H.R.B.M. Kummeling,
ingevolge het besluit van het college voor promoties
in het openbaar te verdedigen op

dinsdag 21 november 2023 des middags te 12.15 uur

door

Wouter Jozef Venema

geboren op 26 februari 1993
te Gouda

Promotoren:
Prof. dr. J.H. de Boer
Dr. J.J.W. Kuiper

Copromotor:
Dr. J. Ossewaarde-van Norel

Beoordelingscommissie:
Prof. dr. P.M. van Hagen
Prof. dr. D. Hamann
Dr. C. Kesmir
Prof. dr. E.J.H.J. Wiertz (voorzitter)
Prof. dr. F. van Wijk

Table of contents

Chapter 1	General introduction	9
Chapter 2	ERAP2 increases the abundance of a peptide submotif highly selective for the Birdshot Uveitis-associated HLA-A29 Published in *Front. Immunol.* **12**, 634441 (2021)	25
Chapter 3	HLA-A29 and Birdshot Uveitis: Further Down the Rabbit Hole Published in *Front. Immunol.* **11**, 599558 (2020)	71
Chapter 4	Retina-arrestin specific CD8+ T cells are not implicated in HLA-A29-positive birdshot chorioretinitis Published in *Clin. Immunol.* **247**, 109219 (2023)	103
Chapter 5	A cis-regulatory element regulates ERAP2 expression through autoimmune disease risk SNPs Manuscript under review	133
Chapter 6	General discussion and future perspectives	173
Chapter 7	Nederlandse samenvatting	187
Appendices	Dankwoord	197
	About the author	205
	List of publications	207

Chapter 1

General introduction

Birdshot uveitis is a sight-threatening inflammatory eye condition

Birdshot uveitis (BU) is an uncommon type of non-infectious uveitis (estimated 0.1-0.6 cases per 100,000 worldwide[1]) characterized by retinal vasculitis and vascular leakage, macular edema, optic disc inflammation and retinal degeneration. Most patients experience floaters and blurred vision and some night blindness. Many patients will have progressive vision loss without treatment[2–4]. Treatment usually involves systemic corticosteroid-sparing immunomodulatory therapy (IMT) for a significant period of time, but it is often not sufficient for preventing progressive decline in visual ability[5–7]. The fundi of patients exhibit distinctive 'shotgun pattern'-like lesions, the cause of which is believed to be T cell-mediated autoimmune reactions directed against yet unidentified antigen(s) expressed in the retina or the vascular layer of the eye (i.e., the choroid)[8] (**Figure 1.1**). This lack of understanding of pathophysiology is reflected by the inconsistent use of terminology to refer to the condition, including *birdshot uveitis*, *birdshot chorioretinopathy*, *birdshot retinochoroiditis,* and *birdshot chorioretinitis*. A chronic, long-term, and progressive disease course is common in BU, leading to significant visual impairment, and treatment side effects, particularly from IMT, can negatively impact quality of life.

Birdshot uveitis as a model to study autoimmunity

*HLA-A*29*

A distinctive molecular feature of BU is the *Human Leukocyte Antigen (HLA)-A*29*, which is a class I *major histocompatibility complex* (MHC-I) antigen involved in *antigen presentation* (see section "antigen presentation via MHC-I"). *HLA-A*29* is one of over 20,000 different MHC-I alleles found in humans. Each MHC-I protein contains a peptide binding cleft with a distinct sequence of amino acids that facilitates the presentation of antigenic peptides at the cell surface. HLA-A*29 is found in all patients with BU, which is viewed as a prerequisite for diagnosis[12–14]. Therefore, the disease mechanisms of BU are likely dependent on HLA-A*29. While BU is a very rare disease, HLA-A*29 is common in the western region of Europe (5-10% of individuals) raising the question as to why only some individuals who carry *HLA-A*29* are prone to developing this blinding eye condition[15,16]. Due to the extreme genetic association between *HLA-A*29* and BU, it may be a useful "model" for understanding the mechanisms of other presumed autoimmune conditions that also have strong genetic associations with MHC-I, such as such as *HLA-B*27-positive* ankylosing spondylitis[17–19], *HLA-C*06:02*-positive psoriasis[20], or *HLA-B*51*-positive Behçet's disease[21,22] (together referred to as the family of "MHC-I-opathies")[23,24].

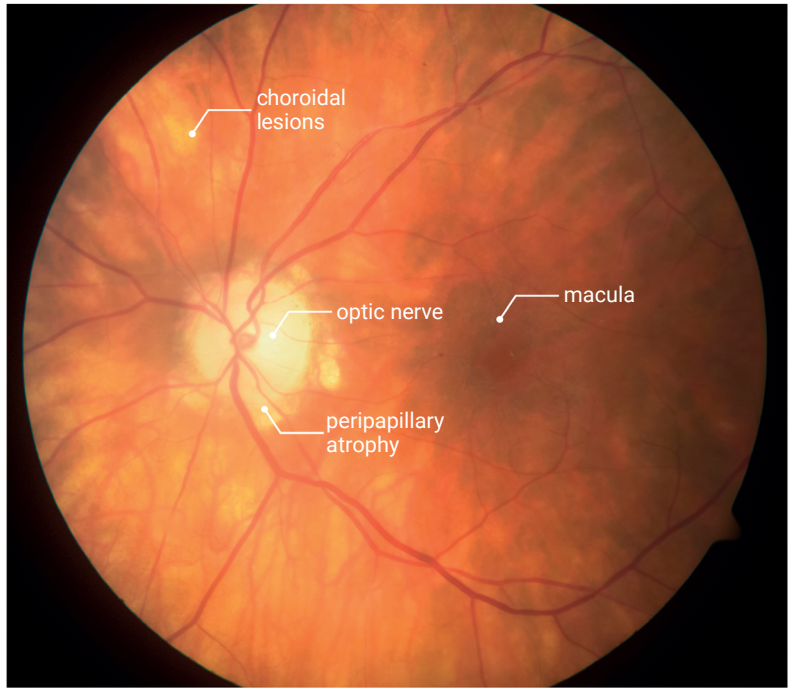

Figure 1.1: Fundus image of a 70 year old female patient with advanced BU. The prominent creamy choroidal lesions are a distinct hallmark of BU. These lesions contain infiltrated T cells[9–11]. There is also peripapillary atrophy around the optic nerve in this patient, which is a sign of choroidal damage.

ERAP1 and ERAP2

Single nucleotide polymorphisms (SNPs) at the *5q15* locus on chromosome 5 near the *ERAP1* and *ERAP2* genes have been implicated in genome-wide association studies (GWAS) of BU[25,26]. These genes encode for *endoplasmic reticulum aminopeptidase* 1 and 2, which are aminopeptidases specialized in peptide processing in the MHC-I pathway. In the endoplasmic reticulum, ERAP1 and ERAP2 trim precursor peptides to a length that allows or prevents their binding to MHC-I for presentation at the cell surface. Across the population, there are more than 10 different allotypes of ERAP1 formed by SNPs that encode amino acid changes in the protein[27]. Allotypes differ in their peptide enzymatic activities and can be considered functionally distinct[28]. The ERAP1 allotype genetically associated with BU is overall inefficient in trimming peptides and often referred to as *Haplotype 10* [*Hap10*], but a standardized nomenclature for ERAP1 allotypes remains to be widely adopted[29]. There is also a genetic association between *Hap10* and other MHC-I-opathies[30].

In contrast, *ERAP2* encodes two haplotypes (*Haplotype A* [*HapA*] and *Haplotype B* [*HapB*]). *HapA* produces a full-length transcript which encodes enzymatically active ERAP2 protein, whereas *HapB* forms a truncated transcript by alternative splicing[31]. Nonsense-mediated mRNA decay removes this alternatively spliced mRNA, which prevents translation into ERAP2 protein. Both haplotypes are actively maintained at intermediate frequencies by *balancing selection*, most likely to preserve beneficial diversity within populations (i.e., host-pathogen co-evolution)[31]. In contrast to disease-risk SNPs in *ERAP1*, SNPs near *ERAP2* that are associated with BU are noncoding and may serve regulatory functions[25]. One particular SNP, rs2248374 is widely believed to control *ERAP2* splicing into either *HapA* or *HapB*, because of its position in a splice region of *ERAP2.* There remains little understanding of the function of other SNPs in the regulation of *ERAP2* and how these contribute to the pathogenesis of BU or inflammatory conditions. To fully understand the disease mechanisms driving BU and other MHC-I-opathies, we need to unravel how disease risk SNPs affect ERAP2 function.

Antigen presentation via MHC-I

Genetic associations with *HLA-A*29*, *ERAP1*, and *ERAP2* point to MHC-I peptide presentation as a key pathway in disease pathogenesis (**Figure 1.2**). As membrane proteins, MHC-I molecules bind peptides in the *endoplasmic reticulum* (ER). These peptides are fragments of cytoplasmic proteins that have been broken down by proteasomes in the cytosol. Therefore, most MHC-I presented peptides are derived from host proteins. The transporter associated with antigen processing (TAP) transports these peptides into the ER lumen. These peptides are further trimmed by ERAP1 and ERAP2 by removing amino acids at their N-termini[30]. As a result of their divergent peptide specificities, ERAP1 and ERAP2 work together to create peptides of the appropriate length and sequence that can be bound and presented by MHC-I[32,33]. This final round of trimming is followed by the loading of peptides onto MHC-I molecules and transport of loaded MHC-I peptide complexes to the cell surface. It is estimated that tens of thousands of peptides are presented on the cell surface by MHC-I[34]. This collection of peptides presented by MHC-I is known as the "immunopeptidome". The T cell receptor (TCR) on $CD8^+$ T cells reads out the MHC-I immunopeptidome and if it recognizes the peptide in complex with MHC-I, it initiates a cytotoxic response that kills the cell presenting the peptide. Although this mechanism is crucial to prevent viral infections or malignant transformations of cells, it can also cause unwanted tissue and cell destruction, such as in autoimmune conditions[35].

It is generally thought that HLA-A*29 presents immunogenic peptides that cause $CD8^+$ T cell-mediated autoimmune reactions to the retina and choroid that lead to BU. This hypothesis is also supported by the genetic association with ERAP genes, since these enzymes modify the immunopeptidome and may alter peptides presented to $CD8^+$ T cells[36].

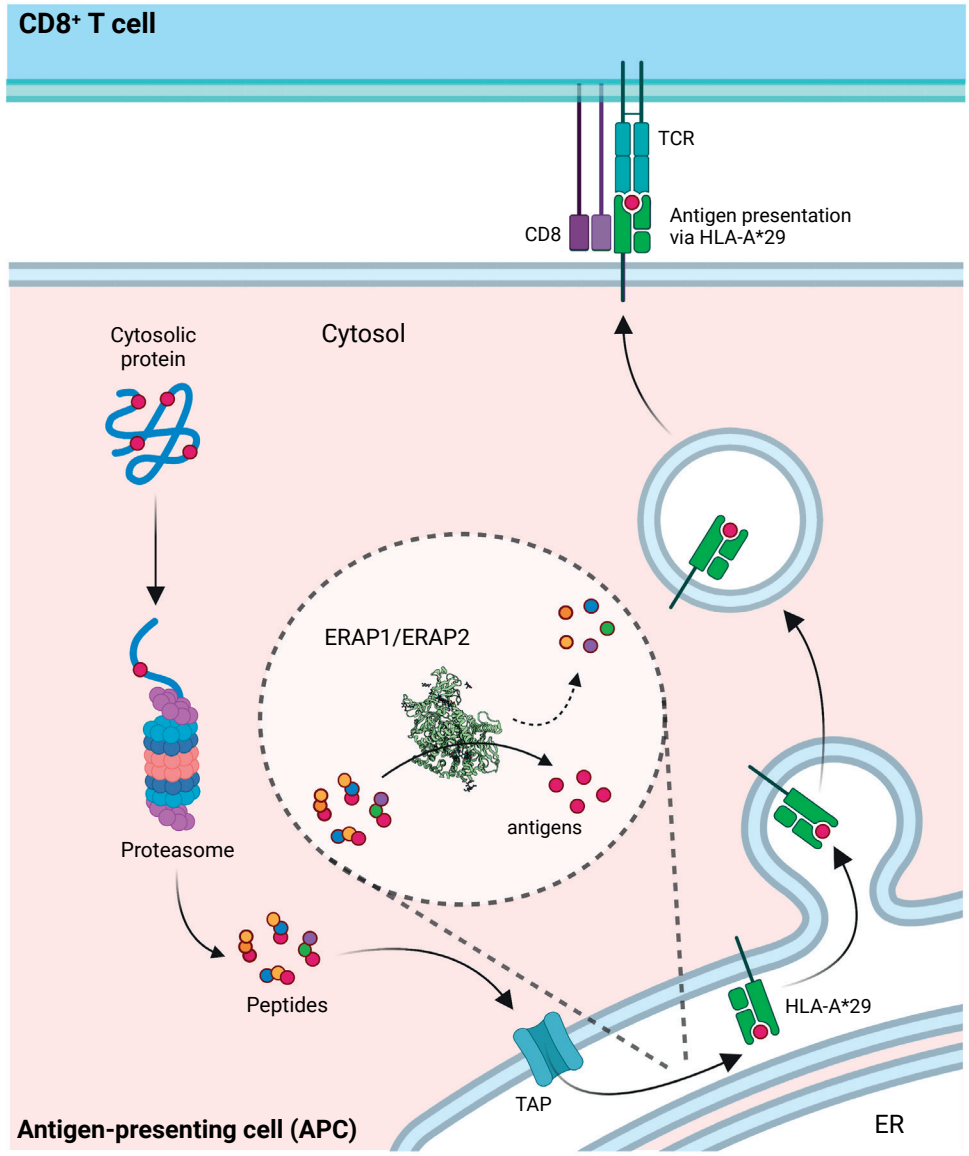

Figure 1.2: **Overview of the MHC-I pathway and antigen presentation via HLA-A29**. Cytosolic proteins are degraded by the proteasome into smaller fragments. These peptides are transported into the endoplasmic reticulum (ER) lumen by the transporter associated with antigen processing (TAP). In the ER lumen, these peptides are further trimmed by ERAP1 and ERAP2, which remove amino acids from their N-termini. After trimming by ERAPs, the antigenic peptides are loaded onto HLA-A*29 (and other MHC-I molecules) followed by transportation of the loaded HLA-A*29 molecule to the cell surface.

Although the disease is quite rare, these molecular characteristics make BU an interesting disease to study how the interplay between a MHC-I molecule and peptide modification by ERAPs lead to the onset/progression of an autoimmune disease. Through the TCR (T

cell receptor), CD8+ T cells interact with the HLA-A*29-peptide complex at their surface, triggering an immune response.

Retinal S-antigen

There has long been speculated that the *retinal arrestin*, also known as *retinal soluble antigen* (encoded by the *SAG gene*), is an autoantigen for BU. SAG is expressed abundantly and specifically by photoreceptors and immunization with SAG causes *experimental autoimmune uveitis* (EAU) in animal models[37,38]. Lymphocyte cultures from BU patients show strong proliferation when stimulated with SAG[13,39]. As a result, SAG is generally considered a candidate autoantigen for BU. It remains unclear whether peptides from SAG are presented by HLA-A*29 in patients and whether this leads to CD8+ T cell activation in the context of HLA-A*29 in patients.

Linkage disequilibrium to identify disease SNP function

The purpose of GWAS is to identify associations between genes and diseases by comparing the allele frequencies of SNPs between patients and a comparable control population[40]. This often results in the identification of "blocks" of correlated SNPs called *genomic loci* that occur more frequently (risk loci) or less frequently (protective loci) in a particular disease. The formation of these genomic loci is due to *linkage disequilibrium* (LD)[41]; An allele of one SNP within a population of interest is said to be in LD if it correlates with (or is 'tagged' by) an allele of another (nearby) SNP. Due to LD, 1 million SNPs are required to tag the ±8 million common (>5% minor allele frequency) SNPs in the human genome[42]. In association studies for complex diseases, LD helps to identify functional SNPs 'tagged' by disease-associated SNPs. An expanding number of studies have linked SNPs to target gene expression or protein expression levels in multiple tissues (termed *expression quantitative trait loci* [eQTL] analysis)[43]. Although these public functional genomic data are useful in understanding the molecular mechanisms that SNPs may be involved in, it remains challenging to distinguish functional variants from non-functional variants in loci with strong LD between SNPs. Using CRISPR-based genome editing approaches (see *CRISPR Cas9 gene editing*), it may be possible to specifically substitute alleles of SNPs to determine if a SNP is 'functional' (i.e., changes the expression of the gene it is associated with). LD information can also be used to deconvolute independent genetic signals. Using *conditional analysis* it is possible to test whether any SNPs are significantly associated with a trait conditioned on a particular SNP at a locus[44]. This approach may be useful to dissect complex association signals and help identify functional SNPs near *ERAP2* that are associated with birdshot uveitis and other autoimmune conditions.

Outstanding questions

Several key questions remain unanswered. We do not know what the immunogenic peptide is that triggers the inflammatory response in BU (if it exists at all) and if it is presented by

HLA-A*29 and dependent on trimming by ERAPs. The immunopeptidome of HLA-A*29 must be investigated to identify the nature of these peptides and ERAP2 must be manipulated to determine how it affects the composition of HLA-A*29 in patients. HLA-A*29 is such a strong risk factor for BU that it is important to determine whether this influence of ERAP2 on HLA-A*29 is specific to HLA-A*29 as compared to other MHC-I alleles.

SAG peptides are considered potential candidates, but are they naturally ligands of HLA-A*29 and are they recognized by $CD8^+$ T cells from patients with BU? In addition, it would be important to determine to what extent SAG peptides are trimmed by ERAP1 and ERAP2.

*HLA-A*29* is prevalent in European and some non-European populations where the condition is not reported, raising the question of why only some individuals carrying this gene are prone to develop this blinding condition. With population genetics data (e.g., the 1000 Genomes project), it may be possible to test if *ERAP1* and *ERAP2* risk variants identified by GWAS are more prevalent in populations in which BU is reported (i.e., Western-European Descent). This is necessary to determine if in BU the disease mechanisms are likely due to an interaction of ERAPs and HLA-A*29.

Furthermore, little is known about how SNPs regulate *ERAP2* and contribute to the development of BU or inflammatory conditions. We need to understand how disease risk SNPs affect *ERAP2* function in order to better understand BU and other MHC-I-opathies.

A model for Birdshot uveitis.

Obtaining an appropriate model to investigate antigen processing and presentation by HLA-A*29 and ERAPs is necessary to establish answers to these outstanding questions. In spite of the fact that the best material would be the primary eye tissues of patients, the supplies of these materials are scarce, and the sample quantities are too small to be easily interrogated by current technologies that probe antigen presentation in depth. For studying the MHC-I pathway in BU, patient-derived cell lines such as *Epstein-Barr virus (EBV) transformed lymphoblastoid cell lines* (LCLs) generated from peripheral blood would be useful because they preserve the patient's genetic background (i.e., HLA-A*29) and provide a constant source of culture material, allowing genetic manipulation by CRISPR-based techniques (i.e., *ERAP2 knock-out*). Such patient-derived cell lines can be further engineered to express proteins of interest, and the presentation of peptides by HLA-A*29 can be monitored experimentally to identify candidate autoantigens (i.e., the retinal S-antigen).

CRISPR-Cas9 gene editing

CRISPR (*Clustered Regularly Interspaced Short Palindromic Repeats*)-based techniques provides an exciting array of tools for genome editing to study the function of DNA sequences (i.e., including the function of SNPs) in cell systems[45]. The *CRISPR-associated 9* (Cas9) nuclease, needed for inducing a double strand break, is derived from the adaptive immune system of bacteria (e.g. *Streptococcus pyogenes*). This technique relies on the use of a guide-RNA (gRNA), which consists of a complementary CRISPR-RNA (crRNA) that can

bind the target genome[46] and a second trans-activating crRNA (tracrRNA) that connects the crRNA to the Cas9 nuclease and subsequently activates Cas9 mediated DNA cleavage[45,47,48] (**Figure 1.3**). Cas9 binds at protospacer adjacent motifs (PAM) in DNA sequences and cleaves the DNA three base pairs upstream of the PAM sequence "NGG" creating a double strand break[45,49]. The human genome contains ~5% "GG" dinucleotide sequences[50], which provides a very large number of regions to modify by CRISPR in a precisely targeted manner.

When Cas9 induces a double strand break on a target sequence the broken DNA ends are joined together with no regard for homology, generating deletions or insertions that disrupt the function of the sequence, a process known as *non-homologous end joining* (NHEJ)[51]. NHEJ is useful to disrupt a coding region, for example to create a gene *knockout*. For a more controlled repair the *alternative homology directed repair* (HDR) can be used, which is based on the use of a DNA template containing the desired DNA sequence with homologous flanking sequence[51]. By using a DNA template, a precise modification can be performed without the *indels* (short for insertions/deletions) created during NHEJ. Double strand repair via the HDR route is most efficient during the G2/S cell phase[52]. Because HDR is usually not very efficient, to generate a cell line with the desired genetic modification, single cell culture, clone screening and validation of the sequence and monitoring of target protein/gene expression is required.

Immunopeptidomics

To study the effect of antigenic peptide processing by ERAP2 on peptide presentation by HLA-A*29, it is desirable to use a technology that captures the immunopeptidome of HLA-A*29. In immunopeptidomics, peptides presented by MHC-I molecules are analyzed using mass spectrometry (MS)[53]. The above-mentioned patient-derived cell lines would be a useful tool to determine the effect of ERAP2 on the immunopeptidome of HLA-A*29.

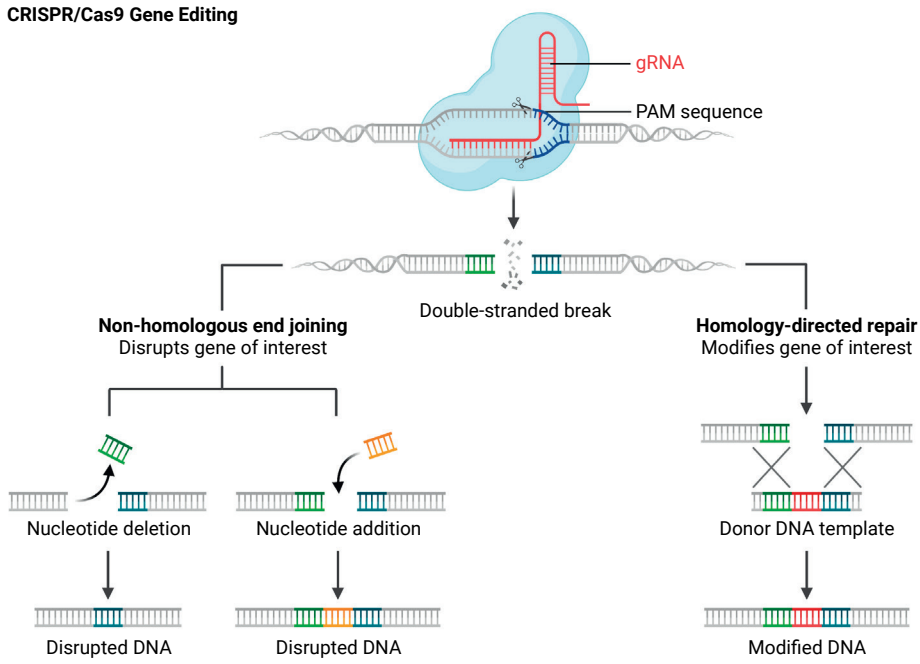

Figure 1.3: Overview of commonly used CRISPR/Cas9 based gene editing approaches. CRISPR/Cas9 mediated DNA modification results in a double stranded break as gRNA bound to the Cas9 nuclease is guided towards the genomic area of interest. The double stranded break can be repaired by non-homologous end joining (NHEJ) or homology directed repair (HDR). The HDR repair mechanism is relatively precise, whereas NHEJ is more error-prone. This makes the HDR repair mechanism a more desirable option for SNP modification.

When combined with CRISPR-Cas9 mediated knockout to permanently silence ERAP2, we can determine the influence of ERAP2 on the presented immunopeptidome. In principle, in immunopeptidomics, HLA (-A*29) bound peptides are obtained by immunoprecipitation of HLA-(A*29) molecules (**Figure 1.4**), followed by elution of the peptides and measurement of their sequence by mass spectrometry. It is possible to simultaneously measure peptides from multiple cell conditions (ERAP2-wildtype versus knockout) by MS using non-radioactive isotopic labeling, such as *Stable Isotope Labeling with Amino acids in Cell culture* (SILAC)[53]. This makes comparing HLA-A*29 peptide abundances between conditions more accurate.

In order to determine if peptides presented by MHC-I are recognized by antigen-specific T cells, MHC Dextramer® technology is commonly used[54]. This technology uses recombinant MHC-I molecules complexed with recombinant peptides of interest and labeled with fluorochromes. By using flow cytometry, antigen-specific $CD8^+$ T cells can be detected in patient samples (for example, peripheral blood), because fluorescence in T cells indicates the presence of binding to a MHC-I peptides complex.

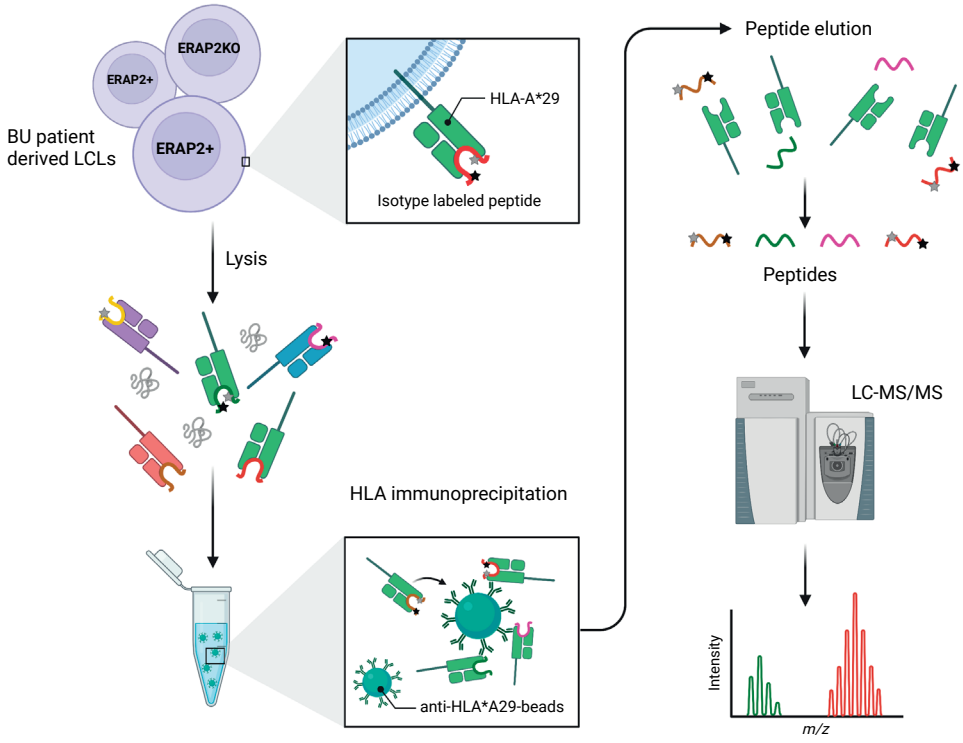

Figure 1.4: **Overview of the immunopeptidomics of HLA-A29 to study the effect of ERAP2.** Isolation and purification of HLA-A*29 bound peptides from BU patient derived lymphoblastoid cell lines (LCLs). LCLs with either functional ERAP2 or LCLs with *ERAP2-knock out* (KO) are used to assess the influence of ERAP2 on the immunopeptidome of HLA-A*29. Stable isotope labeling makes it possible to distinguish peptides from ERAP2^{+} LCLs (heavy peptides) and ERAP2-KO LCLs in a single mass spectrometry measurement. Using immunoprecipitation HLA-A*29 can be isolated, followed by peptide elution. With LC-MS/MS peptide sequences are determined.

Aims and outline of this thesis

In this thesis, we aim to better understand how the genetic predisposition of ERAPs and MHC-I contributes to autoimmunity. Using BU as a prototypic MHC-I associated autoimmunity model, we examine in **Chapter 2** how ERAP2 influences the composition of HLA-A*29-presented peptides in patient-derived cell lines. Further, we demonstrate how the amino acid structure of HLA-A*29 affects peptide binding capacity and discuss how ERAP1 and ERAP2 contribute to the immunopeptidome of HLA-A*29 in **Chapter 3**. Furthermore, we examined in **Chapter 4** whether HLA-A*29 can present peptides derived from the candidate autoantigen *Retinal S-antigen* and assess whether CD8+ T cells of patients recognize these peptides as immunogenic epitopes. Through CRISPR-mediated gene editing, conformational capture assays, and conditional analysis of ERAP2 eQTL datasets, we uncover how multiple SNPs work in concert to regulate ERAP2 expression in **Chapter 5**.

References

1. Minos, E. et al. Birdshot chorioretinopathy: Current knowledge and new concepts in pathophysiology, diagnosis, monitoring and treatment. Orphanet J. Rare Dis. 11, 1–17 (2016).
2. Papadia, M., Jeannin, B. & Herbort, C. P. OCT findings in birdshot chorioretinitis: a glimpse into retinal disease evolution. Ophthalmic surgery, lasers imaging Off. J. Int. Soc. Imaging Eye 43, S25-31 (2012).
3. Testi, I., Ajamil-Rodanes, S., AlBloushi, A. F. & Pavesio, C. Peripheral Capillary Non-perfusion in Birdshot Retinochoroiditis: A Novel Finding on Ultra-widefield Fluorescein Angiography. Ocul. Immunol. Inflamm. 1–4 (2020) doi:10.1080/09273948.2020.1758157.
4. Elahi, S., Lages, V., Jeannin, B. & Herbort, C. P. Advanced Cases of Birdshot HLA-A29 Retinochoroiditis: Prevalence and Characteristics. Klin. Monbl. Augenheilkd. 237, 431–440 (2020).
5. Kiss, S., Ahmed, M., Letko, E. & Foster, C. S. Long-term follow-up of patients with birdshot retinochoroidopathy treated with corticosteroid-sparing systemic immunomodulatory therapy. Ophthalmology 112, 1066–1071 (2005).
6. You, C. et al. Long-term outcomes of systemic corticosteroid-sparing immunomodulatory therapy for Birdshot Retinochoroidopathy. Ocul. Immunol. Inflamm. 1–9 (2019) doi:10.1080/09273948.2019.1641610.
7. Lages, V., Skvortsova, N., Jeannin, B., Gasc, A. & Herbort, C. P. Low-grade 'benign' birdshot retinochoroiditis: prevalence and characteristics. Int. Ophthalmol. 39, 2111—2120 (2019).
8. Kuiper, J., Rothova, A., de Boer, J. & Radstake, T. The immunopathogenesis of birdshot chorioretinopathy; a bird of many feathers. Prog. Retin. Eye Res. 44, 99–110 (2015).
9. Gaudio, P. A., Kaye, D. B. & Crawford, J. B. Histopathology of birdshot retinochoroidopathy. Br. J. Ophthalmol. 86, 1439–1441 (2002).
10. Pulido, J. S. et al. Histological findings of birdshot chorioretinopathy in an eye with ciliochoroidal melanoma. Eye (Lond). 26, 862–865 (2012).
11. Kuiper, J. J. W. et al. Detection of choroid- and retina-antigen reactive CD8+ and CD4+ T lymphocytes in the vitreous fluid of patients with birdshot chorioretinopathy. Hum. Immunol. 75, 570–577 (2014).
12. Papasavvas, I., Kuiper, J. J. W. & Herbort, C. P. J. Some practical issues about HLA-A29 in birdshot retinochoroiditis. J. Ophthalmic Inflamm. Infect. 13, 10 (2023).
13. Nussenblatt, R. B., Mittal, K. K., Ryan, S., Richard Green, W. & Edward Maumenee, A. Birdshot Retinochoroidopathy Associated with Hla-A29 Antigen and Immune Responsiveness to Retinal S-Antigen. Am. J. Ophthalmol. 94, 147–158 (1982).
14. Herbort, C. P. J. et al. Why birdshot retinochoroiditis should rather be called 'HLA-A29 uveitis'? The British journal of ophthalmology vol. 101 851–855 (2017).
15. Wee, R. & Papaliodis, G. Genetics of Birdshot Chorioretinopathy. Semin. Ophthalmol. 23, 53–57 (2008).

16. Baarsma, G. S., Priem, H. A. & Kijlstra, A. Association of birdshot retinochoroidopathy and HLA-A29 antigen. Curr. Eye Res. 9, 63–68 (1990).
17. Evans, D. M. et al. Interaction between ERAP1 and HLA-B27 in ankylosing spondylitis implicates peptide handling in the mechanism for HLA-B27 in disease susceptibility. Nat. Genet. 43, 761–767 (2011).
18. van der Linden, S., Valkenburg, H. & Cats, A. The risk of developing ankylosing spondylitis in HLA-B27 positive individuals: a family and population study. Br. J. Rheumatol. 22, 18–19 (1983).
19. Brewerton, D. A., Nicholls, A., Caffrey, M., Walters, D. & James, D. C. O. ACUTE ANTERIOR UVEITIS AND HL-A 27. Lancet 302, 994–996 (1973).
20. Strange, A. et al. A genome-wide association study identifies new psoriasis susceptibility loci and an interaction between HLA-C and ERAP1. Nat. Genet. 42, 985–990 (2010).
21. Remmers, E. F. et al. Genome-wide association study identifies variants in the MHC class I, IL10, and IL23R-IL12RB2 regions associated with Behçet's disease. Nat. Genet. 42, 698–702 (2010).
22. Ohno, S. et al. Close association of HLA-Bw51 with Behçet's disease. Arch. Ophthalmol. (Chicago, Ill. 1960) 100, 1455–1458 (1982).
23. McGonagle, D., Aydin, S. Z., Gül, A., Mahr, A. & Direskeneli, H. 'MHC-I-opathy'-unified concept for spondyloarthritis and Behçet disease. Nature reviews. Rheumatology vol. 11 731–740 (2015).
24. Kuiper, J. J. W. et al. EULAR study group on 'MHC-I-opathy': identifying disease-overarching mechanisms across disciplines and borders. Ann. Rheum. Dis. annrheumdis-2022-222852 (2023) doi:10.1136/ard-2022-222852.
25. Kuiper, J. J. W. et al. A genome-wide association study identifies a functional ERAP2 haplotype associated with birdshot chorioretinopathy. Hum. Mol. Genet. 23, 6081–6087 (2014).
26. Hanson, A. L. et al. Genetic Variants in ERAP1 and ERAP2 Associated With Immune-Mediated Diseases Influence Protein Expression and the Isoform Profile. Arthritis Rheumatol. 70, 255–265 (2018).
27. Ombrello, M. J., Kastner, D. L. & Remmers, E. F. Endoplasmic reticulum-associated amino-peptidase 1 and rheumatic disease: Genetics. Curr. Opin. Rheumatol. 27, 349–356 (2015).
28. Hutchinson, J. P. et al. Common allotypes of ER aminopeptidase 1 have substrate-dependent and highly variable enzymatic properties. J. Biol. Chem. 296, 100443 (2021).
29. Kuiper, J. J. W. et al. Functionally distinct ERAP1 and ERAP2 are a hallmark of HLA-A29-(Birdshot) Uveitis. Hum. Mol. Genet. 27, 4333–4343 (2018).
30. López de Castro, J. A. How ERAP1 and ERAP2 Shape the Peptidomes of Disease-Associated MHC-I Proteins. Front. Immunol. 9, 2463 (2018).
31. Andrés, A. M. et al. Balancing selection maintains a form of ERAP2 that undergoes nonsense-mediated decay and affects antigen presentation. PLoS Genet. 6, e1001157 (2010).
32. Chang, S.-C., Momburg, F., Bhutani, N. & Goldberg, A. L. The ER aminopeptidase, ERAP1, trims precursors to lengths of MHC class I peptides by a 'molecular ruler' mechanism. Proc. Natl. Acad. Sci. U. S. A. 102, 17107–17112 (2005).

33. Mpakali, A. et al. Structural basis for antigenic peptide recognition and processing by Endoplasmic reticulum (ER) aminopeptidase 2. J. Biol. Chem. 290, 26021–26032 (2015).
34. Rammensee, H.-G., Friede, T. & Stevanović, S. MHC ligands and peptide motifs: first listing. Immunogenetics 41, 178–228 (1995).
35. Collier, J. L., Weiss, S. A., Pauken, K. E., Sen, D. R. & Sharpe, A. H. Not-so-opposite ends of the spectrum: CD8+ T cell dysfunction across chronic infection, cancer and autoimmunity. Nat. Immunol. 22, 809–819 (2021).
36. López de Castro, J. A. et al. Molecular and pathogenic effects of endoplasmic reticulum aminopeptidases ERAP1 and ERAP2 in MHC-I-associated inflammatory disorders: Towards a unifying view. Mol. Immunol. 77, 193–204 (2016).
37. de Smet, M. D., Bitar, G., Roberge, F. G., Gery, I. & Nussenblatt, R. B. Human S-antigen: presence of multiple immunogenic and immunopathogenic sites in the Lewis rat. J. Autoimmun. 6, 587–599 (1993).
38. Gregerson, D. S., Merryman, C. F., Obritsch, W. F. & Donoso, L. A. Identification of a potent new pathogenic site in human retinal S-antigen which induces experimental autoimmune uveoretinitis in LEW rats. Cell. Immunol. 128, 209–219 (1990).
39. Whitcup, S. M., Vistica, B. P., Milam, A. H., Nussenblatt, R. B. & Gery, I. Recoverin-associated retinopathy: a clinically and immunologically distinctive disease. Am. J. Ophthalmol. 126, 230–237 (1998).
40. Evangelou, E. & Ioannidis, J. P. A. Meta-analysis methods for genome-wide association studies and beyond. Nat. Rev. Genet. 14, 379–389 (2013).
41. Slatkin, M. Linkage disequilibrium--understanding the evolutionary past and mapping the medical future. Nat. Rev. Genet. 9, 477–485 (2008).
42. Auton, A. et al. A global reference for human genetic variation. Nature 526, 68–74 (2015).
43. Nica, A. C. & Dermitzakis, E. T. Expression quantitative trait loci: present and future. Philos. Trans. R. Soc. London. Ser. B, Biol. Sci. 368, 20120362 (2013).
44. Yang, J. et al. Conditional and joint multiple-SNP analysis of GWAS summary statistics identifies additional variants influencing complex traits. Nat. Genet. 44, 369–75, S1-3 (2012).
45. Jinek, M. et al. A programmable dual-RNA-guided DNA endonuclease in adaptive bacterial immunity. Science 337, 816–821 (2012).
46. Gasiunas, G., Barrangou, R., Horvath, P. & Siksnys, V. Cas9-crRNA ribonucleoprotein complex mediates specific DNA cleavage for adaptive immunity in bacteria. Proc. Natl. Acad. Sci. U. S. A. 109, E2579-86 (2012).
47. Mali, P. et al. RNA-guided human genome engineering via Cas9. Science 339, 823–826 (2013).
48. Sternberg, S. H., Redding, S., Jinek, M., Greene, E. C. & Doudna, J. A. DNA interrogation by the CRISPR RNA-guided endonuclease Cas9. Nature 507, 62–67 (2014).
49. Anders, C., Niewoehner, O., Duerst, A. & Jinek, M. Structural basis of PAM-dependent target DNA recognition by the Cas9 endonuclease. Nature 513, 569–573 (2014).
50. Scherer, S. A short guide to the human genome. (Cold Spring Harbor Laboratory Press, 2008).

51. Iliakis, G. et al. Mechanisms of DNA double strand break repair and chromosome aberration formation. Cytogenet. Genome Res. 104, 14–20 (2004).
52. Lin, S., Staahl, B. T., Alla, R. K. & Doudna, J. A. Enhanced homology-directed human genome engineering by controlled timing of CRISPR/Cas9 delivery. Elife 3, e04766 (2014).
53. Hassan, C. et al. Accurate quantitation of MHC-bound peptides by application of isotopically labeled peptide MHC complexes. J. Proteomics 109, 240–244 (2014).
54. Batard, P. et al. Dextramers: New generation of fluorescent MHC class I/peptide multimers for visualization of antigen-specific CD8+ T cells. J. Immunol. Methods 310, 136–148 (2006).

Chapter 2

ERAP2 increases the abundance of a peptide submotif highly selective for the Birdshot Uveitis-associated HLA-A29

W.J. Venema[1,2], S. Hiddingh[1,2], J.H. de Boer[1], F.H.J. Claas[3], A Mulder[3], A.I. den Hollander[4], E. Stratikos[5], S. Sarkizova[6,7], L.T. van der Veken[8], G.M.C. Janssen[9], P.A. van Veelen[9], J.J.W. Kuiper[1,2]

1. Department of Ophthalmology, University Medical Center Utrecht, University of Utrecht, Utrecht, The Netherlands.
2. Center for Translational Immunology, University Medical Center Utrecht, University of Utrecht, Utrecht, The Netherlands.
3. Department of Immunology, Leiden University Medical Center, Leiden, The Netherlands
4. Department of Ophthalmology, Donders Institute for Brain, Cognition and Behaviour, Department of Human Genetics, Radboud University Medical Center, Nijmegen, The Netherlands.
5. Department of Chemistry, National and Kapodistrian University of Athens, Panepistimiopolis Zographou 157 84, Greece.
6. Department of Biomedical Informatics, Harvard Medical School, Boston, MA, USA.
7. Broad Institute of MIT and Harvard, Cambridge, MA, USA.
8. Department of Genetics, Division Laboratories, Pharmacy and Biomedical Genetics, University Medical Center Utrecht, University of Utrecht, Utrecht, The Netherlands
9. Center for Proteomics and Metabolomics, Leiden University Medical Center, Leiden, The Netherlands.

Published in Front. Immunol. 12, 634441 (2021)

Abstract

Birdshot Uveitis (BU) is a blinding inflammatory eye condition that only affects HLA-A29-positive individuals. Genetic association studies linked *ERAP2* with BU, an aminopeptidase which trims peptides before their presentation by HLA class I at the cell surface, which suggests that ERAP2-dependent peptide presentation by HLA-A29 drives the pathogenesis of BU. However, it remains poorly understood whether the effects of ERAP2 on the HLA-A29 peptidome are distinct from its effect on other HLA allotypes. To address this, we focused on the effects of ERAP2 on the immunopeptidome in patient-derived antigen presenting cells. Using complementary HLA-A29-based and pan-class I immunopurifications, isotope-labelled naturally processed and presented HLA-bound peptides were sequenced by mass spectrometry. We show that the effects of ERAP2 on the N-terminus of ligands of HLA-A29 are shared across endogenous HLA allotypes, but discover and replicate that one peptide motif generated in the presence of ERAP2 is specifically bound by HLA-A29. This motif can be found in the amino acid sequence of putative autoantigens. We further show evidence for internal sequence specificity for ERAP2 imprinted in the immunopeptidome. These results reveal that ERAP2 can generate an HLA-A29-specific antigen repertoire, which supports that antigen presentation is a key disease pathway in BU.

Introduction

Birdshot uveitis (BU) is a rare form of uveitis characterized by distinctive inflammatory foci across the retina, hypopigmented choroidal lesions, and cystoid macular edema, which causes visual impairment when undertreated[1,2]. Infiltration of T cells and elevated levels of T cell cytokines in eye tissues of patients suggest that T cell-mediated inflammation is among the driving disease mechanisms[3-6]. This is further supported by the fact that all patients with BU carry at least one copy of the Human leukocyte antigen (HLA)-A*29 allele, now widely considered as a prerequisite for diagnosis[7,8]. How HLA-A29 contributes to BU has remained unsolved, however, genetic association studies identified that in addition to the extreme association with the HLA-A*29:02 allele, polymorphisms in endoplasmic reticulum aminopeptidase (ERAP)-1 and ERAP2 confer strong disease risk[9,10]. Within the endoplasmic reticulum, ERAP aminopeptidases destroy or trim peptides to a length that is considered to influence their binding to HLA class I and presentation at the cell surface[11]. Importantly, of the two major haplotypes of ERAP2, the haplotype associated with canonical full-length ERAP2 (termed Haplotype A) is associated with BU[9]. The other common haplotype (haplotype B) encodes a transcript that undergoes alternative splicing and nonsense-mediated RNA decay, resulting in undetectable ERAP2 protein[12]. Because the risk haplotypes of ERAP genes for BU have been shown to result in lower cellular expression and activity of ERAP1 in combination with high cellular expression of functional ERAP2[10], it is likely that ERAP2 generates a so far unknown, but highly HLA-A29-restricted antigen repertoire that dictates T cell- or NK cell responses. This renders antigen processing and presentation a key disease pathway in BU[9].
ERAPs can trim the N-terminal residues of peptide substrates by sequestering the entire substrate inside the enzyme's cavity where the sum of interactions of amino acid side chains are considered to determine the rate and outcome of peptide proteolysis[13,14]. Both ERAP1 and ERAP2 have been shown to have preferences for the internal sequence of the peptide, although these preferences are broad and no specific motif has been identified[13-16]. ERAP1 has been shown to trim peptides in solution by sequestering them in an internal cavity before trimming.[14] However, a number of studies have also shown that ERAPs can also trim peptide while they are bound onto MHC-I[17-21]. These and other observations[22] support that ERAPs modulate both HLA-bound and a significant fraction of the 'free' peptide cargo before binding to HLA, which suggests that physiologically-relevant sequence specificities for ERAP2 may be deciphered from the presented peptide repertoire.
Mass-spectrometry based peptidomic studies of model high-passage cell lines have revealed that ERAPs can influence the peptide repertoire presented by HLA-A29[23,24]. However, to date, no studies have been conducted that studied the interaction of the major genetic risk haplotypes for ERAP1, ERAP2, and HLA-A*29:02 simultaneously in patient-derived tissues and compared the effects of ERAP2 on HLA-A29 to the other competing alleles expressed by the same cell. Knowing the potential effects of ERAP2 across HLA class I alleles is important to be able to separate potential disease effects from canonical antigen processing in studies of

the immunopeptidome and may help predict the outcome of pharmacological interference of ERAP2 activity using small molecule inhibitors[25].

We generated patient-derived lymphoblastoid cells that naturally express high levels of HLA and ERAPs, in which we stably expressed an autoantigen for BU (i.e. the retinal S-antigen, which is only expressed in the retina) to study if can present autoantigen fragments via HLA-A29. An advantage of using lymphoblastoid cells is that they express high levels of the immunoproteasome (e.g., LMP7 subunit)[26], which is also highly expressed in photoreceptors of the retina where the immunoproteasome is essential for the maintenance of normal retinal function and vision transduction[27]. The use of newly established low-passage patient-derived antigen presenting cell lines better preserves the genetic architecture critically involved with BU in the context of physiologically relevant antigen processing.

In this study, we compared the immunopeptidomes of ERAP2-wild-type and ERAP2-deficient cells using mass spectrometry profiling of elutions from immunopurification with an HLA-A29-binding antibody and subsequent pan-class I antibody. Using several unbiased computational analyses, we accurately dissect the immunopeptidomes of HLA-A29 and other allotypes, which revealed commonly shared effects on position (P)1 and P7 of peptides across alleles, and hitherto unknown, specific effects on P2 in the HLA-A29 immunopeptidome with potential implications for the disease mechanisms of BU.

Materials & Methods

Generation of patient-derived EBV-immortalized B cell lines

EBV-immortalized lymphoblastoid cell lines (EBV-LCL) were generated from peripheral blood mononuclear cells (PBMC) from Birdshot patients, from which we selected a cell-line from a female patient (80 years old during sampling) homozygous for the risk haplotypes for *ERAP1* (*Hap10*/*Hap10*) and *ERAP2* (*HapA/HapA*)[10]. B95-8 marmoset-derived EBV supernatant was a kind gift from Dr. Willemijn Janssen, Center for Translational Immunology, UMC Utrecht. Cryopreserved PBMC were thawed and the cell number was determined. In a 24-well plate, 5-10^6 cells were plated and cultured in freshly thawed EBV supernatant overnight at 37°C, 5% CO_2. The next day, transformation-medium (RPMI 1640 + 10% FBS + 1µg/ml cyclosporine) was added into the wells. The EBV-infected cells were observed under the microscope to look for transformed LCLs in clusters. Patient-derived cell lines were cultured in Roswell Park Memorial Institute 1640 medium (RPMI 1640, Thermo Fisher Scientific) supplemented with 10% heat-inactivated fetal bovine serum (FBS, Biowest Riverside) and 1% penicillin/streptomycin (Thermo Fisher Scientific). To obtain stable cell lines overexpressing S-antigen, EBV-LCLs were transduced with the concentrated lentiviral supernatants (see **Supplemental Methods and Info**).

ERAP2 KO using CRISPR-Cas9

For the generation of ERAP2 KO EBV-LCLs the Alt-R CRISPR-Cas9 system (Integrated DNA Technologies) was used and cells were electroporated with the Neon Transfection System (Thermo Fisher Scientific). First, the RNP complex was assembled by combining the crRNA CTAATGGGGAACGATTTCCT with the Alt-R tracrRNA (at a ratio of 1:1) and incubated at 95°C for 5 min, cooled down at room temperature and mixed with the Alt-R S.p Cas9 Nuclease and Buffer R (Neon system). After incubating the RNP complex for 10 minutes at room temperature, 8×10^5 EBV-LCLs were mixed with the crRNA:tracrRNA-Cas9 complex and electroporated with two pulses of 1100 V and 30 ms each using the 10 µl Neon pipette tip. Electroporated cells were immediately taken up in antibiotic-free medium and cultured for minimal 7 days. This procedure was repeated for 3 times before ERAP2 protein expression levels were analyzed by western blot. A total of 5 rounds was required to reduce to levels of ERAP2 expression to near undetectable levels (**Figure 2.1B**).

Cell Culture and HLA-Peptide Immunopurification

For stable isotope labeling by amino acids in cell culture (SILAC), EBV-LCLs were cultured in customized RPMI with the same formula but lacking the two amino acids tyrosine and phenylalanine (Thermo Fisher Scientific) and with dialyzed FBS (Thermo Fisher Scientific) in order to avoid unlabeled (i.e., 'light') amino acid carry-over. The medium was supplemented with L-Tyrosine-$^{13}C_9$,^{15}N (Sigma Aldrich) and L-Phenylalanine-$^{13}C_9$,^{15}N (Cortecnet). Wildtype EBV-LCLs were cultured with the customized medium ('heavy' labeled) and ERAP2-KO EBV-LCLs were cultured in RPMI with 10% non-dialyzed FBS ('light', without the labeled amino acids). Two independent experimental cultures were performed; Biological replicates were defined as two separate experiments starting from the CRISPR-Cas9-mediated ERAP2-KO (i.e., independent SILAC-cultures, immunopurification, elution and mass spectrometry profiling). In each experiment, cells from each condition were cultured to obtain $1x10^9$ cells in total per cell line. Cell pellets were stored at -20°C before mass spectrometry was performed. HLA class I molecules were isolated using standard immunoaffinity purification (IP) as described before[28] from a fixed sample volume of 2.0 ml cell pellet per condition and biological replicate. IP was done using the human monoclonal antibody (mAb) DK1G8 (IgG1)[29] derived from a HLA-A29-negative multiparous woman sensitized to HLA-A29 due to pregnancy, which specifically binds to 63-L-63-Q epitope in *HLA-A*29:01* and *A*29:02* and the very rare allele *A*43:01,* in a single antigen bead test. (https://www.epregistry.com.br/index/databases/ database/ABC/), and a pan-HLA class I-specific mAb W6/32. Cell pellets from light and heavy labeled cell lines (ERAP2-WT and ERAP2-KO conditions) were combined and stored at −80 °C until mass spectrometry analysis.

HLA-A29-binding and W6/32 antibodies.

The hybridoma cell line producing HLA-A29-binding mAb DK1G8 was cultured in protein-free hybridoma medium supplemented with penicillin/streptomycin and L-glutamine in roller bottles. Cell culture supernatant was treated with Protein-A Sepharose beads to capture the mAb and eluted with glycine pH 2.5. Eluted mAb was covalently bound to Protein-A with dimethyl pimelimidate for use in an immunoaffinity column (HLA-A29-Protein-A, W6/32-Protein-A Sepharose at 2.5 mg/ml). The columns were stored in PBS pH 8.0 and 0.02% NaN3 at 4 °C. HLA-bound peptides were extracted as described previously[28].

Isolation of HLA Class I–presented Peptides

The extraction of peptides associated with HLA class I molecules was performed as described elsewhere[28]. Briefly, pellets from a total of 2×10^9 LCLs were lysed for 2 hours at 4 °C in 50 mm Tris-HCl, 150 mm NaCl, 5 mm EDTA, and 0.5% Zwittergent 3-12 (N-dodecyl-N,N-dimethyl-3-ammonio-1-propanesulfonate) (pH 8.0) and the presence of Complete® protease inhibitor (Roche). The preparation was centrifuged for 10 min at 2500 rpm and 4 °C and supernatant was transferred to a new tube and centrifuged for 40 min at 30,000 x g and 4 °C. The supernatant was pre-cleared with a 2-ml CL4B column and subjected to the immunoaffinity column (2ml with 5 mg ml). After washing, bound HLA class I–peptide complexes were eluted from the column and dissociated with 10% acetic acid. Peptides were separated from the HLA class I molecules via passage through a 10 kDa membrane (Microcon YM-10). The filtrate was freeze dried, dissolved in 50mM NH4HCO3 pH 8.4 and the peptides were further purified via 'high pH reverse phase' fractionation on a C18 column (Oasis HLB, Waters, Milford, MA). The peptides were eluted from the C18 Oasis column with successively 400 µl 10/90/0.1, 20/80/0.1 and 50/50/0.1 water/acetonitrile (ACN)/formic acid (FA), v/v/v.

MS analysis

Peptides were lyophilized, dissolved in 95/3/0.1 v/v/v water/acetonitrile/formic acid and subsequently analyzed by on-line C18 nanoHPLC MS/MS with a system consisting of an Easy nLC 1200 gradient HPLC system (Thermo, Bremen, Germany), and a LUMOS mass spectrometer (Thermo). Fractions were injected onto a homemade precolumn (100 µm × 15 mm; Reprosil-Pur C18-AQ 3 µm, Dr. Maisch, Ammerbuch, Germany) and eluted via a homemade analytical nano-HPLC column (30 cm × 50 µm; Reprosil-Pur C18-AQ 3 um). The gradient was run from 2% to 36% solvent B (20/80/0.1 water/acetonitrile/formic acid (FA) v/v) in 120 min. The nano-HPLC column was drawn to a tip of ~5 µm and acted as the electrospray needle of the MS source. The LUMOS mass spectrometer was operated in data-dependent MS/MS mode for a cycle time of 3 seconds, with a HCD collision energy at 32 V and recording of the MS2 spectrum in the orbitrap. In the master scan (MS1) the resolution was 60,000, the scan range 300-1400, at the standard AGC target @maximum fill time of 50 ms. Dynamic exclusion was after n=1 with an exclusion duration of 20s. Charge states

1-3 were included. For MS2 precursors were isolated with the quadrupole with an isolation width of 1.2 Da. Precursors of charge 1 were selected in the range of 800-1400, precursors of charge 2 were selected in the range 400-800, and precursors of charge 3 were selected in the range 300-600. The first mass was set to 110 Da. The MS2 scan resolution was 30,000 at the standard AGC target of 50,000 @dynamic injection time.

In a post-analysis process, raw data were first converted to peak lists using Proteome Discoverer version 2.1 (Thermo Electron), and then submitted to the Uniprot Homo sapiens canonical database (67911 entries), using Mascot v. 2.2.07 (www.matrixscience.com) for protein identification. Mascot searches were with 10 ppm and 0.02 Da deviation for precursor and fragment mass, respectively, and no enzyme was specified. Methionine oxidation was set as a variable modification.

Differential expression analysis

Peptide confidence False Discovery Rates (FDRs) were calculated with the Mascot Percolator[30] plug-in in Proteome Discoverer version 2.1 (Thermo Electron) and we used a strict target FDR of 1% (q<0.01) to obtain peptides detected with high confidence. To retrieve labeled peptides for downstream analysis, the high confidence peptides were further filtered to remove peptides with flags "InconsistentlyLabeled", "NoQuanValues", "Redundant", "IndistinguishableChannels". To detect significant changes in ligand abundance, we used the empirical Bayes workflow for mass spectrometry data based on the limma[31] and *qvalue*[32] R packages following Kammers and associates[33] (see **Supplemental Methods and Info**). The *qvalue* R package was used to provide an unbiased estimate of the false discovery rate (FDR). Changes in peptide abundance between light and heavy conditions below a moderated q<0.01 (i.e., 1% empirical FDR) was considered affected by ERAP2. After differential expression analysis, peptides were assigned to HLA alleles using the *HLAthena* algorithm[34], a state-of-the-art neural-network prediction algorithm trained on mass-spectrometry derived peptides from 95 mono-HLA expressing cell lines, which provides the binding score metric 'MSi' for each peptide and corresponding allele (range [0,1], MSi >0.6 was considered good, MSi>0.8 was considered strong). We used the GibbsCluster 2.0 server[35] to deconvolute the detected 9-mers into a deconvolution solution of maximum three clusters (seeds=5, λ=0.7, σ=5, t=3). We picked a three-cluster solution that best matched the canonical binding motifs of the *HLA-A* alleles *HLA-A*29:02* (PΩ-Tyr/Y or Phe/F) and *HLA-A*03:01* (PΩ-Lys/K or Arg/R). For comparison of the effects of ERAP2 and ERAP1 on the HLA-A29 immunopeptidome, we used the 974 HLA-A29-presented peptides detected in both (identical peptide sequences) datasets from *Sanz-Bravo et al., 2018* (ERAP2, n=1140)[23] and *Alvarez-Navarro et al., 2015* (ERAP1, n=5584)[24] of which 917 showed normalized intensity values >0. In these studies, the normalized intensity ratio [IR] of each peptide in two cell lines was used to infer the relative abundance of each peptide in ERAP positive versus ERAP negative cell lines. The SWEIG cell line has very low ERAP1 levels and was considered functionally 'negative' for ERAP1. We

plotted the normalized intensity ratio for each peptide as reported in the supplemental data from each study in **Figure 2.3I**.

Non-metric multidimensional scaling of peptides

Non-metric multidimensional scaling of 9-mers using entropy-weighted (*MolecularEntropy()* function from *HDMD* R package[36] peptide distances in two-dimensional space was conducted following the method of Sarkizova and associates[34,37]. This method uses a Hamming distance calculated with an amino acid substitution matrix (adapted from Kim *et al*.[38]) that is inversely weighted according to positional entropy to obtain the pairwise "distance" between 9-mers. To map the peptide distances in two dimensions, for each analyzed HLA allele, non-metric multidimensional scaling (NMDS) was used with 10 separate ordinations of 500 iterations using the *nmds()* function from the *ecodist* R package[39]. The configuration with the least stress was used for visualization of the peptidome. We next used *density-based spatial clustering of applications with noise* (DBSCAN)[40] within the *fpc* R package[41] to cluster peptides using the elbow method (*KNNdisplot function()* in *dbscan* R package[40] to estimate the number of clusters that fit the data. Sequence logo plots were generated using the *ggseqlogo* R package[42]. The positional amino acid usage differences were calculated by determining the count for each amino acid at indicated positions (e.g., P1, P2) in the peptides using the *MolecularEntropy()* function from the HDMD *R* package and a fisher exact test was used (*fisher.test ()* function in r base) to assess the differences at indicated positions. A chi-squared test (*chisq.test()* in r base*) was* used to assess for differences in the number of ERAP2 affected peptides per cluster. All *P* values were adjusted (termed *Padj*) using the Bonferroni method as indicated. A *grand average of hydropathicity* (GRAVY) hydrophobicity index on the Kyte-Doolittle scale for each peptide was calculated with the *hydrophobicity()* function in *Peptides* R package[43]. Differences in binding scores and hydrophobicity index were assessed using the *dunnTest()* function in the *FSA* R package[44].

Western Blot analysis

Protein levels of S-antigen, ERAP1 and ERAP2 were analyzed using western blotting. Total cell lysates were prepared using the NP40 lysis buffer (1% NP40, 135 mM NaCl, 5 mM EDTA, 20 mM Tris-HCl, pH = 7.4) complemented with complete protease inhibitor cocktail (Roche). Protein lysates (10 µl/lane) were separated on a 4-20% Mini-PROTEAN TGX gel (Bio-Rad Laboratories) and transferred to a polyvinylidene difluoride membrane (Immobilon-P PVDF, Millipore). Membranes were blocked in 5% nonfat dry milk in TBST and probed overnight at 4°C with antibodies recognizing ERAP1 (AF2334, R&D Systems), ERAP2 (AF3830, R&D Systems), S-antigen (α-mGFP, TA180076, Origene, to detect the fusion protein S-antigen-GFP) or α-tubulin (T6199, Sigma). After washing, membranes were incubated with anti-mouse secondary antibody conjugated to horseradish peroxidase (HRP) (DAKO) or anti-goat secondary antibody conjugated to HRP (DAKO). Protein bands were detected with Amersham Prima Western Blotting (RPN22361, GE Healthcare) on the ChemiDoc Gel Imaging System

(Bio-Rad Laboratories). The ratio of the intensity was calculated using Image Lab 5.1 (Bio-Rad Laboratories) for each experiment.

High-density SNP-array analysis

SNP-array copy number profiling and analysis of regions of homozygosity were performed on DNA isolated from WT and CRISPR-Cas9 edited LCLs (ERAP2-KO) according to standard procedures using the Infinium Human CytoSNP-850K v1.2 BeadChip (Illumina, San Diego, CA, USA). Samples were scanned using the iScan system (Illumina). Subsequently, visualizations of SNP-array results and data analysis were carried out using NxClinical software v5.1 (BioDiscovery, Los Angeles, CA, USA). Human genome build Feb. 2009 GRCh37/hg19 was used.

Data availability.

Analysis code, genotype data, and supporting data files can be found at https://github.com/jonaskuiper/ERAP2_HLA-A29_peptidome. Mass spectrometric raw data has been deposited in the MassIVE depository (MassIVE dataset XXXXX) under the creative commons zero license (CC0 1.0).

Results

Generation of a model for ERAP2-mediated antigen processing and presentation

We generated lymphoblastoid cells (LCLs) from a *HLA-A*29:02*-positive Birdshot patient homozygous for risk haplotypes of *ERAP1* (*Hap10*/*Hap10*) and *ERAP2* (*HapA/HapA*) (**Figure 2.1A**)[9,10] and the retinal S-antigen was stably expressed by lentiviral transduction (see **Supplemental Methods and Info**). Genotyping of the patient revealed *HLA-A*29:02, HLA-A*03:01, HLA-B*40:01*, *HLA-B*44:03*, *HLA-C*16:01*, and *HLA-C*03:04* alleles. Because the risk allotype of ERAP1 shows relatively low aminopeptidase activity[10], we focused our analysis on the effects of ERAP2 on the immunopeptidome. We used CRISPR-Cas9 ribonucleoprotein delivery with a guide-RNA targeting exon 2 in *ERAP2* (**Figure 2.1A**) to disrupt protein expression of ERAP2 and generate an ERAP2-KO LCL, while preserving the protein expression of ERAP1 (**Figure 2.1B**). SNP-array copy number profiling and analysis of regions of homozygosity were performed using the Infinium Human CytoSNP-850K capable of detecting genomic gains and losses with an approximate resolution of ~10 kb by profiling 850,000 single nucleotide polymorphism (SNP) markers spanning the entire genome. SNP-array analysis resulted in a normal female array profile (arr(1-22,X)x2) for both cell conditions (**Supplemental Figure 2.1**), and detected no changes between the WT and ERAP2-KO clones, including the ERAP region *5q15* (**Supplemental Figure 2.2**). This confirms that our editing strategy did not introduce wide spread genomic changes and thus that the

conditions are highly suitable for comparison. Genotype date for 92 SNPs at *5q15* for these cell lines is shown in **Supplemental Table 2.1.**

Next, we used stable isotope labeling by amino acids in cell culture (SILAC) to incorporate "heavy" L-Tyrosine-$^{13}C_9$,^{15}N (Tyr/Y) and L-Phenylalanine-$^{13}C_9$,^{15}N (Phe/F) in the 'wild type' (WT) LCLs and compare these to unlabeled ("light") culture conditions for the ERAP2-KO LCL cells (**Figure 2.1C, 2.1D**). The amino acids Y/F are observed in 95% of previously identified HLA-A29 ligands (**Figure 2.2A**), but are also found in the majority of peptides presented by the other HLA allotypes - with exception of HLA-B40:01.

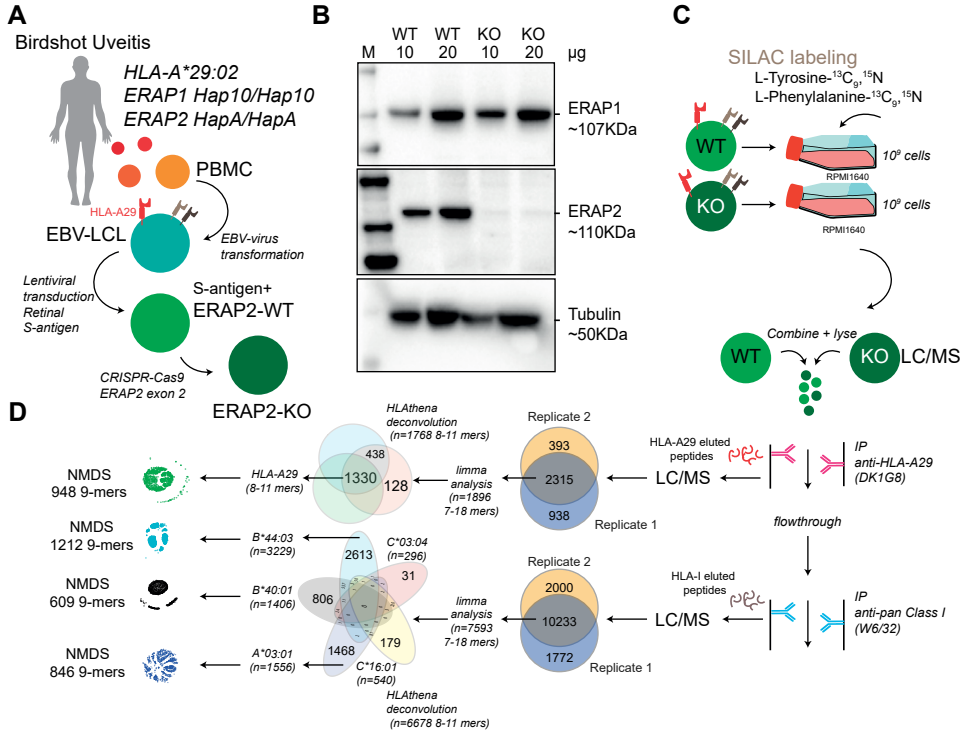

Figure 2.1: Study design and sample preparation. (**a**) Design of the patient-derived model for antigen processing by ERAP2. (**b**) Western blot analysis of the protein expression of ERAP1, ERAP2, and Tubulin as a control in the *HLA-A*29:02*-positive Birdshot uveitis model cell lines in ERAP2-wild type cells (WT) and cells after CRISPR-Cas9 mediated knock-out (KO) of ERAP2. The relative amount of protein (in microgram) used for each lane is indicated. M; marker. (**c**) Overview of cultured SILAC labeled WT LCLs and unlabeled ERAP2 KO LCLs followed by combining the differentially labeled conditions for lysis and immunoprecipitation of HLA-A29 and, subsequently other HLA class I molecules, respectively. HLA-bound peptides were eluted, followed by LC/MS analysis. All steps in (c) were conducted in two separate experiments to generate biological replicates. (**d**) Schematic overview of filtering steps of the identified peptides in this study. All peptides identified in both biological replicates with high confidence were filtered for *limma* analysis (see methods). After differential expression analysis, 8-11 mers were used to deconvolute and assign peptides to HLA alleles using *HLAthena*. The venn diagrams indicate the overlap from data sets and subsetting for subsequent analysis.

Capture of a high-quality HLA-A29 peptidome

Using the HLA-A29-binding antibody, a total of 2315 unique peptides were identified with high confidence (Mascot Percolator q<0.01) between biological replicates (*Jaccard* similarity = 0.64) (**Figure 2.1D**) that were used for further analysis. These were predominantly 9-11 mers (88%), which fits the length distribution[45] of HLA-A29 ligands (**Figure 2.2B**). The HLA-A29-binding antibody may weakly cross-react with other HLA-A allotypes (see ***Methods***). This is of relevance given that *HLA-A*29* alleles are low expressed *HLA-A* alleles[46] compared to high expressed *HLA-A*03* alleles. We used *GibbsCluster 2.0* for unbiased clustering of the peptides, which found a deconvoluted solution that consisted of three clusters; two motifs fitting the canonical HLA-A29:02 binding motif (C-terminal position Y or PΩ-Y) and one cluster highly similar to the dominant HLA-A03:01 motif (PΩ Lysine (K) or Arginine (R) (**Figure 2.2C**) and shows that the HLA-A29 antibody cross-reacts with HLA-A03:01. Indeed, when we used the *HLAthena* algorithm[34], ligands in cluster 1 and 2 were predominantly assigned to HLA-A29:02 (84% and 86%, respectively), and 93% of ligands in cluster 3 were assigned to HLA-A03:01 (**Figure 2.2D**). However, because 66% and 20% of peptides in clusters 1 and 2 assigned to other endogenous HLA alleles also showed high binding scores for HLA-A29:02 (**Figure 2.2E**), we later choose to filter the dataset using bindings scores for HLA-A29:02 (**Figure 2.2G**).

Because we were interested in determining significant changes in peptide abundance associated with ERAP2, we first jointly analyzed the relative abundance (fold change) of light (KO) over heavy (WT) labeled peptides from both experiments using *limma*[33]. A total of 1,896 peptides (**Figure 2.2F**) were detected in both light and heavy channels and used for analysis. Analysis of peptides unique to one of the conditions is shown in the Supplemental Info. Note that the log fold changes of pooled normalized peptides abundances from light and heavy channels by *limma* strongly correlate (spearman r = 0.95) with the light/heavy ratio abundance of each experiment (**Figure 2.2F**), thus the normalization steps preserve the data structure, while improving the power to detect significant changes[33]. From the 1,330 8- to 11-mers HLA-A29 epitopes (MSi>0.6 by *HLAthena*) (**Figure 2.2G**), 1,195/1,330 (89%) of the peptides in our HLA-A29 dataset have been reported as ligands for HLA-A29 of which 78% detected in mono-allelic or homozygous HLA-A29-expressing cell systems[23,34], supporting the notion that the approach taken yields an accurate representation of the peptide-presenting properties of HLA-A29:02.

ERAP2 shapes P1 of HLA-A29 ligands.

At a false discovery rate of 1%, in ERAP2-WT compared to ERAP2-KO cells, a total of 226 peptides were detected at decreased abundance in the binding groove of HLA-A29 (termed ERAP2-"sensitive" peptides), and 228 peptides were increased in abundance (termed ERAP2-"dependent" peptides) (**Figure 2.2H**, **Supplemental Table 2.2**). We detected the 9-mer VTLTCAFRY from retinal S-antigen, which was ~6-fold higher (Log_2[FC] = 2.45) in ERAP2-KO cells compared to ERAP2-WT cells, indicating ERAP2 destroys this epitope (**Figure**

2.2H, **Supplemental Table 2.2**). We observed moderate changes in the length distribution (**Figure 2.2I**, **Supplemental Figure 2.3**) or predicted binding affinities of peptides affected by ERAP2 (Kruskal-Wallis *P* = 0.06) (**Figure 2.2J**).

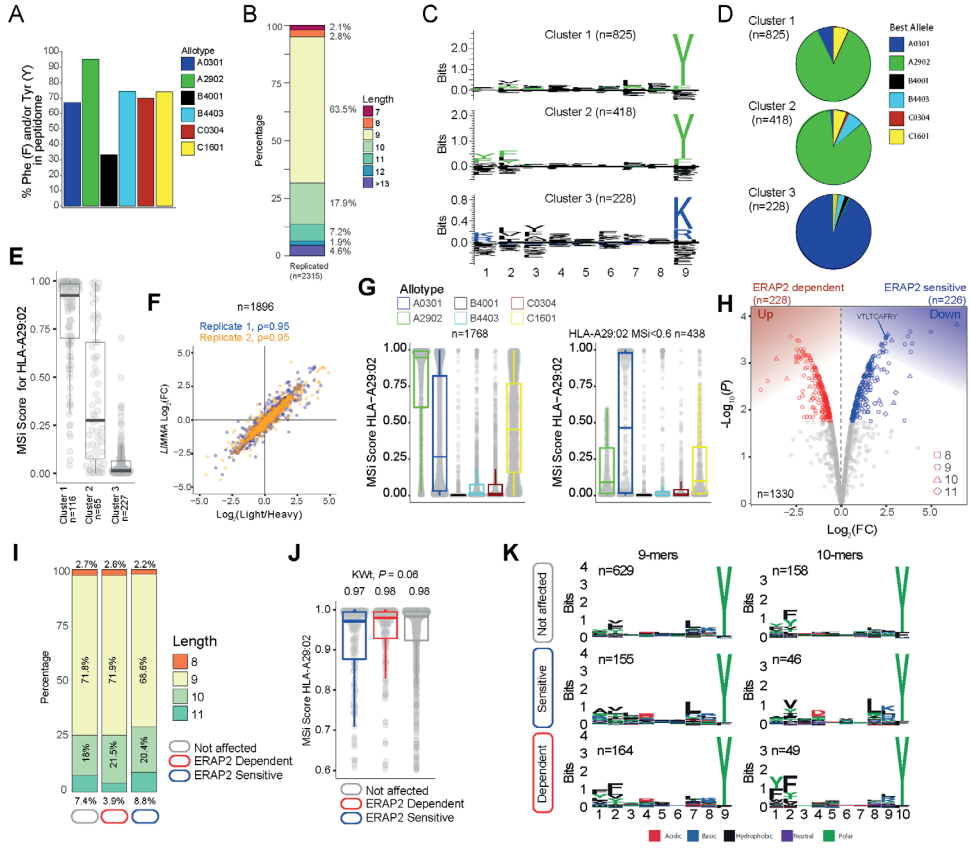

Figure 2.2: ERAP2 shapes the HLA-A29 peptidome. (**a**) The percentage of peptides that contain Phenylalanine and/or Tyrosine in peptidomic studies of monoallelic cell lines by Sarkizova and associates[34]. (**b**) The length distribution of the 2315 peptides detected in both biological replicates. (**c**) *GibbsCluster 2.0* results for unbiased clustering of the 9-mers (n=1471 unique peptides) eluted with the HLA-A29-binding monoclonal antibody. The motifs correspond with the *HLA-A* genotype (*HLA-A*29:02/HLA-A*03:01*) of the sample. Cluster 1 and 2 match the binding motif of HLA-A29:02, and Cluster 3 matches the binding motif of HLA-A03:01. (**d**) Pie diagrams (percentages) of best assigned alleles for the peptides in the clusters identified in (c). The alleles which correspond to the best score for each peptide ('Best Allele' output from *HLAthena*) was used to obtain the percentages of peptides assigned to each of the six *HLA-A, -B*, and *-C* alleles. (**e**) The binding scores for HLA-A29:02 for peptides from the clusters identified in *C* assigned to the other alleles. (**f**) Strong correlation between the raw peptide abundance data (n=1896) and normalized data by *limma* used in the differential expression analysis. (**g**) The 1768 8-11 mers before (left plot) and after (right plot) filtering out the 1330 HLA-A29-binding peptides. (**h**) Volcano plot of the differentially expressed 8-11 mers. In red are peptides that are increased in expression in the presence of ERAP2, while peptides indicated in blue are decreased. The identified peptide VTLTCAFRY from the retinal S-antigen is indicated. (**i**) The length distribution and (**j**) binding scores for HLA-A29 of the peptide groups identified in (h). (**k**) Sequence logos generated using a non-redundant list of 9-mers and 10-mers (11-mers see **Supplemental Figure 2.4**).

In contrast, comparison of the peptide motifs revealed evident and consistent changes at the N-terminal amino acid positions for ERAP2-sensitive 9-11 mer peptides compared to peptides not affected by ERAP2 (**Figure 2.2K**, **Supplemental Figure 2.4**), which aligns with the current view that ERAP2 trims the N-terminal amino acids of peptide substrates[13]. In detail, P1 of 9-mers revealed a contrasting residue preference for ERAP2-sensitive and ERAP2-dependent peptides (**Figure 2.3A**); Alanine(A), K, and R amino acids were seen significantly more often, while amino acids Y and F were seen significantly less often in sensitive peptides compared to non-affected peptides (Fisher's Exact test, *Padj* <0.05, **Supplemental Table 2.3**). In contrast, the most common P1 residues for dependent and non-affected peptides were Y and F (Y/F at P1; 45% and 30%, respectively) with F statistically more abundant at P1 and P2 in dependent peptides (**Figure 2.3A**, **Supplemental Tables 2.3, 2.4**). Intriguingly, we detected no significant effects of ERAP2 at the N-terminal residue of the precursor peptide (position P-1) (**Supplemental Figure 2.5**). Together these data show that ERAP2 has a selective effect on P1 of the HLA-A29 immunopeptidome in part by driving the depletion of peptides with preferred P1 substrates (e.g., A, K, R)[47] of ERAP2. This finding is consistent with previous reports that ERAP2 has primarily a destructive role by over-trimming susceptible peptide sequences and thus removing them from the immune-peptidome[47].

ERAP2 increases the abundance of peptides with a cryptic aromatic P2 motif

ERAP2 trims peptides by sequestering them into the relatively large internal enzyme cavity[13], where peptide side chains across the amino acid sequence can interact with pockets inside the cavity of ERAP2[13,14]. To evaluate if sequence-specific selectivity[16] by *ERAP2* could be interpreted from the HLA-A29 peptidome, we conducted non-metric multidimensional scaling (NMDS) of all 9-mers[34]. This analysis projects peptides in two-dimensional space based on the similarity of the amino acid sequences (**Figure 2.3B**). Considering peptides with significant changes between ERAP2-WT and -KO conditions revealed distinct patterns for co-clustered ("similar") peptides, with ERAP2-sensitive peptides located 'away' from ERAP2-dependent peptides (**Figure 2.3C**). To quantify these differences, we compared the amount of ERAP2-sensitive (**Figure 2.3B** in blue, n=155) versus ERAP2-dependent peptides (in red, n=164) across five clusters of peptides or 'submotifs'[37]. This analysis revealed that ERAP2-sensitive peptides were overrepresented in cluster 3 (X^2, Bonferroni n=clusters, *Padj* = 0.046) and ERAP2-dependent peptides overrepresented in cluster 2 (*Padj* = 5.1×10^{-6}) (**Figure 2.3D**). Cluster 2 (n=172 in total) was defined by nonpolar aromatic residues F (*Padj* = 1.0×10^{-49}), or Y (*Padj* = 2.1×10^{-22}) at P2 (F/Y in 97% of peptides in cluster 2 compared to 13% of peptides in all other clusters). ERAP2-dependent peptides (n=53) made up a considerable proportion of cluster 2 (unaffected peptides; n=106). Peptides in cluster 3 (n=356) were distinguished by a L at P7 (99% of peptides in cluster 3 compared to 3% in other clusters, *Padj* = 2.0×10^{-230})(**Figure 2.3C**, **Supplemental Table 2.5**). Peptides in cluster 3 showed an overall higher binding score for HLA-A29:02 and higher hydrophobicity index compared to cluster 2 (**Figure 2.3E**). Note that submotifs cluster 2 and cluster 3 are *bona fide* submotifs of HLA-A29

that are highly reproducible in other datasets (cluster 1 and 4 in **Figure 2.3F** and **Figure 2.3G** and cluster 1 and 3 in **Supplemental Figure 2.6**). We further replicated our findings in HLA-A29 immunopeptidome data from Sanz-Bravo *et al*.[23] of ERAP2-competent and naturally ERAP2-deficient HLA-A29-positive cell lines (**Figure 2.3H**) and, thus, demonstrate that ERAP2- positive cell lines commonly display selectively increased peptides with the motif of cluster 2.

In contrast, ERAP1 did not selectively contribute to cluster 2 peptides (**Supplemental Figure 2.6**). Also, the effect of ERAP1 and ERAP2 on HLA-A29 peptides correlated weakly (spearman rho=0.12, **Figure 2.3I**), suggesting non-redundant effects for ERAP1 and 2 on the HLA-A29 peptidome. Although the analysis for 10-mers (n=235) in our dataset was considered to lack sufficient resolution to map the effects of ERAP2 on the submotif level, most of the ERAP2-dependent 10-mers also mapped to a submotif of HLA-A29 with F at P2 (**Supplemental Figure 2.7**). In summary, ERAP2 selectively increases the expression of HLA-A29-binding peptides with a submotif with aromatic residues at P2.

ERAP2-dependent peptides of cluster 2 are selective for HLA-A29

HLA class I peptides display promiscuity[48] and it is therefore of interest that HLA-A03:01 can present peptides with a Y at PΩ (similar to HLA-A29) only with L at P7 is present[45]. As expected, peptides from cluster 3 (**Figure 2.3C**) were also predicted as potential binders for HLA-A03:01, while cluster 2 peptides (**Figure 2.3C**) were not (**Supplemental Figure 2.8**). To further test the HLA allotype restriction, we compared the binding scores for the differentially expressed peptides in cluster 2 and 3 for eight alleles which display binding motifs that overlap with HLA-A29:02 (based on Sarkizova *et al*.[34]). As shown in **Figure 2.3J**, ERAP2-sensitive peptides in cluster 3 show relatively good (MSi>0.8) binding scores for several other alleles (e.g., HLA-A30:02). Note that the S-antigen peptide VTLTCAFRY (in cluster 1, **Figure 2.3B**) also shows good binding scores for other alleles (e.g., HLA-A30:02 MSi = 0.86). In contrast, ERAP2-dependent peptides from cluster 2 are predicted to poorly bind the other class I alleles with an overall similar binding motif (median MSi<0.6) (**Figure 2.3J**), indicating that this cluster is highly specific for HLA-A29:02. We extended this analysis to 95 alleles, which supported that the ERAP2-dependent peptides in cluster 2 are highly specific for HLA-A29 (**Supplemental Figure 2.9**), with the exception of *HLA-C*14:03* (>100 times lower allele frequency compared to *HLA-A*29:02* in European populations) (**Supplemental Table 2.6**). The motif of cluster 2 peptides is present in the amino acid sequences of proteins encoded by ~300 genes highly expressed in the retina (**Supplemental Table 2.7**), of which putative HLA-A29-restricted peptides (MSi>0.9 for HLA-A29 and MSi<0.6 for 94 other alleles) were found in key factors in melanocyte biology (ARMC9, OCA2, SLC45A2, PLXNC1) (**Supplemental Table 2.8**). This is of significance, because progressive loss of ocular melanocytes is a hallmark feature of BU[2,5,8,56,57]. We conclude that these data support that ERAP2 may apply selective pressure on the repertoire of HLA-A29.

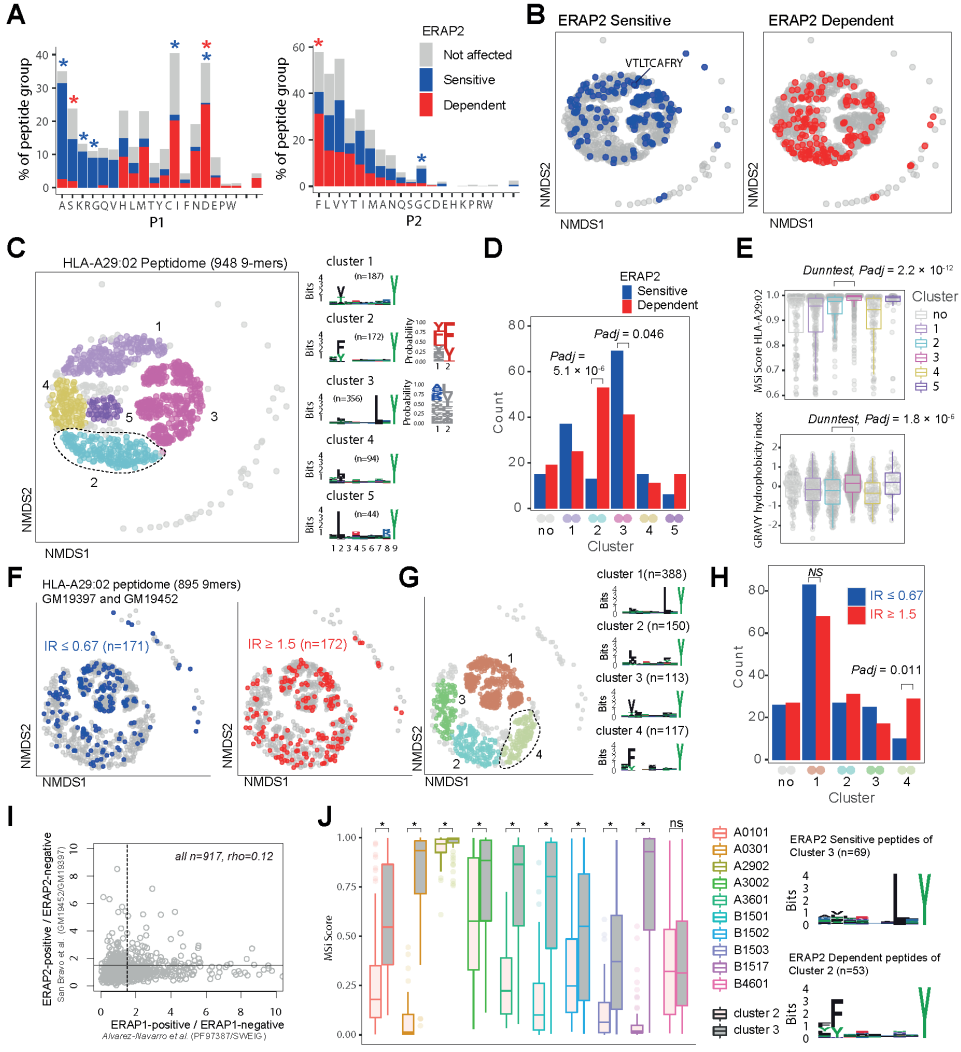

Figure 2.3: ERAP2 increases the abundance of a peptide-motif that is highly selective for HLA-A29. (**a**) Comparison of amino acid proportion at P1 and P2 of 9-mers (% for each group) between peptides that decrease in abundance ('sensitive' peptides, significant changes indicated by the blue asterix), peptides that increase in abundance ('dependent' peptides, significant changes indicated with the red asterix), compared to peptides not affected in ERAP2-WT cells (in grey). Statistics from the fisher tests are indicated in **Supplemental Table 2.3, 2.4**. (**b**) Non-metric multidimensional scaling (NMDS) of 948 9-mers from HLA-A29:02. Peptide distance was defined on the basis of sequence similarity. Each circle represents a unique peptide and is color-coded according to the effect of ERAP2; grey: not affected, blue: Peptides decreased ('sensitive') in abundance and in red peptides that increased ('dependent') in abundance in the ERAP2-WT condition compared to the ERAP2-KO condition. The peptide VTLTCAFRY from the retinal S-antigen is indicated. (**c**) NMDS plot of HLA-A29:02 with 9-mer peptides color-coded according to the clustering by DBSCAN. Sequence logos and two probability plots representing these clusters are shown. (**d**) Comparison of the number of ERAP2-sensitive and -dependent peptides in cluster. *Padj* = Bonferroni corrected (5 clusters) *P* values from X^2 tests. (**e**) Binding scores (MSi metric from *HLAthena*) for HLA-A29:02 and hydrophobicity index for each cluster. (**f**) NMDS of 895 shared 9mers from HLA-A29-positive cell lines GM19452 (ERAP2-positive) and GM19397 (ERAP2-deficient) from *Sanz-Bravo* and associates[23]. In this study, the normalized intensity ratio (GM19452/GM19397) of each peptide in the two cell lines was used to infer the relative abundance of each peptide, which we adapted to assign peptides as ERAP2-sensitive (IR ≤ 0.67, n=171 peptides) or ERAP2-dependent (IR ≥ 1.5, 172 peptides). (**g**) Four clusters were estimated by DBSCAN. (**h**) Comparison of the number of

ERAP2-sensitive and ERAP2-dependent peptides in each peptide cluster identified in *g* similar to *d*. (**i**) Correlation plot of the effects of ERAP1 and ERAP2 on the HLA-A29 peptidome (see methods). The spearman's correlation (rho) is shown for 947 HLA-A29-eluted peptides detected in two studies. The black lines indicate the threshold of the normalized intensity ratio >1.5 used in each of the studies. This analysis suggests very low correlation between the effects of ERAP1 and ERAP2 on similar peptides presented by HLA-A29. (**j**) Predicted binding scores for ERAP2-dependent peptides in cluster 2, and ERAP2-sensitive peptides in cluster 3 for HLA-A29:02 and 9 HLA alleles with relatively similar binding motifs (based on Sarkizova *et al*.[34]). *) indicates Bonferroni corrected $P<0.05$ from a Dunn's Test.

ERAP2 has similar effects on P1 across the HLA class I immunopeptidome

Next, we were interested to see how ERAP2 affects the global peptidome of the other class I alleles. We use the flow-through of the HLA-A29-binding antibody immunopurifications to capture HLA class I molecules (**Figure 2.1D**). After filtering, a total of 10,233 unique peptides were identified between biological replicates (*Jaccard* similarity = 0.73) of which 6,678 8-11 mers were considered for differential expression analysis (**Figure 2.1D**)(**Supplemental Table 2.9**). A total of 2,170 peptides were differentially expressed (**Supplemental Table 2.9**). Notwithstanding allele-specific differences, K, R, and A were seen more often at P1 of ERAP2-sensitive peptides, while F and Y were typically underrepresented across the other five alleles (**Figure 2.4**), **Supplemental Tables 2.10**-**14**). This was supported by a global assessment of all 9-11-mers (**Supplemental Figure 2.10**). These results indicate that ERAP2 has globally similar effects on P1 across HLA allotypes and in line with the observation that the P1 across HLA class I ligands is enrichment for residues A, K, and R[37].

Internal sequence preferences of ERAP2 can be interpreted from the immunopeptidome

We further conducted NMDS of the 9-mers for HLA-A03:01, HLA-B40:01, and HLA-B44:03 (**Figures 2.5A, 2.5D, 2.5G** and **Supplemental Figure 2.11**). The *HLA-C* peptidomes captured were too sparse to provide sufficient resolution (**Supplemental Figure 2.12**). Investigation of HLA-A03:01 was hampered by a relatively high level of submotifs, characteristic for this allele[34,37], in comparison to the density of the peptide data (**Figure 2.5B**), possibly due to loss of peptides by the initial immunopurification (**Figure 2.1D**). Regardless, ERAP2-sensitive peptides were enriched in cluster 4 (X^2, *Padj* = 9.5×10^{-3})(**Figure 2.5C**), but 37/92 (40%) peptides of cluster 4 were also in the HLA-A29 peptidome (20 in cluster 3 of HLA-A29:02, **Figure 2.3C**). Reanalysis of immunopeptidome data from mono-allelic cell lines[34] support that HLA-A29:02 and HLA-A03:01 can each present peptides with the motif of cluster 4 (**Supplemental Figure 2.13**) and demonstrates that ERAP2 influences multiple alleles in part by peptide promiscuity. Considering the other clusters, no evidence for effects of ERAP2 beyond P1 could be observed.

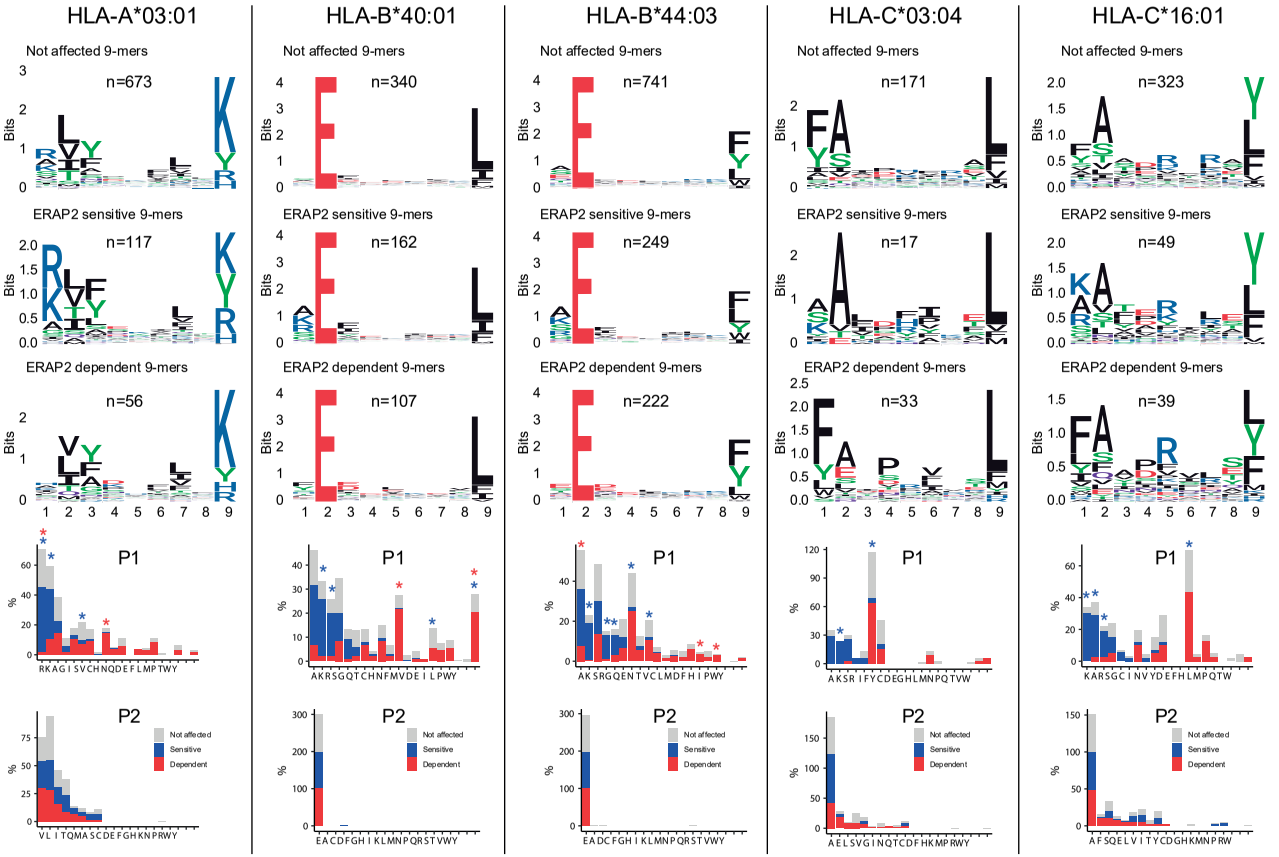

Figure 2.4: ERAP2 shapes P1 across the HLA class I immunopeptidome. Sequence motifs depict specific amino acid preferences at P1-P9 and were generated from a non-redundant list of 9-mers for each class I allele. Comparison of amino acid proportion at P1 and P2 of 9-mers (in percentage for each group of peptides) between peptides that decrease in abundance ('sensitive' peptides, significant changes indicated with the blue asterix), peptides that increase in abundance ('dependent' peptides, significant changes indicated with the red asterix), compared to peptides not affected in ERAP2-WT cells (in grey). The *P* values and summary statistics from the fisher tests are indicated in **Supplemental Table 2.10-14**.

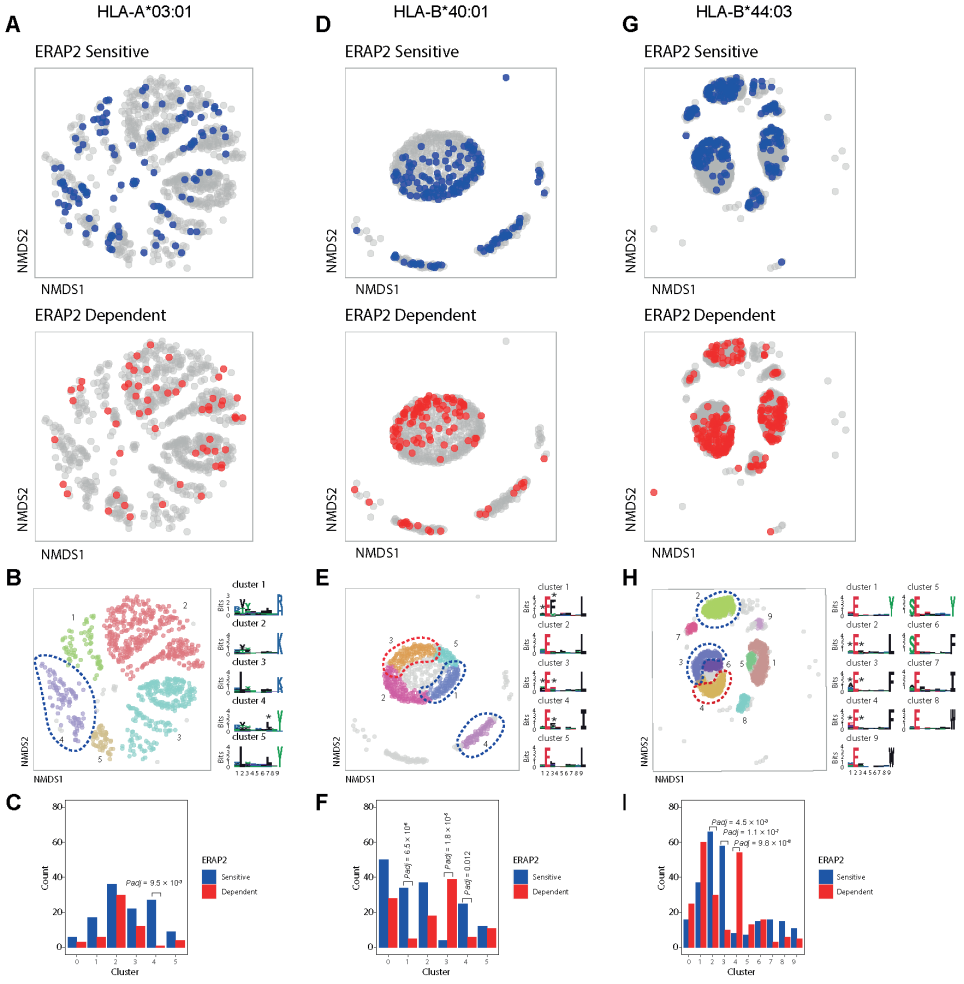

Figure 2.5: NMDS plots showing 9-mer peptide clustering for individual HLA alleles. Non-metric multidimensional scaling (NMDS) visualization of 9-mer peptides and ERAP2 affected peptides for *HLA-A*03:01* (**a**,**b**,**c**), *HLA-B*40:01* (**d**,**e**,**f**), and *HLA-B*44:03* (**g**,**h**,**i**). Peptide distance was defined on the basis of sequence similarity. Each circle represents a unique 9-mer peptide and is color-coded according to the effect of ERAP2; grey: not affected, blue: ERAP2-sensitive peptides red: ERAP2-dependent peptides. The NMDS plot of clusters of peptides for each class I allele peptide are color-coded according to the clustering by DBSCAN. Sequence logos representing these clusters are indicated. * indicates significant changes of amino acid composition tested at P1, P2 and and/or P7 (Fisher's exact test corrected for 20 amino acid residues. Given the entropy-weighted clustering, anchor positions P2 and P9 were not considered for testing. Clusters with significant differences in the count of ERAP2-sensitive and -dependent peptides are highlighted with blue and red ellipses and correspond with the barplots in c,f, and i. The predicted binding scores for each cluster is shown in **Supplemental Figure 2.11**. *Padj* = Bonferroni corrected (n=clusters) *P* values from X^2 tests. All other comparisons were *Padj*>0.05.

In contrast to HLA-A03:01, strong residue preferences at P2 and PΩ of HLA-B40:01 resulted in few submotifs (**Figure 2.5D**). The distribution of ERAP2-sensitive 'away' from dependent peptides in two-dimensional space was reminiscent of the 'pattern' observed in the projection of HLA-A29:02 peptides (**Figure 2.5D**). Submotif analysis revealed that cluster 1 and 4 were enriched for sensitive peptides and were distinguished by a preference for F or Y at P3 (**Figure 2.5E, 2.5F** and **Supplemental Table 2.15**). Cluster 3 (enriched for dependent peptides) was distinguished by a F/Y at P1 (**Figure 2.5E**), similar to the overall motif of ERAP2-dependent peptides.

Finally, HLA-B44:03 submotifs enriched for sensitive peptides (cluster 3 and cluster 2) (**Figure 2.5G-I**) showed a preference for F at P3, similar to HLA-B40:01 (**Supplemental Table 2.15**). These observations are consistent with recognition of P3 by a hydrophobic pocket revealed by structural analysis of ERAP2 (**Supplemental Figure 2.14**). Note that cluster 4 was enriched for dependent peptides (**Figure 2.5I**) and enriched for E at P1 (**Supplemental Table 2.15**), a negatively charged amino acid that is resistant to trimming by ERAP2. In summary, immunopeptidome data revealed internal peptide sequence preferences of ERAP2 that shape the ligand repertoire in a HLA class I-specific manner.

Discussion

In this study, we showed that ERAP2 shapes the HLA-A29 peptidome predominantly by over-trimming peptides carrying susceptible residues at their N-terminus while sparing others carrying a sub-optimal residue at the N-terminal positions. We showed that in the presence of ERAP2 preferred amino acids A, K, and R[47] are underrepresented, while amino acids F and Y are over-represented at P1, but that these effects on P1 are commonly shared with other class I alleles. Strikingly, we identified that ERAP2 specifically increases the abundance of peptides with a distinct submotif (cluster 2, **Figure 2.3C**) defined by nonpolar aromatic residues F or Y at P2 that specifically binds to HLA-A29. Replication of these findings in non-related HLA-A29-positive cell lines suggests that these effects of ERAP2 on HLA-A29 are common. Indeed, in known crystal structures of ERAP2 with peptides, the P2 side-chain is accommodated in a very shallow pocket that cannot easily accommodate large residues such as F and Y due to steric clashes with nearby enzyme residues[13] thus making peptides carrying large hydrophobic bulky residues at P2, poorer substrates (**Supplemental Figure 2.14**). Note that we further showed that the effects of ERAP2 on this cluster of peptides is different from ERAP1, which did not show selectivity for this submotif of HLA-A29 (**Supplemental Figure 2.6**). This fits with the observation that the pocket in ERAP1 that interacts with P2 provides more space for bulky residues[14]. In fact, using correlation as a metric of the effects of ERAP1 and ERAP2, we show that ERAP1 and ERAP2 show non-redundant effects on the HLA-A29 peptidome (**Figure 2.3I**), which is in line with genetic studies that revealed that ERAP1 and ERAP2 independently contribute to the disease risk for BU[10].

Although several studies have shown that ERAPs can trim peptides bound to MHC-I[17-21], structural studies support that ERAP2 can also trim the N-terminal residues from peptide substrates by first sequestering the entire peptide sequence inside the enzyme's cavity. There, the peptide substrate interacts with amino acid side chains of the enzyme, which are considered to influence the stability of the interaction and thus the trimming rates of the peptides[13,14]. The exact internal peptide sequence preferences for ERAP2 remain poorly understood. In an attempt to map its relevance to antigen presentation, here we considered the entire peptide sequence to capture the full effects of ERAP2 on the class I immunopeptidomes, and identify functional submotifs which may be missed using traditional single residue or motif analysis. We describe highly reproducible motifs of HLA-A29 and identified that peptides that are destroyed by ERAP2 (i.e., 'sensitive' to trimming) showed a strong preference for Leucine at P7 and often are presented by multiple alleles (promiscuity). Although we formally cannot exclude the contribution of residual HLA-A29 molecules in the analysis of HLA-A03:01, data from single-HLA cell lines supported overlap in presented peptides with P7-L (**Supplemental Figure 2.13**). Based on the crystal structure of ERAP2[13], the sidechain P7 can be accommodated within a shallow hydrophobic pocket, which suggests that hydrophobic residues like Leucine would be preferred (**Supplemental Figure 2.14**).

Thus, structural analysis indicates that L at P7 is near-optimal for trimming by ERAP2, while bulky residues at P2 (e.g., F) reduce trimming by ERAP2. Therefore, we hypothesize that the increase in peptides with bulky residues at P2 in the presence of ERAP2 is a result of the decreased availability of competing peptides with P7-L due to overtrimming by ERAP2. Importantly, nonpolar aromatic residues F or Y at P3 were associated with peptides that are destroyed in the HLA-B40:01 an HLA-B44:03 peptidome, which is consistent with recognition of P3 by a hydrophobic pocket lined by two other aromatic residues (Tyr892 and Tyr455) that can make favorable pi-stacking interactions with the peptide aromatic side-chain (**Supplemental Figure 2.14**). F at P3 was also the most common residue considering all 9-11-mers detected by immunoprecipitation of HLA class I (**Supplemental Figure 2.10**). The seemingly contrasting preference of F dependent on the position in the peptide substrate, also suggests that predicting substrate specificity based on widely used fluorogenic aminopeptidase substrates (e.g., R-AMC) or peptide series that vary only the N-terminal residue may obscure the full breadth of substrate specificity for this amino peptidase. We do emphasize that the binding motif of HLA-A29 (and other alleles investigated) can obscure the detection of the full internal sequence preferences of ERAP2, but using the presented peptides as a read-out provides the net effect of any internal sequence preferences on antigen presentation.

We showed that the ERAP-sensitive peptides presented by HLA-A29:02 are promiscuous based on their predicted binding scores for other class I alleles, and their detection in the HLA-A29-negative fraction in mass spectrometry analysis. Since these peptides are also characterized by P1 composition (e.g. A, K, R) that is shared with the other HLA allotypes

investigated, it is tempting to speculate that HLA-A29 epitope destruction by ERAP2 is a canonical phenomenon common to class I alleles. This is supported by the observation that HLA class I ligands in general show a depletion for residues A, K, and R at P1 in ERAP2-positive cell lines[37], which are preferred substrates of ERAP2. High hydrophobicity of T-cell receptor contact residues in presented peptides - in particular a hydrophobic P7 - is associated with immunogenicity[49,50]. Perhaps a canonical function of ERAP2 is to destroy epitopes to lower the immunogenic index of peptide cargo presented. This is supported by observations in cancer immunotherapy, where high ERAP2 expression (the risk haplotype for BU) is a strong prognostic predictor of poor survival in patients receiving checkpoint inhibitor therapy to induce T-cell mediated antitumor immunity[51]. Of interest, the size of P1 of the presented peptide modulates the configuration of position 167 in HLA-A[52], which was shown to critically influence T cell recognition[50]. F or Y at P1 gives a similar configuration for position 167, which is different from the conformation mediated by K and R at P1 in one study[52], which suggests that the effects of ERAP2 on P1 may influence T cell receptor recognition.

Given that HLA-A29 is prerequisite for the development of BU, we hypothesize that disease mechanisms associated with antigen presentation are most likely driven by a limited set of epitopes (**Supplemental Table 2.8**) because of promiscuity of peptides[48]. ERAP2 destroyed the only S-antigen peptide detected in the HLA-A29 peptidome, which considering high ERAP2 expression is a risk factor for BU, suggests that HLA-A29-mediated presentation of S-antigen fragments is less likely relevant during disease initiation. However, BU patients show in vitro T cell proliferation towards S-antigen[7]. This makes it tempting to speculate that the retinal S-antigen is more relevant in later stages of the disease via $CD4^+$ T cells responses after the blood retina barrier has been breached. This is supported by the common immune reactivity towards S-antigen in patients with clinically distinct phenotypes of uveitis and the lack of response of patient-derived ocular $CD8^+$ T cells towards this S-antigen peptide[2,4]. Based on the submotifs of peptides (i.e. cluster 2, **Figure 2.3C**), we hypothesize that 'uveitogenic' HLA-A29-restricted peptides may more likely harbor a F or Y at P2. The importance of P2 is supported by the fact that fine mapping studies of the *MHC* linked BU risk to amino acid positions 62-Leu and 63-Gln of *HLA-A*[53], which are unique to HLA-A29 and directly interact with P2 of the anchoring peptide. Although the *HLA-C*14:03* allele also showed good binding scores for the ERAP2-dependent peptides with F or Y at P2, *HLA-C* alleles are notoriously low expressed[54] and the allele frequency of *HLA-C*14:03* is >100 times lower compared to *HLA-A*29:02*. Also, the peptidomes of HLA-A29 and HLA-C14:03 are starkly different (Jaccard similarity index ±1% using peptidome data from Sarkizova and associates[34]) and T cells recognizing the same peptide in a different HLA molecule may not show immune reactivity. Although the overall binding motif of peptides bound to HLA-A29:02 is similar to other alleles (HLA-A1 family members, such as HLA-A01 and HLA-A:30:02[34]), our unbiased submotif analysis had the resolution to discover functional differences not apparent when considering the overall motif of HLA allotypes. The peptide motif of cluster 2 in particular affected by ERAP2 and presented by HLA-A29 (**Figure 2.3C**) did not bind well to the other

alleles (**Figure 2.3J**) and supports that HLA-A29 has unique features in antigen presentation, and is in line with the fact that no other HLA alleles are genetically associated with BU[9]. Note that 'just' P2-F and P2-Y (so without the C-terminal position Y) is not uncommon in the immunopeptidomes of other HLA-A allotypes, such as HLA-A24. We previously showed that peptides with the P2-F/Y+PΩ-Y motif are infrequent on functionally similar HLA allotypes or that these HLA allotypes display very low similarity in the immunopeptidome composition with HLA-A29[55]. This supports that ERAP2 can influence the presentation of peptide that are specific for HLA-A29

Regardless, we show that the amino acid sequence of retina-expressed genes contains peptides with the motif of cluster 2, which supports that ERAP2-mediated HLA-A29-restricted presentation of ocular epitopes could be a key disease mechanism for BU. We hypothesize that ERAP2 facilitates higher expression of HLA-A29-specific peptides derived from proteins related to melanocyte biology – specifically expressed in the ocular retina or choroid. Of course, functional experiments of antigen presentation in the eye and tetramer-analysis of T cell immunity to these putative epitopes is warranted. It is, however, of interest that among the predicted epitopes we found peptides derived from key factors in melanocyte biology. A hallmark feature of BU is the progressive loss of stromal melanocytes in the choroid corresponding to the characteristic cream-colored birdshot fundus lesions[2,8,56,57], and BU has been associated with melanoma[5,6,58].

Previous HLA peptidomic studies of ERAPs are based on single-HLA or long-established cell lines which after years of continuous cultivation are notorious for their profound chromosomal aberrations reported to also affect *ERAP* and *HLA* genes[47,59-61]. In addition, these studies have been conducted with label-free approaches using independent experimental runs, which makes accurate quantification of effects of ERAPs on the immunopeptidome more challenging. To study ERAPs in a physiologically more relevant environment, we exploited MS analysis using newly-established patient-derived cell lines and SILAC labeling to address several potential sources of ambiguity that are non-trivial to resolve with *in silico* methods, including often unaccounted genetic variability (i.e., polymorphisms) in comparing different cell lines or quantitative error caused by the individual analysis of to be compared conditions. Regardless, the results in this study can also be influenced by several factors. Although abundant peptides are more likely to be sufficiently detected in individual elutions (~90% of peptides were reported before), less abundant peptides might be missed. This means that additional undiscovered effects of ERAP2 on the peptidomes investigated could be present. For example, we limited our labeling and analysis to peptides that contain F and/or Y for SILAC labeling, which obscured our capability to cover the majority of the HLA-B40:01 peptidome or potential uncharted domains of the peptidomes of the other alleles.

In conclusion, we show that ERAP2 significantly influences the immunopeptidome across the cellular HLA class I allotypes and ERAP2 increases the expression of a peptide submotif highly selective for HLA-A29. We have narrowed down the potential sequences for autoimmunity-

inducing antigenic peptides based on the selective effect of ERAP2 on the peptide cargo of HLA-A29 in the pathogenesis of Birdshot Uveitis.

Acknowledgements
We express gratitude for constructive input from prof. Debbie van Baarle.

References

1. Minos E, Barry RJ, Southworth S, Folkard A, Murray PI, Duker JS, et al. Birdshot chorioretinopathy: Current knowledge and new concepts in pathophysiology, diagnosis, monitoring and treatment. Orphanet J Rare Dis. (2016) 11(1):1-17. 10.1186/s13023-016-0429-8
2. Kuiper J, Rothova A, de Boer J, Radstake T. The immunopathogenesis of birdshot chorioretinopathy; a bird of many feathers. Prog Retin Eye Res. (2015) 44:99-110. 10.1016/j.preteyeres.2014.11.003
3. Kuiper JJW, Mutis T, de Jager W, de Groot-Mijnes JDF, Rothova A. Intraocular interleukin-17 and proinflammatory cytokines in HLA-A29-associated birdshot chorioretinopathy. Am J Ophthalmol. (2011) 152(2):177-182.e1. 10.1016/j.ajo.2011.01.031
4. Kuiper JJW, Rothova A, Schellekens PAW, Ossewaarde-van Norel A, Bloem AC, Mutis T. Detection of choroid- and retina-antigen reactive CD8+ and CD4+ T lymphocytes in the vitreous fluid of patients with birdshot chorioretinopathy. Hum Immunol. (2014) 75(6):570-577. 10.1016/j.humimm.2014.02.012
5. Pulido JS, Canal I, Salomão D, Kravitz D, Bradley E, Vile R. Histological findings of birdshot chorioretinopathy in an eye with ciliochoroidal melanoma. Eye. (2012) 26(6):862-865. 10.1038/eye.2012.10
6. Gaudio PA, Kaye DB, Crawford JB. Histopathology of birdshot retinochoroidopathy. Br J Ophthalmol. (2002) 86(12):1439-1441. 10.1136/bjo.86.12.1439
7. Nussenblatt RB, Mittal KK, Ryan S, Richard Green W, Edward Maumenee A. Birdshot Retinochoroidopathy Associated with Hla-A29 Antigen and Immune Responsiveness to Retinal S-Antigen. Am J Ophthalmol. (1982) 94(2):147-158. 10.1016/0002-9394(82)90069-1
8. Herbort CP, Pavésio C, LeHoang P, Bodaghi B, Fardeau C, Kestelyn P, et al. Why birdshot retinochoroiditis should rather be called “HLA-A29 uveitis”? Br J Ophthalmol. (2017) 101(7):851-855. 10.1136/bjophthalmol-2016-309764
9. Kuiper JJW, Van Setten J, Ripke S, Van ’T Slot R, Mulder F, Missotten T, et al. A genome-wide association study identifies a functional ERAP2 haplotype associated with birdshot chorioretinopathy. Hum Mol Genet. (2014) 23(22):6081-6087. 10.1093/hmg/ddu307
10. Kuiper JJW, Setten J van, Devall M, Cretu-Stancu M, Hiddingh S, Ophoff RA, et al. Functionally distinct ERAP1 and ERAP2 are a hallmark of HLA-A29-(Birdshot) Uveitis. Hum Mol Genet. (2018) 27(24):4333-4343. 10.1093/hmg/ddy319
11. Saveanu L, Carroll O, Lindo V, Del Val M, Lopez D, Lepelletier Y, et al. Concerted peptide trimming by human ERAP1 and ERAP2 aminopeptidase complexes in the endoplasmic reticulum. Nat Immunol. (2005) 6(7):689-697. 10.1038/ni1208
12. Andrés AM, Dennis MY, Kretzschmar WW, Cannons JL, Lee-Lin S-Q, Hurle B, et al. Balancing selection maintains a form of ERAP2 that undergoes nonsense-mediated decay and affects antigen presentation. PLoS Genet. (2010) 6(10):e1001157. 10.1371/journal.pgen.1001157

13. Mpakali A, Giastas P, Mathioudakis N, Mavridis IM, Saridakis E, Stratikos E. Structural basis for antigenic peptide recognition and processing by Endoplasmic reticulum (ER) aminopeptidase 2. J Biol Chem. (2015) 290(43):26021-26032. 10.1074/jbc.M115.685909
14. Giastas P, Mpakali A, Papakyriakou A, Lelis A, Kokkala P, Neu M, et al. Mechanism for antigenic peptide selection by endoplasmic reticulum aminopeptidase 1. Proc Natl Acad Sci. (2019) 116(52):26709-26716. 10.1073/pnas.1912070116
15. Evnouchidou I, Momburg F, Papakyriakou A, Chroni A, Leondiadis L, Chang SC, et al. The internal sequence of the peptide-substrate determines its N-Terminus trimming by ERAP1. PLoS One. (2008) 3(11). 10.1371/journal.pone.0003658
16. Birtley JR, Saridakis E, Stratikos E, Mavridis IM. The crystal structure of human endoplasmic reticulum aminopeptidase 2 reveals the atomic basis for distinct roles in antigen processing. Biochemistry. (2012) 51(1):286-295. 10.1021/bi201230p
17. Papakyriakou A, Reeves E, Beton M, Mikolajek H, Douglas L, Cooper G, et al. The partial dissociation of MHC class I-bound peptides exposes their N terminus to trimming by endoplasmic reticulum aminopeptidase 1. J Biol Chem. (2018) 293(20):7538-7548. 10.1074/jbc.RA117.000313
18. Chen H, Li L, Weimershaus M, Evnouchidou I, van Endert P, Bouvier M. ERAP1-ERAP2 dimers trim MHC I-bound precursor peptides; implications for understanding peptide editing. Sci Rep. (2016) 6:28902. 10.1038/srep28902
19. Falk K, Rötzschke O, Rammensee HG. Cellular peptide composition governed by major histocompatibility complex class I molecules. Nature. (1990) 348(6298):248-251. 10.1038/348248a0
20. Kanaseki T, Blanchard N, Hammer GE, Gonzalez F, Shastri N. ERAAP synergizes with MHC class I molecules to make the final cut in the antigenic peptide precursors in the endoplasmic reticulum. Immunity. (2006) 25(5):795-806. 10.1016/j.immuni.2006.09.012
21. Reeves E, Edwards CJ, Elliott T, James E. Naturally occurring ERAP1 haplotypes encode functionally distinct alleles with fine substrate specificity. J Immunol. (2013) 191(1):35-43. 10.4049/jimmunol.1300598
22. Mavridis G, Arya R, Domnick A, Zoidakis J, Makridakis M, Vlahou A, et al. A systematic re-examination of processing of MHCI-bound antigenic peptide precursors by endoplasmic reticulum aminopeptidase 1. J Biol Chem. (2020) 295(21):7193-7210. 10.1074/jbc.RA120.012976
23. Sanz-Bravo A, Martín-Esteban A, Kuiper JJW, García-Peydro M, Barnea E, Admon A, et al. Allele-specific alterations in the peptidome underlie the joint association of HLA-A□29:02 and endoplasmic reticulum aminopeptidase 2 (ERAP2) with birdshot chorioretinopathy. Mol Cell Proteomics. (2018) 17(8):1564-1577. 10.1074/mcp.RA118.000778
24. Alvarez-Navarro C, Martín-Esteban A, Barnea E, Admon A, López De Castro JA. Endoplasmic reticulum aminopeptidase 1 (ERAP1) polymorphism relevant to inflammatory disease shapes the peptidome of the birdshot chorioretinopathy-associated HLA-A□29:02 Antigen. Mol Cell Proteomics. (2015) 14(7):1770-1780. 10.1074/mcp.M115.048959

25. Georgiadis D, Mpakali A, Koumantou D, Stratikos E. Inhibitors of ER Aminopeptidase 1 and 2: From Design to Clinical Application. Curr Med Chem. (2019) 26(15):2715-2729. 10.2174/0929867326566180214111849
26. Anderson KS, Zeng W, Sasada T, Choi J, Riemer AB, Su M, et al. Impaired tumor antigen processing by immunoproteasome-expressing CD40-activated B cells and dendritic cells. Cancer Immunol Immunother. (2011) 60(6):857-867. 10.1007/s00262-011-0995-5
27. Hussong SA, Roehrich H, Kapphahn RJ, Maldonado M, Pardue MT, Ferrington DA. A novel role for the immunoproteasome in retinal function. Invest Ophthalmol Vis Sci. (2011) 52(2):714-723. 10.1167/iovs.10-6032
28. Hassan C, Kester MGD, Oudgenoeg G, de Ru AH, Janssen GMC, Drijfhout JW, et al. Accurate quantitation of MHC-bound peptides by application of isotopically labeled peptide MHC complexes. J Proteomics. (2014) 109:240-244. 10.1016/j.jprot.2014.07.009
29. Mulder A, Kardol MJ, Arn JS, Eijsink C, Franke MEI, Schreuder GMT, et al. Human monoclonal HLA antibodies reveal interspecies crossreactive swine MHC class I epitopes relevant for xenotransplantation. Mol Immunol. (2010) 47(4):809-815. 10.1016/j.molimm.2009.10.004
30. Brosch M, Yu L, Hubbard T, Choudhary J. Accurate and Sensitive Peptide Identification with Mascot Percolator. J Proteome Res. (2009) 8(6):3176-3181. 10.1021/pr800982s
31. Ritchie ME, Phipson B, Wu D, Hu Y, Law CW, Shi W, et al. limma powers differential expression analyses for RNA-sequencing and microarray studies. Nucleic Acids Res. (2015) 43(7):e47. 10.1093/nar/gkv007
32. Storey JD, Bass AJ, Dabney A, Robinson D. qvalue: Q-value estimation for false discovery rate control. R package version 2.14.1. (2019) https://github.com/jdstorey/qvalue
33. Kammers K, Cole RN, Tiengwe C, Ruczinski I. Detecting Significant Changes in Protein Abundance. EuPA open proteomics. (2015) 7:11-19. 10.1016/j.euprot.2015.02.002
34. Sarkizova S, Klaeger S, Le PM, Li LW, Oliveira G, Keshishian H, et al. A large peptidome dataset improves HLA class I epitope prediction across most of the human population. Nat Biotechnol. (2020) 38(2):199-209. 10.1038/s41587-019-0322-9
35. Andreatta M, Lund O, Nielsen M. Simultaneous alignment and clustering of peptide data using a Gibbs sampling approach. Bioinformatics. (2013) 29(1):8-14. 10.1093/bioinformatics/bts621
36. McFerrin L. HDMD: Statistical Analysis Tools for High Dimension Molecular Data (HDMD). R package version 1.2. (2013) https://CRAN.R-project.org/package=HDMD
37. Abelin JG, Keskin DB, Sarkizova S, Hartigan CR, Zhang W, Sidney J, et al. Mass Spectrometry Profiling of HLA-Associated Peptidomes in Mono-allelic Cells Enables More Accurate Epitope Prediction. Immunity. (2017) 46(2):315-326. 10.1016/j.immuni.2017.02.007
38. Kim Y, Sidney J, Pinilla C, Sette A, Peters B. Derivation of an amino acid similarity matrix for peptide: MHC binding and its application as a Bayesian prior. BMC Bioinformatics. (2009) 10:394. 10.1186/1471-2105-10-394
39. Goslee SC, Urban DL. The ecodist Package for Dissimilarity-based Analysis of Ecological Data. J. Stat. Software. (2007) 1(7). 10.18637/jss.v022.i07

40. Hahsler M, Piekenbrock M, Doran D. dbscan: Fast Density-Based Clustering with R. J Stat Software. (2019) 1(1). 10.18637/jss.v091.i01
41. Hennig C. fpc: Flexible Procedures for Clustering. R package version 2.2-5. (2020) https://CRAN.R-project.org/package=fpc
42. Wagih O. ggseqlogo: A 'ggplot2' Extension for Drawing Publication-Ready Sequence Logos. R package version 0.1. (2017) https://CRAN.R-project.org/package=ggseqlogo
43. Osorio D, Rondón-Villarreal P, Torres Sáez R. Peptides: A Package for Data Mining of Antimicrobial Peptides. R J. (2015) 7:4-14. 10.32614/RJ-2015-001
44. Ogle DH, Wheeler P, Dinno A. FSA: Fisheries Stock Analysis. R package version 0.8.30. (2020) https://github.com/droglenc/FSA.
45. Gfeller D, Guillaume P, Michaux J, Pak H-S, Daniel RT, Racle J, et al. The Length Distribution and Multiple Specificity of Naturally Presented HLA-I Ligands. J Immunol. (2018) 201(12):370516. 10.4049/jimmunol.1800914
46. René C, Lozano C, Villalba M, Eliaou J-F. 5' and 3' untranslated regions contribute to the differential expression of specific HLA-A alleles. Eur J Immunol. (2015) 45(12):3454-3463. 10.1002/eji.201545927
47. López de Castro JA, Alvarez-Navarro C, Brito A, Guasp P, Martín-Esteban A, Sanz-Bravo A. Molecular and pathogenic effects of endoplasmic reticulum aminopeptidases ERAP1 and ERAP2 in MHC-I-associated inflammatory disorders: Towards a unifying view. Mol Immunol. (2016) 77:193-204. 10.1016/j.molimm.2016.08.005
48. Rao X, Hoof I, Costa AICAF, van Baarle D, Kesmir C. HLA class I allele promiscuity revisited. Immunogenetics. (2011) 63(11):691-701. 10.1007/s00251-011-0552-6
49. Chowell D, Krishna S, Becker PD, Cocita C, Shu J, Tan X, et al. TCR contact residue hydrophobicity is a hallmark of immunogenic CD8+ T cell epitopes. Proc Natl Acad Sci U S A. (2015) 112(14):E1754-1762. 10.1073/pnas.1500973112
50. Riley TP, Keller GLJ, Smith AR, Davancaze LM, Arbuiso AG, Devlin JR, et al. Structure Based Prediction of Neoantigen Immunogenicity. Front Immunol. (2019) 10:2047. 10.3389/fimmu.2019.02047
51. Lim YW, Chen-Harris H, Mayba O, Lianoglou S, Wuster A, Bhangale T, et al. Germline genetic polymorphisms influence tumor gene expression and immune cell infiltration. Proc Natl Acad Sci U S A. (2018) 115(50):E11701-11710. 10.1073/pnas.1804506115
52. Coles CH, McMurran C, Lloyd A, Hock M, Hibbert L, Raman MCC, et al. T Cell Receptor interactions with Human Leukocyte Antigen govern indirect peptide selectivity for the cancer testis antigen MAGE-A4. J Biol Chem. (2020) 295:11486-11494. 10.1074/jbc.RA120.014016
53. Márquez A, Cordero-Coma M, Martín-Villa JM, Gorroño-Echebarría MB, Blanco R, Díaz Valle D, et al. New insights into the genetic component of non-infectious uveitis through an Immunochip strategy. J Med Genet. (2017) 54(1):38-46. 10.1136/jmedgenet-2016-104144
54. Apps R, Meng Z, Del Prete GQ, Lifson JD, Zhou M, Carrington M. Relative Expression Levels of the HLA Class-I Proteins in Normal and HIV-Infected Cells. J Immunol. (2015) 1403234. 10.4049/jimmunol.1403234

55. Kuiper JJW, Venema WJ. HLA-A29 and Birdshot Uveitis: Further Down the Rabbit Hole. Front Immunol. (2020) 11:599558. 10.3389/fimmu.2020.599558
56. Elahi S, Herbort CPJ. Vogt-Koyanagi-Harada Disease and Birdshot Retinochoroidopathy, Similarities and Differences: A Glimpse into the Clinicopathology of Stromal Choroiditis, a Perspective and a Review. Klin Monbl Augenheilkd. (2019) 236(4):492-510. 10.1055/a-0829-6763
57. Papadia M, Herbort CP. New concepts in the appraisal and management of birdshot retinochoroiditis, a global perspective. Int Ophthalmol. (2015) 35(2):287-301. 10.1007/s10792-015-0046-x
58. Hassman L, Warren M, Huxlin KR, Chung MM, Xu L. Evidence of melanoma immunoreactivity in patients with Birdshot retinochoroidopathy. Invest Ophthalmol Vis Sci. (2017) 58(8):5745.
59. Chen L, Shi H, Koftori D, Sekine T, Nicastri A, Ternette N, et al. Identification of an Unconventional Subpeptidome Bound to the Behçet's Disease-associated HLA-B*51:01 that is Regulated by Endoplasmic Reticulum Aminopeptidase 1 (ERAP1). Mol Cell Proteomics. (2020) 19(5):871-883. 10.1074/mcp.ra119.001617
60. Guasp P, Lorente E, Martín-Esteban A, Barnea E, Romania P, Fruci D, et al. Redundancy and Complementarity between ERAP1 and ERAP2 revealed by their effects on the behcet's disease-associated HLA-B*51 peptidome. Mol Cell Proteomics. (2019) 18(8):1491-1510. 10.1074/mcp.RA119.001515
61. Heterozygosity of the 721.221-B*51:01 Cell Line Used in the Study by Guasp et (Arthritis Rheumatol, February 2016). Arthritis Rheumatol. (2017) 69(3):686. 10.1002/art.40073

Supplemental figures

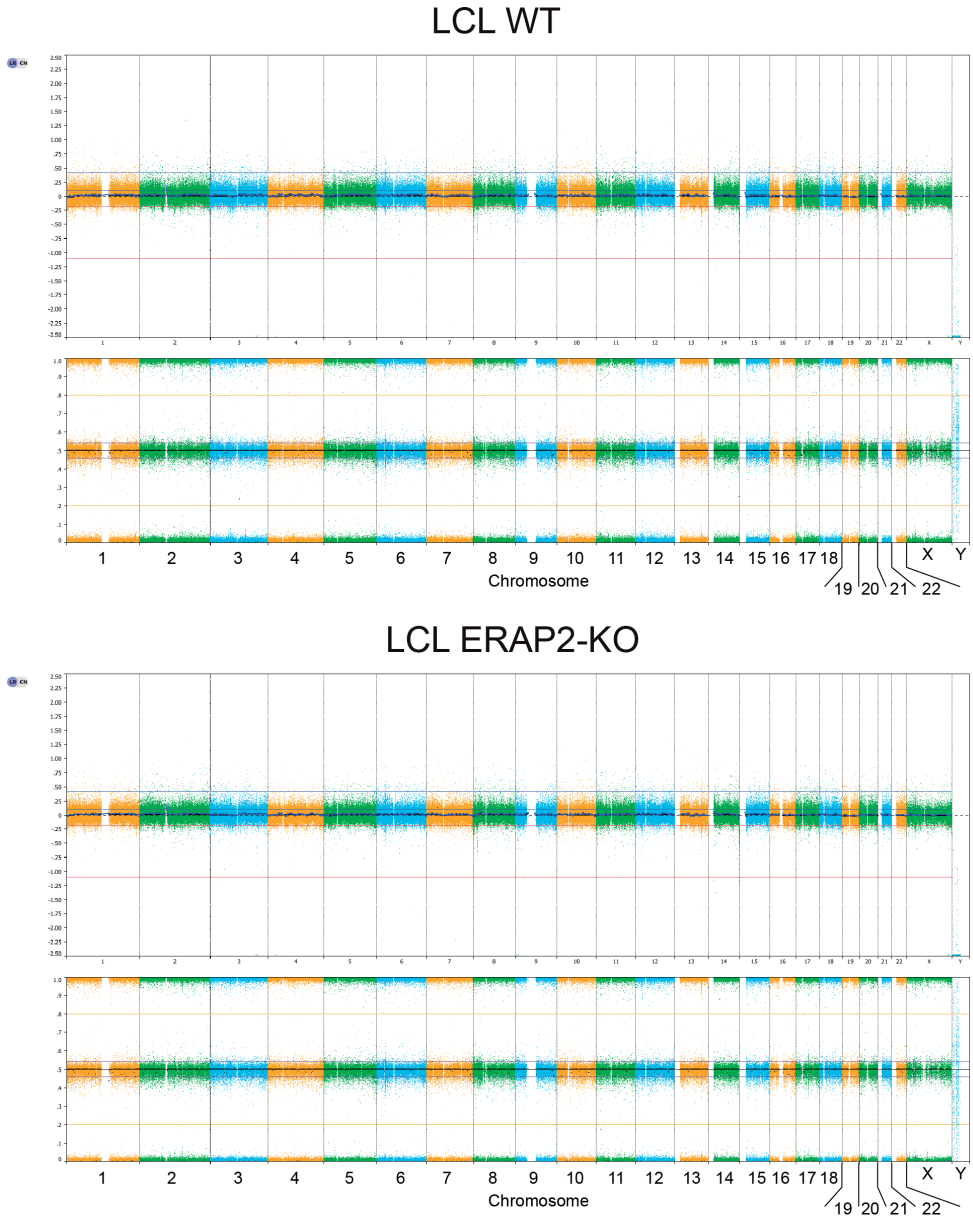

Supplemental Figure 2.1. Whole genome analysis using SNP arrays on unedited (LCL Wildtype, WT) and edited (ERAP2-KO) cell lines used in this study. SNPs were detected by the Infinium Human CytoSNP-850K v1.1 BeadChip (Illumina, San Diego, CA, USA) and show highly consistent genomes. The panels show the array results for the whole. On the X-axis the chromosomes and chromosomal region are indicated. The upper Y-axis shows the Log2 R ratio and the lower Y-axis indicates the B allele frequency for each SNP.

LCL WT

LCL ERAP2-KO

Supplemental Figure 2.2. Whole genome analysis using SNP arrays on unedited (LCL Wildtype, WT) and edited (ERAP2-KO) cell line using the Infinium Human CytoSNP-850K v1.1 BeadChip (Illumina, San Diego, CA, USA), similar to **Supplemental Figure 2.1**, but here the panels show the array results for the region near *5q15* including *ERAP1, ERAP2,* and *LNPEP*. The SNP probes are indicated by black dots. The upper Y-axis shows the Log2 R ratio for the probes and the lower Y-axis indicates the B allele frequency for each SNP (BAF).

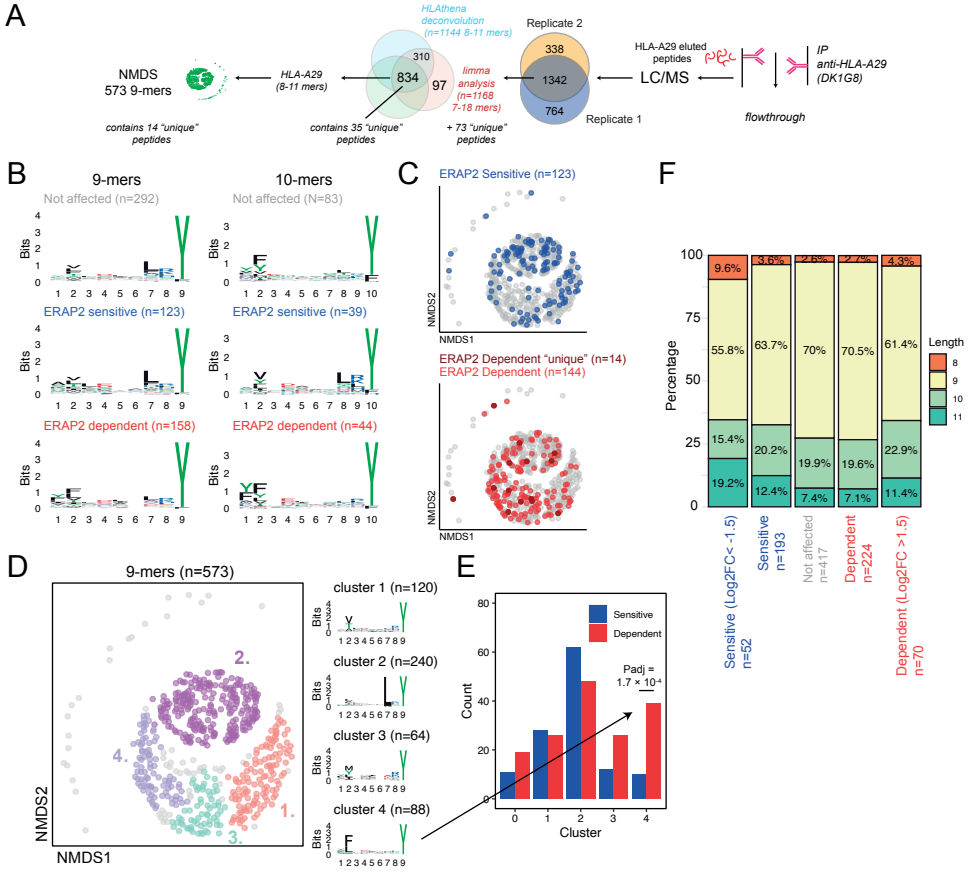

Supplemental Figure 2.3. HLA-A29 peptidome data analysis including peptides unique to either ERAP2-KO or ERAP2-WT cells. (**a**) A total of 1342 peptides overlapping between the two biological replicates with percolator q<0.01 and Mascot Ions score >30, were filtered according to the steps indicated. Note that after the limma analysis, the 73 "unique" peptides detected in either the heavy or light labeled conditions (with consistent detection in the same channel in both experiments) were added to the dataset before deconvolution with *HLAthena* to filter for HLA-A29 ligands. (**b**) The sequence logos for 9-mers and 10-mers in this dataset. ERAP2-sensitive peptides are peptides that decrease in amount in the presence of ERAP2 and ERAP2-dependent peptides increase in amount in the presence of ERAP2. **c**) Nonmetric multidimensional scaling of 573 9-mers in this dataset. The ERAP2-sensitive and ERAP2-dependent peptides are indicated in blue and red, respectively. Peptides uniquely identified in the ERAP2 WT-condition are shown in dark red (n=14). (**d**) Four clusters were estimated (eps parameter for DBSCAN, using k=5) using the elbow method. The sequence logos for each cluster are indicated on the right. (**e**) Comparison of the number of ERAP2-sensitive and ERAP2-dependent peptides in each peptide cluster identified in *b*. *Padj* = bonferroni corrected (n=clusters) *P* values from X^2 tests. All other comparisons were Padj>0.05. (**f**) The percentage of 8-11-mers in peptides sets of this dataset. This analysis shows length dependent effects seen for ERAP2 in an hypoactive ERAP1 background.

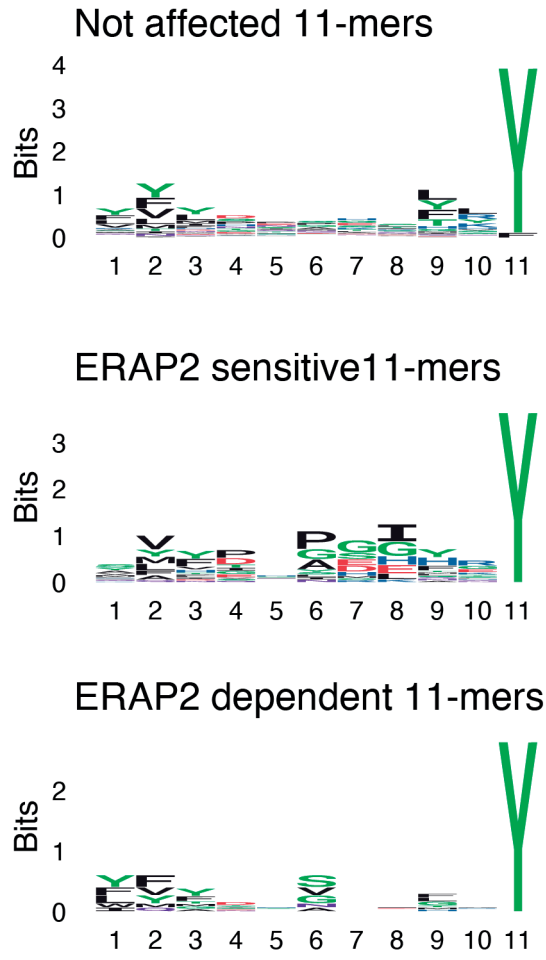

Supplemental Figure 2.4. The sequence logos for non-redundant 11-mers from HLA-A29. Peptides that decrease in the presence of ERAP2 are termed ERAP2-sensitive, peptides that increased in relative amounts are termed ERAP2-dependent. Peptides that did not change in relative amounts in the presence of ERAP2 are termed 'not affected'.

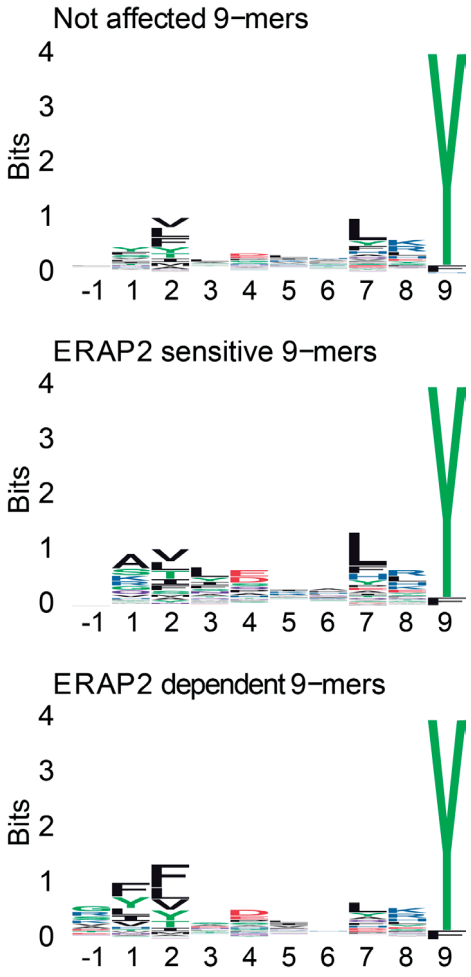

Supplemental Figure 2.5. The sequence logos for 948 non-redundant 9-mers and their designated P-1 derived from the amino acid sequence of the putative proteins. Peptides that decrease in the presence of ERAP2 are termed ERAP2-sensitive, peptides that increase in abundance are termed ERAP2-dependent. Peptides that did not change in abundance in the presence of ERAP2 are termed 'not affected'.

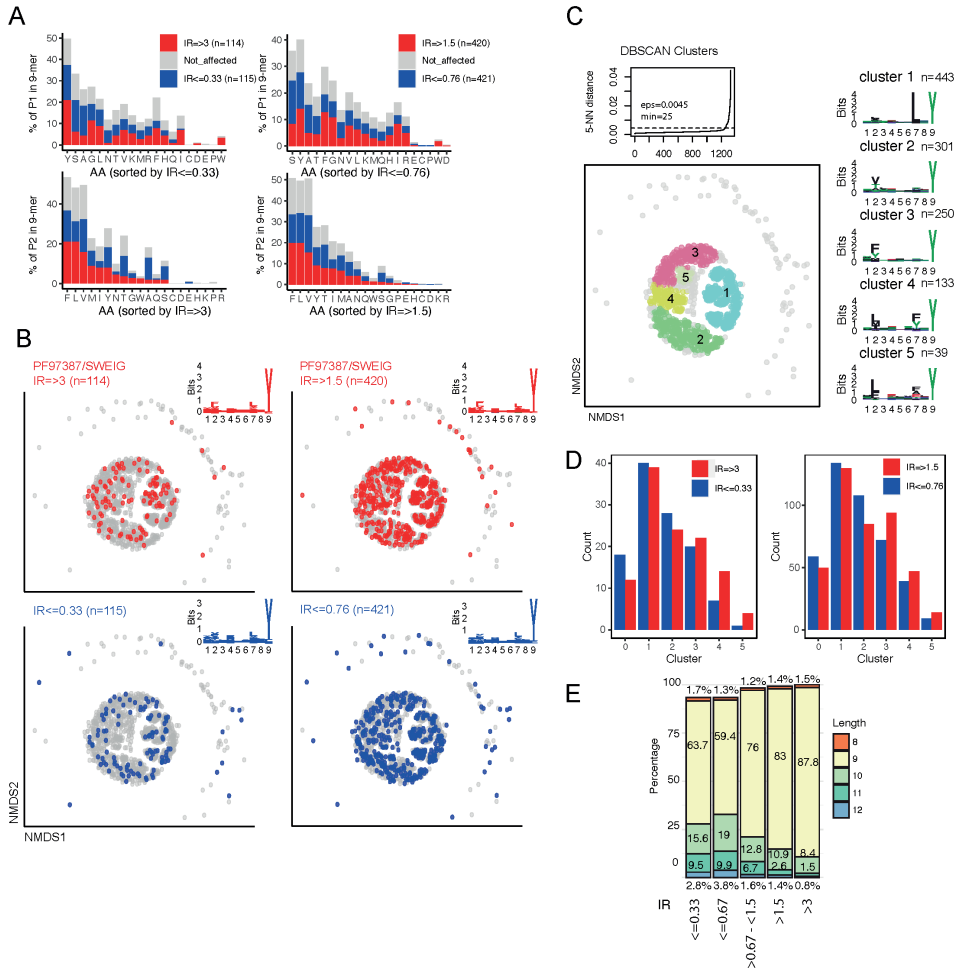

Supplemental Figure 2.6. **Non-metric multidimensional scaling of the 1329 shared 9-mers eluted from the HLA-A29-positive cell lines PF97387 (ERAP1 high expression/activity) and SWEIG (ERAP1 low expression/activity)**. The 1329 9-mers were filtered (removed peptides with value 0 in any of the 3 replicates from PF97387 or SWEIG) from a total of 5584 (3828 9-mers) peptides from *Alvarez-Navarro et al.,2015.* In this study, the normalized intensity ratio (PF97387/SWEIG) of each peptide in the two cell lines was used to infer the relative abundance of each peptide, which we adapted to assign peptides as ERAP2-dependent (IR ≥ 1.5 or IR ≥ 3) or ERAP2-sensitive (IR ≤ 0.76 or IR ≤ 0.33). We used IR≤ 0.76 (instead of 0.67) compared to IR ≥ 1.5 so the peptide datasets would be of equal size. (**a**) Comparison of amino acid proportion at P1 and P2 of 9-mers (in percentage for each group of peptides) between peptides that decrease in abundance (in blue) in the presence of ERAP1 or that increase in abundance (red), compared to peptides not affected by ERAP1 cells (in grey). All comparisons were not significant; *Padj*>0.05. (**b**) Non-metric multidimensional scaling of the 1329 9-mers. (**c**) Five clusters were estimated (eps parameter for DBSCAN, using k=5, based on Figure 3C) using the elbow method. The sequence logos for each cluster are indicated on the right. (**d**) Comparison of the number of ERAP1-dependent (IR ≥ 1.5 or IR ≥ 3) and ERAP1-sensitive peptides (IR ≤ 0.76 or IR ≤ 0.33) in each peptide cluster identified in *b*. *Padj* = Bonferroni corrected (n=clusters) X^2 tests. The difference between the count of sensitive and dependent peptides in each cluster was not significant or *Padj*>0.05. (**e**) The percentage of 9-mers and 10-mers in peptides sets using different cut-offs for the intensity ratio (IR). This analysis confirms the length effects seen for ERAP1 as reported by *Alvarez-Navarro et al., 2015* in these cell lines (which are ERAP2-deficient).

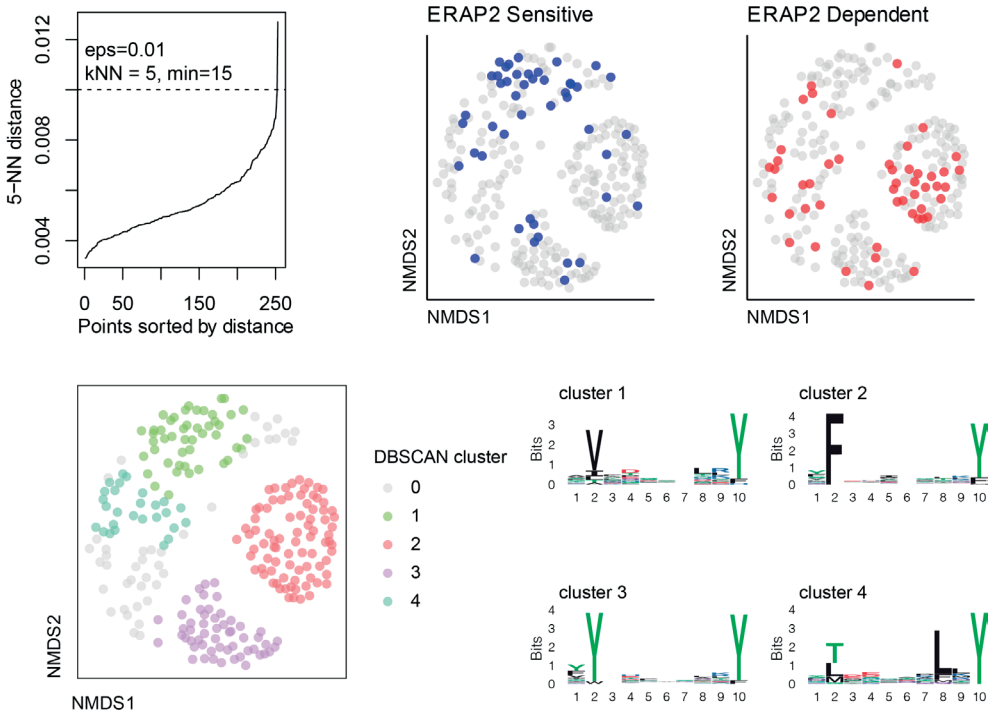

Supplemental Figure 2.7. Non-metric multidimensional scaling plot of 235 10-mers eluted from HLA-A29:02. Differentially expressed peptides are indicated in blue (ERAP2 sensitive that decrease in abundance in the presence of ERAP2) and red (ERAP2-dependent peptides that increase in abundance in the presence of ERAP2). A total of four clusters were identified and the sequence logos for each cluster are indicated. Cluster 0 indicates the unassigned peptides. 10-mer peptides of cluster 2 also show the P2-F motif for HLA-A29 and contains enrichment for ERAP2-dependent peptides compared to ERAP2-sensitive peptides, which reflects the results from 9-mers in **Figure 2.3**.

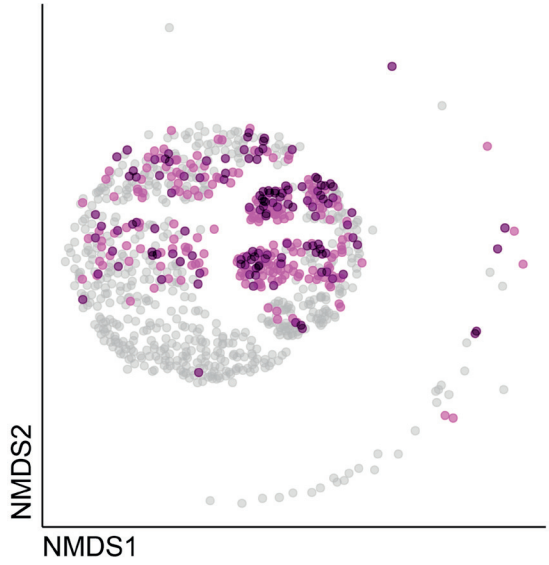

Supplemental Figure 2.8. Non-metric multidimensional scaling plot of 948 9-mers eluted from HLA-A29:02 in this study. Peptides with a binding score MSi>0.6 for HLA-A03:01 from *HLAthena* (https://HLAthena.tools) are highlighted in magenta. Peptides with a binding score MSi>0.6 for HLA-A03:01 that are differentially expressed (moderate q<0.01) are indicated in black.

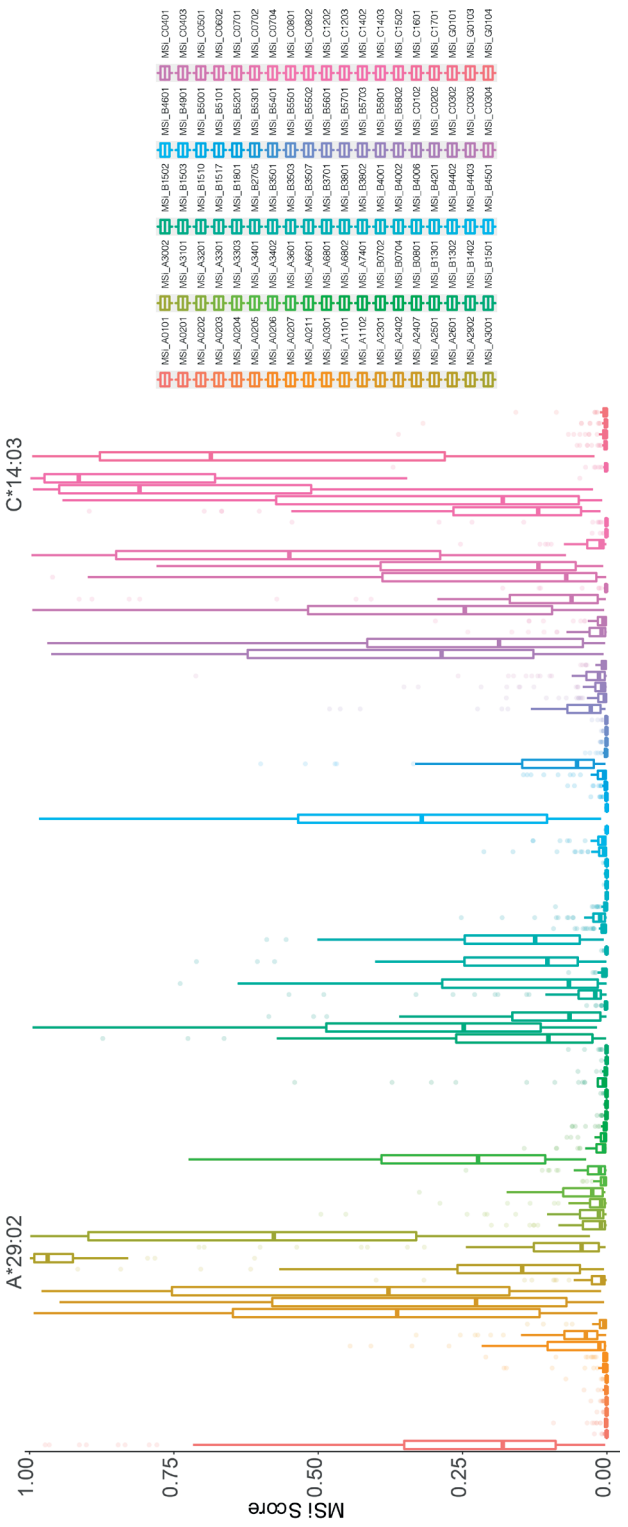

Supplemental Figure 2.9. Predicted binding scores (in MSi from HLAthena) for the 53 ERAP2-dependent peptides in cluster 2 (**Figure 2.3C**) across 95 HLA alleles (selection of alleles tested based on Sarkizova *et al., 2020*).

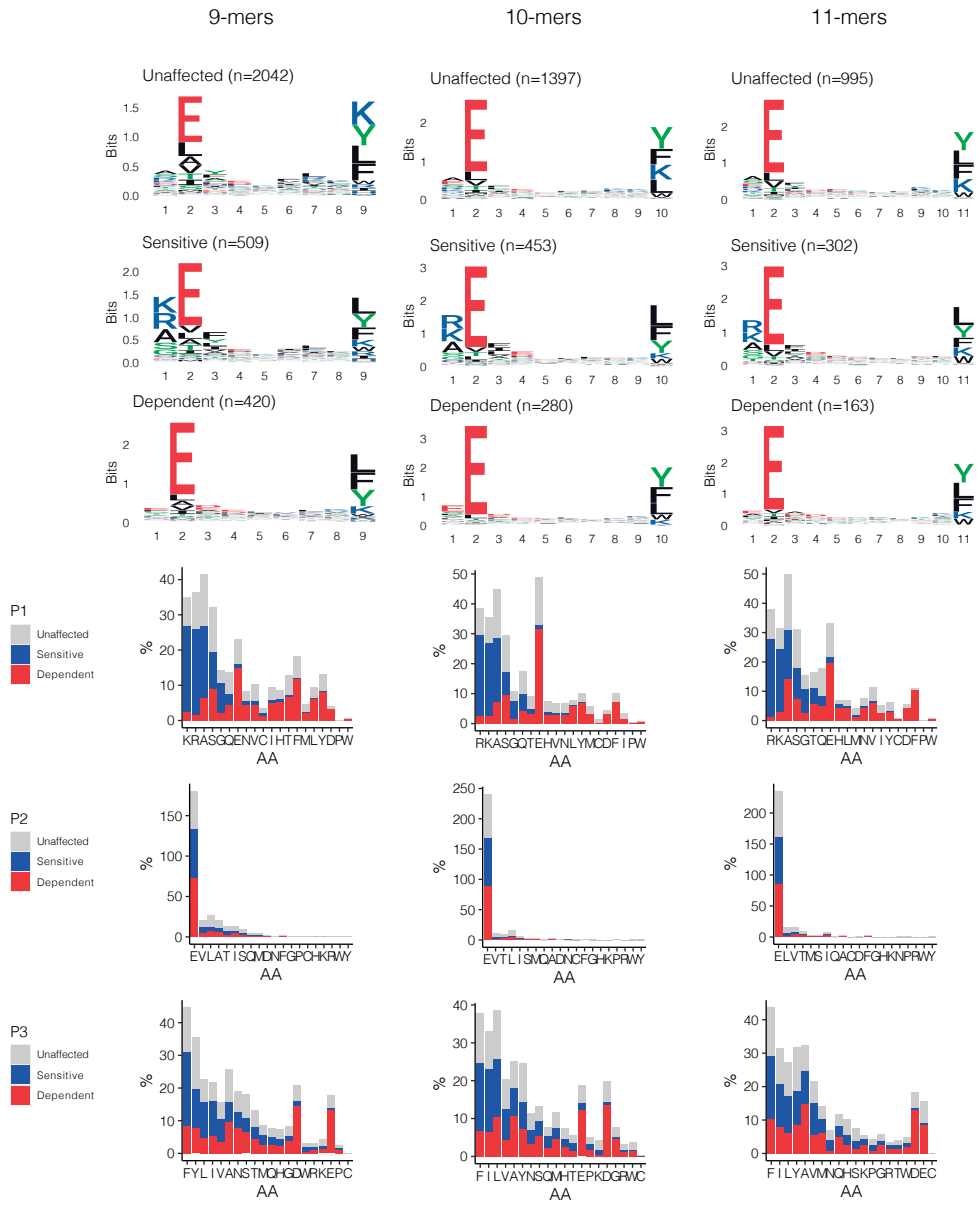

Supplemental Figure 2.10. The effect of ERAP2 on the HLA class I peptidome. Sequence motifs depict specific amino acid preferences for 9-, 10-, and 11-mers were generated from a non-redundant list of peptides from HLA class I (W6/32). Comparison of amino acid proportion at P1, P2, and P3 of (in percentage for each group of peptides) between peptides that decrease in abundance ('sensitive'), peptides that increase in abundance ('dependent' peptides) compared to peptides not affected in ERAP2-WT cells (in grey).

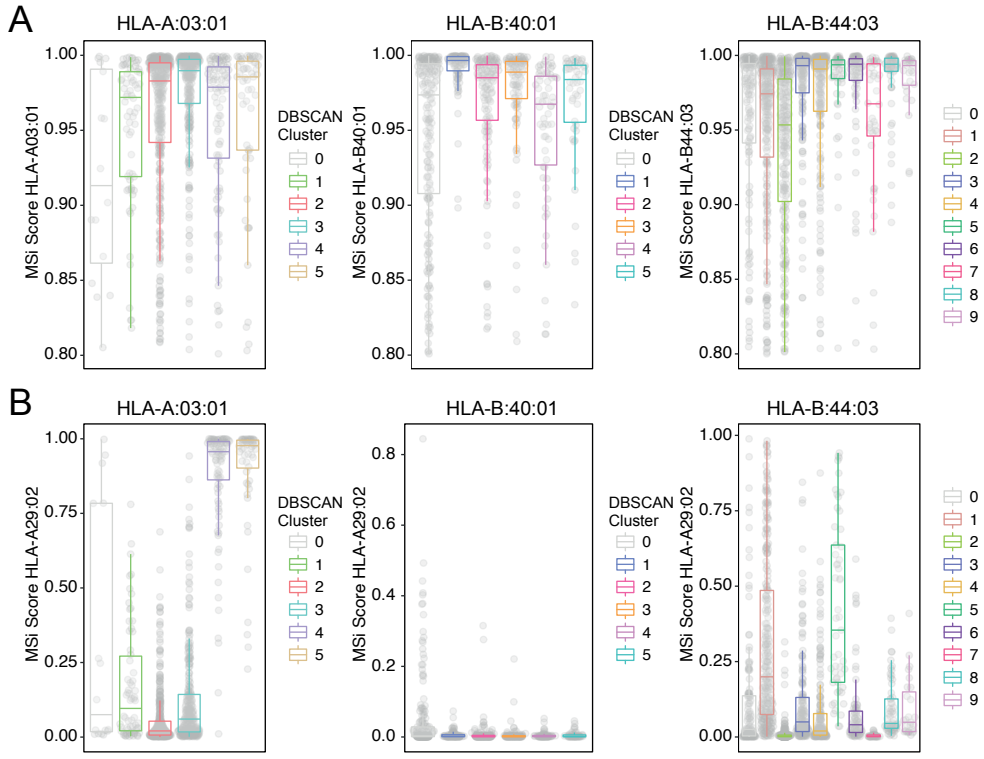

Supplemental Figure 2.11. Peptide bindings scores from *HLAthena* (HLAthena.tools) for peptide clusters from **Figure 2.4**. (**a**) The binding score (MSi) for 9-mers with a MSi>0.8 used for the non-metric multidimensional scaling of *HLA-A*03:01*, *HLA-B*40:01*, and *HLA-B*44:03*. The binding score ranges from 0 (low) to 1 (high). Clusters identified by DBSCAN are indicated and color-coded. (**b**) The binding score for *HLA-A*29:02* (MSi) for the same 9-mers and clusters as shown in *a*.

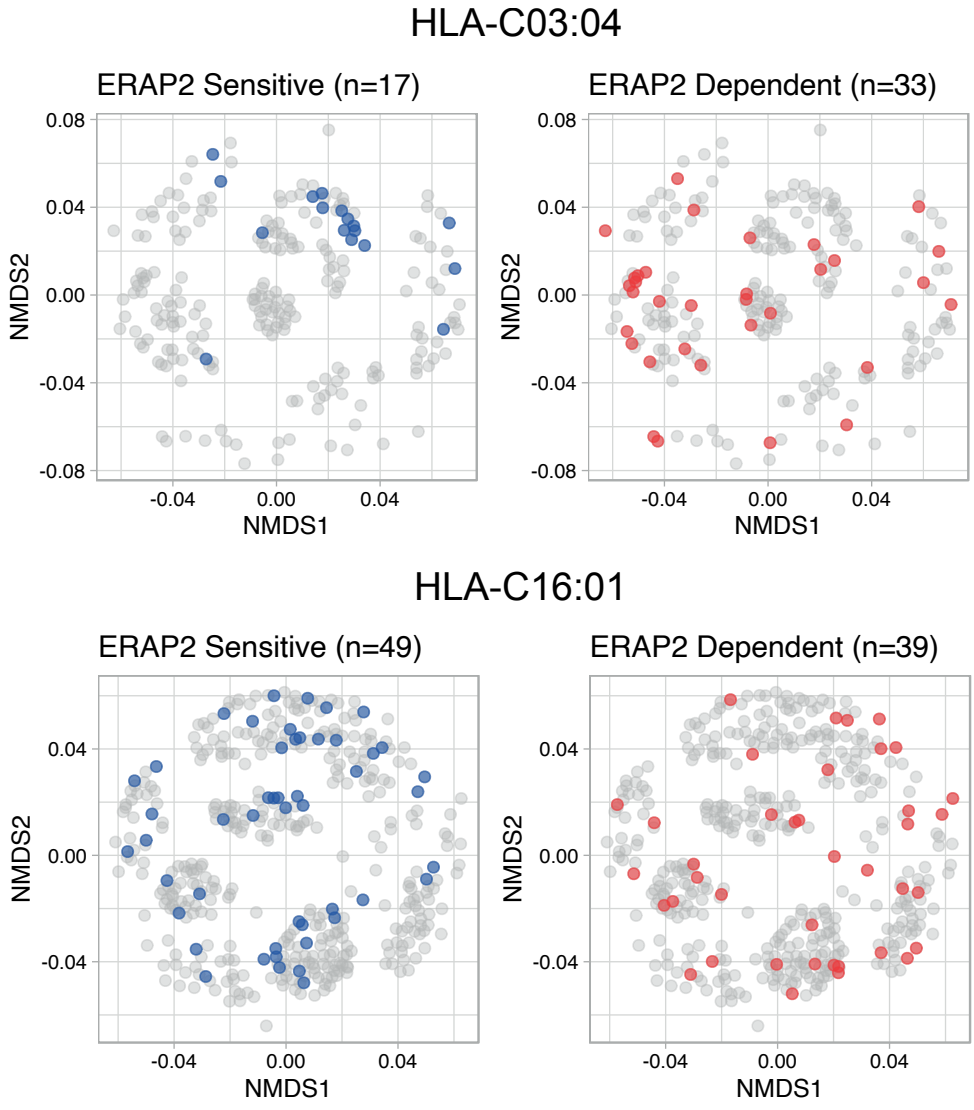

Supplemental Figure 2.12. Non-metric multidimensional scaling plot of 221 and 411 9-mers from HLA-C03:04 and HLA-C16:01. Differentially expressed peptides are indicated in blue (ERAP2 sensitive that decrease in abundance in the presence of ERAP2) and red (ERAP2-dependent peptides that increase in abundance in the presence of ERAP2).

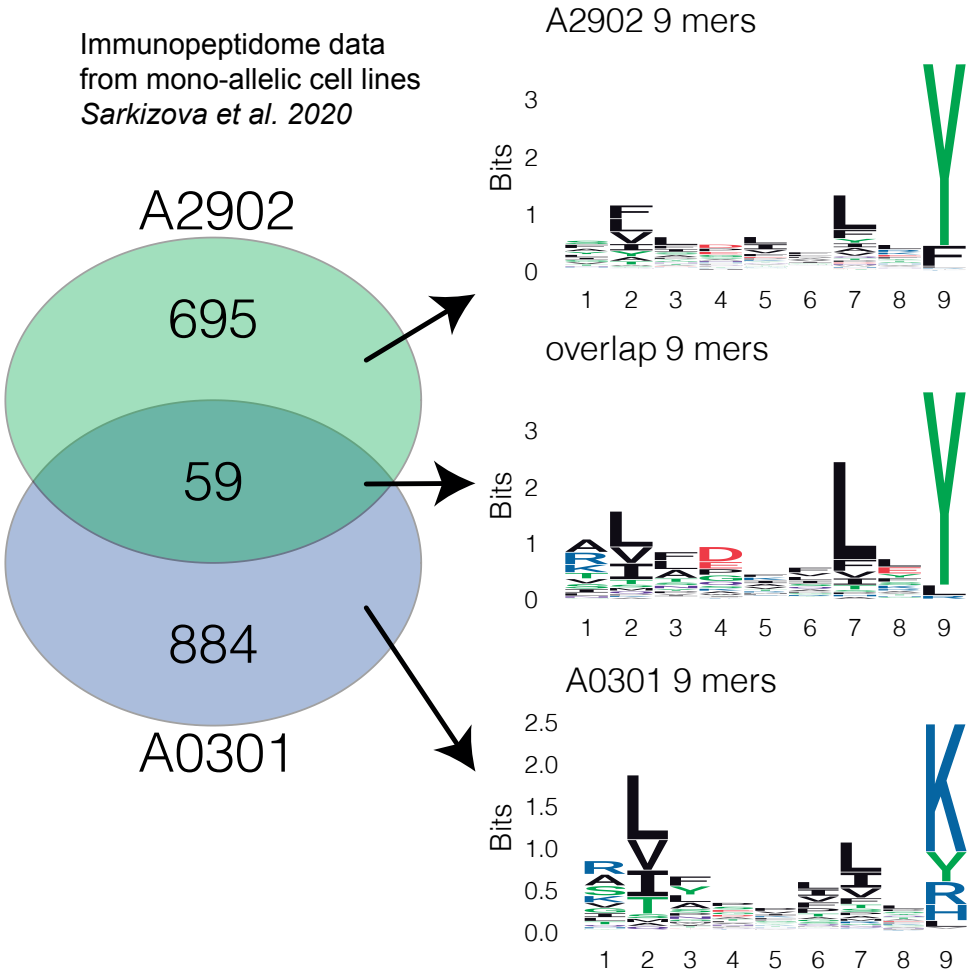

Supplemental Figure 2.13. Venn diagram of 9-mers presented by monoallelic cell lines expressing only HLA-A29:02 or only HLA-A03:01 from *Sarkizova et al., 2020* A total of 59 9-mers were detected in both datasets. The sequence logos for peptides uniquely observed in HLA-A29, overlapping peptides found in both monoallelic datasets, and peptides uniquely observed in HLA-A03 are indicated on the right.

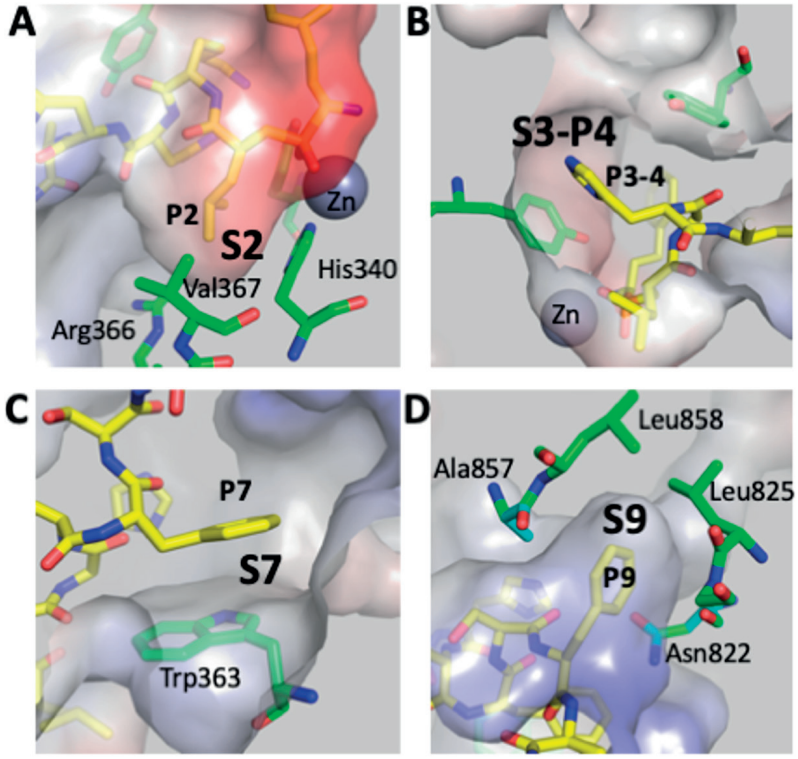

Supplemental Figure 2.14. Putative specificity pockets of ERAP2 that help explain observed sequence motifs. ERAP2 (from PDB code *5AB0*) is shown in surface representation colored by electrostatic potential (red=negative, white=neutral, blue=negative). Peptide analogue DG025 that was crystallized bound onto ERAP2 is shown in yellow sticks (carbon=yellow, oxygen=red, nitrogen=blue). Nearby ERAP2 residues that help form indicated specificity pockets are shown in green sticks. Specificity pockets are indicated as (**a**) S2, (**b**) S3-P4, (**c**) S7 and (**d**) S9. Peptide residue side-chains that are accommodated in the pockets are indicated as P2, P3-4, P7 and P9.

Supplemental Methods and Info

Lentiviral vector production

HEK-293T cells were seeded into 10 cm dishes (2×10^6 cells/dish) and cultured in Dulbecco's Modified Eagle Medium (DMEM, Thermo Fisher Scientific). The next day, 293T cells were co-transfected with 2 µg transfer vector (Lenti ORF clone of Human S-antigen mGFP tagged, RC220057L2 from Origene) and components of 2nd generation packaging vectors: 8.33 µg psPAX2 packaging vector and 2.77 µg pMD2.G envelope vector at a ratio of 4:1. Transfection was done in serum-free DMEM using Lipofectamine 2000 (Thermo Fisher Scientific) according to manufacturer's instructions. Medium was replaced with 10 mL DMEM supplemented with 10% FBS and incubated at 37°C, 5% CO_2 after 24 hours. The conditioned medium containing lentiviral particles was collected 48 hours after transfection and an additional 10 mL of fresh culture medium was added to the cells. After 12 hours, harvested supernatants were combined and cleared by centrifugation at 1500 rpm for 5 minutes at 4°C then passed through a 0.45 µm filter. Lentiviral supernatants were concentrated using ultracentrifugation with a Beckman Coulter Optima centrifuge using a SW32Ti rotor. Filtered supernatant was added to 38.5 mL Ultra-Clear tubes (Beckman Coulter). Centrifugation was performed for 120 minutes at 32,000 rpm. Supernatant was completely removed and virus pellets were resuspended in 1 mL RPMI (containing 10% FBS and 1% penicillin/streptomycin) and stored at -80°C.

Lentiviral transduction of S-antigen in EBV-LCL

To obtain stable cell lines overexpressing S-antigen, EBV-LCLs were transduced with the concentrated lentiviral supernatants. To transduce EBV-LCLs, $1x10^6$ cells were seeded in a 24-wells plate with the lentivirus and a final polybrene concentration of 6 µg/mL. After 24 hours, the medium was replaced and the cells were cultured for another 3 days, without exceeding a cell concentration of 1.5×10^6 cells/mL. Transduction efficiency was monitored by fluorescent light microscopy. GFP-positive EBV-LCLs were sorted using the BD FACSAria™ III sorter and S-antigen expression levels were detected by western blot. Western blot analysis to detect the fusion protein S-antigen-GFP was done as described in the Method section. **Supplemental Figure 2.15** below shows the high protein expression of S-antigen and Tubulin detected from the same cell lysate samples of the patient-derived LCL, but run on two separate blots in parallel because the proteins are detected in close proximity on the blot.

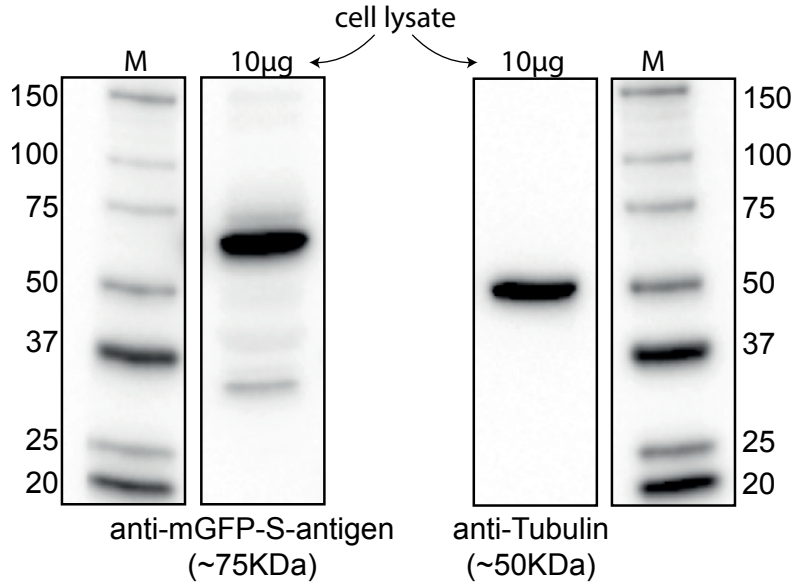

Supplemental Figure 2.15. Western blot analysis of retinal S-antigen after transduction of the patient-derived LCLs.

Differential expression analysis of peptides using limma

For differential expression analysis we used the workflow from Kammers *et al.,* 2015 available at http://www.biostat.jhsph.edu/~kkammers/software/eupa/R_guide.html. Their method exploits the R package *limma* for shrinking a peptide's sample variance towards a pooled estimate that boosts power for stable detection of (truly) significant changes in small proteomic data sets. Peptide data were preprocessed using the *read.peptides()* function, which excludes peptides with missing values (i.e., not detected in either the light or heavy channel). We computed dummy variables for the "I*solation.Interference*", "*Quan. Usage*", "*Quan.info*" variables, because quality control of the input data was completed as described in the main manuscript. The peptide sequence was used as the "*Protein. Group.Accessions*" variable. Overlapping peptide data from the biological replicates were independently normalized using the *quantify.proteins()* function. Following the workflow of Kammers et al., we used peptides (with a Mascot Percolator q<0.01 in all analyses) detected in both biological replicates (i.e., peptides unique to one of the conditions are left out for normalization and statistical analysis). For example, for peptides detected by DK1G8 (anti-HLA-A29) with a *HLAthena* binding score [MSi]>0.6 for HLA-A*29:02 a total of 1330 peptides were detected in both channels, while 41 peptides in either the light or heavy channel (with consistent detection in the same channel in both experiments) and were not considered for statistical analyses. We blocked for batch effect (two independent experiments) in *limma* by including them in the design matrix. HLA-A29 peptidome analysis considering also peptides detected in either the heavy or light channels is provided in **Supplemental**

Figure 2.3. Here, we used dummy variables for the moderate q-value (set to 1×10^{-6}) and $\log_2$FC ($\log_2$FC= -6.6 for peptides only detected in the ERAP2 KO-cell line and $\log_2$FC=6.6 for peptides detected only in the ERAP2 WT-cell line), because these parameters were only used to subset peptides unique to either of the conditions (using moderate q<0.01 as a threshold) together with the differentially expressed peptides detected in both channels. Also, although Mascot Percolator exploits a number of relevant peptide features and has been shown to be superior in accurate peptide identification compared to previous Mascot scoring based on one metric (Borsch et al.,2009), we also conducted this analysis of the HLA-A29 peptidome using the percolator q-value in conjunction with the Mascot ions score >30, which showed similar effects for ERAP2 at the submotif level as the analysis using the percolator q-value (see **Supplemental Figure 2.3**).

References Supplemental Info

Alvarez-Navarro C, Martín-Esteban A, Barnea E, Admon A, López de Castro JA. Endoplasmic Reticulum Aminopeptidase 1 (ERAP1) Polymorphism Relevant to Inflammatory Disease Shapes the Peptidome of the Birdshot Chorioretinopathy- Associated HLA-A*29:02 Antigen. Mol Cell Proteomics. 2015 Jul;14(7):1770-80.

Brosch M, Yu L, Hubbard T, Choudhary J. Accurate and sensitive peptide identification with Mascot Percolator. J Proteome Res. 2009 Jun;8(6):3176-81.

Kammers K, Cole RN, Tiengwe C, Ruczinski I. Detecting Significant Changes in Protein Abundance. EuPA Open Proteom. 2015 Jun;7:11-19.

Sanz-Bravo A, Martín-Esteban A, Kuiper JJW, García-Peydró M, Barnea E, Admon A, López de Castro JA. Allele-specific Alterations in the Peptidome Underlie the Joint Association of HLA-A*29:02 and Endoplasmic Reticulum Aminopeptidase 2 (ERAP2) with Birdshot Chorioretinopathy. Mol Cell Proteomics. 2018 Aug;17(8):1564-1577.

Sarkizova S, Klaeger S, Le PM, Li LW, Oliveira G, Keshishian H, Hartigan CR, Zhang W, Braun DA, Ligon KL, Bachireddy P, Zervantonakis IK, Rosenbluth JM, Ouspenskaia T, Law T, Justesen S, Stevens J, Lane WJ, Eisenhaure T, Lan Zhang G, Clauser KR, Hacohen N, Carr SA, Wu CJ, Keskin DB. A large peptidome dataset improves HLA class I epitope prediction across most of the human population. Nat Biotechnol. 2020 Feb;38(2):199-209.

Chapter 3

HLA-A29 and Birdshot Uveitis: Further Down the Rabbit Hole

J.J.W. Kuiper[1,2] and W.J. Venema[1,2]

1. Department of Ophthalmology, University Medical Center Utrecht, University of Utrecht, Utrecht, Netherlands
2. Center for Translational Immunology, University Medical Center Utrecht, University of Utrecht, Utrecht, Netherlands

Published in Front. Immunol. 11, 599558 (2020)

Abstract

HLA class I alleles constitute established risk factors for non-infectious uveitis and preemptive genotyping of HLA class I alleles is standard practice in the diagnostic work-up. The HLA-A29 serotype is indispensable to Birdshot Uveitis (BU) and renders this enigmatic eye condition a unique model to better understand how the antigen processing and presentation machinery contributes to non-infectious uveitis or chronic inflammatory conditions in general. This review will discuss salient points regarding the protein structure of HLA-A29 and how key amino acid positions impact the peptide binding preference and interaction with T cells. We discuss to what extent the risk genes ERAP1 and ERAP2 uniquely affect HLA-A29 and how the discovery of a HLA-A29-specific submotif may impact autoantigen discovery. We further provide a compelling argument to solve the long-standing question why BU only affects HLA-A29-positive individuals from Western-European ancestry by exploiting data from the 1000 Genomes Project. We combine novel insights from structural and immunopeptidomic studies and discuss the functional implications of genetic associations across the HLA class I antigen presentation pathway to refine the etiological basis of Birdshot Uveitis.

Introduction into birdshot uveitis

Birdshot Uveitis (also known as *Birdshot chorioretinopathy* or *Birdshot retinochoroidopathy*) is a well-characterized form of autoimmune uveitis (inflammation of the uveal layer of the eye) mostly known for its ovoid light lesions, which appear 'shotgun pattern'-like distributed along the vascular arcades in the back of the eye (i.e., the 'fundus' of the eye where these lesions are visible by photography)[1]. Inflammation and extensive depigmentation of the choroid, macular edema, peripheral ischemia[2], degeneration of the retina, and the progressive formation of thin layer of scar tissue on the retina ("epiretinal membrane")[3,4], progressively impair vision in a substantial proportion of patients. BU is unusual in the young[5] and typically affects patients over 50 years of age of Western-European ancestry, with more women than men affected[6]. Long-term systemic corticosteroid-sparing immunomodulatory therapy is the mainstay of treatment[7,8], but a fraction of patients may exhibit a more benign disease course that does not require systemic therapy[9]. Histopathology studies of eye tissues and modern imaging technologies show that early lesions are located deep inside the vascular layer of the eye (the "choroid") between the retina and the white outer layer of the eyeball (sclera). In the choroid, the large-vessel layer (choroidal stroma)—densely populated with pigmented "melanocyte" cells—shows abnormalities before the characteristic fundus lesions are visible[10,11]. Because BU shows early inflammation of the choroidal stroma[12], Herbort and associates proposed to classify BU as a primary *stromal choroiditis*, together with *Vogt-Koyanagi-Harada* (VKH) disease. VKH is a condition characterized by chronic inflammation toward melanocytes that affect multiple parts of the body, including the choroidal stroma and the larger choroidal vessels[11,13]. In VKH no retinal involvement at early stages of disease are noticeable. In contrast, retinal inflammation (e.g., leakage of vessels) is an early clinical characteristic of BU[14], which suggests that retina involvement is not merely the result of inflammation spilling over from the choroid. However, the cause and interdependence of the retinal and choroidal inflammation are unknown, which is reflected in the use of multiple terms to define the eye condition; birdshot *retinitis*, birdshot *chorioretinopathy*, or birdshot *retinochoroidopathy*. For lack of understanding the disease pathology, here the broader term "birdshot uveitis" was chosen.

Microscopic anatomy studies (or *histological* studies) of eye tissue of patients with BU are scarce because of the rarity of the condition (estimated 1 to 5 cases per 500,000)[6,15]. The most recent histological study by Sohn and coworkers[16] in a patient with end-stage BU showed extensive degeneration of the retina and near complete loss of choroidal layers and the retinal pigment epithelium, a highly specialized cell layer critical to the homeostasis photoreceptors of the retina. Changes in retinal pigment epithelium are also evident by retinal imaging in patients with established disease[17]. Each of the histological studies show massive infiltration of blood leukocytes into the choroid and retina layers; mostly T lymphocytes not only express the glycoproteins CD4 ("T helper" cells) and CD8 ("Cytotoxic" T cells)[16,18,19] but also relatively increased numbers of other immune cells, such as myeloid

cells and B lymphocytes. The cases in two of these studies were remarkable for a history of malignant melanoma, but evidence that directly links melanoma to BU is lacking. At most, the evidence is circumstantial, such as "Birdshot-like disease" in melanoma cancer patients that develop autoimmune uveitis due to checkpoint inhibitor therapy (a treatment setting T cells free to kill tumor, but also normal tissue)[20] or the presence of blood antibodies that can bind to proteins in melanoma tumor cell lines[21]. These phenomena may be explained by the fact the proteins involved in immunity toward melanoma are also expressed in normal melanocytes[22] and may actually support that choroidal melanocytes are among target cells deliberately attacked by the derailed immune system in BU.

The genetic association with HLA-A29

Short after BU was first described in 1980[23], the unusually strong genetic association of the *Human-Leukocyte Antigen A*29* (*HLA-A*29*) with BU was discovered in 1982 by Nussenblatt and coworkers[24]. HLA-A29-positive testing is now widely considered critical to diagnosis and led key opinion leaders in the field propose to rename the condition to "HLA-A29 uveitis"[25]. *HLA-A*29* is one of the hundreds of variants of the *HLA-A* gene that together with different versions of *HLA-B* and *HLA-C* genes form the HLA class I complex of functionally related proteins in humans. The *HLA-A* gene encodes slightly different versions of a the cell-surface protein HLA-A. Like other HLA class I proteins, HLA-A plays a central role in the immune system by instructing immune cells (e.g., cytotoxic T cells) if a cell must be destroyed because it is infected by foreign invaders (e.g., a virus) or when a cell has become cancerous after mutation of the DNA[26]. In most cells of the body, HLA-A achieves this by constant sampling of protein fragments from foreign invaders or self-proteins (termed "antigenic" peptides, or antigens in short) from the inside of the cell and "presenting" these peptides on the outside of the cell for scrutiny by surveilling immune cells[26,27]. This "antigen presenting pathway" is critical to monitor cellular integrity and is based on differentiating "self" from "non-self" (pathogen) or "altered-self" (cancer)[26]. Aberrant function of this pathway can result in persistent infection, cancer or autoimmune disease[27].

Because all patients with BU carry a copy of the HLA-A29 *allele* (the term for "gene variant"), it is considered to be critically involved in the unidentified disease mechanisms[1]. This is supported by rare familiar cases of BU that show that all cases with the eye phenotype are also HLA-A29-positive[28]. Also, the allele frequency of HLA-A29 is high in Western-European countries[29], where also the vast majority of BU patients are reported in Europe, while BU is anecdotally reported in populations with low occurrence of HLA-A29[30,31]. How exactly HLA-A29 contributes to eye inflammation is unknown, but several unique properties of HLA-A29 distinguish this allele from others *HLA-A* alleles in the population; A gel electrophoresis study from 1992 indicated that HLA-A29 in cases is identical to unaffected controls that carry HLA-A29 (~5–10% of the Western-European populations)[32],

which is supported by small DNA sequencing studies[29]). In two genome-wide association studies[33,34], we used detailed genetic analysis of HLA alleles in BU cases that revealed that the main risk allele for BU is *HLA-A*29:02*, the most common HLA-A29 allele in Europe. These studies further ascertained that other associations in the *MHC* locus (the DNA region where HLA genes are embedded) are a result of positive linkage disequilibrium (LD) with HLA-A29. In other words, near-by gene variants such as for example the *HLA-B*44* allele are often (yet not always) inherited together with HLA-A29 but most likely not relevant for the disease. One study of a murine model in which a copy of HLA-A29 DNA from a BU patient was genetically expressed initially showed an eye disease similar to BU[35], but in a later underappreciated study, the mice strain used for the BU model was found to harbor a wide-spread and previously unnoticed genetic mutation that causes retinal degenerative disease (not uveitis) that also affected the control mice[36]. This supports that the HLA-A29 allele itself is not sufficient and that the susceptibility to BU is mediated by additional etiological triggers. This also fits the observation that HLA-A29 is a common allele (~10% of the Western-European population is HLA-A29-positive), but BU is a rare condition (~250 cases in the Netherlands at 17 Mill. citizens as of June 2020). Also, *HLA-A*29:02* is also very common among specific ethnic groups of non-European ancestry where BU has not been reported, such as the South African Zulu[37] or the Luhya in Webuye of Kenya in Africa (~10% HLA-A*29:02-positive individuals)[38,39].

The HLA-A29 protein structure

In 2020, the *immuno polymorphism database*[40] contains >200 reported HLA-A29 alleles, but only the most common alleles—*HLA-A*29:02*, *HLA-A*29:01*, and *HLA-A*29:10*—have been reported in cases with birdshot[41]. Structurally, HLAA*29:01 (D102H) and HLA-A*29:10 (E177K) differ from HLA-A*29:02 at single amino acids positions in the external alpha 2 domain of HLA-A29 (**Figure 3.1A**), but these positions do not influence the expression, conformation, or interaction of the HLA-A complex with T cells[46-48]. In other words, these alleles can be considered functionally similar. The most relevant amino acid positions in HLA-A29 for disease risk were statistically linked to amino acids at positions 62 and 63 in the protein sequence[33]. As shown in **Figure 3.2**, the amino acids *Leucine* at position 62 (62-L) and *Glutamine* at position 63 (63-Q) distinguish HLA-A29 from other *HLA-A* alleles.

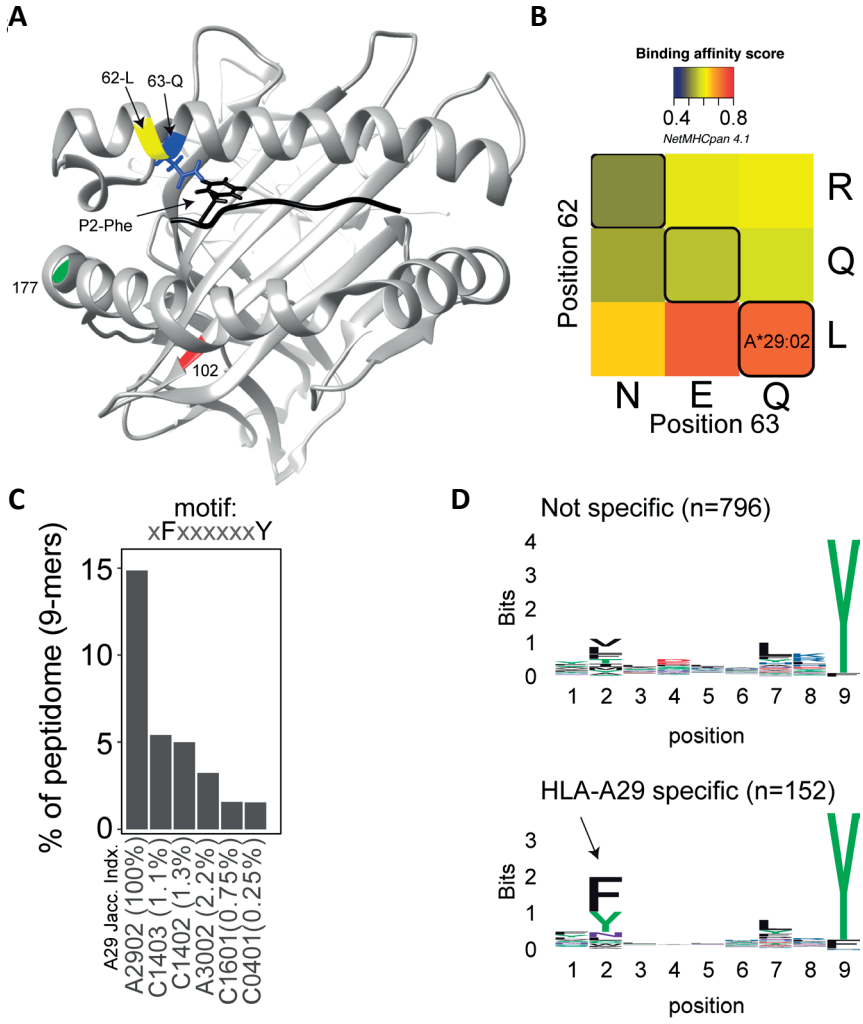

Figure 3.1: Structure and function of amino acid positions 62 and 63 in HLA-A29. (**A**) View into the peptide-binding groove of a three-dimensional ribbon model for HLA-A29 (Based on Protein Data Bank entry: 6J1W modelling using UCSF Chimera[42]. The amino acids Leucine (L in yellow) at position 62 and Glutamine (Q in blue) at position 63 defining HLA-A29 are indicated. The binding peptide is shown in black with phenylalanine at position 2 (P2-Phe) interacting with position 63-Q (with energy-minimized positions of side chains). Polymorphic amino acid positions associated with the alleles *HLA-A29:01* (pos 102 in red) and *HLA-A29:10* (position 177 in green) are also shown. (**B**) The effect of amino acid substitutions for position 62 and 63 on predicted binding affinity for HLA-A29-presented peptides. The average binding scores of 9-mers (n = 948) detected by mass-spectrometry analysis of HLA-A29 reported by Venema *et al*.[43]. Replacement of position 62 and 63 with the most commonly occurring amino acids at that position encoded by *HLA-A* alleles was done in netMHCpan 4.1 server[44]. Naturally occurring motifs are indicated with black lines, other motifs (e.g., QN) do not occur in human HLA-A allotypes. (**C**) The percentage of 9-mer peptides with P2-Phe and P9-Tyr detected in immunopeptidomes of HLA class I alleles as reported by Sarkizova *et al*.[45]. The top 5 (of 95 alleles tested) class I alleles other than HLA-A29 are shown. The jaccard similarity index for the HLA-A*29:02 peptidome (overlap in presented peptides) and each allele is indicated (in %). Peptidome data were derived from Sarkizova *et al*.[45]. (**D**) Sequence logos of 9-mers (n = 948) from HLA-A29 [the same peptides as in (C)] stratified into non-specific for HLA-A29 (with binding score MSi > 0.6 for HLA-A*43:01 or HLA-A*68:130 according to the *HLAthena* server[45]) or specific for HLA-A29 (MSi < 0.6 for HLA-A*43:01 and HLA-A*68:130). The arrow indicates the aromatic P2 in the binding motif specific for HLA-A29.

This is of interest because computational modelling of HLA-A by changing amino acids at indicated positions (or amino acid substitution modelling) revealed that position 63 has the largest effect on the ability to bind antigenic peptides over all polymorphic positions in the peptide-binding "groove" of HLA-A *allotypes* (the term for "protein variants")[49]. Specific mutation of the positions 62-63 can completely abrogate HLA peptide recognition by T cells[50]. Most other *HLA-A* alleles encode the amino acids *asparagine* (N) or *glutamic acid* (E) at amino acid position 63 (**Figure 3.2**). Despite the degree of similarity of the chemical characteristics of the side chains of the amino acids, the effects of Q and N on the local structure of protein are different[51] and changing the chemically related glutamine (Q) to glutamic acid (E) at single amino acid position in the HLA-A molecule can modulate the interaction with CD8 of T cells[52].

AA Pos.	10	20	30	40	50	60	70	80	90	100
A*01:01:01:01	GSHSMRYFFT	SVSRPGRGEP	RFIAVGYVDD	TQFVRFDSDA	ASQKMEPRAP	WIEQEGPEYW	DQETRNMKAH	SQTDRANLGT	LRGYYNQSED	GSHTIQIMYG
A*02:01:01:01	----------	----------	----------	----------	---R------	----------	-G---KV---	---H-VD---	---------A	----V-R---
A*03:01:01:01	----------	----------	----------	----------	---R------	----------	------V--Q	-----VD---	---------A	----------
A*11:01:01:01	--------Y-	----------	----------	----------	---R------	----------	------V--Q	-----VD---	----------	----------
A*23:01:01:01	--------S-	----------	----------	----------	---R------	----------	-E--GKV---	-----E--RI	ALR------A	----L-M-F-
A*24:02:01:01	--------S-	----------	----------	----------	---R------	----------	-E--GKV---	-----E--RI	ALR------A	----L-M-F-
A*26:01:01:01	--------Y-	----------	----------	----------	---R------	----------	-RN---V---	----------	----------	------R---
A*29:01:01:01	--------T-	----------	----------	----------	---R------	----------	-LQ---V--Q	----------	---------A	------M---
A*29:02:01:01	--------T-	----------	----------	----------	---R------	----------	-LQ---V--Q	----------	---------A	------M---
A*29:10:01	--------T-	----------	----------	----------	---R------	----------	-LQ---V--Q	----------	---------A	------M---
A*30:01:01:01	--------S-	------S---	----------	----------	---R------	-----R----	------V--Q	-----VD---	---------A	----------
A*31:01:02:01	--------T-	----------	----------	----------	---R------	-----R----	------V---	--I--VD---	---------A	------M---
A*32:01:01:01	----------	----------	----------	----------	---R------	----------	------V---	-----ES-RI	ALR------A	------M---
A*33:01:01:01	--------T-	----------	----------	----------	---R------	----------	-RN---V---	--I--VD---	---------A	------M---
A*43:01	--------Y-	----------	----------	----------	---R------	----------	-LQ---V---	----------	----------	------R---
A*66:01:01:01	--------Y-	----------	----------	----------	---R------	----------	-RN---V--Q	-----VD---	----------	------R---
A*68:01:01:01	--------Y-	----------	----------	----------	---R------	----------	-RN---V--Q	-----VD---	---------A	------M---
A*74:01:01:01	----------	----------	----------	----------	---R------	----------	------V---	-----VD---	---------A	------M---
A*80:01:01:01	----------	----------	----------	S---Q-----	---R------	-----E----	-E----V---	---N------	----------	----------

Figure 3.2: The amino acid sequence of HLA-A alleles. The first 100 amino acids for 19 HLA-A alleles from the IPD-IMGT/HLA Database[40]. The amino acids at positions 62 and 63 distinguish HLA-A29 alleles, with the exception of the rare HLA-A43 (± 15,000 times lower allele frequency compared to *HLA-A29:02* in the European population).

Indeed, amino acid substitution modelling of position 62 and 63 in HLA-A29 demonstrates that the strength of binding of peptides (i.e., the binding "affinity") into the peptide-binding groove of HLA-A29 is decreased if the amino acids at these positions are changed to any of the other naturally occurring combinations of amino acids at positions 62-63 in HLA-A (**Figure 3.1B**). Curiously, substituting position 62 is predicted to have a larger effect than substitutions on position 63. Also, the 'theoretical' motif 62-L 63-E (which does not occur in any known *HLA-A* alleles) provides a globally similar binding capacity for peptides compared to the 62-L 63-Q of HLA-A29. Phylogenetically related alleles of HLA-A29 (i.e., *HLA-Aw19* complex)[53] encode 62-Q 63-E and would require changing 'only' position 62 to achieve a globally similar functionality. However, as mentioned, the local structural effects of the chemically related E and Q can be quite distinct and functional analysis is required to better understand the hierarchy of impact of these positions on defining the HLA-A29 peptidome. Also, these amino acids do not completely account for the peptide specificity

of HLA-A29. In fact, 62-L 63-Q is detected in some other alleles such as *HLA-A*43:01*, *HLA-A*11:11*, and *HLA-A*68:130* (allele frequency of *HLA-A*43:01* and *HLA-A*11:11* in the European population >15,000 times less than *HLA-A*29:02*[54], and *HLA-A*68:130* is not well documented[40]). However, these alleles differ from HLA-A29 alleles on various other key positions that influence peptide binding in the peptide binding groove, including amino acid position 9[55], 70, 76, 77, or positions 97 or 152, which influence the interaction with T cells[56,57]. Notwithstanding these exceptional alleles, the amino acid motif 62-L 63-Q near exclusively accounts for HLA-A29 in the European population[54]. Amino acid residues 62 and 63 are positioned at the edge of the peptide binding groove (**Figure 3.1A**) in a cavity that directly interacts with the side chain of the amino acid at position 2 (P2) of the displayed antigenic peptide[58]. Therefore, the 62-63 motif may influence the flexibility to accommodate antigenic peptides with distinct P2 residues, a feature most likely relevant to autoantigen discovery for BU.

The HLA-A29 peptide motif

The peptide binding motif—or the 'conserved' positional residue preference considering the amino acid sequences of all "presented" peptides—of HLA-A29 is relatively flexible on condition of a C-terminal (the last amino acid in a peptide) *Tyrosine* (Y) or less frequently a *Phenylalanine* (F)[45]. Peptides with a C-terminal Y also make up a significant proportion of the peptides presented on other HLA-A alleles, including HLA-A*01:01, HLA-A*03:01, and HLA-A*30:02[45] (but also HLA-A*43:01 and HLA-A*68:130). This includes peptides that are detected in the binding groove of more than one HLA-A allotype (demonstrated by mass-spectrometry studies of single-HLA-expressing cell lines), a phenomenon termed peptide 'promiscuity'[59]. We and others have studied the complete set of antigenic peptides (termed the 'immunopeptidome') bound by HLA-A29 and used multidimensional scaling (a visual representation of the immunopeptidome where all peptides are positioned in a graph based on their relative similarity or difference in amino acid sequence) to cluster the peptides into subdominant binding motifs (or "submotifs")[43,45,60]. This approach facilitates the identification of clusters of antigenic peptides (submotifs) that are shared with other HLA class allotypes or that are unique to HLA-A29. These studies revealed patterns of submotif preferences easy to miss in conventional studies when considering the immunopeptidome as a whole. In short, HLA-A29 presents a palette of submotifs mostly defined by distinct amino acids at position 2 (P2) and 7 (P7) in the antigenic peptide sequence. As discussed, a fraction of peptides presented by HLA-A29 is also found in the binding groove of other HLA-A alleles and consequently some submotifs of HLA-A29 were also detected in immunopeptidome data of other HLA allotypes. This helped to narrow down a submotif that is specific to HLA-A29[43], which is characterized by the amino acids F or Y at P2 in conjunction with the HLA-A29-characteristic C-terminal (PC) Y (F/Y-P2 + Y-PC motif). This motif makes up ~15%

of the HLA-A29 immunopeptidome (**Figure 3.1C**). Peptides with this motif are substantially less frequently presented on other HLA allotypes and those that do are uncommon in the Western-European population and/or display very low similarity in the immunopeptidome composition with HLA-A29 (<3% of the peptides are shared, **Figure 3.1C**). Note that 'just' P2-F and P2-Y (so without PC-Y) is not uncommon in the immunopeptidomes of other HLA-A allotypes, such as HLA-A24 (see supplemental data of Sarkizova *et al*.[45]), but the amino acids that occupy the pocket accommodating P2 of binding peptides is completely different from HLA-A29. Although we were unable to find immunopeptidome studies of the HLA-A*43:01 and HLA-A*68:130 alleles, binding prediction shows that peptides with the motif F/Y-P2 + Y-PC are poorly presented by these alleles, most likely as a consequence of the differences in other key positions in the binding groove (**Figure 3.1D**), which further support that this motif is specific to HLA-A29.

The *ERAP1-ERAP2* haplotype links BU to the Western-European ancestry

Key to progress in understanding why merely a fraction of HLA-A29-positive individuals develop BU came from genetic studies, including work from our lab. We identified that beyond HLA-A29, genetic polymorphisms (or common variations in the DNA sequence among individuals) at chromosome *5q15* confer strong disease risk[34,61]. The signal on chromosome 5 covers the endoplasmic reticulum aminopeptidase (*ERAP*)-1 and *ERAP2* genes, and *LNPEP*, all enzymes involved in trimming the peptide fragments before they are bound by HLA class I (e.g., HLA-A29). Importantly, the combination of two polymorphisms functionally linked to *ERAP1* (rs2287987) and *ERAP2* (rs10044354), conferred a risk for BU that was significantly larger than the risk from either one the two polymorphisms individually[61]. Analysis of patients and HLA-A29-positive controls showed that the combined polymorphisms linked to *ERAP1* and *ERAP2* also showed the largest disease risk (detected in 50% of 130 cases and 25% of 439 HLA-A29-positive controls). This indicates that the genetic changes affecting both ERAP1 and ERAP2 in tandem increase the risk in the HLA-A29-positive population[61]. Indeed, if we look at publicly available data from the 1000 genomes project, the risk-variant linked to *ERAP2* (rs10044354-T) or the risk-variant linked to *ERAP1* (rs2287987-C) are also observed in HLA-A29-positive individuals of non-European ancestry (**Figure 3.4**).

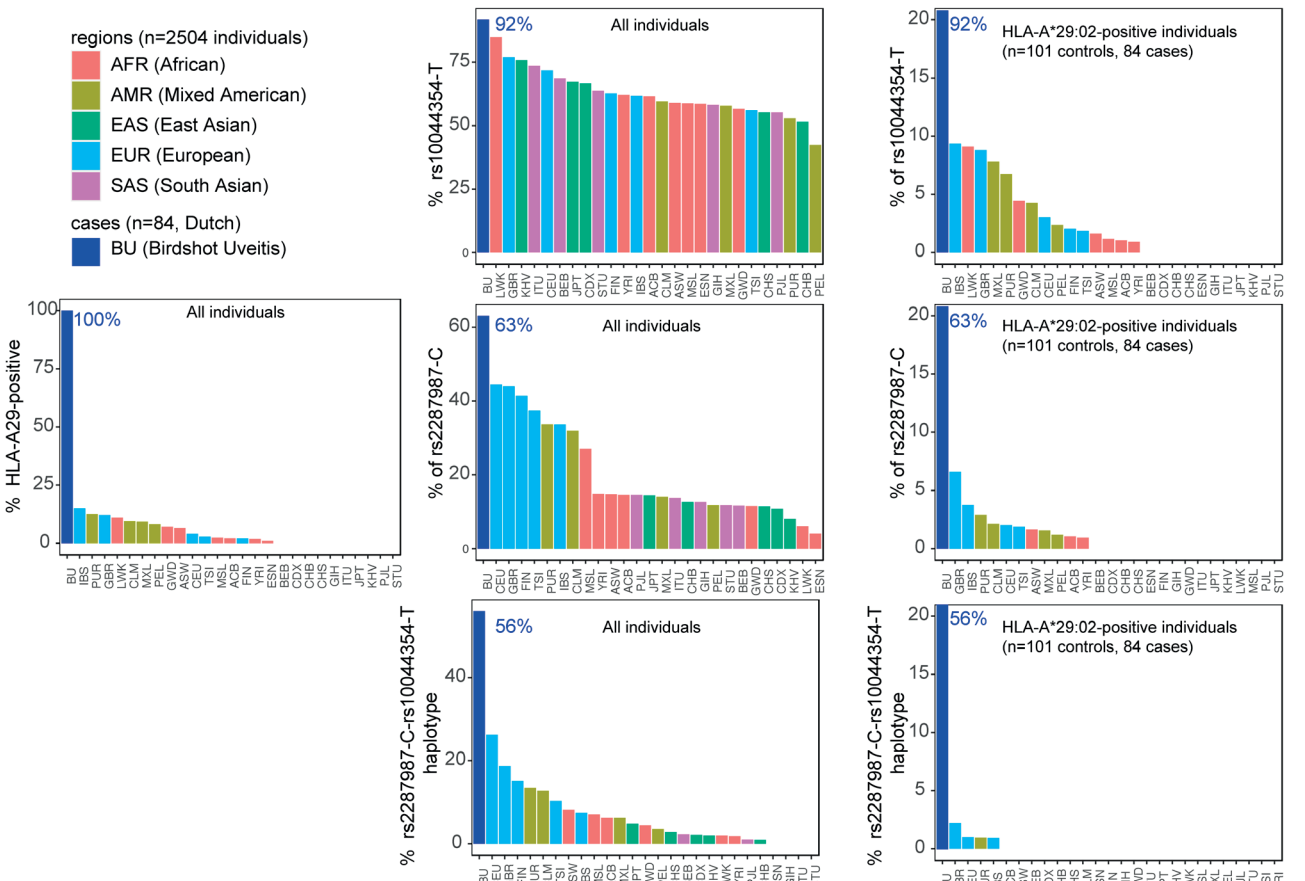

Figure 3.3: The combined risk factors HLA-A29 and the ERAP1-ERAP2 haplotype are restricted to populations of Western-European ancestry. The percentage of individuals that carry a copy of *HLA-A*29:02*, the C allele of the polymorphism rs2287987 (in *ERAP1*), and the T allele of rs10044354 (near *ERAP2*) in 84 BU patients and the 2504 individuals of 26 ethnic populations of the 1000 Genomes Project. Data from BU patients was derived from Kuiper *et al*.[61]. The graphs in the middle are the data for all 2504 individuals of

the 1000 Genomes. The graphs on the right are the genotype data limited to HLA-A*29:02-positive individuals. This data demonstrates that the combined risk haplotype of rs2287987-rs10044354 in HLA-A29 is rare or absent in populations of non-Western-European ancestry. HLA data was obtained from Abi-Rached *et al.*[39] and genotype data for rs10044354 and rs22878987 from the 1000 Genomes project[63]. The regions and populations are indicated using the following abbreviations: CHB, Han Chinese in Beijing; JPT, Japanese in Tokyo; CHS, Southern Han Chinese; CDX, Chinese Dai in Xishuangbanna; KHV, Kinh in Ho Chi Minh City; CEU, Utah Residents (CEPH) with Northern and Western European Ancestry; TSI, Tuscans in Italy; FIN, Finnish in Finland; GBR, British in England and Scotland; IBS, Iberian Population in Spain; YRI, Yoruba in Ibadan; LWK, Luhya in Webuye; GWD, Gambian in Western Divisions in the Gambia; MSL, Mende in Sierra Leone; ESN, Esan in Nigeria; ASW, Americans of African Ancestry in SW USA; ACB, African Caribbeans in Barbados; MXL, Mexican Ancestry from Los Angeles USA; PUR, Puerto Ricans from Puerto Rico; CLM, Colombians from Medellin; PEL, Peruvians from Lima; GIH, Gujarati Indian from Houston; PJL, Punjabi from Lahore; BEB, Bengali from Bangladesh; STU, Sri Lankan Tamil from the UK; ITU, Indian Telugu from the UK.

For example, most of the HLA-A29-positive cases in the Luhya in Webuye (LWT in **Figure 3.3**) of Kenya also carry the BU risk variant near *ERAP2*, a population where no BU has been reported. In contrast, the combined risk polymorphisms are only observed in HLA-A29-positive individuals in Western-European populations in which BU is "endemic", with the exception of Puerto Ricans (PUR in **Figure 3.4**). However, the majority (>60%) of Puerto Ricans is of European ancestry and the samples from this population were collected throughout the entire country (i.e., predominantly Caucasian)[64]. Furthermore, BU is reported in Puerto Ricans (several Puerto Rican BU cases are reported in the *Retina Image Bank*; file numbers 6191 and 6178)[65]. In contrast, the Tuscany population (TSI in **Figure 3.4)** includes samples collected from a small town near Florence in Italy. In this population the combination of HLA-A29 and the ERAP1-ERAP2 polymorphisms is rare. These data do not necessarily represent all individuals of a population of a country that is of mixed ancestry (e.g., BU is reported in Northern Italy[66]), but serves to explain why BU is very rare or non-existing in populations where the genetic combination associated with BU risk is exceptional.

This also implies that the ERAP1, ERAP2, and HLA-A29 collectively drive the pathogenesis of BU. We do like to emphasize that the number of individuals "burdened" with the "birdshotgenotype" still exceeds the estimated cases in each population (~1% of people from Western-European ancestry, of which about 1 in 500 develop BU as a rough estimate). Here, it is good to consider that the cause of HLA-A29-dependent BU is most likely heterogenous and in some patients may be mediated by genetic susceptibility imprinted in *ERAP* genes, while in others ERAPs may be dysregulated by alternative mechanisms. For example, ERAP1 is tightly regulated by TNF-alpha, a pro-inflammatory cytokine that is increased in concentration in eye fluids of BU patients and blocking TNF-alpha by anti-TNF therapy alleviates severe symptoms of BU[67-70]. Polymorphisms linked to *ERAP1* and *ERAP2* genes are also associated with other HLA class I associated conditions that manifest with non-infectious uveitis, including HLA-B27-associated anterior uveitis and ankylosing spondylitis, or HLA-B51-associated Behcet's disease[71-73]. This supports the interdependence of ERAPs and HLA class I in the pathophysiology of non-infectious uveitis.

ERAP1 and ERAP2 in the antigen presentation pathway

The antigen presenting pathway for HLA(-A) starts with the degradation of cellular proteins (proteolysis) by the proteasome, a continuous and normal process to eliminate dysfunctional or mature proteins into shorter peptides[26,27]. A selection of peptides up to 20 amino acids long are transported into the endoplasmic reticulum (ER) by the *Transporter associated with antigen processing* (or TAP) and trimmed to generally 8-10 amino acid long peptides by ERAP1 and ERAP2[26,27,74]. ERAP1 and ERAP2 are specialized aminopeptidases that reside in ER (hence their name) where they each trim a proportion of the antigenic peptide pool before the peptides bind to HLA class I molecules for presentation at the cell surface[74].

Structural studies have shown that the trimming process involves sequestering the entire peptide sequence inside the enzyme's cavity after which the N-terminal (first amino acid in the peptide sequence) is trimmed off[75,76], which indicates that the majority of peptides are trimmed before binding[77] to HLA class I (e.g. HLA-A29). Some HLA class II alleles lack protection of their peptide-binding groove when exposed to peptides in the endoplasmic reticulum and bind these peptides before their transportation to the cell surface[78]. It's not unlikely that ERAPs may influence the peptide cargo presented by a selective group of these 'unprotected' HLA class II alleles, but this is unexplored. Also, 'free' ERAP1 and ERAP2 is found in body fluids and blood[79], and can be secreted by stimulated immune cells[80]. Notwithstanding these other functions, the strong genetic association with HLA-A29-associated BU implicates ERAP-dependent antigen presentation by HLA-A29 as a key disease pathway in BU. To better understand how ERAP1 and ERAP2 modulate HLA-A29, let's first detail the genetic associations mapped to these genes.

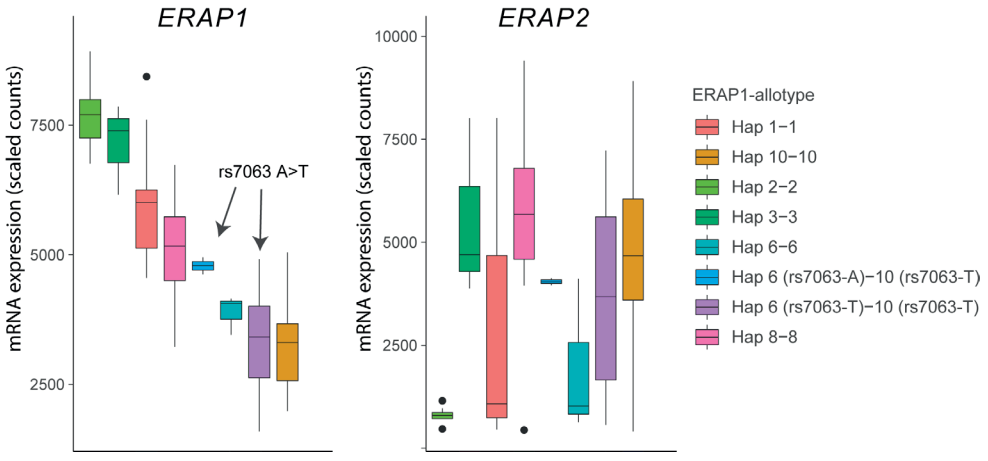

Figure 3.4: The splice associated variant rs7063 associated with haplotype 6 (97% of all *Hap6*) and 10 (99% of all *Hap10*) of *ERAP1* mediates low expression of these haplotypes in lymphoblastoid cells. Gene expression data for *ERAP1* and *ERAP2* from 85 homozygous or heterozygous cell lines with indicated haplotypes (and rs7063 allele) were obtained from available RNA-sequencing data of 358 lymphoblastoid cell lines from European ancestry of the GEUVADIS cohort (loaded using the *recount* R package)[62]. Note that in cell lines that harbor the haplotype 10 containing the T allele of rs7063 genotype, the rs7063 genotype in Hap6 governs the expression of total *ERAP1* and that Hap6/Hap10 cell lines homozygous for the T allele of rs7063 show similar low expression compared to Hap10/Hap10 cell lines. The gene expression pattern for *ERAP2* (right plot) in the same samples does not mimic *ERAP1* gene expression patterns, but reflects the nonrandom distribution of the ERAP2-protein coding haplotype across common *ERAP1* haplotypes, as we previously described[61]. In particular haplotype 2 (Hap2; encoding *allotype 2*) is found infrequently in conjunction with ERAP2 haplotype A and, thus, shows low overall expression for ERAP2 in the *Hap2* homozygous cell lines in this example (n = 9).

ERAP1 and birdshot

The *ERAP1* gene encodes various distinct ERAP1 haplotypes (a group of polymorphisms inherited together) that encode functionally different protein variants (which are termed "allotypes") with markedly different capacity to cut antigen peptides in terms of speed and specificity[61,81]. Genetics studies showed that the C allele of the polymorphism rs2287987 was more frequently seen in patients with BU[61]. The rs2287987-C is found almost exclusively in the haplotype (named *Hap10*) that encodes *Allotype 10*[61]. Detailed description of ERAP1 polymorphisms and their effects on functions of ERAP1 can be found elsewhere[74,82]. Briefly, the minor C allele of rs2287987 located in exon 6 of ERAP1 results in the change of Methionine to Valine at amino acid position 349 in ERAP1. This amino acid change occurs in the active site of ERAP1 next to the hallmark zinc-binding motif of the family of M1 zinc metallopeptidases (H-E-X-X-H-(X)18-E motif) and affects the enzymatic activity of the enzyme. However, the rs2287987 bearing allotype 10 contains additional polymorphisms that indirectly affect the specificity or activity by changing the structural conformation of the enzyme[83,84]. Note that rs2287987-C is also common in African populations (**Figure 3.3**) but it often resides in ERAP1 haplotypes different from Hap10. Allotype 10 is characterized by enzymatic activity that is magnitudes lower compared to other characterized allotypes of ERAP1, but also shows relatively low expression[61]. The latter feature is caused by moderate LD between the C allele of rs2287987 and a splice interfering variant (T allele of rs7036[85] located upstream in an untranslated region of *ERAP1* (rs7063 is present in >90% of *Hap10* and typically <5-10% of other common haplotypes of *ERAP1*[61]). Although low expression and low enzymatic activity of *Hap10* is often mentioned in the same breath in discussions of its pathogenic contribution to disease, rs2287987 is associated with BU independently from rs7063, thus, the BU risk linked to rs2287987 represents more likely the diminished enzymatic activity of ERAP1[61]. In fact, rs7063-T is also found in >90% of another common haplotype of ERAP1 named Hap6[61].

Because the vast majority of Hap6 shares the T allele of rs7063 with Hap10[61], gene expression data from the 1000 Genomes project shows that consequently the expression of the two haplotypes is comparably low (**Figure 3.4**). Although the ERAP1 expression levels have been shown to influence the immunopeptidome of HLA-A29[86], the low expressed Hap6 is not associated with BU[61] and makes it more plausible that the highly distinct enzymatic features of Hap10 contribute to the susceptibility to BU. This is further supported by the fact that the highly active ERAP1 allotype encoded by *Hap2*, the functional "antagonist" of Hap10, is protective against BU[61]. Because of these differences in trimming capacity, the lack of destruction of a uveitogenic epitope is a plausible mechanism for disease.

ERAP2 and birdshot

Of the two common haplotypes (A and B) of *ERAP2* detected in the population, *haplotype A* (HapA) encodes the canonical full length ERAP2 protein[87], but is consists of many polymorphisms that are located also far outside *ERAP2* and deep into the *LNPEP* gene. The polymorphisms of *HapA* outside *ERAP2* are located in the intragenic regions of the *LNPEP* gene and are not encoded into the *LNPEP* gene products. *Haplotype B* (HapB) contains a polymorphism (the G allele of rs2248734) that changes a splice region and facilitates intronic read-through until a stop codon, which under steady state conditions targets the transcript for

destruction and results in barely detectable levels of the full length ERAP2 protein[87]. However, HapB has been shown to produce a truncated ERAP2 protein in response to infection by various microbial pathogens, interferon alpha or bacterial lipopolysaccharides[88-90]. The strongest association at *5q15* is linked to the polymorphisms in HapA (tagged by rs10044354 in an intragenic location of *LNPEP*). We showed that this signal did not influence the splicing or expression of the *LNPEP* gene, but showed that high *ERAP2* expression controlled by this genetic signal embedded in HapA is a risk factor for BU[34,61]. Here we note that the polymorphism rs10044354 (and variants in LD) is independently associated with BU from the polymorphism rs2248374 that governs splicing of *ERAP2* into its main haplotypes[61]. Data from the *The Genotype-Tissue Expression (GTEx) project* supports that rs10044354 is strongly associated with the expression of *ERAP2* and mildly impacts the expression of *LNPEP* across various tissues[91]. However, the effect sizes of rs10044354 on the expression of other nearby genes *ERAP1* and *CAST* are in the same range as for *LNPEP* and of unknown biological significance. In summary, high ERAP2 expression is a significant risk factor for BU in HLA-A29-positive individuals. The generation of *uveitogenic* peptides by ERAP2, which hypoactive ERAP1 fails to destroy, is a plausible disease mechanism for BU.

ERAP1 and ERAP2 shape the HLA-A29 immunopeptidome

Both ERAP1 and ERAP2 have been shown to affect the HLA-A29 peptidome of cell model systems[86,92], which has been reviewed in detail elsewhere[74]. In short, by global assessment of the immunopeptidome, active ERAP1 allotypes (e.g. *Hap2*) decrease the length of peptides of 10 amino acids or longer (10-mers), with a net increase of 9-mers[86]. In the presence of active ERAP1 allotypes, the number of peptides with phenylalanine (F) and tyrosine (Y) at the first two amino acids of the peptide sequence (the N-terminal position 1 [P1] or 2 [P2]) of the binding peptides was slightly increased[86]. ERAP2 shapes the HLA-A29 immunopeptidome predominantly by destruction of peptides with a P1 amino acid that are preferred substrates for ERAP2, predominantly Lysine (K), Arginine (R), and Alanine (A)[93]. Large aromatic amino acids F and Y are poor substrates for ERAP2. Because ERAP2 destroys competing peptides

that harbor optimal residues (K, R, or A at P1) for ERAP2, peptides that contain F or Y at P1 consequently make up a relatively larger proportion of the available antigen peptides to bind HLA-A29 and become "over-represented" in the presence of ERAP2[43,92].

Other studies from the López de Castro group also demonstrated these ERAP2 effects on the immunopeptidome of risk HLA allotypes of other types of uveitis, such as HLA-B27[94]. In a recent study, we demonstrated that the effect of ERAP2 on P1 is actually a common feature of ERAP2 observable in the immunopeptidomes of all HLA class I alleles expressed by the cell[43]. Intriguingly, Abelin and coworkers showed that peptides presented by HLA class I allotypes show a depletion for K, R and A residues at P1, which we believe can be attributed to the fact that their studied cell line expresses ERAP2[60]. So perhaps ERAP2 is evolutionary designed to destroy epitopes with these characteristics as a means to lower the immunogenicity of the presented immunopeptidome. This hypothesis comes from the observation that cancer patients with high ERAP2 expression showed worse overall survival after checkpoint inhibitor therapy (allowing T cells to kill cancer cells), relative to those with low ERAP2 expression[95]. In other words, when T cells are "licensed" to attack tumors unrestrictedly, immune responses are more dependent on the level of antigen presentation to T cells. Here, ERAP2 may influence the HLA class I immunopeptidome so it provides less T cell epitopes to destroy tumors (and perhaps normal tissue, but this was not evaluated). This may in part be explained by the fact that the side chains of the amino acids at P1 influence the spatial configuration of amino acid position 167 in HLA-A, which has been shown to tune the peptide recognition by T cells and affect the peptide binding repertoire[49,96]. Here, the amino acids K and R induce a similar configuration of position 167 that is distinct from the configuration the alpha domain adapts at this position if P1 contains a F or Y[96], which functionally parallels the preference for trimming these amino acids by ERAP2. Beyond the universal effects on P1, peptides that are destroyed by ERAP2 may also share additional characteristics. For example, ERAP2 also showed preference for amino acids at position 3 and 7 in the antigenic peptide[43], which matches the pockets of ERAP2 that would interact with the sidechain of these residues[75]. Similar to the effects of P1, as mentioned, the destruction of HLA-A29 epitopes by ERAP2 most likely represents a canonical function of ERAP2.

The ERAP1-ERAP2 risk-haplotype exhibits HLA-A29-specific effects

In contrast to the shared effects of ERAP2 across HLA class I immunopeptidomes, in patient derived cell lines homozygous for the risk ERAP1 allotype *Hap10*, ERAP2 facilitated the increased presentation of peptides with F or Y at P2 specifically for HLA-A29[43,92]. Because this is the same submotif that distinguishes HLA-A29 from other HLA class I alleles, this observation provides a possible explanation for the association of these genes with BU. These submotif-specific effects of ERAP2 were also detected in different source data regarding

immunopeptidomics of HLA-A29[43]. This indicates these effects of ERAP2 on HLA-A29 are generalizable, but may also help narrow down the putative disease modifying effects of the antigen presentation pathway. Recall that active ERAP1 allotypes (other than *Hap10* and in ERAP2-deficient cells) also showed a moderate increase of F at P2 in the HLA-A29 immunopeptidome[86]. However, submotif analysis of this data revealed that ERAP1 did not bias the immunopeptidome in favor of the HLA-A29-specific submotif like ERAP[43]. This may be because the pocket in which the side chain of P2 binds in ERAP2 has limited space which doesn't allow bulky aromatic residues[75], while the analogous pocket in which P2 would bind in ERAP1 is more open and could accommodate bulky residues to some degree (i.e., F or Y)[76]. Furthermore, considering individual peptides, there is low correlation between the effects of ERAP1 and ERAP2 on HLA-A29[43], which indicates context specificity and possible non-redundant pathogenic contributions to antigen presentation by HLA-A29 that increase the risk for BU. Such independent pathogenic contributions by ERAP1 and ERAP2 are supported by the genetic studies[61] of BU as discussed.

HLA-A29 and autoantigen presentation

Given that HLA-A29 is prerequisite for the development of BU, we hypothesize that disease mechanisms associated with antigen presentation are most likely driven by a limited set of epitopes (or single peptide) because of promiscuity of peptides across HLA class I[59]. Based on the submotif that is specific to HLA-A29 and supported by ERAP2, we hypothesize that 'uveitogenic' HLA-A29-restricted peptides may more likely harbor a F or Y at P2 (and a Y at PC). The importance of P2 in HLA-A29-restricted peptides is in line with the fact that the amino acids at position 62-63—which define HLA-A29—directly interact with P2 of the binding peptide (**Figure 3.1**). The hypoactive ERAP1 allotype strongly linked to BU predominantly may prevent the destruction of 9-mers or longer peptides[43,73,92]. There are examples of HLA-A29-presented 10-mers that cause strong T cell-mediated responses in humans, such as AELLNIPFLY encoded by *UGT2B17*[97,98].

Curiously, the *HLA-A*29* alleles are among the lowest expressed HLA-A alleles[99]. However, the amount of peptides presented by HLA class I only weakly correlates with HLA levels at the cell surface, plus immunopeptidome studies support that HLA-A29 is potent in presentation of peptides at the cell surface[43,45,92]. Of interest, HLA class I is generally low expressed in the retina[100], while HLA class I expression is relatively high around endothelial cells of large vessels of the choroid[101], the presumed epicenter of inflammation in BU[12]. Choroid melanocytes are densely located around these endothelial cells and have been proposed as an autoantigen source in BU etiology[1]. Perhaps BU is driven by HLA-A29-presented ERAP-dependent melanocyte-derived peptides[1,61]. This also fits the "*autoimmune surveillance of hypersecreting mutants*" (ASHM) theory, which predicts that autoantigens involved in organ-specific autoimmunity (the eye) should be linked to secreting cells such

as melanocytes[102], where autoimmunity is considered a natural tradeoff to prevent lethal disease mediated by hypersecreting mutants. Besides their more commonly known role in pigment production, choroid melanocytes have also been shown to contribute to the maintenance of the normal vasculature structure of the choroid[103]. Of interest, melanocytes can produce powerful angiogenic factors upon suppression of tyrosinase activity, the key enzyme in pigment production[104]. It is conceivable that proteins highly expressed in choroidal melanocytes are closely monitored by surveilling self-reactive T cells (following the ASHM theory), because of the potential devastating effects of hypersecreting mutants, at the cost of autoimmunity. The autoimmune conditions VKH, *vitiligo*, and *psoriasis* are a proof of principle that melanocytes harbor autoantigens that are targets for autoreactive T cells[105-108]. Gene expression or proteomic studies comparing cutaneous and choroid melanocytes are warranted to understand their potential differences to better understand the restriction of BU inflammation to the eye. Of interest, the ERAP2-promoted HLA-A29-specific peptide motif (P2-F + PC-Y) is observed in the amino acid sequence of key proteins of melanogenesis that are expressed in the eye[43]. These include a number of putative candidate peptides from melanocyte proteins, such as CFVALFVRY (SLC45A2), CFPLLRLLY (OCA2), or SFSKLLLPY (PLXNC1)[43]. Of course, functional experiments are required to validate if any of these 'potential' peptides are actually presented by HLA-A29. As mentioned, the circumstantial association with melanoma (i.e., a 'hyper' antimelanoma response) has sparked interest for this theory, but lacks evidence for any causal relation[109]. Remarkably, although HLA-A29 can effectively present melanoma epitopes[1], HLA-A29 is associated with worse survival compared to HLA-A29-negative melanoma patients[110]. This could indicate that perhaps similar to the effects of ERAP2, in general, HLA-A29 and ERAP2 may 'lower' the immunogenic peptide cargo presented to T cells, but only increase the expression of a very limited (perhaps single) antigen under specific conditions that cause BU. Alternatively, the loss of choroidal melanocytes may be collateral damage from dysfunction in the choroidal endothelium. More specifically, the disruption of a *Hedgehog*-signaling axis from choroidal endothelial cells to choroidal stromal cells (i.e., perivascular mesenchymal stem cell-like cells that suppress T cell function) resulted in the loss of choroid melanocytes and illustrates a key role for the choroidal endothelium for the maintenance of choroidal immune homeostasis[111].

The retinal S-antigen has long been considered as a major autoantigen for BU, because S-antigen causes a birdshot-like phenotype in primate models[112,113] and T cells from patients proliferate after stimulation with S-antigen[24,114]. However, S-antigen immune reactivity is widespread among clinically distinct phenotypes of uveitis and linked to T helper cell responses (linked to HLA class II), which suggests it plays a role in BU independent of HLA-A29, perhaps at later stages of the disease. This is in line with the retinal lesions observed in BU patients and suggests the retinal S-antigen may have a role at the clinical stage. However, also other retinal proteins contain peptides that may be presented by HLA-A29[109]. Previous *in vitro* studies determined that peptides derived from the S-antigen can bind to HLA-A29[115],

but further research using immunopeptidomics of cells expressing S-antigen are required to define the HLA-A29 presented epitopes of S-antigen. We recently identified that a naturally HLA-A29-presented peptide of S-antigen is VTLTCAFRY and currently assess if this peptide is also recognized by T cells of patients[43].

The microbiome, TH17 cells, and HLA-A29

The *commensal microbiome* is a fast universe of diverse and mostly uncharacterized microbial species which inhabit tissues such as the skin and gastrointestinal tract where they collectively influence the functions of the immune system[116]. For example, CD8+ T cells are primed by microbial derived metabolites and MHC-I presented microbial derived peptides to cross-react with cancer antigens as a means to facilitate anti-tumor immunity[117,118]. Gut microbiome dysbiosis is observed in patients with inflammatory conditions and considered to cause disturbance of systemic immune homeostasis in uveitis[119]. In animal models, gut commensals have been shown to directly activate T helper 17 (Th17) cells to trigger uveitis[120]. This is of interest, because BU patients show increased numbers of blood Th17 cells and elevated levels of Th17-cytokines[68,121-123]. Of interest, Th17 cells induced by infection such as the fungal commensal *C. Albicans* may persist and aggravate autoimmune disease of the kidney[124]. Protective anti-*C. albicans* responses by Th17 cells have also paradoxically been shown to result in inflammatory lung disease or inflammatory bowel disease in some individuals[125]. Although *C. albicans* infection can affect the choroid and retina in a small percentage of patients[126], this shows a very different clinical phenotype. Regardless, the Th17-signature in BU could be related to changes in the microbiome. Studies of the microbiome of patients with BU are not yet conducted, the first study of HLA-A29-positive individuals as a whole show a distinct intestinal microbiome composition[127] as demonstrated for HLA-B27-positive or HLA-DRB1-positive controls[128]. In fact, microbiome similarity is observed in individuals who shared HLA alleles[129], which suggests that HLA influences the composition of the gut microbiome in part as a canonical feature of the immune homeostasis. The interaction of the microbiome in antigen-presentation via HLA-A29 in the disease mechanisms of BU requires further investigation, ideally by integrating the novel insights from studies of ERAP1 and ERAP2. Of interest, HLA class I bound by *Killer immunoglobulin-Like Receptors* (KIRs) on T cells promotes the expansion of Th17 cells in patients with HLA-B27 pathologies[130]. Furthermore, specific modulation of ERAP1 has been shown to influence Th17 expansion[131]. Therefore, it would be interesting to determine if similar biological mechanisms are linking HLA-A29 to Th17 responses in BU.

KIR receptors and birdshot

BU may be driven by additional inflammatory genes since its genetic profile displayed shared genetic contributions with other inflammatory conditions, including *systemic lupus erythema* and *Neuromyelitis optica*, that both involve the eye[132]. Among these may also be additional factors of the antigen presentation pathway, including the autophagy gene *TECPR2* previously reported[34] or *Killer immunoglobulin-Like Receptor* (KIR, KIRs) genes[133]. *KIR* genes have been associated with BU, however, the allele frequencies of controls used in a study of BU patients may not be representative for European populations and stringent correction for multiple testing is required to avoid false-positives, which may influence the outcomes of *KIR* associations in BU[133,134]. Regardless, KIRs are important receptors for T cells, but also *Natural Killer* (NK) *cells*, an understudied immune cell in the context of non-infectious uveitis that is decreased in the circulation of BU patients[135]. Curiously, immunosuppression therapy restores the number of NK cells in patients with uveitis[136]. The role of KIRs in BU also merits further functional investigation because NK cells have been shown to get activated by HLA class I by altering the presented peptide[137]. It will be interesting to explore the role of the *ERAP1-ERAP2* haplotype in peptide presentation by HLA-A29 and NK cell responses in patients. However, in HLA-B27-associated ankylosing spondylitis, the strong genetic interaction of *ERAP1* with *HLA-B*27* was independent from genetic associations with *KIR* genes, suggesting that the disease mechanisms of ERAP and HLA class I may be mostly distinct from interaction of KIRs with HLA class I[138], and perhaps represent complementary mechanisms such as shown for free heavy chain expression by HLA-B27 and KIR interaction[131], while ERAP may mediated antigen-specific T cell responses. Indeed, T cell receptor (TCR) analysis of CD8+ T cells in patients with AS suggest differential antigen exposure[139] and similar studies of TCR repertoires of BU are currently underway.

Concluding remarks

In this review, we discussed how key features of the antigen presentation pathway predispose to eye-specific autoimmunity in BU. The prerequisite forHLA-A29 and the enrichment for functional polymorphisms that affect the function of antigen processing enzymes ERAP1 and ERAP2 point toward a key contribution for the antigen presentation pathway in the etiology of BU. Using functional studies, we are beginning to understand how ERAPs shape the immunopeptidome of HLA-A29 and a growing body of evidence is closing in on their disease modifying effects. This will help to better predict the outcome of pharmacological interference of ERAPs activity using newly available small molecule inhibitors[140] that may soon be applied as a high precision medicine to halt autoimmunity and restore eye health in patients, while leaving immunity toward pathogens and cancerous tissues intact.

References

1. Kuiper J, Rothova A, de Boer J, Radstake T. The immunopathogenesis of birdshot chorioretinopathy; a bird of many feathers. Prog Retin Eye Res (2015) 44:99–110. doi: 10.1016/j.preteyeres.2014.11.003
2. Testi I, Ajamil-Rodanes S, AlBloushi AF, Pavesio C. Peripheral Capillary Non-perfusion in Birdshot Retinochoroiditis: A Novel Finding on Ultrawidefield Fluorescein Angiography. Ocul Immunol Inflamm (2020) 1–4. doi: 10.1080/09273948.2020.1758157
3. Papadia M, Jeannin B, Herbort CP. OCT findings in birdshot chorioretinitis: a glimpse into retinal disease evolution. Ophthalmic surgery, lasers imaging. Off J Int Soc Imaging Eye (2012) 43:S25–31. doi: 10.3928/15428877-20120816-01
4. Elahi S, Lages V, Jeannin B, Herbort CP. Advanced Cases of Birdshot HLAA29 Retinochoroiditis: Prevalence and Characteristics. Klin Monbl Augenheilkd (2020) 237:431–40. doi: 10.1055/a-1081-1683
5. Lee J, Smith WM, Goldstein DA. Birdshot chorioretinopathy presenting in a teenager. Am J Ophthalmol Case Rep (2020) 19:100807. doi: 10.1016/j.ajoc.2020.100807
6. Minos E, Barry RJ, Southworth S, Folkard A, Murray PI, Duker JS, et al. Birdshot chorioretinopathy: Current knowledge and new concepts in pathophysiology, diagnosis, monitoring and treatment. Orphanet J Rare Dis (2016) 11:1–17. doi: 10.1186/s13023-016-0429-8
7. Kiss S, Ahmed M, Letko E, Foster CS. Long-term follow-up of patients with birdshot retinochoroidopathy treated with corticosteroid-sparing systemic immunomodulatory therapy. Ophthalmology (2005) 112:1066–71. doi:10.1016/j.ophtha.2004.12.036
8. You C, Lasave AF, Kubaisi B, Syeda S, Ma L, Wai KCK, et al. Long-term outcomes of systemic corticosteroid-sparingimmunomodulatory therapy for Birdshot Retinochoroidopathy. Ocul Immunol Inflamm (2020) 28(6):966–74. doi: 10.1080/09273948.2019.1641610
9. Lages V, Skvortsova N, Jeannin B, Gasc A, Herbort CP. Low-grade 'benign' birdshot retinochoroiditis: prevalence and characteristics. Int Ophthalmol (2019) 39:2111—2120. doi: 10.1007/s10792-018-1050-8
10. Pepple KL, Chu Z, Weinstein J, Munk MR, Van Gelder RN, Wang RK, et al. Use of En Face Swept-Source Optical Coherence Tomography Angiography in Identifying Choroidal Flow Voids in 3 Patients With Birdshot Chorioretinopathy. JAMA Ophthalmol (2018) 136:1288–92. doi: 10.1001/jamaophthalmol.2018.3474
11. Elahi S, Herbort CPJ. Vogt-Koyanagi-Harada Disease and Birdshot Retinochoroidopathy, Similarities and Differences: A Glimpse into the Clinicopathology of Stromal Choroiditis, a Perspective and a Review. Klin Monbl Augenheilkd (2019) 236:492–510. doi: 10.1055/a-0829-6763
12. Böni C, Thorne JE, Spaide RF, Ostheimer TA, Sarraf D, Levinson RD, et al. Choroidal Findings in Eyes With Birdshot Chorioretinitis Using Enhanced-Depth Optical Coherence Tomography. Invest Ophthalmol Vis Sci (2016) 57:OCT591–9. doi: 10.1167/iovs.15-18832

13. Balci O, Jeannin B, Herbort CPJ. Contribution of dual fluorescein and indocyanine green angiography to the appraisal of posterior involvement in birdshot retinochoroiditis and Vogt-Koyanagi-Harada disease. Int Ophthalmol (2018) 38:527–39. doi: 10.1007/s10792-017-0487-5
14. Papadia M, Herbort CP. New concepts in the appraisal and management of birdshot retinochoroiditis, a global perspective. Int Ophthalmol (2015) 35:287–301. doi: 10.1007/s10792-015-0046-x
15. Shah KH, Levinson RD, Yu F, Goldhardt R, Gordon LK, Gonzales CR, et al. Birdshot chorioretinopathy. Surv Ophthalmol (2005) 50:519–41. doi:10.1016/j.survophthal.2005.08.004
16. Sohn EH, Chirco KR, Folk JC, Mullins RF. Clinicopathological Correlation In A Patient With Previously Treated Birdshot Chorioretinopathy. Retin cases Brief Rep (2017) 11:344–7. doi: 10.1097/ICB.0000000000000367
17. Böni C, Thorne JE, Spaide RF, Ostheimer TA, Sarraf D, Levinson RD, et al. Fundus Autofluorescence Findings in Eyes With Birdshot Chorioretinitis. Invest Ophthalmol Vis Sci (2017) 58:4015–25. doi: 10.1167/iovs.17-21897
18. Pulido JS, Canal I, Salomão D, Kravitz D, Bradley E, Vile R. Histological findings of birdshot chorioretinopathy in an eye with ciliochoroidal melanoma. Eye (2012) 26:862–5. doi: 10.1038/eye.2012.10
19. Gaudio PA, Kaye DB, Crawford JB. Histopathology of birdshot retinochoroidopathy. Br J Ophthalmol (2002) 86:1439–41. doi: 10.1136/bjo.86.12.1439
20. Acaba-Berrocal LA, Lucio-Alvarez JA, Mashayekhi A, Ho AC, Dunn JP, Shields LA, et al. Birdshot-like Chorioretinopathy Associated With Pembrolizumab Treatment. JAMA Ophthalmol (2018) 136:1205–7. doi:10.1001/jamaophthalmol.2018.1851
21. Hassman L, Warren M, Huxlin KR, Chung MM, xu l. Evidence of melanoma immunoreactivity in patients with Birdshot retinochoroidopathy. Invest Ophthalmol Vis Sci (2017) 58:5745.
22. Naveh HP, Rao UNM, Butterfield LH. Melanoma-associated leukoderma - immunology in black and white? Pigment Cell Melanoma Res (2013) 26:796–804. doi: 10.1111/pcmr.12161
23. Ryan SJ, Maumenee AE. Birdshot retinochoroidopathy. Am J Ophthalmol (1980) 89:31–45. doi: 10.1016/0002-9394(80)90226-3
24. Nussenblatt RB, Mittal KK, Ryan S, Richard Green W, Edward Maumenee A. Birdshot Retinochoroidopathy Associated with Hla-A29 Antigen and Immune Responsiveness to Retinal S-Antigen. Am J Ophthalmol (1982) 94:147–58. doi: 10.1016/0002-9394(82)90069-1
25. Herbort CP, Pavésio C, LeHoang P, Bodaghi B, Fardeau C, Kestelyn P, et al. Why birdshot retinochoroiditis should rather be called 'HLA-A29 uveitis'? Br J Ophthalmol (2017) 101:851–5. doi: 10.1136/bjophthalmol-2016-309764
26. Rock KL, Reits E, Neefjes J. Present Yourself! By MHC Class I and MHC Class II Molecules. Trends Immunol (2016) 37:724–37. doi: 10.1016/j.it.2016.08.010
27. Neefjes J, Ovaa H. A peptide's perspective on antigen presentation to the immune system. Nat Chem Biol (2013) 9:769–75. doi: 10.1038/nchembio.1391

28. Tsui E, Takhar JS, Joye A, Ahmad TR, Acharya NR, Gonzales JA. High Resolution DNA Typing of Human Leukocyte Antigen A29 in Familial Birdshot Chorioretinopathy. Ocul Immunol Inflamm (2019) 1–4. doi: 10.1080/09273948.2019.1682173
29. Arnaiz-Villena A, Gomez-Casado E, Martinez-Laso J. Population genetic relationships between Mediterranean populations determined by HLA allele distribution and a historic perspective. Tissue Antigens (2002) 60:111–21. doi: 10.1034/j.1399-0039.2002.600201.x
30. Knezevic A, Munk MR, Pappas F, Merrill PT, Goldstein DA. HLA-A29-Positive Birdshot Chorioretinopathy In An African American Patient. Retin cases Brief Rep (2016) 10:201–4. doi: 10.1097/ICB.0000000000000224
31. Baddar D, Goldstein DA. HLA-A29-positive Birdshot Chorioretinopathy in a Hispanic Patient. Ocular Immunol Inflammation (2016) 24:110–2. doi:10.3109/09273948.2014.928733
32. LeHoang P, Ozdemir N, Benhamou A, Tabary T, Edelson C, Betuel H, et al. HLA-A29.2 subtype associated with birdshot retinochoroidopathy. Am J Ophthalmol (1992) 113:33–5. doi: 10.1016/S0002-9394(14)75749-6
33. Márquez A, Cordero-Coma M, Martín-Villa JM, Gorroño-Echebarría MB, Blanco R, Díaz Valle D, et al. New insights into the genetic component of non-infectious uveitis through an Immunochip strategy. J Med Genet (2017) 54:38–46. doi: 10.1136/jmedgenet-2016-104144
34. Kuiper JJW, Van Setten J, Ripke S, Van 'T Slot R, Mulder F, Missotten T, et al. A genome-wide association study identifies a functional ERAP2 haplotype associated with birdshot chorioretinopathy. Hum Mol Genet (2014) 23:6081–7. doi: 10.1093/hmg/ddu307
35. Szpak Y, Vieville JC, Tabary T, Naud MC, Chopin M, Edelson C, et al. Spontaneous retinopathy in HLA-A29 transgenic mice. Proc Natl Acad Sci USA (2001) 98:2572–6. doi: 10.1073/pnas.051595998
36. Mattapallil MJ, Wawrousek EF, Chan CC, Zhao H, Roychoudhury J, Ferguson TA, et al. The Rd8 mutation of the Crb1 gene is present in vendor lines of C57BL/6N mice and embryonic stem cells, and confounds ocular induced mutant phenotypes. Invest Ophthalmol Vis Sci (2012) 53:2921–7. doi: 10.1167/iovs.12-9662
37. Middleton D, Williams F, Meenagh A, Daar AS, Gorodezky C, Hammond M, et al. Analysis of the distribution of HLA-A alleles in populations from five continents. Hum Immunol (2000) 61:1048–52. doi: 10.1016/S0198-8859(00)00178-6
38. Luo M, Embree J, Ramdahin S, Ndinya-Achola J, Njenga S, Bwayo JB, et al. HLA-A and HLA-B in Kenya, Africa: allele frequencies and identification of HLA-B*1567 and HLA-B*4426. Tissue Antigens (2002) 59:370–80. doi:10.1034/j.1399-0039.2002.590503.x
39. Abi-Rached L, Gouret P, Yeh J-H, Di Cristofaro J, Pontarotti P, Picard C, et al. Immune diversity sheds light on missing variation in worldwide genetic diversity panels. PloS One (2018) 13:e0206512. doi: 10.1371/journal.pone.0206512
40. Robinson J, Barker DJ, Georgiou X, Cooper MA, Flicek P, Marsh SGE. IPDIMGT/HLA Database. Nucleic Acids Res (2020) 48:D948–55. doi: 10.1093/nar/gkz950

41. Donvito B, Monnet D, Tabary T, Delair E, Vittier M, Réveil B, et al. A new HLA extended haplotype containing the A*2910 allele in birdshot retinochoroidopathy: susceptibility narrowed to the HLA molecule itself. Invest Ophthalmol Vis Sci (2010) 51:2525–8. doi: 10.1167/iovs.09-4329
42. Pettersen EF, Goddard TD, Huang CC, Couch GS, Greenblatt DM, Meng EC, et al. UCSF Chimera–a visualization system for exploratory research and analysis. J Comput Chem (2004) 25:1605–12. doi: 10.1002/jcc.20084
43. Venema WJ, Hiddingh S, de Boer JH, Claas FHJ, Mulder A, Den Hollander AI, et al. ERAP2 facilitates a subpeptidome of Birdshot Uveitis-associated HLA-A29. bioRxiv (2020) 2020.08.14.250654. doi: 10.1101/2020.08.14.250654
44. Reynisson B, Alvarez B, Paul S, Peters B, Nielsen M. NetMHCpan-4.1 and NetMHCIIpan-4.0: improved predictions of MHC antigen presentation by concurrent motif deconvolution and integration of MS MHC eluted ligand data. Nucleic Acids Res (2020) 48:W449–54. doi: 10.1093/nar/gkaa379
45. Sarkizova S, Klaeger S, Le PM, Li LW, Oliveira G, Keshishian H, et al. A large peptidome dataset improves HLA class I epitope predictionacross most of the human population. Nat Biotechnol (2020) 38:199–209. doi: 10.1038/s41587-019-0322-9
46. Dellgren C, Ekwelum VAC, Ormhøj M, Pallesen N, Knudsen J, Nehlin JO, et al. Low Constitutive Cell Surface Expression of HLA-B Is Caused by a Posttranslational Mechanism Involving Glu180 and Arg239. J Immunol (2016) 197:4807–16. doi: 10.4049/jimmunol.1502546
47. Moots RJ, Matsui M, Pazmany L, McMichael AJ, Frelinger JA. A cluster of mutations in HLA-A2 alpha 2 helix abolishes peptide recognition by T cells. Immunogenetics (1991) 34:141–8. doi: 10.1007/BF00205816
48. Serçinoğlu O, Ozbek P. Sequence-structure-function relationships in class I MHC: A local frustration perspective. PloS One (2020) 15:e0232849. doi: 10.1371/journal.pone.0232849
49. van Deutekom HWM, Keşmir C. Zooming into the binding groove of HLA molecules: which positions and which substitutions change peptide binding most? Immunogenetics (2015) 67:425–36. doi: 10.1007/s00251-015-0849-y
50. McMichael AJ, Gotch FM, Santos-Aguado J, Strominger JL. Effect of mutations and variations of HLA-A2 on recognition of a virus peptide epitope by cytotoxic T lymphocytes. Proc Natl Acad Sci USA (1988) 85:9194–8. doi: 10.1073/pnas.85.23.9194
51. Vasudev PG, Banerjee M, Ramakrishnan C, Balaram P. Asparagine and glutamine differ in their propensities to form specific side chain-backbone hydrogen bonded motifs in proteins. Proteins (2012) 80:991–1002. doi:10.1002/prot.24001
52. Wooldridge L, van den Berg HA, Glick M, Gostick E, Laugel B, Hutchinson SL, et al. Interaction between the CD8 coreceptor and major histocompatibility complex class I stabilizes T cell receptor-antigen complexes at the cell surface. J Biol Chem (2005) 280:27491–501. doi:10.1074/jbc.M500555200
53. McKenzie LM, Pecon-Slattery J, Carrington M, O'Brien SJ. Taxonomic hierarchy of HLA class I allele sequences. Genes Immun (1999) 1:120–9. doi: 10.1038/sj.gene.6363648

54. Hurley CK, Kempenich J, Wadsworth K, Sauter J, Hofmann JA, Schefzyk D,et al. Common, intermediate and well-documented HLA alleles in world populations: CIWD version 3.0.0. HLA (2020) 95:516–31. doi: 10.1111/tan.13811
55. Binkowski TA, Marino SR, Joachimiak A. Predicting HLA class I nonpermissive amino acid residues substitutions. PloS One (2012) 7:e41710. doi:10.1371/journal.pone.0041710
56. Maeurer MJ, Chan HW, Karbach J, Salter RD, Knuth A, Lotze MT, et al. Amino acid substitutions at position 97 in HLA-A2 segregate cytolysis from cytokine release in MART-1/Melan-A peptide AAGIGILTV-specific cytotoxic T lymphocytes. Eur J Immunol (1996) 26:2613–23. doi: 10.1002/eji.1830261112
57. Hogan KT, Clayberger C, Bernhard EJ, Walk SF, Ridge JP, Parham P, et al. A panel of unique HLA-A2 mutant molecules define epitopes recognized by HLA-A2-specific antibodies and cytotoxic T lymphocytes. J Immunol (1989)142:2097–104.
58. Doytchinova IA, Guan P, Flower DR. Identifiying human MHC supertypes using bioinformatic methods. J Immunol (2004) 172:4314–23. doi: 10.4049/jimmunol.172.7.4314
59. Rao X, Hoof I, Costa AII, van Baarle D, Kesmir C. HLA class I allele promiscuity revisited. Immunogenetics (2011) 63:691–701. doi: 10.1007/s00251-011-0552-6
60. Abelin JG, Keskin DB, Sarkizova S, Hartigan CR, Zhang W, Sidney J, et al. Mass Spectrometry Profiling of HLA-Associated Peptidomes in Mono-allelic Cells Enables More Accurate Epitope Prediction. Immunity (2017) 46:315–26. doi: 10.1016/j.immuni.2017.02.007
61. Kuiper JJW, Van Setten J, Devall M, Cretu-Stancu M, Hiddingh S, Ophoff RA, et al. Functionally distinct ERAP1 and ERAP2 are a hallmark of HLAA29-(Birdshot) Uveitis. Hum Mol Genet (2018) 27:4333–43. doi: 10.1101/338228
62. Lappalainen T, Sammeth M, Friedländer MR, ’t Hoen PAC, Monlong J, Rivas MA, et al. Transcriptome and genome sequencing uncovers functional variation in humans. Nature (2013) 501:506–11. doi: 10.1038/nature12531
63. Auton A, Brooks LD, Durbin RM, Garrison EP, Kang HM, Korbel JO, et al. A global reference for human genetic variation. Nature (2015) 526:68–74. doi: 10.1038/nature15393
64. Pérez-Mayoral J, Soto-Salgado M, Shah E, Kittles R, Stern MC, Olivera MI, et al. Association of genetic ancestry with colorectal tumor location in Puerto Rican Latinos. Hum Genomics (2019) 13:12. doi: 10.1186/s40246-019-0196-4
65. Marrero FM, De Jesus E, Alvarez S, Mendez Bermudez IJ, Vila M, Marrero FM, Santos C, et al. Characteristics, Upon Presentation, of a Cohort of Hispanic Patients with Birdshot Retinochoroidopathy. P R Health Sci J (2020) 39(3):249–53. doi: 10.1007/s10792-016-0434-x
66. Cimino L, Aldigeri R, Marchi S, Mastrofilippo V, Viscogliosi F, Coassin M, et al. Changes in patterns of uveitis at a tertiary referral center in Northern Italy: analysis of 990 consecutive cases. Int Ophthalmol (2018) 38:133–42. doi: 10.1007/s10792-016-0434-x
67. Garancher A, Suzuki H, Haricharan S, Chau LQ, Masihi MB, Rusert JM, et al. Tumor necrosis factor overcomes immune evasion in p53-mutant medulloblastoma. Nat Neurosci (2020) 23:842–53. doi: 10.1038/s41593-020-0628-4

68. Kuiper JJW, Mutis T, de Jager W, de Groot-Mijnes JDF, Rothova A. Intraocular interleukin-17 and proinflammatory cytokines in HLA-A29-associated birdshot chorioretinopathy. Am J Ophthalmol (2011) 152:177–82.e1. doi: 10.1016/j.ajo.2011.01.031
69. Huis in het Veld PI, van Asten F, Kuijpers RWAM, Rothova A, De Jong EK, Hoyng CB. Adalimumab Therapy For Refractory Birdshot Chorioretinopathy. Retina (2019) 39:2189–97. doi: 10.1097/IAE.0000000000002281
70. Steeples LR, Spry P, Lee RWJ, Carreño E. Adalimumab in refractory cystoid macular edema associated with birdshot chorioretinopathy. Int Ophthalmol (2018) 38:1357–62. doi: 10.1007/s10792-017-0592-5
71. Kirino Y, Bertsias G, Ishigatsubo Y, Mizuki N, Tugal-Tutkun I, Seyahi E, et al. Genome-wide association analysis identifies new susceptibility locifor Behcet's disease and epistasis between HLA-B*51 and ERAP1. NatGenet (2013) 45:202–7. doi: 10.1038/ng.2520
72. Evans DM, Spencer CCA, Pointon JJ, Su Z, Harvey D, Kochan G, et al. Interaction between ERAP1 and HLA-B27 in ankylosing spondylitis implicates peptide handling in the mechanism for HLA-B27 in disease susceptibility. Nat Genet (2011) 43:761–7. doi: 10.1038/ng0911-919a
73. Huang X-F, Li Z, De Guzman E, Robinson P, Gensler L, Ward MM, et al. Genomewide Association Study of Acute Anterior Uveitis Identifies New Susceptibility Loci. Invest Ophthalmol Vis Sci (2020) 61:3. doi: 10.1167/iovs.61.6.3
74. López de Castro JA. How ERAP1 and ERAP2 Shape the Peptidomes of Disease-Associated MHC-I Proteins. Front Immunol (2018) 9:2463. doi:10.3389/fimmu.2018.02463
75. Mpakali A, Giastas P, Mathioudakis N, Mavridis IM, Saridakis E, Stratikos E. Structural basis for antigenic peptide recognition and processing by Endoplasmic reticulum (ER) aminopeptidase 2. J Biol Chem (2015) 290:26021–32. doi: 10.1074/jbc.M115.685909
76. Giastas P, Mpakali A, Papakyriakou A, Lelis A, Kokkala P, Neu M, et al. Mechanism for antigenic peptide selection by endoplasmic reticulum aminopeptidase 1. Proc Natl Acad Sci (2019) 116:26709–16. doi: 10.1073/pnas.1912070116
77. Mavridis G, Arya R, Domnick A, Zoidakis J, Makridakis M, Vlahou A, et al. A systematic re-examination of processing of MHCI-bound antigenic peptide precursors by endoplasmic reticulum aminopeptidase 1. J Biol Chem (2020) 295:7193–210. doi: 10.1074/jbc.RA120.012976
78. Yamashita Y, Anczurowski M, Nakatsugawa M, Tanaka M, Kagoya Y, Sinha A, et al. HLA-DP(84Gly) constitutively presents endogenous peptides generated by the class I antigen processing pathway. Nat Commun (2017) 8:15244. doi: 10.1038/ncomms15244
79. Suhre K, Arnold M, Bhagwat AM, Cotton RJ, Engelke R, Raffler J, et al. Connecting genetic risk to disease end points through the human blood plasma proteome. Nat Commun (2017) 8:14357. doi: 10.1038/ncomms15345
80. Goto Y, Ogawa K, Nakamura TJ, Hattori A, Tsujimoto M. TLR-mediated secretion of endoplasmic reticulum aminopeptidase 1 from macrophages. J Immunol (2014) 192:4443–52. doi: 10.4049/jimmunol.1300935

81. Ombrello MJ, Kastner DL, Remmers EF. Endoplasmic reticulum-associated amino-peptidase 1 and rheumatic disease: Genetics. Curr Opin Rheumatol (2015) 27:349–56. doi: 10.1097/BOR.0000000000000189
82. Reeves E, James E. The role of polymorphic ERAP1 in autoinflammatory disease. Biosci Rep (2018) 38(4):BSR20171503. doi: 10.1042/BSR20171503
83. Harvey D, Pointon JJ, Evans DM, Karaderi T, Farrar C, Appleton LH, et al. Investigating the genetic association between ERAP1 and ankylosing spondylitis. Hum Mol Genet (2009) 18(21):4204–12. doi: 10.1093/hmg/ddp371
84. Nguyen TT, Chang SC, Evnouchidou I, York IA, Zikos C, Rock KL, et al. Structural basis for antigenic peptide precursor processing by the endoplasmic reticulum aminopeptidase ERAP1. Nat Struct Mol Biol (2011) 18(5):604–13. doi: 10.1038/nsmb.2021
85. Hanson AL, Cuddihy T, Haynes K, Loo D, Morton CJ, Oppermann U, et al. Genetic Variants in ERAP1 and ERAP2 Associated With Immune-Mediated Diseases Influence Protein Expression and the Isoform Profile. Arthritis Rheumatol (2018) 70:255–65. doi: 10.1002/art.40369
86. Alvarez-Navarro C, Martín-Esteban A, Barnea E, Admon A, López De Castro JA. Endoplasmic reticulum aminopeptidase 1 (ERAP1) polymorphism relevant to inflammatory disease shapes the peptidome of the birdshot chorioretinopathy-associated HLA-A*29:02 Antigen. Mol Cell Proteomics (2015) 14:1770–80. doi: 10.1074/mcp.M115.048959
87. Andrés AM, Dennis MY, Kretzschmar WW, Cannons JL, Lee-Lin S-Q, Hurle B, et al. Balancing selection maintains a form of ERAP2 that undergoes nonsense-mediated decay and affects antigen presentation. PloS Genet (2010) 6:e1001157. doi: 10.1371/journal.pgen.1001157
88. Tanioka T, Hattori A, Masuda S, Nomura Y, Nakayama H, Mizutani S, et al. Human leukocyte-derived arginine aminopeptidase. The third member of the oxytocinase subfamily of aminopeptidases. J Biol Chem (2003) 278:32275–83. doi: 10.1074/jbc.M305076200
89. Ye CJ, Chen J, Villani AC, Gate RE, Subramaniam M, Bhangale T, et al. Genetic analysis of isoform usage in the human anti-viral response reveals influenza-specific regulation of ERAP2 transcripts under balancing selection. Genome Res (2018) 28:1812–25. doi: 10.1101/gr.240390.118
90. Saulle I, Vanetti C, Goglia S, Vicentini C, Tombetti E, Garziano M, et al. A New ERAP2/Iso3 Isoform Expression Is Triggered by Different Microbial Stimuli in Human Cells. Could It Play a Role in the Modulation of SARSCoV-2 Infection? Cells (2020) 9:1951. doi: 10.3390/cells9091951
91. GTEx Consortium. The Genotype-Tissue Expression (GTEx) project.Nat Genet (2013)45:580–5. doi: 10.1038/ng.2653
92. Sanz-Bravo A, Martín-Esteban A, Kuiper JJW, García-Peydro M, Barnea E, Admon A, et al. Allele-specific alterations in the peptidome underlie the joint association of HLA-A*29:02 and endoplasmic reticulum aminopeptidase 2 (ERAP2) with birdshot chorioretinopathy. Mol Cell Proteomics (2018) 17:1564–77. doi: 10.1074/mcp.RA118.000778
93. López de Castro JA, Alvarez-Navarro C, Brito A, Guasp P, Martín-Esteban A, Sanz-Bravo A, et al. Molecular and pathogenic effects of endoplasmic reticulum aminopeptidases ERAP1 and ERAP2 in MHC-I-associated inflammatory disorders: Towards a unifying view. Mol Immunol (2016) 77:193–204. doi: 10.1016/j.molimm.2016.08.005

94. Martín-Esteban A, Guasp P, Barnea E, Admon A, López de Castro JA. Functional Interaction of the Ankylosing Spondylitis-Associated Endoplasmic Reticulum Aminopeptidase 2 With the HLA-B*27 Peptidome in Human Cells. Arthritis Rheumatol (Hoboken NJ) (2016) 68:2466–75. doi: 10.1002/art.39734
95. Lim YW, Chen-Harris H, Mayba O, Lianoglou S, Wuster A, Bhangale T, et al. Germline genetic polymorphisms influence tumor gene expression and immune cell infiltration. Proc Natl Acad Sci USA (2018) 115:E11701–10. doi:10.1073/pnas.1804506115
96. Coles CH, McMurran C, Lloyd A, Hock M, Hibbert L, Raman MCC, et al. T Cell Receptor interactions with Human Leukocyte Antigen govern indirect peptide selectivity for the cancer testis antigen MAGE-A4. J Biol Chem (2020) 295:11486–94. doi: 10.1074/jbc.RA120.014016
97. Terakura S, Murata M, Warren EH, Sette A, Sidney J, Naoe T, et al. A single minor histocompatibility antigen encoded by UGT2B17 and presented by human leukocyte antigen-A*2902 and -B*4403. Transplantation (2007) 83:1242–8. doi: 10.1097/01.tp.0000259931.72622.d1
98. Koziel MJ, Dudley D, Wong JT, Dienstag J, Houghton M, Ralston R, et al. Intrahepatic cytotoxic T lymphocytes specific for hepatitis C virus in persons with chronic hepatitis. J Immunol (1992) 149:3339–44.
99. René C, Lozano C, Villalba M, Eliaou J-F. 5' and 3' untranslated regions contribute to the differential expression of specific HLA-A alleles. Eur J Immunol (2015) 45:3454–63. doi: 10.1002/eji.201545927
100. Boegel S, Löwer M, Bukur T, Sorn P, Castle JC, Sahin U, et al. HLA and proteasome expression body map. BMC Med Genomics (2018) 11:36. doi:10.1186/s12920-018-0354-x
101. Goverdhan SV, Howell MW, Mullins RF, Osmond C, Hodgkins PR, Self J, et al. Association of HLA class I and class II polymorphisms with age-related macular degeneration. Invest Ophthalmol Vis Sci (2005) 46:1726–34. doi: 10.1167/iovs.04-0928
102. Korem Kohanim Y, Tendler A, Mayo A, Friedman N, Alon U. Endocrine Autoimmune Disease as a Fragility of Immune Surveillance against Hypersecreting Mutants. Immunity (2020) 52:872–84. e5. doi: 10.1016/j.immuni.2020.04.022
103. Shibuya H, Watanabe R, Maeno A, Ichimura K, Tamura M, Wakana S, et al. Melanocytes contribute to the vasculature of the choroid. Genes Genet Syst(2018) 93:51–8. doi: 10.1266/ggs.17-00058
104. Adini I, Ghosh K, Adini A, Chi Z-L, Yoshimura T, Benny O, et al. Melanocyte-secreted fibromodulin promotes an angiogenic microenvironment. J Clin Invest (2014) 124:425–36. doi: 10.1172/JCI69404
105. Sugita S, Takase H, Taguchi C, Imai Y, Kamoi K, Kawaguchi T, et al. Ocular infiltrating CD4+ T cells from patients with Vogt-Koyanagi-Harada disease recognize human melanocyte antigens. Invest Ophthalmol Vis Sci (2006)47:2547–54. doi: 10.1167/iovs.05-1547
106. Otani S, Sakurai T, Yamamoto K, Fujita T, Matsuzaki Y, Goto Y, et al. Frequent immune response to a melanocyte specific protein KU-MEL-1 in patients with Vogt-Koyanagi-Harada disease. Br J Ophthalmol (2006)90:773–7. doi: 10.1136/bjo.2005.086520

107. Frączek A, Owczarczyk-Saczonek A, Placek W. The Role of T(RM) Cells in the Pathogenesis of Vitiligo-A Review of the Current State-Of-The-Art. Int J Mol Sci (2020) 21(10):3552. doi: 10.3390/ijms21103552
108. Arakawa A, Siewert K, Stöhr J, Besgen P, Kim S-M, Rühl G, et al. Melanocyte antigen triggers autoimmunity in human psoriasis. J Exp Med (2015) 212:2203–12. doi: 10.1084/jem.20151093
109. Kuiper JJW, Rothova A, Schellekens PAW, Ossewaarde-van Norel A, BloemAC, Mutis T. Detection of choroid- and retina-antigen reactive CD8+ and CD4+ T lymphocytes in the vitreous fluid of patients with birdshot chorioretinopathy. Hum Immunol (2014) 75:570–7. doi: 10.1016/j.humimm.2014.02.012
110. Dhall A, Patiyal S, Kaur H, Bhalla S, Arora C, Raghava GPS. Computing Skin Cutaneous Melanoma Outcome From the HLA-Alleles and Clinical Characteristics. Front Genet (2020) 11:221. doi: 10.3389/fgene.2020.00221
111. Lehmann G, Hanke-Gogokhia C, Hu Y, Bareja R, Salfati Z, Ginsberg M, et al. Single-cell profiling reveals an endothelium-mediated immunomodulatory pathway in the eye choroid. J Exp Med (2020) 217(6):e20190730. doi: 10.1084/jem.20190730
112. Nussenblatt RB, Kuwabara T, de Monasterio FM,WackerWB. S-antigen uveitis in primates. A newmodel for human disease. Arch Ophthalmol (Chicago Ill 1960) (1981) 99:1090–2. doi: 10.1001/archopht.1981.03930011090021
113. Faure JP, Phuc LH, Takano S, Sterkers M, Thillaye B, De Kozak Y. [Experimental uveoretinitis induced in monkeys by retinal S antigen. Induction, histopathology (author's transl)]. J Fr Ophtalmol (1981) 4:465–72.
114. Nussenblatt RB, Gery I, Ballintine EJ, Wacker WB. Cellular immune responsiveness of uveitis patients to retinal S-antigen. Am J Ophthalmol (1980) 89:173–179. doi: 10.1016/0002-9394(80)90108-7
115. Boisgerault F, Khalil I, Tieng V, Connan F, Tabary T, Cohen JH, et al. Definition of the HLA-A29 peptide ligand motif allows prediction of potential T-cell epitopes from the retinal soluble antigen, a candidate autoantigen in birdshot retinopathy. Proc Natl Acad Sci U S A (1996) 93:3466–3470. doi: 10.1073/pnas.93.8.3466
116. Yadava K, Pattaroni C, Sichelstiel AK, Trompette A, Gollwitzer ES, Salami O, et al. Microbiota Promotes Chronic Pulmonary Inflammation by Enhancing IL-17A and Autoantibodies. Am J Respir Crit Care Med (2016) 193:975–87. doi: 10.1164/rccm.201504-0779OC
117. Fluckiger A, Daillère R, Sassi M, Sixt BS, Liu P, Loos F, et al. Cross-reactivity between tumor MHC class I-restricted antigens and an enterococcal bacteriophage. Science (2020) 369:936–42 doi: 10.1126/science.aax0701
118. Mager LF, Burkhard R, Pett N, Cooke NCA, Brown K, Ramay H, et al. Microbiome-derived inosine modulates response to checkpoint inhibitor immunotherapy. Science (2020). doi: 10.1126/science.abc3421
119. Fu X, Chen Y, Chen D. The Role of Gut Microbiome in Autoimmune Uveitis. Ophthalmic Res (2020). doi: 10.1159/000510212 120. Horai R, Caspi RR. Microbiome and Autoimmune Uveitis. Front Immunol (2019) 10:232. doi: 10.3389/fimmu.2019.00232

121. Daien V, Mura F, Martin G, Audo R, Rivière S, Konate A, et al. Th17 and regulatory T cells are increased in blood of patients with birdshot chorioretinopathy. Acta Ophthalmol (2017) 95:e161–3. doi: 10.1111/aos.12949
122. Molins B, Mesquida M, Llorenç V, de la Maza M, Adán A. Elevated Serum Immune Mediators and Subclinical Inflammation in HLA-A29-associated Birdshot Chorioretinopathy. Ocul Immunol Inflamm (2016) 24:647–52. doi:10.3109/09273948.2015.1057601
123. Yang P, Foster CS. Interleukin 21, interleukin 23, and transforming growth factor b1 in HLA-A29-associated birdshot retinochoroidopathy. Am J Ophthalmol (2013) 156:400–6.e2. doi: 10.1016/j.ajo.2013.03.004
124. Krebs CF, Reimers D, Zhao Y, Paust H-J, Bartsch P, Nuñez S, et al. Pathogeninduced tissue-resident memory T(H)17 (T(RM)17) cells amplify autoimmune kidney disease. Immunol (2020) 5:eaba4163 doi: 10.1126/sciimmunol.aba4163
125. Bacher P, Hohnstein T, Beerbaum E, Röcker M, Blango MG, Kaufmann S, et al. Human Anti-fungal Th17 Immunity and Pathology Rely on Cross-Reactivity against Candida albicans. Cell (2019) 176:1340–55.e15. doi:10.1016/j.cell.2019.01.041
126. Donahue SP, Greven CM, Zuravleff JJ, Eller AW, Nguyen MH, Peacock JEJ, et al. Intraocular candidiasis in patients with candidemia. Clinical implications derived from a prospective multicenter study. Ophthalmology (1994) 101:1302–9. doi: 10.1016/S0161-6420(94)31175-4
127. Sternes PR, Martin TM, Paley M, Diamond S, Asquith MJ, Brown MA, et al. HLA-A alleles including HLA-A29 affect the composition of the gutmicrobiome: a potential clue to the pathogenesis of birdshot retinochoroidopathy Sci Rep (2020) 10(1):17636. doi: 10.1038/s41598-020-74751-0.
128. Asquith M, Sternes PR, Costello M-E, Karstens L, Diamond S, Martin TM, et al. HLA Alleles Associated With Risk of Ankylosing Spondylitis and Rheumatoid Arthritis Influence the Gut Microbiome. Arthritis Rheumatol (Hoboken NJ) (2019) 71:1642–50. doi: 10.1002/art.40917
129. Andeweg SP, Keşmir C, Dutilh BE. Quantifying the impact of Human Leukocyte Antigen on the human gut microbiome. bioRxiv (2020). doi: 10.1101/2020.01.14.907196 2020.01.14.907196.
130. Ridley A, Hatano H, Wong-Baeza I, Shaw J, Matthews KK, Al-Mossawi H, et al. Activation-Induced Killer Cell Immunoglobulin-like Receptor 3DL2 Binding to HLA-B27 Licenses Pathogenic T Cell Differentiation in Spondyloarthritis. Arthritis Rheumatol (Hoboken NJ) (2016) 68:901–14. doi: 10.1002/art.39515
131. Chen L, Ridley A, Hammitzsch A, Al-Mossawi MH, Bunting H, Georgiadis D, et al. Silencing or inhibition of endoplasmic reticulum aminopeptidase 1 (ERAP1) suppresses free heavy chain expression and Th17 responses in ankylosing spondylitis. Ann Rheumatol Dis (2016) 75:916–23. doi: 10.1136/annrheumdis-2014-206996
132. Burren OS, Reales G, Wong L, Bowes J, Lee JC, Barton A, et al. Informed dimension reduction of clinically-related genome-wide association summary data characterises cross-trait axes of genetic risk. bioRxiv (2020). doi: 10.1101/2020.01.14.905869 2020.01.14.905869.
133. Levinson RD, Du Z, Luo L, Monnet D, Tabary T, Brezin AP, et al. Combination of KIR and HLA gene variants augments the risk of developing birdshot chorioretinopathy in HLA-A*29-positive individuals. Genes Immun (2008) 9:249–58. doi: 10.1038/gene.2008.13

134. Singh KM, Phung YT, Kohla MS, Lan BY-A, Chan S, Suen DL, et al. KIR genotypic diversity can track ancestries in heterogeneous populations: a potential confounder for disease association studies. Immunogenetics (2012) 64:97–109. doi: 10.1007/s00251-011-0569-x
135. Verhagen FH, Hiddingh S, Rijken R, Pandit A, Leijten E, Olde Nordkamp M, et al. High-Dimensional Profiling Reveals Heterogeneity of the Th17 Subset and Its Association With Systemic Immunomodulatory Treatment in Noninfectious Uveitis. Front Immunol (2018) 9:2519. doi: 10.3389/fimmu.2018.02519
136. Li Z, Lim WK, Mahesh SP, Liu B, Nussenblatt RB. Cutting edge: in vivo blockade of human IL-2 receptor induces expansion of CD56(bright) regulatory NK cells in patients with active uveitis. J Immunol (2005) 174:5187–91. doi: 10.4049/jimmunol.174.9.5187
137. Mbiribindi B, Mukherjee S, Wellington D, Das J, Khakoo SII. Spatial Clustering of Receptors and Signaling Molecules Regulates NK Cell Response to Peptide Repertoire Changes. Front Immunol (2019) 10:605. doi: 10.3389/fimmu.2019.00605
138. Hanson AL, Vukcevic D, Leslie S, Harris J, Lê Cao K-A, Kenna TJ, et al. Epistatic interactions between killer immunoglobulin-like receptors and human leukocyte antigen ligands are associated with ankylosing spondylitis. PloS Genet (2020) 16:e1008906. doi: 10.1371/journal.pgen.1008906
139. Hanson AL, Nel HJ, Bradbury L, Phipps J, Thomas R, Lê Cao K-A, et al. Altered Repertoire Diversity and Disease-Associated Clonal Expansions Revealed by T Cell Receptor Immunosequencing in Ankylosing Spondylitis Patients. Arthritis Rheumatol (Hoboken NJ) (2020) 72(8):1289–302. doi: 10.1002/art.41252
140. Georgiadis D, Mpakali A, Koumantou D, Stratikos E. Inhibitors of ER Aminopeptidase 1 and 2: From Design to Clinical Application. Curr Med Chem (2019) 26:2715–29. doi: 10.2174/0929867325666180214111849

Chapter 4

Retina-arrestin specific CD8+ T cells are not implicated in HLA-A29-positive birdshot chorioretinitis

W.J. Venema[1,2,#], S. Hiddingh[1,2,#], G.M.C. Janssen[3], J. Ossewaarde-van Norel[1], N. Dam van Loon[1], J.H. de Boer[1], P.A. van Veelen[3], J.J.W. Kuiper[1,2]

1. Department of Ophthalmology, University Medical Center Utrecht, University of Utrecht, Utrecht, the Netherlands
2. Center for Translational Immunology, University Medical Center Utrecht, University of Utrecht, Utrecht, the Netherlands
3. Center for Proteomics and Metabolomics, Leiden University Medical Center, Leiden, the Netherlands

[#]These authors contributed equally

Published in Clin. Immunol. 247, 109219 (2023)

Abstract

Background

HLA-A29-positive birdshot chorioretinitis (BCR) is an inflammatory eye disorder that is generally assumed to be caused by an autoimmune response to HLA-A29-presented peptides from retinal arrestin (SAG), yet the epitopes recognized by CD8+ T cells from patients remain to be identified.

Objectives

The identification of natural ligands of SAG presented by HLA-A29. To quantify CD8+ T cells reactive to antigenic SAG peptides presented by HLA-A29 in patients and controls.

Methods

We performed mass-spectrometry based immunopeptidomics of HLA-A29 of antigen-presenting cell lines from patients engineered to express SAG. MHC-I Dextramer technology was utilized to determine expansion of antigen-specific CD8+ T cells reactive to SAG peptides in complex with HLA-A29 in a cohort of BCR patients, HLA-A29-positive controls, and HLA-A29-negative controls.

Results

We report on the naturally presented antigenic SAG peptides identified by sequencing the HLA-A29 immunopeptidome of antigen-presenting cells of patients. We show that the N-terminally extended SAG peptide precursors can be trimmed in vitro by the antigen-processing aminopeptidases ERAP1 and ERAP2. Unexpectedly, no enhanced antigen engagement by CD8+ T cells upon stimulation with SAG peptides was observed in patients or HLA-A29-positive controls. Multiplexed HLA-A29-peptide dextramer profiling of a case-control cohort revealed that CD8+ T cells specific for these SAG peptides were neither detectable in peripheral blood nor in eye biopsies of patients.

Conclusions

Collectively, these findings demonstrate that SAG is not a CD8+ T cell auto-antigen and sharply contrast the paradigm in the pathogenesis of BCR. Therefore, the mechanism by which HLA-A29 is associated with BCR does not involve SAG.

Introduction

Birdshot chorioretinitis (BCR) is a rare inflammatory eye disease characterized by progressive T-cell infiltrates in the posterior eye segment, destruction of photoreceptors, gradual deterioration of retinal function, and declining visual abilities[1-3]. Selective inhibition of T cells by Cyclosporin A is effective for treatment of birdshot chorioretinitis which supports a T-cell mediated autoimmune aetiology[4,5].

The most distinguished molecular trait of BCR is its extreme genetic association with the *Human Leukocyte Antigen class I A*29 allele* (HLA-A29). This gene-disease link is so robust that testing positive for HLA-A29 is considered essential for diagnosis[2,6]. Other more recently identified susceptibility genes are the closely related *endoplasmic reticulum aminopeptidase* (*ERAP)1* and *ERAP2* genes[7-9], which encode enzymes specialized to shorten intracellular precursor peptides to a length that facilitates or prevents their binding to HLA class I molecules. Collectively, these molecular features strongly implicate CD8+ T-cell activation by self-antigen presentation via HLA-A29 as a key disease mechanism for BU. To date, however, the evidence for pathogenic CD8+ T cell involvement in BCR remains limited to the detection of CD8+ T-cell infiltrates in eye tissues of BCR patients[10-12].

The identification of bona fide CD8+ T cell autoantigens is challenging and highly labor and resource intensive. Consequently, to date, very few autoantigens for MHC-I-associated conditions are identified[13-15]. A long presumed (since 1982) autoantigen for BCR is the *retinal arrestin* (also known as the *retinal Soluble (S-)antigen* (SAG)), which is abundantly and specifically expressed by photoreceptors. Immunization with SAG in primates or rodents causes *experimental autoimmune uveitis* characterized by T-cell immunity directed towards the retina, with close resemblance to BCR[16,17]. Pharmacological inhibition of T cells blocks SAG-induced experimental uveitis[17]. Peripheral blood lymphocyte cultures from BCR patients show strong proliferation in response to stimulation with SAG[18] and *in vitro* binding studies support that synthetic peptides identical to fragments of the SAG can bind to HLA-A29 [19]. Consequently, SAG is generally viewed as a causal autoantigen for BCR[2,18-20], but there are no studies have provided evidence for SAG peptide recognition by CD8+ T cells in the context of HLA-A29.

In this study, we characterized the self-antigen-presenting function of HLA-A29 by lentiviral transduction of full-length SAG in antigen presenting cells from patients. We used mass-spectrometry based peptide sequencing of ligands eluted from HLA-A29 at the cell surface for unbiased SAG ligand discovery. We report on the identification of two HLA-A29-presented peptides from SAG and reveal that these peptides in complex with HLA-A29 are not recognized by CD8+ T-cells of patients with BU.

Materials & Methods

Patient-derived antigen presenting cell lines

This study was performed in compliance with the guidelines of the Declaration of Helsinki and has the approval of the local Institutional Review Board (University Medical Center Utrecht). Antigen presenting cell lines were generated by the induction of EBV-immortalised lymphoblastoid cells (LCLs) with B95-8 marmoset-derived EBV supernatant as described earlier[21]. Briefly, peripheral blood mononuclear cells (PBMCs) from two BCR patients were cultured in B95-8 marmoset-derived EBV supernatant with *Roswell Park Memorial Institute 1640* medium (RPMI 1640) supplemented with 10% heat-inactivated fetal bovine serum (FBS, Biowest Riverside), and 1μg/ml cyclosporine to remove T cells. LCL cluster formation was monitored by light microscopy and established patient-derived LCLs maintained in RPMI 1640 (10% FBS + 1% penicillin/streptomycin (Thermo Fisher Scientific)). Genotype data for single nucleotide polymorphisms at *5q15* (**Table 4.1**) from the two patients were obtained from a previous genotyping study[8]. High-resolution HLA class I typing (**Table 4.1**) was performed on genomic DNA of cell lines using SSO DNA typing (LABType HD; One Lambda).

Table 4.1. Demographics and genotype data of the patient-derived lymphoblastoid cell lines used for HLA-A29 immunopeptidomics in this study. The genotype data for HLA class I alleles and key polymorphisms (and derived haplotypes) are indicated.

Patient-derived cell line	LCL1	LCL2
Age	80	65
Sex	Female	Female
HLA class I alleles		
HLA-A	*A*29/A*03*	*A*29/A*31*
HLA-B	*B*40/B*44*	*B*40/B*45*
HLA-C	*C*03/C*16*	*C*03/C*06*
ERAP1		
Haplotype	Hap10/Hap10	Hap7/Hap8
rs27044	C/C	C/C
rs17482078	T/T	C/C
rs10050860	T/T	C/C
rs30187	C/C	C/C
rs2287987	C/C	T/T
rs27895	C/C	C/C
rs26618	T/T	T/C
rs26653	G/G	G/G
rs3734016	C/C	T/C
rs72773968	G/G	G/G
ERAP2		
Haplotype	HapA/HapA	HapA/HapA
rs2248374	A/A	A/A

S-antigen lentiviral transduction

We seeded HEK-293T cells into 10 cm dishes at a concentration of 2×10^6 cells per dish overnight in *Dulbecco's Modified Eagle Medium* (DMEM, Thermo Fisher Scientific). Cells were transfected in serum-free DMEM using Lipofectamine 2000 (Thermo Fisher Scientific) with 2nd generation packaging vectors (8.33 µg psPAX2 packaging vector and 2.77 µg pMD2.G envelope vector at a ratio of 4:1) and 2 µg of the transfer vector (Lenti ORF clone of Human S-antigen mGFP tagged, RC220057L2, *Origene*) and cultured at 37°C, 5% CO_2 for 24 hours. We replaced the medium with 10 mL DMEM supplemented with 10% FBS and collected the conditioned medium containing lentiviral particles 48 hours after transfection. We added an additional 10 mL of fresh culture medium, which was harvested after 12 hours. The first and second rounds of harvested supernatants were combined and cleared by centrifugation at 1500 rpm for 5 minutes at 4°C. Cleared supernatant was passed through a 0.45 µm filter and concentrated by ultracentrifugation (Beckman Coulter Optima centrifuge, SW32Ti rotor) for 120 minutes at 32,000 rpm. After removal of supernatant, virus pellets were resuspended in 1 mL RPMI (10% FBS, 1% penicillin/streptomycin) and stored until use at -80°C. Established LCLs ($1x10^6$ cells) were seeded in a 24-well plate and transduced with lentiviral particles and polybrene (final concentration 6 µg/mL). After 24 hours of culture, the medium was replaced for fresh RPMI (10% FBS, 1% penicillin/streptomycin) and the cells were cultured for another 3 days, without exceeding a cell concentration of $1.5x10^6$ cells/mL. Successful lentiviral transduction was evaluated by detection of GFP-positive cells by fluorescent light microscopy. We sorted GFP-positive LCLs using the BD FACSAria™ III sorter.

Western blot analysis

Immunoblotting was performed to assess protein levels of S-antigen after lentiviral transduction (S-antigen fusion protein with GFP), ERAP2 and α-tubulin (loading control) with the following antibodies: ERAP2 and α-mGFP to detect the fusion protein S-antigen-GFP. Cell lysates of LCL1 and LCL2 were prepared using the NP40 lysis buffer (1% NP40, 135 mM NaCl, 5 mM EDTA, 20 mM Tris-HCl, pH=7.4) complemented with 1:25 cOmplete protease inhibitor cocktail (Roche). The protein lysates (10 µg/lane) were separated on a 4%–20% Mini-PROTEAN TGX gel (Bio-Rad Laboratories) and transferred to a polyvinylidene difluoride membrane (Immobilon-P PVDF, Millipore). Precision Plus Protein All Blue Standards was used as the protein marker (Bio-Rad Laboratories). Membranes were blocked in 5% nonfat dry milk in TBS-T and incubated overnight at 4°C with antibodies targeting ERAP2 (1:2500, AF3830, R&D Systems), α-mGFP (1:2000, clone 2F6, TA180076, Origene). Detection of ERAP2 was done using anti-goat secondary antibody staining conjugated to horseradish peroxidase (HRP) (1:5000, DAKO) and α-mGFP was measured with anti-mouse secondary antibody conjugated to HRP (1:5000, DAKO). Protein bands were detected with Amersham ECL™ Prime Western Blotting Detection System (RPN2236, GE Healthcare) on the ChemiDoc Gel Imaging System (Bio-Rad Laboratories).

HLA-A29 immunopeptidome analysis

The immunopeptidome analysis of HLA-A29 was performed as described previously[21]. Briefly, LCL1-SAG+ cells were cultured in a medium supplemented with stable isotope labelled amino acids and combined with unlabelled CRISPR-edited cells for SILAC-labelled immuno peptidomics as described in detail in *Venema et al.*[21]. LCL2-SAG+ cells were cultured in unlabelled conditions. Frozen cell pellets (-20°C) of 1-2 × 10^9 SAG-positive LCLs were lysed in Tris-HCL buffer (Tris-HCl 50 mM, NaCl 150 mM, EDTA 5mM) with 0.5% Zwittergent® 3-12 Detergent and Roche cOmplete Protease Inhibitor Cocktail and 4°C for 2 hours. Lysates were cleared by centrifugation (10 min. 2,500 rpm, 4°C). Supernatant was harvested and centrifuged for 40 min (30,000 x g, 4°C) and pre-cleared with a 2mL CL4B column. The final supernatant was subjected to the HLA-A29-binding mAb *DK1G8*[21,22] (IgG1) immunoaffinity column for standard immunoaffinity purification[23]. Columns were washed and HLA-A29-peptide complexes eluted from the column. We dissociated complexes with 10% acetic acid filtered for peptides using a 10 kDa membrane (Microcon YM-10). Freeze dried filtrate was dissolved in 50 mM ammonium bicarbonate (pH 8.3) and subjected to C18 reverse phase columns (Oasis HLB, Waters, Milford, MA). Peptides were eluted from the C18 columns using 400 µl 10/90/0. water/acetonitrile/formic acid, v/v/v., 20/80/0.1 and 50/50/0.1 water/acetonitrile/formic acid, v/v/v, lyophilized and finally dissolved in 95/3/0.1 v/v/v water/acetonitrile/formic acid.

Mass spectrometry was performed using on-line C18 nanoHPLC MS/MS with a system consisting of an Easy nLC 1200 gradient HPLC system (Thermo, Bremen, Germany), and a (for LCL1) LUMOS mass spectrometer (Thermo) or (for LCL2) a Q Exactive Plus Hybrid Quadrupole-Orbitrap as described in detail in Venema *et al*.[21].

Mass Spectrometry Data Analysis

Processed mass spectrometry (MS) data from LCL1 (available via https://github.com/jonaskuiper/ERAP2_HLA-A29_peptidome) were obtained by filtering peptides detected in both biological replicates for 'heavy' labelled amino acids (see **Supplemental Figure 4.1**). Peptide data from LCL1 and LCL2 were filtered for peptides with a Best Mascot ion score >35 and length between 8-11 amino acids (typical length for T-cell epitopes)[24,25] (**Supplemental Table 4.1 and 4.2**).

ERAP1 and ERAP2 S-antigen peptide digestions

Recombinant ERAP1 (2334-ZN-010, R&D Systems) and ERAP2 (3830-ZN-010, R&D Systems) were used for digestion of SAG peptides (VTLTCAFRY and TVLGILVSY) and their respective natural N-terminal extended 10-mer precursor (all custom order from Pepscan Presto, NL) (**Key Resources Table**). We used the peptide SVLKSLPFTII and RGRFSGLLGR as positive controls for ERAP1 and ERAP2, and SVLKSLPFTII was also used to evaluate potential tryptic activity. Each peptide (1 µg) was individually digested with either ERAP1, ERAP2 or a combination of both ERAPs (100 ng per condition). Reactions were terminated by addition

of 5% trifluoroacetic acid (TFA) after 60 minutes incubation at 37°C. N-terminal peptide trimming was assessed using mass spectrometry comparing peptide cleavage between T0 and T1. All reactions have been performed *in duplo* in separate experiments.

HLA-A29-peptide dextramer analysis

To determine the presence of antigen-specific T cells reactive to retinal S-antigen peptides, peripheral blood mononuclear cells (PBMCs) from Birdshot patients, anonymous HLA-A29-positive controls (Buffy coat, Sanquin, Amsterdam), and HLA-A29-negative anonymous healthy blood donors with no history of ocular inflammatory disease served as controls (HC) were isolated from heparinized venous blood by standard ficoll gradient centrifugation immediately after blood withdrawal and stored in liquid nitrogen. For flow cytometry analysis the liquid nitrogen stored PBMCs were quickly thawed and washed once with ice cold phosphate buffered saline. The cells were stained with Fixable Viability Dye eFluor 450 (eBioscience) to determine the viability. After 10 minutes of incubation, samples were stained with APC-labeled dextramer *HLA-A*29:02-TVLGILVSY*, PE-labeled dextramer *HLA-A*29:02-VTLTCAFRY* and a FITC-labelled negative control (*HLA-B*08:01* dextramer loaded with nonsense AAKGRGAAL peptide) (Immudex, DK). The incubation was performed in FACS Buffer (1% bovine serum albumin (BSA) and 0.1% sodium azide in PBS) at room temperature for 10 minutes, followed by washing and further surface staining with V500-labeled anti-human CD8 (Becton Dickinson), PerCP-Cy5.5-labeled anti-human CD4 (BioLegend), BV605-labeled anti-human CD3 (BioLegend), PE-CF594-labeled anti-human CD56 (Becton Dickinson) and a dump channel of APC-eF780-labeled antibodies (CD14 and C19; eBioscience) for 20 minutes at 4°C. Flow cytometric analyses were performed on the BD FACSAria™ III and the data were analyzed using FlowJo software (TreeStar Inc.). Fluorescence minus one (FMO) control samples were used to set the dextramer gates.

As a control, CompBead Plus Anti-Mouse Ig,κ beads and unlabeled negative control beads (both BD Biosciences) were mixed with anti-human HLA-A,B,C antibody (clone W6/32; BioLegend), followed by washing and further staining with either one of the dextramers. Analysis of the beads was performed on the BD FACSAria™ III. For the analysis of aqueous humor (n=1), and vitreous fluid (n=1), samples from two BCR patients were stained and analyzed as described above. However, only one wash step after staining was performed to minimize cell loss given the limited number of cells present in the samples.

PBMC stimulation with S-antigen peptides

PBMCs from 12 BCR patients and 6 HLA-A29-positive controls were seeded in 96-well flat-bottom plates (1×10^6 cells/well) and cultured in RPMI 1640 medium supplemented with 5 IU/ml IL-2 and 10% human AB serum. The cells were stimulated with either one of the synthetic peptides TVLGILVSY or VTLTCAFRY (Pepscan Presto, NL) for 48 hours at a concentration of 10 ng/ml. After 48 hours of peptide stimulation, cells were re-stimulated for 4 hours with 20ng/mL ionomycin and 1µg /mL phorbol myristate acetate (PMA) (both from Sigma Aldrich).

GolgiStop (BD Biosciences; 2µL in 150µL culture medium) was added after 30 minutes and the cells were cultured for an additional 3.5 hours before the intracellular cytokine staining was performed.
Cells were surface stained with APC/Cy7-labeled anti-human CD8 (Becton Dickinson), BV785-labeled anti-human CD4 (BioLegend), BV605-labeled anti-human CD3 (BioLegend), fixed, and permeabilized in fixation buffer (Becton Dickinson) and intracellularly stained using antibodies against TNFα (BioLegend), IL-17A (eBioscience) and IFNγ (Becton Dickinson). Flow cytometric analyses were performed on the BD LSR Fortessa™ Cell analyzer (BD Bioscience). Data were analyzed using FlowJo software (TreeStar Inc.).

Peptide prediction algorithms and Statistical analysis

Peptide binding to HLA alleles was predicted using neural-network based prediction algorithm HLAthena[26]. HLAthena provides a binding score metric 'MSi' between 0-1 with MSi>0.9 considered strong binding. Prediction of antigen processing of N-terminally extended precursor peptides was conducted by subjecting the full amino acid sequence of of SAG (Uniprot: P10523, ARRS_HUMAN), β-arrestin-1 (Uniprot: P49407, ARRB1_HUMAN) and β-arrestin-2 (Uniprot: P32121, ARRB2_HUMAN) to NetChop - 3.1 web server[27] using the *Cterm* method, which best predicts cellular antigen processing outcome (proteasome+proteases)[28]. The mean protein copy number of beta-arrestin 1 and beta-arrestin 2 isoforms in purified peripheral blood immune cell subsets were calculated using the mass-spectrometry-based proteomic data as reported by Rieckmann and co-workers[29]. Group differences were assessed using the Kruskal-Wallis rank sum test with the *kruskal.test()* function in base R or a Dunn's Kruskal-Wallis Multiple Comparisons by *dunnTest()* function in the *FSA R* package[30]. *P* values were adjusted using the bonferroni method.

Data availability

Descriptions of how to reproduce the analysis workflows (showing code and R package version numbers) using data underlying the figures presented in this paper are available at https://github.com/jonaskuiper/SAG_birdshot

Results

Peptides from the retinal S-antigen (SAG) are bona fide ligands of HLA-A29

We reasoned that a powerful way to discover peptide antigen ligands derived from the retinal S-antigen (SAG) would be to determine if they can be presented by HLA-A29 using patient-derived antigen presenting cells (**Figure 4.1A**). To do so, we initiated the study by using immunopeptidome data from an *HLA-A29:02*-positive birdshot chorioretinitis patient derived lymphoblastoid cells (LCL1, female, 80 years) that we subjected to lentiviral transduction for stable expression of full-length SAG protein (SAG-GFP fusion protein) (**Figure**

4.1B, 4.1C). We filtered the amino peptidome data for 8-11 amino acids long peptides (i.e., typical length for T-cell epitopes)[25] with an ion Mascot Score >35 (n=820 unique peptide ligands) (**Figure 4.2A** and **Supplemental Figure 4.1**) and identified the 9-mer peptides VTLTCAFRY [amino acid positions 63-71 in SAG] and TVLGILVSY [323-331] that matched with the amino acid sequence of SAG (**Table 4.1, Supplemental Table 4.1**).

To validate these findings, we generated LCLs from a second *HLA-A*29:02*-positive birdshot chorioretinitis patient (LCL2; female, 65 years old) (**Table 4.1**) and SAG was also stably expressed by lentiviral transduction in this cell line (**Figure 4.1B, 4.1C**). Using mass spectrometry analysis, we sequenced peptides eluted from anti-HLA-A29 immunoprecipitations from LCL2 and filtered the immunopeptidome data (n=910 unique 8-11-mers, **Supplemental Figure 4.1**) and detected 295 peptides (Ion Mascot Score >35) in common with LCL1 (**Supplemental Table 4.2, 4.3**). This independent analysis also detected VTLTCAFRY (SAG[63-71]) and TVLGILVSY (SAG[323-331]) as the only SAG derived peptides in the HLA-A29 immunopeptidome data of LCL2. Comparing the tandem mass spectrometry (MS/MS) spectra of the SAG ligands identified in the elutions from HLA-A29 immunoprecipitations with the fragment-spectrum we generated from their synthetic peptide analogues supported accurate identification of SAG derived peptides bound to HLA-A29 (**Figure 4.2B, Supplemental Figure 4.2**). In silico binding analysis by HLAthena[26] corroborated that these peptides were also predicted as very strong ligands for HLA-A29 (**Table 4.2**).

Using the amino acid sequence of these peptides as a query in BLAST[31] revealed that TVLGILVSY is unique to SAG. In contrast, the peptide sequence of VTLTCAFRY is also present in the amino acid sequence of other non-vision arrestins (*e.g.,* β-arrestin-1 and -2).

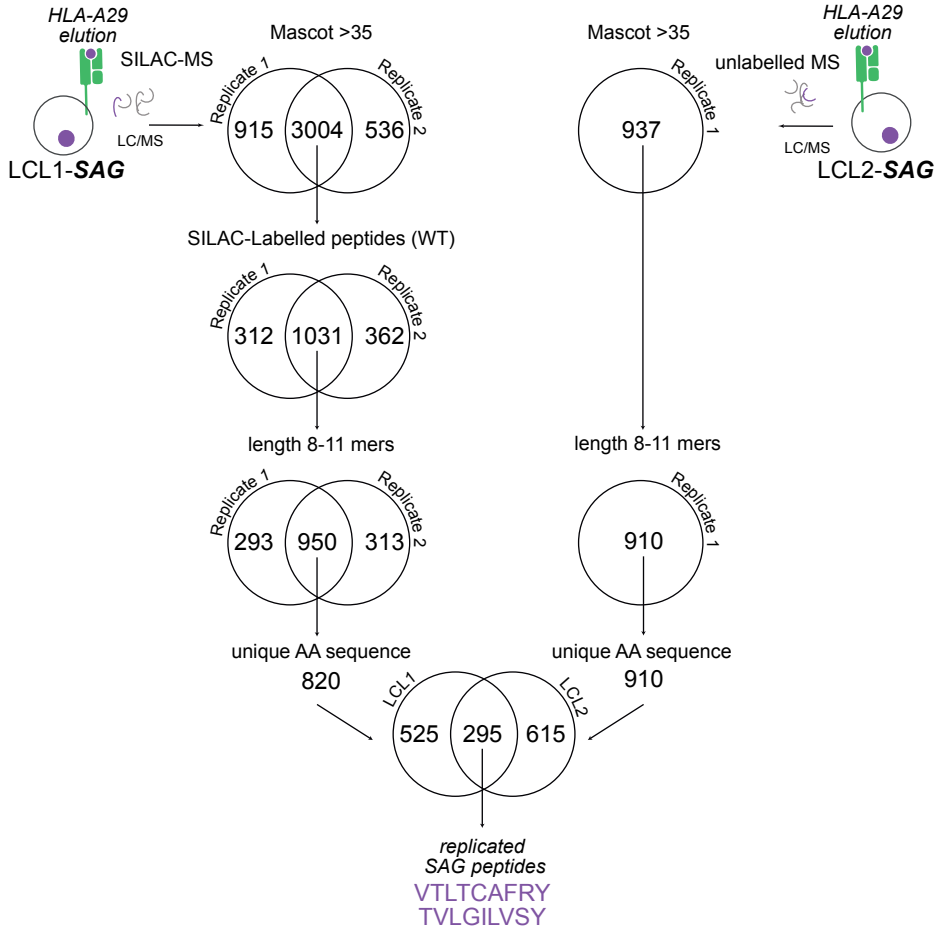

Figure 4.1: **Study design and generation of patient-derived antigen presentation models for SAG**. (**a**) Schematic overview of the generation of a birdshot chorioretinitis patient-derived lymphoblastoid cells [LCL1 and LCL2] expressing the retinal S-antigen (SAG)-GFP fusion protein by lentiviral transduction. We used mass-spectrometry-based peptide sequencing (i.e., *immuno-peptidomics*) of HLA-A29-eluted peptides for identification of SAG-derived ligands of HLA-A29. (**b**) Western blot of SAG+mGFP fusion protein (27.3 kD mGFP + 44.6 kD S-antigen) expression and ERAP2 (control) in "WT" and LCL1s transduced with SAG. Two separate blots using the same protein lysates for each sample were run in parallel for the detection of either anti-ERAP2 or anti-mGFP. (**c**) Brightfield microscope image with GFP overlay of LCLs after stable expression of SAG-GFP.

Although we are formally unable to assign VTLTCAFRY to the SAG, β-arrestins are low expressed in B cells (**Figure 4.2C**) and this peptide has not been reported in HLA-A29 immunopeptidome studies of lymphoblastoid cell lines[26,32-34]. Because the amino acids upstream (N-terminal) of VTLTCAFRY in the source proteins differ between the SAG and other arrestins (**Table 4.1**), we asked if this may influence the probability of antigen processing and presentation of the mature peptide VTLTCAFRY. To this end, we used neural network-based prediction of the likelihood of the generation of N-terminally extended precursors peptides of VTLTCAFRY from full-length SAG, and β-arrestin-1 and -2 by the cellular antigen

processing machinery (combined proteasomal and proteases)[27,28]. This analysis revealed that whole-cell antigen processing is predicted to generate the 9-mer ligand and a N-terminally extended 11-mer for SAG, but not for other arrestins (**Figure 4.1D**). Of interest, the nearest N-terminal cleavage site "shared" between arrestins is predicted 5 amino acid positions before the 9-mer ligand, which would introduce N-terminal acidic residues (D and E) that are unfavorable for antigen processing[35]. Collectively, these observations make it reasonable to assume that also the VTLTCAFRY peptide is derived specifically from SAG. Based on these results, we conclude that two 9-mer peptides derived from SAG are *bona fide* ligands of HLA-A29.

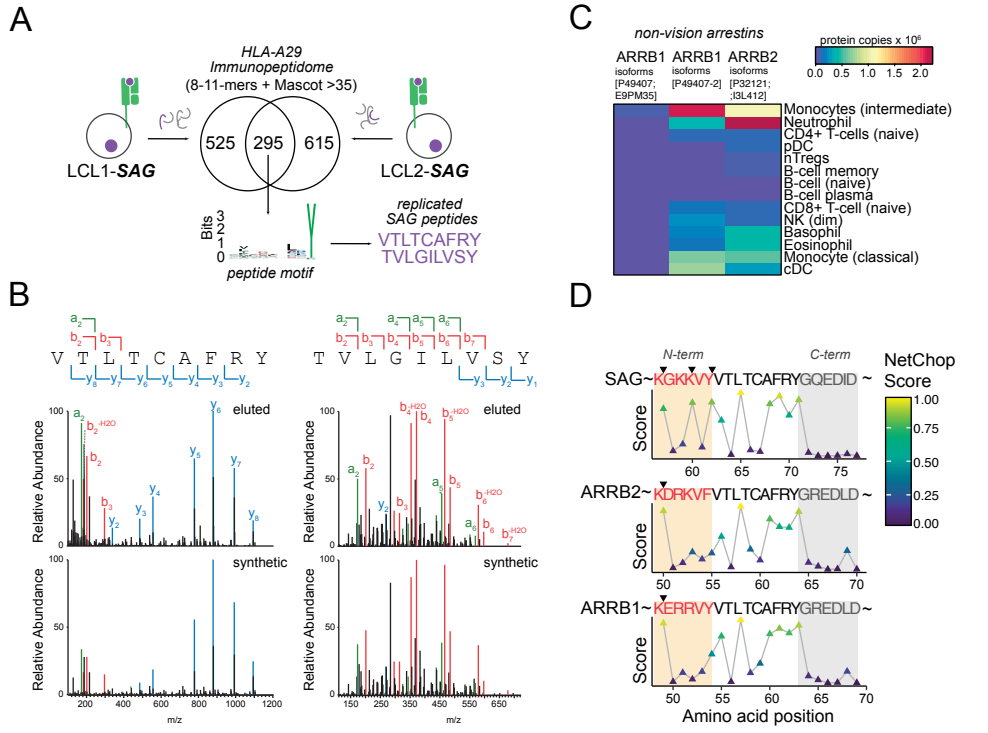

Figure 4.2: Identification of two SAG derived ligands of HLA-A29. (**a**) Venn diagram of HLA-A29 immunopeptidomes (8-11 mers with Mascot Ion score >35) of LCL1-*SAG* and LCL2-*SAG*. Detailed filtering steps for peptides in the immunopeptidome data is provided in **Supplemental Figure 4.1.** A sequence logo is shown based on the non-redundant list of 9-mers detected in both cell lines and includes the SAG-derived peptides (VTLTCAFRY, TVLGILVSY) highlighted in purple. (**b**) The MS/MS spectrum of the peptide fragment ions derived from the SAG peptides identified in elutions from HLA-A29 immunoprecipitations of the patient derived cell lines ("eluted") and from recombinant peptides with identical amino acid sequence ("synthetic"). The relative abundance and mass/charge (m/z) of characteristic (a-, b- and y-) ions from the fragmentation of the peptides are highlighted. Detailed MS/MS fragment spectrum is shown in **Supplemental Figure 4.2**. (**c**) Heatmap showing the mean protein copy numbers for protein isoforms of β-arrestin-1 and -2 (ARRB1, -2) in peripheral blood immune subsets (data from Rieckmann *et al*.[29] (**d**) The predicted in vivo whole-cell proteolysis (proteasomal + all other proteases) of SAG, and β-arrestin-1 and -2 (ARRB1, -2) of full-length protein by *NetChop Cterm* algorithm[27]. The predicted cleavage sites in the source protein N-terminally of the identified ligand VTLTCAFRY that exceed the threshold (>0.5) are highlighted with black triangles.

Table 4.2. Identified S-antigen derived peptides in immunopeptidome data of LCL1 and LCL2. The flanking sequence in the source protein(s) is shown. The predicted binding affinity [range 0-1, from HLAthena[26]) for HLA*A29:02 and other class I alleles are also provided.

S-antigen peptide	Flanking sequence of Source protein (Uniprot).	Predicted binding affinity HLA*A29:02	High affinity >0.9 for other HLA alleles
VTLTCAFRY	S-antigen (P10523): ...GKKVY**VTLTCAFRY**GQEDI... B-arrestin 1 (P49407): ...ERRVY**VTLTCAFRY**GREDL... B-arrestin 2 (P32121): ...DRKVF**VTLTCAFRY**GREDL...	0.92	HLA-B*15:17
TVLGILVSY	S-antigen (P10523): ...EGIDR**TVLGILVSY**QIKVK...	0.99	HLA-A*03:01 HLA-A*25:01 HLA-A*26:01 HLA-A*30:02 HLA-A*34:02 HLA-B*15:01 HLA-B*15:02 HLA-B*18:01 HLA-B*35:01 HLA-B*35:07 HLA-B*46:01 HLA-C*12:02

HLA-A29 ligands of SAG are trimmed by ERAP1 and ERAP2

Because the antigen processing aminopeptidases ERAP1 and ERAP2 are genetically implicated in the pathogenesis of birdshot chorioretinitis[7-9], we next were interested to determine whether the two SAG-derived peptides could be generated through trimming N-terminal elongated peptide precursors by ERAP1 and ERAP2. We used recombinant ERAP1 and ERAP2 to *in vitro* digest VTLTCAFRY, TVLGILVSY and their respective 10-mer precursor peptides (N-terminal extended with the amino acid at that position in the retinal S-antigen amino acids sequence, **Table 4.2**). ERAP1 clearly processed the control peptides RGRFSGLLGR and SVLKSLPFTII, as well as the precursor peptide 10-mer YVTLTCAFRY to the 9-mer HLA-A29 ligand VTLTCAFRY after 60 minutes of incubation (**Figure 4.3A, 4.3B**). However, we observed no trimming of the 10-mer precursor RTVLGILVSY. No tryptic activity was detected in the ERAP preparations since the tryptic peptide SLPFTII peptide was not efficiently formed from SVLKSLPFTII. ERAP1 also trimmed the 9-mer HLA-A29 ligand VTLTCAFRY to the 8-mer TLTCAFRY. In contrast, ERAP2 left the precursor peptide 10-mer YVTLTCAFRY unaffected, but did show limited activity towards the precursor 10-mer RTVLGILVSY to yield the HLA-A29 ligand TVLGILVSY (**Figure 4.3C**). These *in vitro* results show that SAG-derived ligands of HLA-A29 can potentially be generated from N-terminally trimming of precursor peptides by ERAP1 and ERAP2.

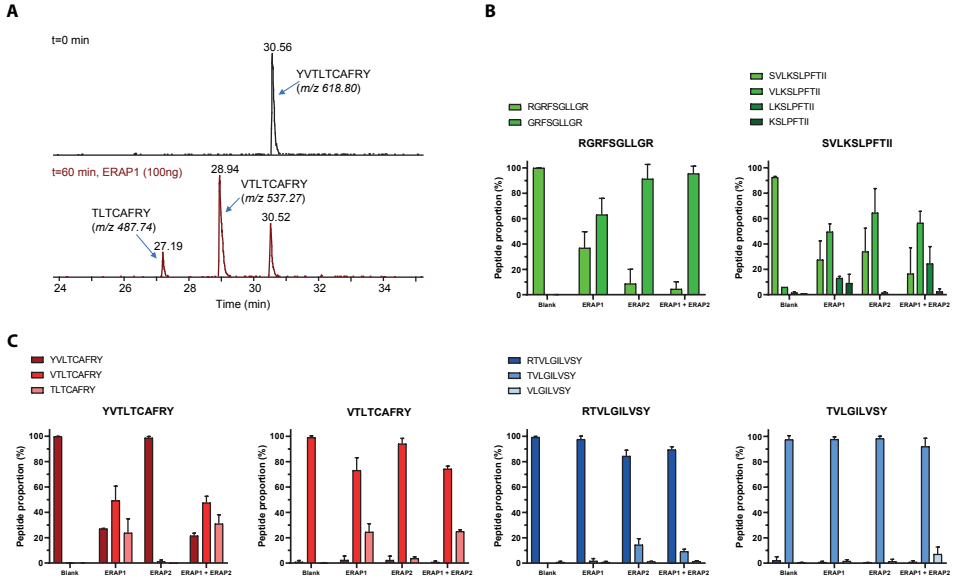

Figure 4.3: **In vitro S-antigen peptide digestion by ERAP1 and ERAP2.** (**a**) Representative mass spectrometry chromatogram showing ERAP1 digestion of S-antigen derived peptide YVTLTCAFRY into the respective 9- and 8-mer after the 60 min. incubation (**b**) Positive control RGRFSGLLGR, showing the proportional abundance digestion products (%) of the original peptide and measured digestion products as a result of ERAP1, ERAP2 or ERAP1 + ERAP2 digestion respectively. Control peptide SVLKSLPFTII to assess tryptic activity on lysine (K) at P4 to validate ERAP1/ERAP2 purity. (**c**) Digestion of VTLTCAFRY and its respective 10-mer YVTLTCAFRY, TVLGILVSY and its respective 10-mer RTVLGILVSY. Peptide digestion assay data is shown in **Supplemental Table 4.2**.

SAG-specific CD8+ T cells are not detectable in birdshot chorioretinitis patients.

We next assessed whether the two identified peptides from the retinal S-antigen were detected by CD8+ T-cells from patients, HLA-A29-positive or HLA-A29-negative controls (n=34) using fluorescent-dextramerized recombinant HLA-A*29:02 molecules complexed with either VTLTCAFRY or TVLGILVSY. Comparing empty beads and beads coated with pan-class I antibody (W6/32) mixed with either one of the dextramers, revealed good performance for our assembled HLA-A29/VTLTCAFRY and HLA-A29/TVLGILVSY dextramers (**Figure 4.4A**). Enumeration of dextramer-positive events revealed no difference between cases and HLA-A29-positive, and HLA-A29-negative controls (**Figure 4.4B**). Importantly, the frequency of detected events was in the same range as the negative control dextramer, indicating that no SAG-specific CD8+ T cells were detectable in peripheral blood.

To ascertain the absence of CD8+ T cell activation by these SAG peptides, we assessed antigen engagement at the single cell level. To this end, we conducted peptide stimulations of PBMCs from 18 BCR patients and 6 HLA-A29-positive controls and monitored intracellular cytokine (TNF-alpha, interferon-gamma, and interleukin-17) production by CD8+ T-cells after 48 hours.

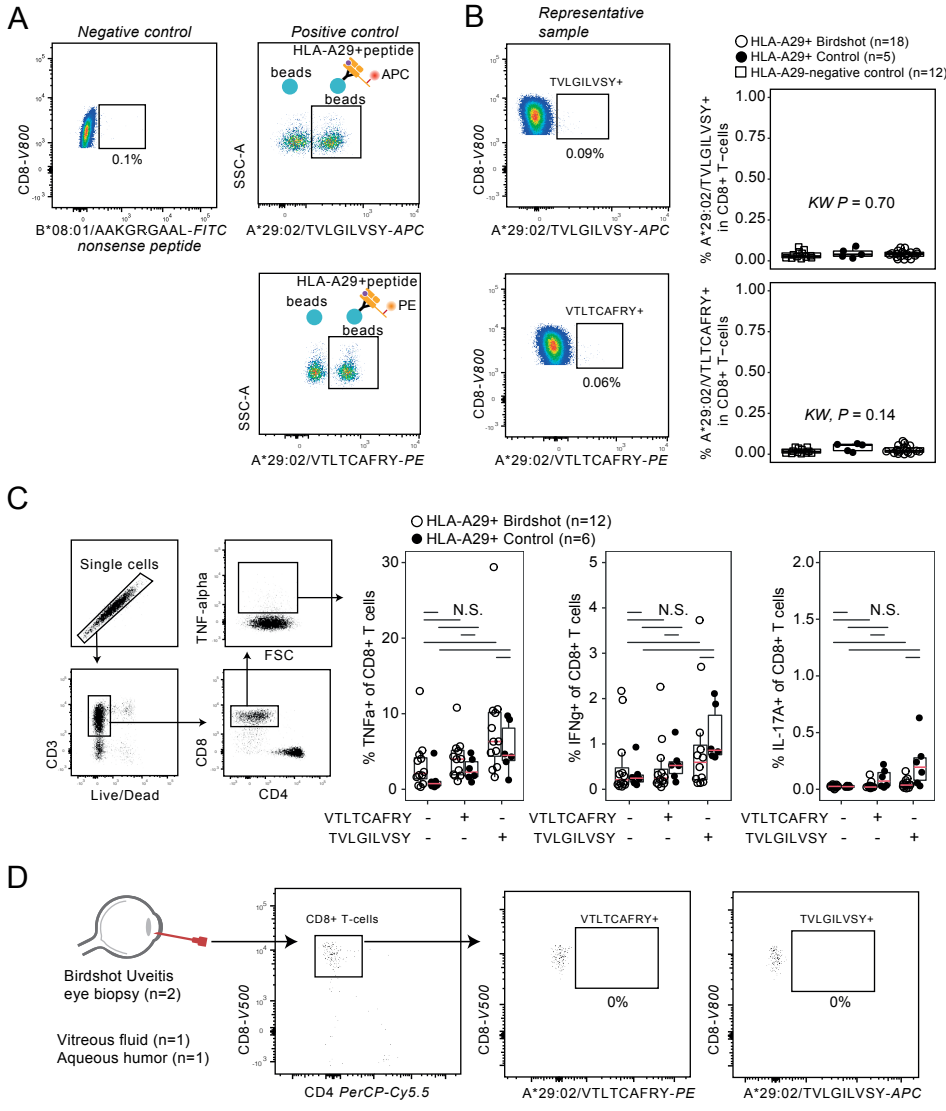

Figure 4.4. HLA-A29/SAG-specific CD8+ T cells are absent in peripheral blood or eye biopsies of birdshot chorioretinitis patients. (**a**) Biplot of flow cytometry analysis using a positive control for HLA-A29-TVLGILVSY dextramer and HLA-A29-VTLTCAFRY dextramer by using beads coated with or without pan anti-HLA class I antibody (W6/32) and dextramers. As a negative control, we used a dextramer complexed with a nonsense peptide. (**b**) Representative biplot for the percentage of the blood CD8+ T cells binding to each of the HLA-A29 dextramers. A scatterplot of the percentage of dextramer-positive CD8+T cells in peripheral blood mononuclear cell (PBMC) samples from HLA-A29+ birdshot chorioretinitis patients, HLA-A29+ healthy controls, and HLA-A29-negative healthy controls. *P* values are from a *Kruskal Wallis* test). (**c**) Intracellular cytokine detection by flow cytometry of TNF-alpha, IFN-gamma, and IL-17-producing CD8+ T-cells after peptide stimulated PBMC cultures. The comparison of the percentage of cytokine producing CD8+ T-cells in unstimulated PBMC cultures, or stimulated with VTLTCAFRY, or TVLGILVSY, is shown. None of the comparisons were statistically significant by Dunn's test with correction for multiple testing. NS = non-significant. (**d**) Representative flow cytometry biplots of vitreous fluid of one birdshot chorioretinitis patient. Eye-infiltrating CD8+ T-cells were stained with the S-antigen peptide HLA-A29-TVLGILVSY dextramer and HLA-A29-VTLTCAFRY dextramer.

Stimulation with synthetic VTLTCAFRY or TVLGILVSY did not induce a significant increase in the frequency of cytokine-producing CD8+ T-cells in cases and controls (**Figure 4.4C**). Because we also detected VTLTCAFRY peptide with post-translational modifications in the immunopeptidome data, we also determined cytokine production by CD8+ T cells after 48 stimulation with VTLTCAFRY with phosphorylated Threonine (at amino acid position 2, position 4, or both position 2 and 4) or cysteinylated Cysteine (C-cys) at amino acid position 5 in VTLTCAFRY, but detected also no significant increase in the frequency of cytokine-producing CD8+ T cells in cases and controls using stimulation with these modified peptides (**Supplemental Figure 4.3**).

Finally, we had the opportunity to study fresh intraocular eye biopsies from two BCR patients. Although flow cytometry analysis revealed evident infiltration of CD8+ T cells, no SAG-peptide dextramer-positive T cells were detected in inflamed eyes of patients (**Figure 4.4D**). Collectively, we conclude that SAG peptides in complex with HLA-A29 are not recognized by CD8+ T-cells of BCR patients.

Discussion

In this study, we investigated the candidate autoantigen SAG in BCR using patient-derived cell lines and identified two naturally presented peptides of SAG. We demonstrated that these peptides in complex with HLA-A29 are not recognized by circulating and eye-infiltrating CD8+ T cells of patients.

SAG has been postulated as the primary autoantigen ever since the discovery of HLA-A29 in cases with BCR over forty years ago[18]. In 1982, Nussenblatt and coworkers established the extreme genetic association between *HLA-A*29* and BCR and concurrently reported that PBMC cultures of BCR patients showed enhanced proliferation upon stimulation with SAG compared to healthy controls[18]. The nomination of SAG as candidate autoantigen for BCR was also based upon the observation that injecting rhesus monkeys with SAG or its derived 18-mer DTNLASSTIIKEGIDRTV (peptide "M") induced experimental uveitis, characterised by focal retinal lesions and histopathological features with high resembles to BCR[36,37]. However, *in vitro* SAG-stimulated T cell proliferation as well as SAG-induced experimental autoimmune uveitis is predominantly T helper cell-driven and mediated by MHC class II[38-42]. Also, in humans, cellular and humoral *in vitro* hyperresponsiveness to SAG is not limited to BCR and commonly observed in patients with a wide variety of inflammatory eye conditions. Our study revealed that peptides from SAG presented by HLA-A29 are not immunogenic.

Using immunopeptidomics of newly-generated patients' cell lines with low passage, we ensured preservation of canonical antigen processing for unbiased discovery of peptide antigens presented by HLA-A29. Although we consider this a significant improvement compared to more widely used long-established cell lines that suffer from genomic aberrations, also in the MHC-I pathway[43,44], ideally, we would have liked to determine if SAG ligands

are also presented by photoreceptors in the eye under inflammatory conditions. Recently, it was shown that shortage in cellular tryptophan promotes tryptophan to phenylalanine substitution in proteins, which could alter the HLA antigenic peptide repertoire and activate T cells[45]. HLA-A29 immunopeptidomics of inflamed retina is technically and ethically highly challenging considering the limited amount of tissue available for such analysis. However, even when considering the possibility of inflammation-induced tryptophan breakdown in the retina[46-49], SAG contains merely a single tryptophan in its amino acid sequence (W198), which after substitution does not influence predicted binding to HLA-A29 (NetCTLpan server after *in silico* W198F substitution, data not shown). We therefore consider it likely that our model captured all *in situ* SAG ligands of HLA-A29, also when presented by antigen presenting cells under inflammatory conditions.

Another limitation of our work is that we did not evaluate if CD8+ T cells recognize SAG-derived epitopes via other HLA class I alleles in linkage disequilibrium with HLA-A29 (e.g., HLA-B44, HLA-C16). However, in our reanalysis of previously reported pan-MHC-I immunopeptidome analysis of LCL1[21] we detected only one other SAG-derived peptide (at Mascot Ion score >35): the 11-mer SEVATEVPFRL most likely derived from *HLA-B*44:03* (*HLAthena* binding score, MSI = 0.88) which is in linkage disequilibrium with *HLA-A*29:02*[50]. Although the amino acid sequence of this 11-mer overlaps with peptides that are highly potent for induction of uveitis in a rat model of experimental autoimmune uveitis[51,52], this model is not mediated by CD8+ T cells[53]. Therefore, we speculate that other putative HLA class I presented SAG epitopes will have negligible contribution to CD8+ T cell immunity in BCR. Given that PBMC cultures of BCR patients showed enhanced T cell proliferation upon stimulation with SAG[18,41], our current view is that SAG functions as a “collateral” or “secondary” autoantigen involved in CD4+ T helper-mediated responses induced by epitope spreading subsequent to (yet unidentified) primary autoantigen-directed immunity via HLA-A29 and CD8+ T cells.

Peptide-MHC multimers represent a powerful technology for the detection of antigen-specific CD8+ T cells. However, the low frequency in peripheral blood and relatively low affinity T-cell receptors (TCR) of self-specific T-cells pose a significant challenge since the signal in peripheral blood may become obscured within the inherent background noise. To ascertain high quality detection and quantification, we used several strategies in line with current recommendations[54], such as an optimized staining protocol (stain with dextramers before staining for coreceptor CD8[55]), use of “dump” channels to eliminate nonspecific binding events[56], FMO controls, and anti-multimer bead positive controls to ensure an accurate gating strategy. We also used dextramers which outperform conventional tetramers, because they carry a greater number of both peptide-HLA complexes and fluorochromes[57]. Although the frequency of dextramer-positive events in this study were in the range of frequencies reported for blood CD8+ T-cells specific for viral or tumor peptides[58-60], we observed no differences to unaffected controls. Although we can formally not exclude HLA

alloreactivity by CMV- and EBV-specific T-cells[61-63] known to cross-react specifically with HLA-A29 in HLA-A29-negative donors[64].

The use of optimized protocols in future studies to prevent TCR triggering and internalization, and reduce reagent dissociation during washing steps may further increase sensitivity[65]. We would like to point out that SAG-specific CD8+ T cells may be detected by magnetic bead enrichment protocols or long-term peptide stimulation-based expansion[66,67]. However, these approaches may also target low-frequency or non-expanded T cells while our approach assumed that during active uveitis SAG-specific CD8+ T cells should be expanded to a degree that is detectable in patients' blood using highly sensitive dextramer technology. Low-frequency self-reactive CD8+ T-cells are common in blood from healthy individuals[60,68]. Because healthy people with self-reactive T cells do not spontaneously develop autoimmune diseases, this does not imply that their cognate antigens are clinically relevant for autoimmunity. This line of reasoning may lead to a paradox where absence of their ex vivo detection without enrichment does not mean there are no self-reactive T cells, whereas detection after stimulation/enrichment does not proof their in vivo expansion unambiguously. Hence, we required evidence of expansion of self-reactive CD8+ T cells to consider their cognate antigens as autoantigens, because high frequency of self-reactive T cells in the peripheral repertoire correlates with the susceptibility to develop autoimmune disease[69]. Furthermore, autoimmune T cells are enriched for low-affinity TCRs, since low-affinity T cells are more prone to escape negative selection. However, this means they must be present in substantially larger numbers in order to induce autoimmunity, so an increase in self-reactive cells is required to cause autoimmunity[70–72]. Consequently, dextramers have been shown to have sufficient sensitivity for the ex vivo quantification to expanded CD8+ T cells to a variety of autoantigens in other autoimmune diseases, including rheumatoid arthritis, spondylarthritis, and psoriasis[65,73–77]. Because we show that ERAPs can influence the generation of the SAG peptides, one limitation of the study is that we did not stratify our antigen-specific response assay by functional polymorphisms in ERAP genes in the samples. Using this non-enriched approach, we demonstrated that the detected frequency in patients was similar to HLA-A29-positive controls, and indistinguishable from the negative control dextramer. Importantly, no dextramer-positive T cells were detected among the eye-infiltrating CD8+ T cells in patients. We also found no induction of antigen-specific cytokine production in CD8+ T cells after stimulation with these SAG peptides. This supports our conclusion that we did not detect SAG-specific CD8+ T cells in patients and that SAG is unlikely of relevance to the HLA-A29-mediated - and thus disease defining - pathogenic mechanisms.

Genome-wide genetic studies identified *HLA-A29*, *ERAP1*, and *ERAP2* genes as risk genes for BCR[7,9]. This substantiates peptide processing by ERAP1 and ERAP2 in the endoplasmic reticulum and subsequent peptide presentation by HLA-A29 at the cell surface as a key disease mechanism for BU. Functional studies have revealed that ERAP2 promotes HLA-A29 presentation of peptides with a motif that is found in the amino acid sequence of melanocyte

proteins[1,21]. This is significant, because in *HLA-C*06-associated psoriasis* melanocytes trigger autoreactive CD8+ T cells via ERAP1[14,15]. These findings are significant because inflammation in BCR may originate in the melanocyte-rich ocular choroid and suggest that tissue resident autoantigens of the choroid may provide the targets for autoreactive CD8+ T cells[1]. If melanocytes are a target tissue in BCR remains to be determined. Regardless, identification of autoantigens in upcoming studies may benefit from the rapid advancement in sequencing technologies, such as *single-cell TCR sequencing*, which will allow the identification of the full-length alpha and beta TCR chains of eye-infiltrating CD8+ T cells, which can be used for functional evaluation (i.e., cloning into cell lines) and screening of large peptide libraries to identify their cognate peptide antigen(s)[15,78]. In conclusion, we demonstrate that the longstanding autoantigen candidate SAG is not implicated as a CD8+ T cell target in BCR and that the disease mechanisms that involve antigen presentation via HLA-A29 involve possibly other yet unidentified peptides.

References

1. J.J.W. Kuiper, W.J. Venema, HLA-A29 and birdshot uveitis: further down the rabbit hole, Front. Immunol. 11 (2020), 599558.
2. J. Kuiper, A. Rothova, J. de Boer, T. Radstake, The immunopathogenesis of birdshot chorioretinopathy; a bird of many feathers, Prog. Retin Eye Res. [Internet]. 44 (2015) 99–110, https://doi.org/10.1016/j.preteyeres.2014.11.003.
3. E.H. Sohn, K.R. Chirco, J.C. Folk, R.F. Mullins, Clinicopathological correlation in a patient with previously treated birdshot chorioretinopathy, Retin Cases Brief Rep.11 (4) (2017) 344–347.
4. A.T. Vitale, A. Rodriguez, C.S. Foster, Low-dose cyclosporine therapy in the treatment of birdshot retinochoroidopathy, Ophthalmology. 101 (5) (1994 May) 822–831.
5. P. Le Hoang, B. Girard, G. Deray, H. Le Minh, Y. De Kozak, B. Thillaye, et al., Cyclosporine in the treatment of birdshot retinochoroidopathy, Transplant. Proc. 20 (3 Suppl 4) (1988 Jun) 128–130.
6. C.P. Herbort, C. Pav´esio, P. LeHoang, B. Bodaghi, C. Fardeau, P. Kestelyn, et al., Why birdshot retinochoroiditis should rather be called “HLA-A29 uveitis”? Br. J. Ophthalmol. 101 (7) (2017) 851–855.
7. J.J.W. Kuiper, J. Van Setten, S. Ripke, R. Van ’T Slot, F. Mulder, T. Missotten, et al., A genome-wide association study identifies a functional ERAP2 haplotype associated with birdshot chorioretinopathy, Hum. Mol. Genet. 23 (22) (2014) 6081–6087.
8. Kuiper JJW, Setten J van, Devall M, Cretu-Stancu M, Hiddingh S, Ophoff RA, et al. Functionally distinct ERAP1 and ERAP2 are a hallmark of HLA-A29-(birdshot) uveitis. Hum. Mol. Genet. 2018;27(24):4333–43.
9. S. Gelfman, D. Monnet, A.J. Ligocki, T. Tabary, A. Moscati, X. Bai, et al., ERAP1, ERAP2, and two copies of HLA-Aw19 alleles increase the risk for birdshot Chorioretinopathy in HLA-A29 carriers, Invest. Ophthalmol. Vis. Sci. 62 (14) (2021 Nov) 3.
10. J.S. Pulido, I. Canal, D. Salom˜ao, D. Kravitz, E. Bradley, R. Vile, Histological findings of birdshot chorioretinopathy in an eye with ciliochoroidal melanoma, Eye. 26 (6) (2012) 862–865.
11. P.A. Gaudio, D.B. Kaye, J.B. Crawford, Histopathology of birdshot retinochoroidopathy, Br. J. Ophthalmol. 86 (12) (2002 Dec) 1439–1441.
12. J.J.W. Kuiper, A. Rothova, P.A.W. Schellekens, A. Ossewaarde-van Norel, A. C. Bloem, T. Mutis, Detection of choroid- and retina-antigen reactive CD8+ and CD4+ T lymphocytes in the vitreous fluid of patients with birdshot chorioretinopathy, Hum. Immunol. [Internet]. 75 (6) (2014) 570–577, https://doi.org/10.1016/j.humimm.2014.02.012.
13. D. McGonagle, S.Z. Aydin, A. Gül, A. Mahr, H. Direskeneli, ‘MHC-I-opathy’-unified concept for spondyloarthritis and Behçet disease, in: Nature reviews. Rheumatology. United States 11, 2015, pp. 731–740.
14. A. Arakawa, E. Reeves, S. Vollmer, Y. Arakawa, M. He, A. Galinski, et al., ERAP1 controls the autoimmune response against melanocytes in psoriasis by generating the melanocyte autoantigen and regulating its amount for HLA-C*06:02 presentation, J. Immunol. 207 (9) (2021 Nov) 2235–2244.

15. A. Arakawa, K. Siewert, J. St¨ohr, P. Besgen, S.-M. Kim, G. Rühl, et al., Melanocyte antigen triggers autoimmunity in human psoriasis, J. Exp. Med. 212 (13) (2015 Dec) 2203–2212.
16. R.B. Nussenblatt, T. Kuwabara, F.M. de Monasterio, W.B. Wacker, S-antigen uveitis in primates. A new model for human disease, Arch. Ophthalmol. (Chicago, Ill 1960) 99 (6) (1981 Jun) 1090–1092.
17. R.B. Nussenblatt, M.M. Rodrigues, W.B. Wacker, S.J. Cevario, M.C. Salinas-Carmona, I. Gery, Cyclosporin a. inhibition of experimental autoimmune uveitis in Lewis rats, J. Clin. Invest. 67 (4) (1981 Apr) 1228–1231.
18. R.B. Nussenblatt, K.K. Mittal, S. Ryan, W. Richard Green, Maumenee A. Edward, Birdshot Retinochoroidopathy associated with HLA-A29 antigen and immune responsiveness to retinal S-antigen, Am. J. Ophthalmol. [Internet]. 94 (2) (1982 Aug 1) 147–158, https://doi.org/10.1016/0002-9394(82)90069-1.
19. F. Boisgerault, I. Khalil, V. Tieng, F. Connan, T. Tabary, J.H. Cohen, et al., Definition of the HLA-A29 peptide ligand motif allows prediction of potential T-cell epitopes from the retinal soluble antigen, a candidate autoantigen in birdshot retinopathy, Proc. Natl. Acad. Sci. U S A [Internet]. 93 (8) (1996 Apr) 3466–3470, https://doi.org/10.1073/pnas.93.8.3466.
20. T. Tabary, P. Lehoang, H. Betuel, A. Benhamou, R. Semiglia, C. Edelson, et al., Susceptibility to birdshot chorioretinopathy is restricted to the HLA-A29.2 subtype, Tissue Antigens 36 (4) (1990 Oct) 177–179.
21. W.J. Venema, S. Hiddingh, J.H. de Boer, F.H.J. Claas, A. Mulder, A.I. den Hollander, et al., ERAP2 increases the abundance of a peptide submotif highly selective for the birdshot uveitis-associated HLA-A29, Front. Immunol. 12 (2021), 634441.
22. A. Mulder, M.J. Kardol, J.S. Arn, C. Eijsink, M.E.I. Franke, G.M.T. Schreuder, et al., Human monoclonal HLA antibodies reveal interspecies crossreactive swine MHC class I epitopes relevant for xenotransplantation, Mol. Immunol. 47 (4) (2010 Jan) 809–815.
23. C. Hassan, M.G.D. Kester, G. Oudgenoeg, A.H. de Ru, G.M.C. Janssen, J.W. Drijfhout, et al., Accurate quantitation of MHC-bound peptides by application of isotopically labeled peptide MHC complexes, J. Proteom. [Internet]. 109 (2014) 240–244. Available from, http://www.sciencedirect.com/science/article/pii/S1874391914003613.
24. C. Hassan, M.G.D. Kester, A.H. de Ru, P. Hombrink, J.W. Drijfhout, H. Nijveen, et al., The human leukocyte antigen-presented ligandome of B lymphocytes, Mol. Cell. Proteomics 12 (7) (2013 Jul) 1829–1843.
25. R. Vita, S. Mahajan, J.A. Overton, S.K. Dhanda, S. Martini, J.R. Cantrell, et al., The immune epitope database (IEDB): 2018 update, Nucleic Acids Res. 47 (D1) (2019 Jan) D339–D343.
26. S. Sarkizova, S. Klaeger, P.M. Le, L.W. Li, G. Oliveira, H. Keshishian, et al., A large peptidome dataset improves HLA class I epitope prediction across most of the human population, Nat. Biotechnol. [Internet]. 38 (2) (2020 Feb 16) 199–209, https://doi.org/10.1038/s41587-019-0322-9.

27. M. Nielsen, C. Lundegaard, O. Lund, C. Kes¸mir, The role of the proteasome in generating cytotoxic T-cell epitopes: insights obtained from improved predictions of proteasomal cleavage, Immunogenetics. 57 (1–2) (2005 Apr) 33–41.
28. J.J.A. Calis, P. Reinink, C. Keller, P.M. Kloetzel, C. Kes¸mir, Role of peptide processing predictions in T cell epitope identification: contribution of different prediction programs, Immunogenetics. 67 (2) (2015 Feb) 85–93.
29. J.C. Rieckmann, R. Geiger, D. Hornburg, T. Wolf, K. Kveler, D. Jarrossay, et al., Social network architecture of human immune cells unveiled by quantitative proteomics, Nat. Immunol. 18 (5) (2017 May) 583–593.
30. D. Ogle, P. Wheeler, A. Dinno, FSA: Fisheries Stock Analysis. R Packag version 0830 [Internet], Available from: https://github.com/droglenc/FSA, 2020.
31. S.F. Altschul, W. Gish, W. Miller, E.W. Myers, D.J. Lipman, Basic local alignment search tool, J. Mol. Biol. 215 (3) (1990 Oct) 403–410.
32. C. Alvarez-Navarro, A. Martín-Esteban, E. Barnea, A. Admon, J.A. L´opez De Castro, Endoplasmic reticulum aminopeptidase 1 (ERAP1) polymorphism relevant to inflammatory disease shapes the peptidome of the birdshot chorioretinopathy associated HLA-A*29:02 Antigen, Mol. Cell. Proteomics 14 (7) (2015) 1770–1780.
33. A. Sanz-Bravo, A. Martín-Esteban, J.J.W. Kuiper, M. García-Peydro, E. Barnea, A. Admon, et al., Allele-specific alterations in the peptidome underlie the joint association of HLA-A*29:02 and endoplasmic reticulum aminopeptidase 2 (ERAP2) with birdshot chorioretinopathy, Mol. Cell. Proteomics 17 (8) (2018) 1564–1577.
34. D.P. Granados, W. Yahyaoui, C.M. Laumont, T. Daouda, T.L. Muratore-Schroeder, C. Cˆot´e, et al., MHC I-associated peptides preferentially derive from transcripts bearing miRNA response elements, Blood. 119 (26) (2012 Jun) e181–e191.
35. A. Hearn, I.A. York, K.L. Rock, The specificity of trimming of MHC class I-presented peptides in the endoplasmic reticulum, J. Immunol. 183 (9) (2009 Nov) 5526–5536.
36. R.B. Nussenblatt, T. Kuwabara, F.M. de Monasterio, W.B. Wacker, S-antigen uveitis in primates. A new model for human disease, Arch. Ophthalmol. (Chicago, Ill 1960) 99 (6) (1981 Jun) 1090–1092.
37. S. Hirose, V.K. Singh, L.A. Donoso, T. Shinohara, S. Kotake, T. Tanaka, et al., An 18-mer peptide derived from the retinal S antigen induces uveitis and pinealitis in primates, Clin. Exp. Immunol. 77 (1) (1989 Jul) 106–111.
38. M.J. Mattapallil, P.B. Silver, J.J. Mattapallil, R. Horai, Z. Karabekian, J. H. McDowell, et al., Uveitis-associated epitopes of retinal antigens are pathogenic in the humanized mouse model of uveitis and identify autoaggressive T cells, J. Immunol. 187 (4) (2011 Aug) 1977–1985.
39. M.D. de Smet, G. Bitar, S. Mainigi, R.B. Nussenblatt, Human S-antigen determinant recognition in uveitis, Invest. Ophthalmol. Vis. Sci. 42 (13) (2001 Dec) 3233–3238.
40. P. Tripathi, S. Saxena, V.S. Yadav, S. Naik, V.K. Singh, Human S-antigen: peptide determinant recognition in uveitis patients, Exp. Mol. Pathol. 76 (2) (2004 Apr) 122–128.

41. M.D. de Smet, J.H. Yamamoto, M. Mochizuki, I. Gery, V.K. Singh, T. Shinohara, et al., Cellular immune responses of patients with uveitis to retinal antigens and their fragments, Am J. Ophthalmol. 110 (2) (1990 Aug) 135–142.
42. S.A. Tamm, S.M. Whitcup, I. Gery, B. Wiggert, R.B. Nussenblatt, M.I. Kaiser-Kupfer, Immune response to retinal antigens in patients with gyrate atrophy and other hereditary retinal dystrophies, Ocul. Immunol. Inflamm. 9 (2) (2001 Jun) 75–84.
43. Heterozygosity of the 721.221-B*51:01 Cell Line Used in the Study by Guasp et (Arthritis Rheumatol, February 2016), Arthritis Rheumatol. [Internet] 69 (3) (2017 Mar 1) 686, https://doi.org/10.1002/art.40073.
44. L. Chen, H. Shi, D. Koftori, T. Sekine, A. Nicastri, N. Ternette, et al., Identification of an unconventional Subpeptidome bound to the Behçet's disease-associated HLA-B*51:01 that is regulated by endoplasmic reticulum aminopeptidase 1 (ERAP1), Mol Cell Proteomics [Internet]. 19 (5) (2020) 871–883. Available from, https:// europepmc.org/articles/PMC7196583.
45. A. Pataskar, J. Champagne, R. Nagel, J. Kenski, M. Laos, J. Michaux, et al., Tryptophan depletion results in tryptophan-to-phenylalanine substitutants, Nature. 603 (7902) (2022 Mar) 721–727.
46. L. Lanser, P. Kink, E.M. Egger, W. Willenbacher, D. Fuchs, G. Weiss, et al., Inflammation-induced tryptophan breakdown is related with Anemia, fatigue, and depression in cancer, Front. Immunol. 11 (2020) 249.
47. J. Brown, B. Robusto, L. Morel, Intestinal Dysbiosis and tryptophan metabolism in autoimmunity, Front. Immunol. 11 (2020) 1741.
48. S.S. Palabiyik, S. Keles, G. Girgin, E. Arpali-Tanas, E. Topdagi, T. Baydar, Neopterin release and tryptophan degradation in patients with uveitis, Curr. Eye Res. 41 (11) (2016 Nov) 1513–1517.
49. B. Li, T. Zhang, W. Liu, Y. Wang, R. Xu, S. Zeng, et al., Metabolic features of mouse and human retinas: rods versus cones, macula versus periphery, Retina versus RPE. iScience. 23 (11) (2020 Nov), 101672.
50. E. Enrich, E. Campos, L. Martorell, M.J. Herrero, F. Vidal, S. Querol, et al., HLA-A, -B, -C, -DRB1, and -DQB1 allele and haplotype frequencies: an analysis of umbilical cord blood units at the Barcelona cord blood Bank, HLA. 94 (4) (2019 Oct) 347–359.
51. M.D. de Smet, G. Bitar, F.G. Roberge, I. Gery, R.B. Nussenblatt, Human S-antigen: presence of multiple immunogenic and immunopathogenic sites in the Lewis rat, J. Autoimmun. 6 (5) (1993 Oct) 587–599.
52. D.S. Gregerson, C.F. Merryman, W.F. Obritsch, L.A. Donoso, Identification of a potent new pathogenic site in human retinal S-antigen which induces experimental autoimmune uveoretinitis in LEW rats, Cell. Immunol. 128 (1) (1990 Jun) 209–219.
53. M. Diedrichs-M¨ohring, U. Kaufmann, G. Wildner, The immunopathogenesis of chronic and relapsing autoimmune uveitis - lessons from experimental rat models, Prog. Retin. Eye Res. 65 (2018 Jul) 107–126.
54. G. Dolton, K. Tungatt, A. Lloyd, V. Bianchi, S.M. Theaker, A. Trimby, et al., More tricks with tetramers: a practical guide to staining T cells with peptide-MHC multimers, Immunology. 146 (1) (2015 Sep) 11–22.

55. L. Wooldridge, A. Lissina, D.K. Cole, H.A. van den Berg, D.A. Price, A.K. Sewell, Tricks with tetramers: how to get the most from multimeric peptide-MHC, Immunology. 126 (2) (2009 Feb) 147–164.
56. P.K. Chattopadhyay, J.J. Melenhorst, K. Ladell, E. Gostick, P. Scheinberg, A. J. Barrett, et al., Techniques to improve the direct ex vivo detection of low frequency antigen-specific CD8+ T cells with peptide-major histocompatibility complex class I tetramers, Cytom. Part A J. Int. Soc. Anal. Cytol. 73 (11) (2008 Nov) 1001–1009.
57. G. Dolton, A. Lissina, A. Skowera, K. Ladell, K. Tungatt, E. Jones, et al., Comparison of peptide-major histocompatibility complex tetramers and dextramers for the identification of antigen-specific T cells, Clin. Exp. Immunol. 177 (1) (2014 Jul) 47–63.
58. S.A. Hunsucker, C.S. McGary, B.G. Vincent, A.A. Enyenihi, J.P. Waugh, K. P. McKinnon, et al., Peptide/MHC tetramer-based sorting of CD8+ T cells to a leukemia antigen yields clonotypes drawn nonspecifically from an underlying restricted repertoire, Cancer Immunol. Res. 3 (3) (2015 Mar) 228–235.
59. C. Vandamme, R. Xicluna, L. Hesnard, M. Devaux, N. Jaulin, M. Guilbaud, et al., Tetramer-based enrichment of preexisting anti-AAV8 CD8(+) T cells in human donors allows the detection of a T(EMRA) subpopulation, Front. Immunol. 10 (2019) 3110.
60. W. Yu, N. Jiang, P.J.R. Ebert, B.A. Kidd, S. Müller, P.J. Lund, et al., Clonal deletion prunes but does not eliminate self-specific αβ CD8(+) T lymphocytes, Immunity. 42 (5) (2015 May) 929–941.
61. A.L. Amir, L.J.A. D'Orsogna, D.L. Roelen, M.M. van Loenen, R.S. Hagedoorn, R. de Boer, et al., Allo-HLA reactivity of virus-specific memory T cells is common, Blood. 115 (15) (2010 Apr) 3146–3157.
62. L.J. D'Orsogna, H. van den Heuvel, E.M.W. van der Meer-Prins, D.L. Roelen, I.I. N. Doxiadis, F.H.J. Claas, Stimulation of human EBV- and CMV-specific cytolytic effector function using allogeneic HLA molecules, J. Immunol. 189 (10) (2012 Nov) 4825–4831.
63. H. van den Heuvel, K.M. Heutinck, E.P.M.W. van der Meer-Prins, Yong S. La, F.H. J. Claas, I.J.M. Ten Berge, Detection of virus-specific CD8+ T cells with cross-reactivity against Alloantigens: potency and flaws of present experimental methods, Transplant direct. 1 (10) (2015 Nov), e40.
64. A. van Egmond, C. van der Keur, G.M.J.S. Swings, S.A. Scherjon, F.H.J. Claas, The possible role of virus-specific CD8(+) memory T cells in decidual tissue, J. Reprod. Immunol. 113 (2016 Feb) 1–8.
65. G. Dolton, E. Zervoudi, C. Rius, A. Wall, H.L. Thomas, A. Fuller, L. Yeo, M. Legut, S. Wheeler, M. Attaf, D.M. Chudakov, E. Choy, M. Peakman, A.K. Sewell, Optimized peptide-MHC Multimer protocols for detection and isolation of autoimmune T-cells, Front. Immunol. 29 (9) (2018 Jun) 1378.
66. C. Vandamme, R. Xicluna, L. Hesnard, M. Devaux, N. Jaulin, M. Guilbaud, J. Le Duff, C. Couzini´e, P. Moullier, X. Saulquin, O. Adjali, Tetramer-based enrichment of preexisting anti-AAV8 CD8+ T cells in human donors allows the detection of a TEMRA subpopulation, Front. Immunol. 21 (10) (2020 Jan) 3110.
67. E. Barnes, S.M. Ward, V.O. Kasprowicz, G. Dusheiko, P. Klenerman, M. Lucas, Ultra-sensitive class I tetramer analysis reveals previously undetectable populations of antiviral CD8+ T cells, Eur. J. Immunol. 34 (6) (2004 Jun) 1570–1577.

68. D.M. Richards, E. Ruggiero, A.C. Hofer, J.P. Sefrin, M. Schmidt, C. von Kalle, M. Feuerer, The contained self-reactive peripheral T cell repertoire: size, diversity, and cellular composition, J. Immunol. 195 (5) (2015 Sep 1) 2067–2079, https:// doi.org/10.4049/jimmunol.1500880. Epub 2015 Jul 20. PMID: 26195815.
69. P.S. Ohashi, S. Oehen, K. Buerki, H. Pircher, C.T. Ohashi, B. Odermatt, B. Malissen, R.M. Zinkernagel, H. Hengartner, Ablation of "tolerance" and induction of diabetes by virus infection in viral antigen transgenic mice, Cell. 65 (2) (1991 Apr 19) 305–317.
70. D. Zehn, M.J. Bevan, T cells with low avidity for a tissue-restricted antigen routinely evade central and peripheral tolerance and cause autoimmunity, Immunity. 25 (2) (2006 Aug) 261–270.
71. T.C. Butler, M. Kardar, A.K. Chakraborty, Quorum sensing allows T cells to discriminate between self and nonself, Proc. Natl. Acad. Sci. U. S. A. 110 (29) (2013 Jul 16) 11833–11838.
72. S. Koehli, D. Naeher, V. Galati-Fournier, D. Zehn, E. Palmer, Optimal T-cell receptor affinity for inducing autoimmunity, Proc. Natl. Acad. Sci. U. S. A. 111 (48) (2014 Dec 2) 17248–17253, https://doi.org/10.1073/pnas.1402724111. Epub 2014 Nov 19. PMID: 25411315; PMCID: PMC4260541.
73. I. Cammarata, C. Martire, A. Citro, D. Raimondo, D. Fruci, O. Melaiu, V. D'Oria, C. Carone, G. Peruzzi, C. Cerboni, A. Santoni, J. Sidney, A. Sette, M. Paroli, R. Caccavale, E. Milanetti, M. Riminucci, E. Timperi, S. Piconese, A. Manzo, C. Montecucco, R. Scrivo, G. Valesini, E. Cariani, V. Barnaba, Counter-regulation of regulatory T cells by autoreactive CD8+ T cells in rheumatoid arthritis, J. Autoimmun. 99 (2019 May) 81–97.
74. R. Lande, E. Botti, C. Jandus, D. Dojcinovic, G. Fanelli, C. Conrad, G. Chamilos, L. Feldmeyer, B. Marinari, S. Chon, L. Vence, V. Riccieri, P. Guillaume, A. A. Navarini, P. Romero, A. Costanzo, E. Piccolella, M. Gilliet, L. Frasca, The antimicrobial peptide LL37 is a T-cell autoantigen in psoriasis, Nat. Commun. 3 (5) (2014 Dec) 5621, https://doi.org/10.1038/ncomms6621. Erratum in: Nat. Commun. 2015;6:6595. (PMID: 25470744).
75. M. Paul, D. Badal, N. Jacob, D. Dayal, R. Kumar, A. Bhansali, S.K. Bhadada, N. Sachdeva, Pathophysiological characteristics of preproinsulin-specific CD8+ T cells in subjects with juvenile-onset and adult-onset type 1 diabetes: a 1-year follow-up study, Pediatr. Diabetes 19 (1) (2018 Feb) 68–79.
76. N. Sachdeva, M. Paul, D. Badal, R. Kumar, N. Jacob, D. Dayal, A. Bhansali, S. K. Arora, S.K. Bhadada, Preproinsulin specific CD8+ T cells in subjects with latent autoimmune diabetes show lower frequency and different pathophysiological characteristics than those with type 1 diabetes, Clin. Immunol. 157 (1) (2015 Mar) 78–90.
77. A. Citro, R. Scrivo, H. Martini, C. Martire, P. De Marzio, A.R. Vestri, J. Sidney, A. Sette, V. Barnaba, G. Valesini, CD8+ T cells specific to apoptosis-associated antigens predict the response to tumor necrosis factor inhibitor therapy in rheumatoid arthritis, PLoS One 10 (6) (2015 Jun 10), e0128607.
78. S. Valkiers, N. de Vrij, S. Gielis, S. Verbandt, B. Ogunjimi, K. Laukens, et al., Recent advances in T-cell receptor repertoire analysis: bridging the gap with multimodal single-cell RNA sequencing, ImmunoInformatics [Internet]. 5 (2022), 100009.

Supplemental figures

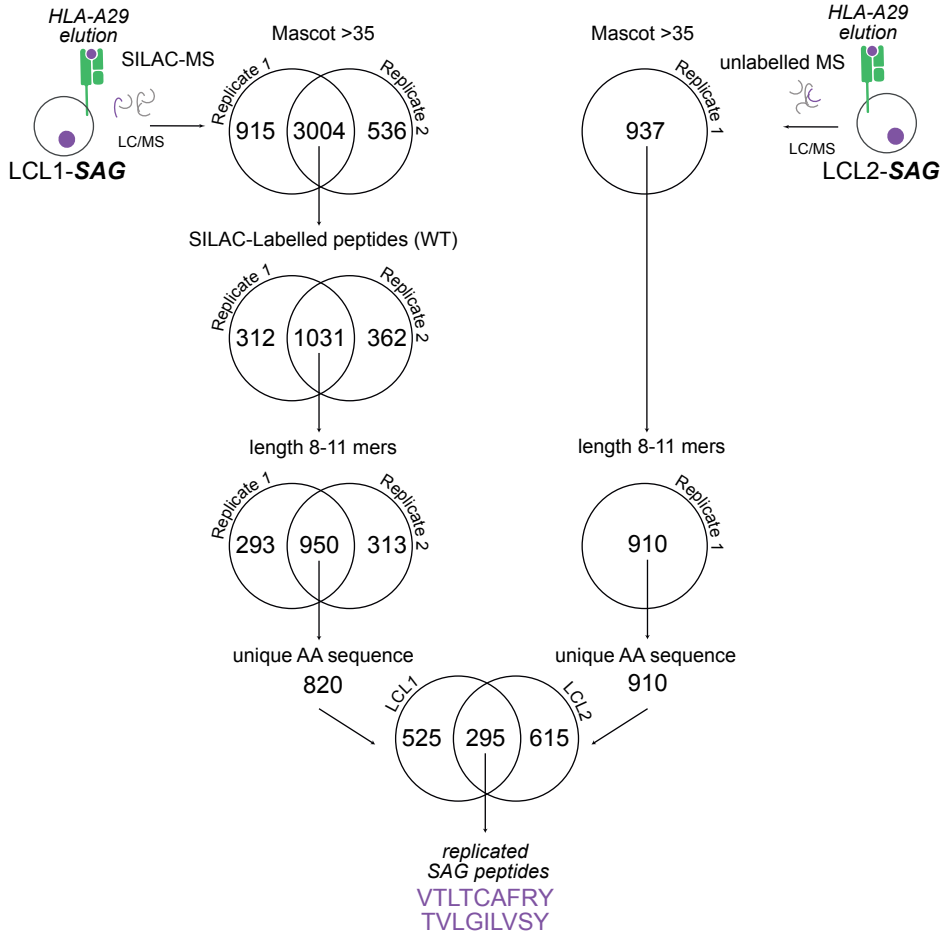

Supplemental Figure 4.1. Venn diagram of filtering steps of the peptides identified by mass spectrometry in the HLA-A29 immunopeptidomes of LCL1 and LCL2.

>>

Supplemental Figure 4.2. The MS/MS spectrum of the peptide fragment ions derived from the SAG peptides identified in elutions from HLA-A29 immunoprecipitations of the patient derived cell lines ("eluted") and from recombinant peptides with identical amino acid sequence ("synthetic"). The relative abundance and mass/charge (m/z) of characteristic (a-,-b-, and y-) ions from the fragmentation of the peptides are highlighted.

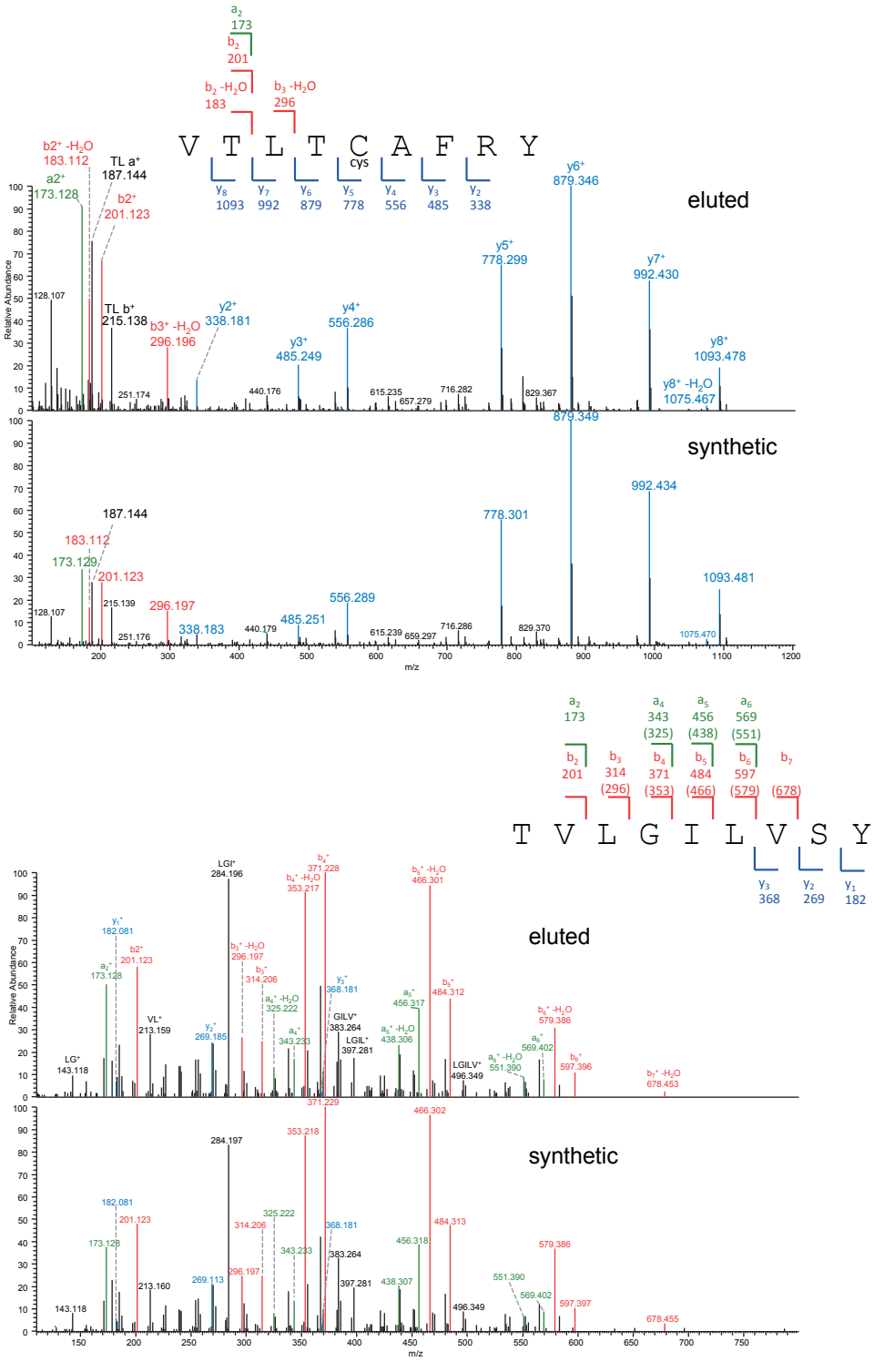
a2 173
b2 201
b2 -H2O 183
b3 -H2O 296
V T L T C A F R Y
cys
y8 1093
y7 992
y6 879
y5 778
y4 556
y3 485
y2 338
b2+ -H2O 183.112
TL a+ 187.144
a2+ 173.128
b2+ 201.123
y6+ 879.346
y5+ 778.299
y7+ 992.430
y8+ 1093.478
y8+ -H2O 1075.467
TL b+ 215.138
b3+ -H2O 296.196
y2+ 338.181
y4+ 556.286
y3+ 485.249
eluted
synthetic
Relative Abundance
m/z
a2 173
a4 343 (325)
a5 456 (438)
a6 569 (551)
b2 201
b3 314 (296)
b4 371 (353)
b5 484 (466)
b6 597 (579)
b7 (678)
T V L G I L V S Y
y3 368
y2 269
y1 182
LGI+ 284.196
VL+ 213.159
LG+ 143.118
GILV+ 383.264
LGIL+ 397.281
LGILV+ 496.349
eluted
synthetic

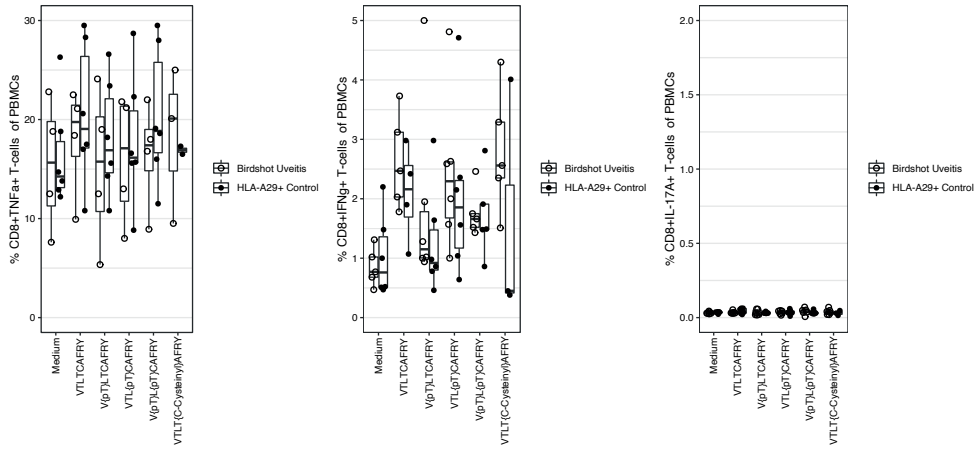

Supplemental Figure 4.3. Intracellular cytokine detection by flow cytometry of TNF-alpha, IFN-gamma, and IL-17 producing CD8+ T-cells after S-antigen peptide stimulated cultures of PBMCs. The comparison of the percentage of cytokine producing CD8+ T-cells in unstimulated PBMC cultures, or stimulated with VTLTCAFRY, VTLTCAFRY with the phosphorylated T as position 2 (V{pT}LTCAFRY, VTLTCAFRY with the phosphorylated T as position 4 (VTL{pT} CAFRY, VTLTCAFRY with phosphorylated T as position 2 and 4 (V{pT}L{pT}CAFRY, and VTLTCAFRY with a cysteinyl to C at position 5 (VTLT{C-Cystenyl}AFRY is shown. None of the comparisons were statistically significant by Dunn's test with correction for multiple testing.

Chapter 5

A *cis*-regulatory element regulates *ERAP2* expression through autoimmune disease risk SNPs

W.J. Venema[1,2], S. Hiddingh[1,2], J. van Loosdregt[2], J. Bowes[3], B. Balliu[4], J.H. de Boer[1], J. Ossewaarde-van Norel[1], S.D. Thompson[5], C.D. Langefeld[6], L.T. van der Veken[7], P.H.L. Krijger[8], W. de Laat[8], J.J.W. Kuiper[1,2]

1. Department of Ophthalmology, University Medical Center Utrecht, Utrecht University, Utrecht, the Netherlands.
2. Center for Translational Immunology, University Medical Center Utrecht, Utrecht University, Utrecht, the Netherlands.
3. Centre for Genetics and Genomics Versus Arthritis, Centre for Musculoskeletal Research, Manchester Academic Health Science Centre, The University of Manchester, Manchester, UK.
4. Department of Computational Medicine, David Geffen School of Medicine, University of California, Los Angeles, CA, USA.
5. Department of Pediatrics, University of Cincinnati College of Medicine, Division of Human Genetics, Cincinnati Children's Hospital Medical Center, Cincinnati, Ohio, USA
6. Department of Biostatistics and Data Science, and Center for Precision Medicine, Wake Forest University School of Medicine, Winston-Salem, NC, USA
7. Department of Genetics, Division Laboratories, Pharmacy and Biomedical Genetics, University Medical Center Utrecht, Utrecht University, Utrecht, The Netherlands.
8. Oncode Institute, Hubrecht Institute-KNAW and University Medical Center Utrecht, 3584 CT Utrecht, the Netherlands.

Manuscript under review

Abstract

Single nucleotide polymorphisms (SNP) near the *ERAP2* gene are associated with autoimmune conditions such as *Crohn's disease*, and *birdshot chorioretinopathy*, as well as protection against lethal infections, including the *Black Death*. Due to high linkage disequilibrium (LD), a great number of trait-associated SNPs are correlated with *ERAP2* expression, however their functional mechanisms remain unidentified.

We used genome editing and functional genomics to identify causal variants that remain obscured by LD. We demonstrate by reciprocal allelic replacement that *ERAP2* expression is directly controlled by the genotype of splice region SNP rs2248374. However, we demonstrate that autoimmune disease-risk SNPs located near the downstream *LNPEP* gene promoter are independently associated with *ERAP2* expression. Allele-specific conformation capture assays revealed long-range chromatin contacts between the *LNPEP* promoter region and the *ERAP2* promoter and showed that interactions were stronger in patients carrying the alleles that increase susceptibility to autoimmune diseases. Replacing the disease-associated SNPs in the *LNPEP* promoter by reference sequences lowered *ERAP2* expression.

These findings show that clustered GWAS signals associated with diverse autoimmune conditions and lethal infections act in concert to control ERAP2 expression and that disease-associated variants can convert a gene promoter region into a potent enhancer of a distal gene.

Introduction

MHC class I molecules (MHC-I) display peptides derived from intracellular proteins allowing CD8+ T cells to detect infection and malignancy[1,2]. In the endoplasmic reticulum, aminopeptidases ERAP1 and ERAP2 shorten peptides that are presented by MHC-I[3-5]. Dysfunctional ERAP may alter the repertoires of peptides presented by MHC-I, potentially activating CD8+ T cells and causing adverse immune responses[6-8].

In *genome-wide association studies* (GWAS), polymorphisms at *5q15* (chromosome 5, *q* arm, G-band *15*) near the *ERAP1* and *ERAP2* genes have been associated with multiple autoimmune conditions. Among them are ankylosing spondylitis[9,10], Crohn's disease [CD][11], juvenile idiopathic arthritis [JIA][12], birdshot chorioretinopathy [BCR][13,14], psoriasis, and Behcet's disease[15,16]. The SNPs identified in GWAS as disease-risk SNPs in *ERAP1* usually correspond to changes in amino acid residues, resulting in proteins with different peptide trimming activities and expression levels[8,17-20].

On the other hand, many SNPs near *ERAP2* are highly correlated with the level of *ERAP2* expression (i.e., *expression quantitative trait loci* [eQTLs] for *ERAP2*)[21,22]. Due to linkage disequilibrium (LD) between these SNPs, there are two common *ERAP2* haplotypes; one haplotype encodes enzymatically active ERAP2 protein while the alternative haplotype encodes transcript with an extended exon 10 that contains premature termination codons, inhibiting mRNA and protein expression[23]. The haplotype that produces full-size *ERAP2* increases the risk of autoimmune diseases such as CD, JIA, and BCR, but it also protects against severe respiratory infections like pneumonia[24], as well as historically the *Black Death*, caused by the bacterium *Yersinia pestis*[11-13,25]. There is a SNP rs2248374 (allele frequency ~50%) located within a donor splicing site directly after exon 10 that tags these common haplotypes[14,23,26]. Consequently, rs2248374 is assumed to be the sole variant responsible for ERAP2 expression. Although this is supported by association studies and minigene based assays[23,26], strikingly, there have been no studies evaluating *ERAP2* expression after changing the allele of this SNP in genomic DNA. This leaves the question of whether the rs2248374 genotype is essential for *ERAP2* expression unanswered.

More than a hundred additional *ERAP2* eQTLs located in and downstream of the *ERAP2* gene, form a large 'extended ERAP2 haplotype'[13]. It is commonly assumed that these *ERAP2* eQTLs work solely by tagging (i.e., in LD with) rs2248374[23,25,27-30]. There is however, evidence that some SNPs in the extended *ERAP2* haplotype may influence *ERAP2* expression independent of rs2248374[20,32]. The use of CRISPR-Cas9 genome editing and functional genomics may be able to unravel the *ERAP2* haplotypes and identify causal variants that regulate *ERAP2* expression but are obscured by LD with rs2248374 in association studies.

We investigated whether rs2248374 is sufficient for the expression of *ERAP2*. Polymorphisms influencing *ERAP2* expression were identified using allelic replacement by CRISPR-mediated homologous repair and conformation capture assays. We report that rs2248374 was indeed

critical for *ERAP2* expression, but that *ERAP2* expression is further influenced by additional SNPs that facilitate a local conformation that increases promoter interactions.

Materials & methods

Cell culture

The THP1 cell line (ATCC, TIB-202™ ECACC Cat# 88081201, RRID:CVCL_0006, monocyte isolated from peripheral blood from an acute monocytic leukemia patient) and Jurkat cell line (ATCC, Clone E6-1,TIB-152™; established from the peripheral blood of a 14-year-old, male, acute T-cell leukemia patient) were purchased from ATCC. Cell lines were cultured in Roswell Park Memorial Institute 1640 medium (RPMI 1640, Thermo Fisher Scientific) supplemented with 10% heat-inactivated fetal bovine serum (FBS, Biowest Riverside) and 1% penicillin/streptomycin (Thermo Fisher Scientific). The authenticity of each cell line was monitored by genome-wide SNP-array analysis (for technical details see *High-density SNP-array analysis* below). On the SNP array, 41 SNPs from a 97-SNP fingerprint for cancer cell line authentication (COSMIC Cell Line repository, available via https://cancer.sanger.ac.uk) were present. Jurkat and THP-1 cell lines used in this study had genotypes identical to those in the COSMIC Cell Line repository (**Supplemental Table 5.1**).

Table 5.1a: **DNA oligonucleotides used as guide RNA and DNA donor template for modification of rs2248374 in both THP-1 and Jurkat cell lines.** Sequences (5'→3') of the used Alt-R® CRISPR-Cas9 crRNAs and Ultramer® DNA Oligos. Rs2248374 is highlighted in red in both crRNAs and DNA templates; the introduced *TaqI* motif sequence in each donor template is underscored (CGA). The template design of the Ultramer DNA oligos follows the work by Richardson *et al*.[69], which proposed that a template should be 127 bp in length (36 bp 5', 91 bp 3' of cut site respectively).

Oligo	THP-1 (rs2248374-GG)	Jurkat (rs2248374-AGG)
Alt-R® CRISPR-Cas9 crRNA	AGATGACAAGTAACATGGTG	AGATGACAAGTAACATGGTA
Ultramer® DNA Oligo	AGGGACAGGTGGGCTACTCTGTATGTCATACT CACTCTAGGTCAGGCTATTCCACAGATCTCTTC TACTCTGTGACTCTCTTTATCCTTACCATGTTC GATGTCATCTTGGGATCCGAATGACAAAC	AGGGACAGGTGGGCTACTCTGTATGTCATACT CACTCTAGGTCAGGCTATTCCACAGATCTCTTC TACTCTGTGACTCTCTTTATCCTCACCATGTT CGATGTCATCTTGGGATCCGAATGACAAAC

CRISPR-Cas9-mediated allelic substitution

We used the Alt-R gRNA system (Alt-R® CRISPR-Cas9 tracrRNA ligated to custom Alt-R® CRISPR-Cas9 crRNA) together with recombinant Alt-R® S.p. Cas9 Nuclease V3 (Integrated DNA Technologies) and custom Ultramer® DNA Oligo (Integrated DNA Technologies) as donor templates to modify rs2248374 through homology directed repair (**Table 5.1a**). The guide RNA with the recombinant Cas9 nuclease (RNP complex) was assembled by incubating the Alt-R® tracrRNA with the custom crRNA (**Table 5.1a**) at 95°C for 5 min (1:1 ratio), followed by cooling down at room temperature. The RNP complex was mixed with the Alt-R® S.p. Cas9 Nuclease and Buffer R (Neon system), followed by 10 min incubation. The custom DNA

template was added to the mixture after RNP assembly. THP-1 cells or Jurkat cells were electroporated with the Neon Transfection System (Thermo Fisher Scientific) (for Jurkat cells: protocol A in **Table 5.3**).

Table 5.1b: DNA oligonucleotides used as guide RNA and DNA donor template (1500bp) for modification of LNPEP promoter. Sequences (5'→3') of the used Alt-R® CRISPR-Cas9 crRNAs and Megamer™ DNA Oligo. The protective alleles of the seven SNPs in the regulatory region are highlighted in red (from '5 to 3') rs2548224-T, rs3842058-AAA, rs2548225-A, rs2617435-T, rs1046395-G, rs1046396-G, and rs2762-C respectively , in the Megamer™ sequence, as well as both gRNA binding locations (green = crRNA sequence; red = PAM sequence).

Oligo	Oligo sequences 5' → 3' for CRISPR-knock in experiment in Jurkat (Figure 5.3C)
Alt-R® CRISPR-Cas9 crRNA	crRNA 1: CCTGTAGGAGCGTTAAGTTG crRNA 2: ATGAGGCTGACTCACCCATT
Megamer™ DNA Oligo	GTGGGCAGTGGGAAAGTTGGCAGCTCAGGTTTGCCCCCGGAGGAGGCGGTGTCGG CCCGACTCTCCTGTAGGAGCGTTAAGTTGTGGCAGCTGCCGAGCCCAACTTTTGTG GGGCGCCAGGAGCTGTCCCCCTGCCCTTCAGTGAGCTGCCGGCGTGACTTTTCCTA ATAGGGCGGGGTGGGGGTGGGAGGCTTGGCAGGTTAATGTTGTGGAAGGAAGG GAAACTTCAGGAAAGGCTTGCTCACCTCGCTCGGTGCCGCGGAGGTGCCTGGCCA CAGTGCCACCCTCCTGACCCTGCCGAGGTACTCGGCAGGGCCACCACGCATCCCCTCACT GGCTGCAGATCACATCAGTTTTTCAGTCAAAGACTTGTTAATGTCAAGGGTCCGTCAC GGTGGTGATACCACTGTGTGACAGGAAGCGAGAGTCAACGCAGGGAGCCTGCACCCT GCAAACAGCCACAGCCCTTCACTGAACGGGGAGCATAAATCCCACCCTAGTTAGAAC CATGGCTTTTGTGCGGACCAGAAGTGCCAGAGCCACAATATAGGGGTGAGATGTCTTAC CGTTTTGCGGTGTTGAGTGTGTGGATTCCCTTTTAAGATAGAAAGTAGGAAAACTGC CAGTAAGGGAGACGACTCACTAAAAGAGGATTCAGTCTCTGGTTGACATGTTTTGCT GAGTGTGGTTGGTTACTTCAGGTACAGTATCACATTAATAGGGGCCACAGTCTATATCCCT GTTTAGTTTGTTAGTTACCACTCAAGAGCAGACAGATATTGTCCACTTTATCCCAAATC CCAGCCAGACTTTGTTGTATGCTGTGCTTCATTCATGGGGCTGTGAACTACTGATTATAT TCTCCCTATTCCTAATGTAGAATGCTTTATTCTACTGCCATCTTTCTGTCTGCACTGTTTA ATTAGGCTTACTGATAACAACTTTAATTCTGAATTTTCTTTCTCATTCAGGTTCTATTTG TAATTACTAAGACTTAAAGAATAGTCTGGTGAAGTTACTCGAAGAATTAAGGAAG GTTTGAGCTAAAATGAACTAGAGACCATCTAGTACTTTAGTGTAAAATATGTTTAATA CAAGTCGTTAAGTCCTTGTAAGTGACTATTCCAATGTTCATTCTTTGTTTTTGGAAGAAT- GCTTGGAGTTACCATGTTTTTAAATGTGAAATTTCATCTAAATTAAAAAAAAAATCTCTGT GATGAGGCTGACTCACCCATTTGGTCAAGATTAGTGCTAGCTGATTTGCTGAACCTTTG CCTACAGAATTAAAGTACTTTCTCAAGTTTTAAAATTGGTGTCTTTTCTCTTATAGAA TATGCTTCTAGATTGCTTCTAGATGTGGGTATTTGCAAACTGTCACATTTGGGAGGA CAATGGAAAAATCCCACAGAAGAGAACAAAAAAAGAAGCAATGCTTCAACTTTCAT GTAGGAAATTGGATTTCTGATTCTTTCCTATCTTTCAGAGTTGATGCTGGAGACA

After electroporation the cells were incubated overnight with antibiotic-free culture medium with 20 µM Alt-R® HDR Enhancer (Integrated DNA Technologies). The next day, cells were diluted in 10x dilution steps until a final concentration of 30 cells/mL was reached (total volume 10 mL). Cells were seeded in multiple flat-bottom 96-well plates at 20 µL cell suspension per well (<1 cell/well) and transferred to 24 well plates once grown confluently. Confluent cultured clones were lysed (~80% of total volume) in RLT buffer (Qiagen, Cat# 1030963) and DNA was isolated using Qiagen AllPrep DNA/RNA/miRNA Universal Kit (Cat# 80224). The flanking sequence of rs2248374 was amplified by PCR (Forward primer:

Table 5.2. Details on the SNPs investigated in this study. The minor allele frequency (MAF) and linkage disequilibrium (LD) for each SNP is indicated for the European [EUR] superpopulation of the 1000 Genomes. Data was obtained from LDlink[70].

SNP	Context in this study	Coord (GRChr37)	Alleles	MAF (EUR)	Distance from rs7705093	LD (D')	LD (R2)	Correlated Alleles
rs2248374	ERAP2 splice variant	chr5:96235896	(A/G)	0.4801	-54751	0.99	0.75	C=G,T=A
rs2549794	lead SNP 5q15 in Crohn's disease[11]	chr5:96244549	(C/T)	0.4046	-46098	0.98	0.92	C=T,T=C
rs2548224	ERAP2 eQTL in regulatory region	chr5:96272420	(T/G)	0.4175	-18227	0.99	0.98	C=T,T=G
rs3842058	ERAP2 eQTL in regulatory region	chr5:96272528	(AA/-)	0.4175	-18119	0.99	0.98	C=AA,T=-
rs2548225	ERAP2 eQTL in regulatory region	chr5:96273033	(A/T)	0.4155	-17614	1.0	0.98	C=A,T=T
rs2617435	ERAP2 eQTL in regulatory region	chr5:96273034	(T/C)	0.4155	-17613	1.0	0.98	C=T,T=C
rs1046395	ERAP2 eQTL in regulatory region	chr5:96273180	(G/A)	0.4016	-17467	1.0	0.93	C=G,T=A
rs1046396	ERAP2 eQTL in regulatory region	chr5:96273187	(G/A)	0.4155	-17460	0.99	0.98	C=G,T=A
rs2762	ERAP2 eQTL in regulatory region	chr5:96273298	(C/T)	0.4145	-17349	1.0	0.99	C=C,T=T
rs7705093	lead SNP 5q15 in birdshot chorioretinopathy[13]	chr5:96290647	(C/T)	0.4175	0	1.0	1.0	C=C,T=T
rs27290	lead SNP 5q15 in JIA[12]	chr5:96350088	(G/A)	0.4145	59441	1.0	0.99	C=A,T=G

Jurkat cells were incubated overnight with antibiotic-free culture medium with 20 μM Alt-R® HDR Enhancer (Integrated DNA Technologies), followed by single cell seeding. PCR (Forward primer: GTGGGCAGTGGGAAAGTTGG; Reverse primer: TGTCTCCAGCATCAACTCTGA) and restriction analysis by TaqI (TaqI-v2, cleaves PCR products containing the G allele of rs1046396 tagging the protective allele) was used to identify clones without cleaved PCR bands (i.e., loss of risk haplotype), and allelic substitutions were validated by sanger sequencing.

AGGGAAAGAGAAGAATTGGA; Reverse primer: TCTCTTTCCTGTAGTGATTC) and PCR products incubated with the TaqI-v2 (R0149S, New England Biolabs) restriction enzyme (15 min at 65 °C). Next, the PCR products were loaded on a 1% agarose gel (agarose, Acros Organics; 10x TAE UltraPure™, Invitrogen) to assess restriction by TaqI. Samples with a cleaved PCR product were prepared for sanger sequencing to validate in-frame integration of donor DNA and correct modification of rs2248374. CRISPR-Cas9-mediated haplotype substitution (i.e., disease-risk alleles to protective alleles) was achieved by using a large single-strand DNA template (**Table 5.1b**, 1500 bp Megamer™, Integrated DNA Technologies) with the alternative allele for SNPs (from '5 to 3') rs2548224, rs3842058, rs2548225, rs2617435, rs1046395, rs1046396, and rs2762 and two guide RNAs (assembled separately) targeting upstream of rs2548224 and downstream of rs2762 respectively (**Table 5.2**) to introduce two double strand breaks. The two RNP complexes were transfected together with the Megamer™ in Jurkat cells (**Table 5.3**, Jurkat protocol B).

CRISPR-Cas9 knock-out of *ERAP2* eQTLs

To delete a 116 kb region downstream of *ERAP2* in Jurkat cells, two RNP complexes were assembled in parallel using Alt-R gRNA system (Alt-R® CRISPR-Cas9 tracrRNA ligated to custom Alt-R® CRISPR-Cas9 crRNA) together with recombinant Alt-R® S.p. Cas9 Nuclease V3 (Integrated DNA Technologies). RNPs with guide RNAs (guide RNA1; GGCATTCCTTAAGGGTATCA and guide RNA2; GCGTTGCTTCACATATAAGT, see for details **Supplemental Figure 5.1**) were transfected by electroporation into Jurkat cells (Jurkat protocol B in **Table 5.3**). Following transfection, Jurkat cells were diluted to 16.67 cells/mL and seeded in 96 well flat bottom plates (<1 cell/well at 50 µL cell suspension/well) for single cell cultures. Jurkat clones were screened by PCR (Fw: GTCCTTTCGCTGCTGATTTG; Rv: AGGTCATTCCACCACTTCATTGT), The PCR products were loaded on a 1% agarose gel (agarose, Acros Organics; 10x TAE UltraPure™, Invitrogen) with the anticipated PCR product size only detectable after deletion of the entire DNA region, which was verified by sanger sequencing (**Supplemental Figure 5.1**).

Table 5.3: **Settings used for transfection with the Neon Transfection System.**

Cell type	Cell #	Pulse (V)	Pulse width (ms)	Pulse #	Pipet tip type (µL)
THP-1	3.0×10^5	1600	10	3	10
Jurkat (Protocol A)	2×10^5	1100	30	2	10
Jurkat (Protocol B)	2×10^5	1325	10	3	10

Western Blot analysis

Western blotting was used to determine the protein levels of ERAP2. NP40 lysis buffer was used to prepare total cell lysates (1% NP40, 135 mM NaCl, 5 mM EDTA, 20 mM Tris-HCl, pH = 7.4), complemented with cOmplete protease inhibitor cocktail (Roche). Protein lysates

(20 µg/lane) were separated on a 4-20% Mini-PROTEAN TGX gel (Bio-Rad Laboratories) and transferred to a polyvinylidene difluoride membrane (Immobilon-P PVDF, Millipore). After blocking in 5% non-fat dry milk in TBST, membranes were probed overnight at 4°C with antibodies that recognize ERAP2 (AF3830, R&D Systems) or α-tubulin (T9026, Sigma-Aldrich). Following washing, membranes were incubated with either anti-goat or anti-mouse secondary antibodies conjugated to HRP (DAKO). Protein bands were detected with Amersham ECL™ Prime Western Blotting (RPN2236, GE Healthcare) on the ChemiDoc Gel Imaging System (Bio-Rad Laboratories).

qPCR analysis

Gene expression was quantified by using qPCR. For *ERAP2* we used primers (**Table 5.4**) which bind to exon 10 (Fw: CATTCGGATCCCAAGATGAC) and exon 11 (Rv: GGAGTGAACACCCGTCTTGT) to determine functional *ERAP2* transcript based on rs2248374 variant. Primers targeting the control gene *RPL32* were used to calculate relative expression. (Fw: AGGGTTCGTAGAAGATTCAAGG; Rv: GGAAACATTGTGAGCGATCTC). The nucleotide sequence for the primers used for qPCR of *ERAP1* and *LNPEP* are shown in **Table 5.4**.

Table 5.4: qPCR primers

Gene	Primer sequence (5' → 3')
ERAP2 Forward	CATTCGGATCCCAAGATGAC
ERAP2 Reverse	GGAGTGAACACCCGTCTTGT
ERAP1 Forward	GCAAACCTTACCACGCTGAC
ERAP1 Reverse	GGTTCTTCCGATAGCCTCTCTC
LNPEP Forward	AGGGATGAGCAATACACCGC
LNPEP Reverse	AGCAACCAAGTAAGTGCTCA
RPL32 Forward	AGGGTTCGTAGAAGATTCAAGG
RPL32 Reverse	GGAAACATTGTGAGCGATCTC

ERAP2 activity assay

To assess ERAP2 enzymatic function in THP-1 cells after introduction of the A allele of rs2248374, total cellular ERAP2 protein was enriched by immunoprecipitation and incubated with L-Arginine-7-amido-4-methylcoumarin hydrochloride (R-AMC, A2027, Sigma-Aldrich). Briefly, THP-1 cells were lysed (50 mM Tris, 150 mM NaCl, 1% Triton X-100, pH 7.5) and 500 µg cell lysate was incubated for 2h at 4°C with Protein-G-sepharose beads (BV-6511, BioVision) and anti-ERAP2 (AF3830, R&D Systems). Beads were washed in assay buffer (50 mM Tris, 1 mM DTT, pH 7.5) and resuspended in 100 µL assay buffer. Duplicate samples containing 40 µL beads solution were incubated with 40 µM of R-AMC (total volume 50 µL) for 1h at 37°C, while the fluorescent signal was measured (E_x: 370-10, E_m: 440-20) with a CLARIOstar plate reader (BMG Labtech).

Allele-specific 4C-seq

EBV-immortalised lymphoblastoid cell lines (LCL) were generated from peripheral blood mononuclear cells (PBMC) from 3 birdshot chorioretinopathy patients as previously described[33]. The integrity of the genomes of the LCLs was assessed with whole genome SNP-array analysis, showing no abnormalities (**Supplemental Figure 5.2**). 4C template preparation was performed as described[34]. Patient-derived cell lines were cultured in RPMI 1640 supplemented with 10% FBS 1% penicillin/streptomycin (Thermo Fisher Scientific), washed and cross-linked in 2% formaldehyde. DNA was digested in situ with MboI (NEB) and Csp6I (Thermo Scientific). Primers used for inverse PCR (5'-TACACGACGCTCTTCCGATCTTGTGGTTGGTTACTTCAGGT-3', 5'-ACTGGAGTTCAGACGTGTGCTCTTCCGATCTGGACCCTTGACATTAACAAG-3') allow reading of the ERAP2 eQTL rs3842058 (indel within the regulatory element) in the viewpoint fragment that is associated with the risk allele. Products were sequenced using Illumina sequencing (Illumina NextSeq 500). 4C-seq reads were demultiplexed by matching the 5'-ends of the R1 reads to the reading primer sequence (allowing 2 mismatches), and split into risk and non-risk reads based on the presence of the indel and its flanking sequence (GGACCCTTGACATTAACAAGTCTGAC for the risk allele and GGACCCTTGACATTAACAAGTCTTTG for the non-risk allele). Finally reads were mapped to the hg19 reference genome and processed using pipe4C[34] (github.com/deLaatLab/pipe4C) with the following parameters: normalization to 1 million reads in cis, window size 21, removal of top 2 read counts. Overlay plots were generated using R (https://www.R-project.org/).

High-density SNP-array analysis

Genomic DNA of unedited and edited clones of THP-1 and Jurkat cell lines, and patient-derived LCLs was used for SNP-array copy number profiling and analysis of regions of homozygosity with the Infinium Human CytoSNP-850K v1.2 BeadChip (Illumina, San Diego, CA, USA). This array has ~850,000 single nucleotide polymorphisms (SNPs) markers across the genome and can detect genomic insertions and deletions as well as stretches of homozygosity. Data analysis was conducted using NxClinical software v6.0 (Bionano genomics, San Diego, CA, USA). Human genome build Feb. 2009 GRCh37/hg19 was used. Results were classified with BENCH Lab CNV software (Agilent, Santa Clara, CA, USA). The genotype data were used for cell line verification and monitoring for potential genomic alterations in single cell cultures.

ERAP2 eQTL colocalization and conditional analysis

Summary statistics of GWAS from CD (obtained via https://www.ibdgenetics.org/uploads/cd-meta.txt.gz)[11], JIA[12], and BCR[13] were used in visualization of disease associated SNPs at *5q15*. ERAP2 eQTL data for 'whole blood' were downloaded from the GTEx portal and used for GWAS colocalization analysis with the *coloc* R package (v.5.1.0.1)[35]. We assessed the likelihood of colocalization using the posterior probability (PP) for hypothesis 4 (that there is an association between both traits and they are driven by the same causal variant(s)). The likelihood of colocalization was deemed high for associations with PP4 > 0.8. The posterior

probability of colocalization (H4) was calculated using the *coloc.abf()* function using default priors. For cross tissue ERAP2 eQTL conditional analyses, we used the "FastGxC" shared *ERAP2* eQTL data as reported by *Lu* et al., which is calculated using RNA-seq data from the Genotype-Tissue Expression (GTEx) Consortium v8[36]. To identify *ERAP2* eQTLs and pQTLs with association signals independent from rs2248374, conditional analysis was conducted using *conditional and joint multiple-SNP analysis* (GCTA-COJO) using the *ERAP2* eQTL data from FastGxC or ERAP2 pQTL data from targeted plasma proteomics from the INTERVAL study[37] using LD information from the EUR superpopulation as a reference panel. More details on colocalization and conditional association analysis are outlined in ***Appendix 5.I***. The GWAS regional association data for CD, BCR, and JIA and ERAP2 eQTL and pQTL are shown in **Supplemental Table 5.2-5.7**.

Splice prediction of rs2248374

We used the deep neural network *SpliceAI*[38] and *Pangolin*[39] to predict the effects of the A>G allele substitution in pre-mRNA transcript sequences. Masked scores were predicted via https://spliceailookup.broadinstitute.org/[38] using "chr5 96900192 A G" as input for hg38, and "chr5 96235896 G A" for hg19.

ERAP2 promotor-interacting SNP selection.

The promoter-interacting eQTL summary statistics for *ERAP2* determined by H3K27ac HiChIP assays in primary immune cells were obtained from Chandra *et al.*[40]. We selected *ERAP2* eQTLs located in active enhancer regions at *5q15* (i.e., H3K27ac peaks) that significantly interacted with the transcriptional start site of *ERAP2* for each immune cell type (P<0.05). We visualised *H3K27* acetylation data from primary tissue analysis from ENCODE using the *WASHU Epigenome Browser*[41] (v54.00) at http://epigenomegateway.wustl.edu/browser/ (direct link to used data at *5q15* via: https://tiny.one/2p92f7tb). Massive parallel sequence data results for *ERAP2* eQTLs were obtained from supplementary data from Abell *et al*.[32].

Data availability

Additional data underlying figures is shown in **Supplemental Table 5.1-5.11.** The full reproducible code will be made available via dataverseNL. https://dataverse.nl/

Results

ERAP2 expression depends on the genotype of rs2248374.

The SNP rs2248374 is located downstream of exon 10 of *ERAP2* and its genotype strongly correlates with ERAP2 expression. Predictions by deep neural network-based algorithms *SpliceAI* and *Pangolin* indicate that the A>G allelic substitution by rs2248374 inhibits constitutive splicing three base pairs upstream at the canonical exon-intron junction

(*SpliceAI,* donor loss Δ score = 0.51, *Pangolin* Δ score = 0.58). Despite widespread assumption that this SNP controls *ERAP2* expression, functional studies are lacking[23]. Therefore, we first aimed to determine whether ERAP2 expression is critically dependent on the genotype of this SNP. Allelic replacement by CRISPR-mediated homologous repair using a donor DNA template was used to specifically mutate rs2248374 G>A by homology directed repair (HDR) (**Figure 5.1A**). Because HDR is inefficient[42], a silent mutation was inserted into the donor template to produce a *TaqI* restriction site, which can be used to screen clones with correctly edited SNPs. As THP-1 cells are homozygous for the G allele of rs2248374 (**Figure 5.1B**), we used this cell line for experiments because it can be grown in single-cell derived clones. We targeted rs2248374 in THP-1 cells and established a clone that was homozygous for the A allele of rs2248374 (**Figure 5.1B**). Sequencing of the junctions confirmed that the integrations were seamless and precisely positioned in-frame.

SNP-array analysis was performed to exclude off-target genomic alterations giving rise to duplications and deletions in the genome of the gene edited cell lines (**Supplemental Figure 5.3**). We did not observe any of such unfavorable events. This confirmed that our editing strategy did not induce widespread genomic changes[43]. While THP-1 cells are characterized by genomic alterations, including large regions of copy number neutral loss of heterozygosity of chromosome 5 (including *5q15*)[44,45] (**Supplemental Figure 5.3**), the results confirmed that single-cell clones from the unedited 'wild-type' (WT, rs2248374-GG) THP-1 cells and "edited" THP-1 (rs2248374-AA) were genetically identical at *5q15*, which justifies their comparison (**Figure 5.1C**). In contrast with WT THP-1, *ERAP2* transcript became well detectable in THP-1 cells in which we introduced the A allele of rs2248374 (**Figure 5.1D**). According to Western Blot analysis, WT THP-1 cells lack ERAP2 protein, while the rs2248374-AA clone expressed full-length ERAP2 (**Figure 5.1E**), which was enzymatically functional as determined by a fluorogenic *in vitro* activity assay (**Figure 5.1F**).

Oppositely, we then examined whether mutation of rs2248374 A>G would abolish *ERAP2* expression in cells naturally expressing ERAP2. The Jurkat T cell line was chosen because they are heterozygous for rs2248374 and express ERAP2, and they possess the ability to grow in single-cell clones required to overcome the low-efficiency of CRISPR knock-in by HDR. To alter the single A allele of rs2248374 in the Jurkat cell line, we used a donor DNA template encoding the G variant (**Supplemental Figure 5.4A**) and established a clone homozygous for rs2248374 G (**Supplemental Figure 5.4B**)**.** We found no changes between our unedited population and rs2248374 edited Jurkat cells at *5q15* by whole genome homozygosity mapping (**Supplemental Figure 5.4C**). The A>G substitution at position rs2248374 depressed *ERAP2* mRNA expression (**Supplemental Figure 5.4D**) and abolished ERAP2 protein expression (**Supplemental Figure 5.4E**). These results show that *ERAP2* mRNA and protein expression is critically dependent on the genotype of rs2248374 at steady-state conditions.

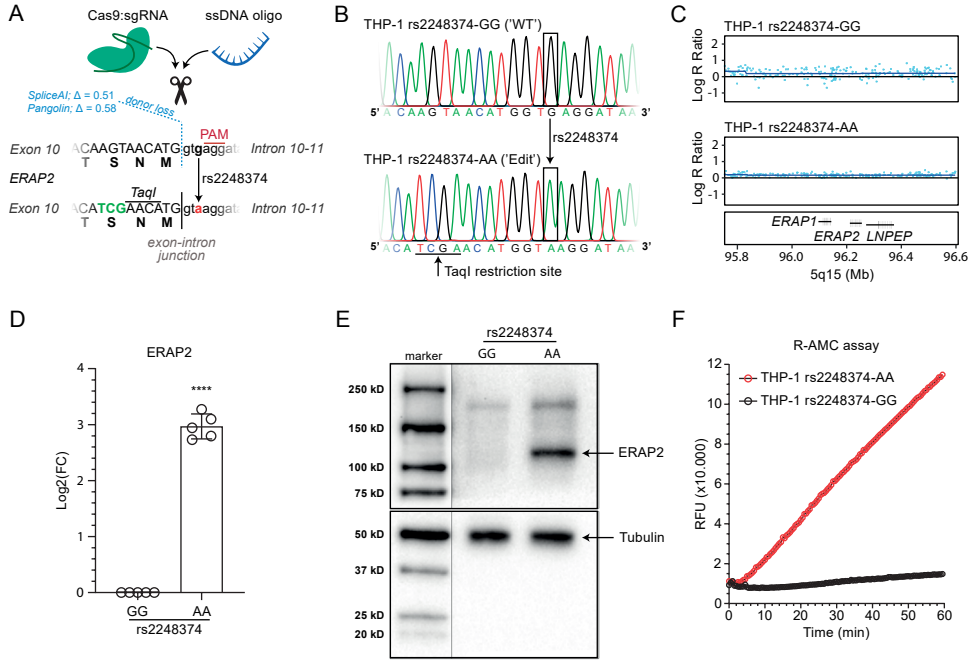

Figure 5.1: The A allele of rs2248374 is essential for full-length ERAP2 expression. (**a**) Overview of the CRISPR-Cas9 mediated homology-directed-repair (HDR) strategy for SNP allelic replacement of the G allele of rs2248374 to the A allele in THP-1 cells. The ssDNA oligo template introduces the A allele at position rs2248374 and a silent *TaqI* restriction site used for screening successfully edited clones. The predicted effect size (delta scores from *SpliceAI* and *Pangolin*) and intended position that exhibits altered splicing induced by the G allele of rs2248374 is shown in blue. (**b**) Sanger sequence data showing THP-1 'WT' with the single rs2248374-G variant and the successful SNP modification to the A allele of rs2248374. (**c**) SNP-array based copy number profiling and analysis of regions of homozygosity of unedited and edited THP-1 clones demonstrating no other genomic changes. Plot is zoomed on *5q15.* Genome-wide results are outlined in **Supplemental Figure 5.3**. (**d**) *ERAP2* gene expression determined by qPCR in cellular RNA from THP-1 cells unedited or edited for the genotype of rs2248374. (**e**) Western blot analysis of ERAP2 protein in cell lysates from THP-1 cells unedited or edited for the genotype of rs2248374. ****) t.test, *P*<0.001 (**f**) Hydrolysis [expressed as relative fluorescence units (RFU)] of the substrate L-Arginine-7-amido-4-methylcoumarin hydrochloride (R-AMC) by immunoprecipitated ERAP2 protein from THP-1 cell lines unedited or edited for the genotype of rs2248374. The generation of fluorescent AMC indicates ERAP2 enzymatic activity.

Disease risk SNPs are associated with ERAP2 levels independent of rs2248374.

Many additional SNPs at chromosome *5q15* show strong associations with *ERAP2* gene expression levels (also known as *ERAP2* eQTLs). Despite LD between the other *ERAP2* eQTLs and rs2248374, rs2248374 does not appear to be the strongest *ERAP2* eQTL in the GTEx database (data for GTEx 'whole blood' shown **Figure 5.2A, Supplemental Table 5.2**). Following this, we investigated the SNPs near the *ERAP2* gene that are associated with several T-cell-mediated autoimmune conditions, such as CD, JIA, and BCR (**Figure 5.2B-D**). We found strong evidence for colocalization between GWAS signals at *5q15* for BCR, CD, and JIA and *cis*-eQTLs for *ERAP2* (**Supplemental Table 5.3**-**5.5**) (posterior probability of colocalization >90%). This indicates that these SNPs alter the risk for autoimmunity through their effects on *ERAP2* gene expression. It is noteworthy, however, that the GWAS hits at *5q15* for CD, BCR, and JIA are in high LD (r^2>0.9) with each other but not in high LD with rs2248374 (r^2<0.8) (**Figure 5.2E**). Furthermore, the GWAS association signal at *5q15* for JIA (lead variant rs27290; $P_{dominant} = 7.5 \times 10^{-9}$) did not include rs2248374 (JIA, $P_{dominant} = 0.65$) (**Figure 5.2D**). In line with this, we previously reported that the lead variant rs7705093 (**Figure 5.2C**) is associated with BCR after conditioning on rs2248374[31]. These findings reveal that SNPs implicated in these complex human diseases by GWAS may affect *ERAP2* expression through mechanisms other than rs2248374.

We therefore sought to determine if *ERAP2* eQTLs function independently of rs2248374. In agreement with the role ERAP2 plays in the MHC-I pathway that operates in most cell types, *ERAP2* eQTLs are shared across many tissues[46,47]. As a proof of principle, we used tissue-shared *ERAP2* eQTLs from a previous analysis of RNA-seq data from the GTEx Consortium (**Figure 5.2F**). To test whether the disease-associated top association signals were independent from rs2248374, we performed conditional testing of the *ERAP2* eQTL signal by first including the genotype of rs2248374 as a covariate in the regression model. Conditioning on rs2248374 revealed a complex independent *ERAP2* eQTL signal composed of many SNPs extending far downstream into the *LNPEP* gene (**Figure 5.2F**). This secondary *ERAP2* eQTL signal included the lead variants at *5q15* for CD, BCR, and JIA ($P_{conditioned} < 5.9 \times 10^{-9}$), consistent with earlier findings in association studies (**Supplemental Table 5.6**)[20,31]. We further strengthened these observations by using summary statistics from SNPs associated with plasma levels of ERAP2 from the INTERVAL study (called protein quantitative trait loci, or pQTLs)[37]. In agreement with the mRNA data from GTEx, conditioning on rs2248374 revealed a strong independent association between GWAS lead variants and ERAP2 protein levels ($P_{conditioned} < 1.6 \times 10^{-62}$) (**Figure 5.2F**). Based on these results, we conclude that GWAS signals at *5q15* are associated with ERAP2 levels independently of rs2248374.

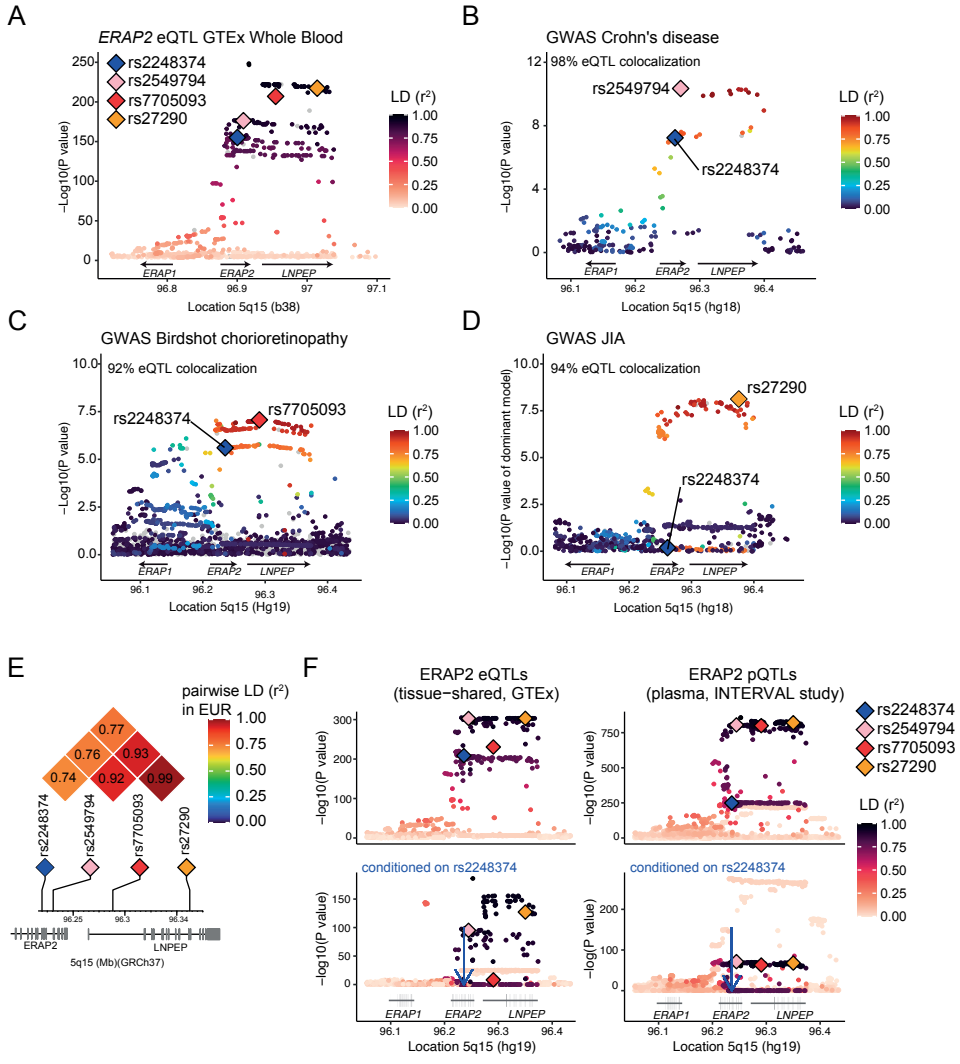

Figure 5.2: **Autoimmune disease-risk SNPs associated with ERAP2 levels independent from rs2248374 genotype.** (**a**) *ERAP2* eQTL data from GTEx whole blood (**Supplemental Table 5.2**). GWAS lead variants at *5q15* for Crohn's disease [CD] (rs2549794, see *b*), birdshot chorioretinopathy [BCR] (rs7705093, see *c*), and juvenile idiopathic arthritis [JIA] (rs27290, see *d*) and rs2248374 are denoted by colored diamonds. The color intensity of each symbol reflects the extent of LD (r^2 from 1000 Genomes EUR samples) with rs2927608. Grey dots indicate missing LD information. (**b**-**d**) Regional association plots of GWAS from CD, BCR, and JIA (**Supplemental Table 5.3-5.5**). For the CD we used the *P* value of rs2549782 (LD [r2]=1.0 with rs2248374 in EUR). The color intensity of each symbol reflects the extent of LD (r^2 estimated using 1000 Genomes EUR samples) with rs2927608. The results from colocalization analysis between GWAS signals and *ERAP2* eQTL data from whole blood (in *a*) is denoted (details in Appendix I). (**e**) Pairwise LD (r^2 estimated using 1000 Genomes EUR samples) comparison between splice variant rs2248374 (*ERAP2*), and disease-risk SNPs rs2549794 (CD), rs7705093 (BCR) and rs27290 (JIA). (**f**) Initial association results and conditional testing of *ERAP2* tissue-shared eQTL data from GTEx consortium and ERAP2 pQTL data from plasma proteomics of the INTERVAL study (**Supplemental Table 5.6**, **5.7**)[37]. Conditioning on rs2248374 (dark blue diamond) revealed independent *ERAP2* eQTL and ERAP2 pQTL signals that include lead variants at *5q15* for CD, BCR, and JIA (P <5.0 x 10^{-8}). The human reference sequence genome assembly annotations are indicated.

SNPs in a downstream cis-regulatory element modulate ERAP2 promoter interaction.

Computational tools to predict the functional impact of non-coding variants may be highly inaccurate[48]. To prioritize likely causal variants by experimentally monitoring their effects on ERAP2, we aimed to resolve the function of SNPs that correlated with ERAP2 expression independent from rs2248374. First, we aimed to generate a large 116 kb heterozygous deletion downstream of *ERAP2* in *Jurkat* cells. This deletion included all downstream SNPs as well as the entire *LNPEP* gene (**Supplemental Figure 5.1**). *ERAP2* expression by qPCR was not significantly reduced by this approach, which may be due to only partial deletion of the region as shown by whole genome zygosity mapping (**Supplemental Figure 5.1**), or the non-selective removal of all downstream putative regulatory elements.

Since allelic replacement would provide a more physiological relevant approach, we next aimed to specifically alter the SNP alleles and evaluate the impact on *ERAP2* expression. The large size of the region containing all the "independent" *ERAP2* eQTLs prevents efficient HDR[43], so we decided to prioritize a regulatory interval with *ERAP2* eQTLs. Genetic variation in non-coding enhancer sequences near genes can influence gene expression by interacting with the gene promoter[49]. Therefore, we leveraged chromosome conformation capture coupled with sequencing (Hi-C) data enriched by chromatin immunoprecipitation for the activating histone H3 lysine 27 acetylation (*H3K27ac*, an epigenetic mark of active chromatin that marks enhancer regions) in primary T cells, B cells, and monocytes[40], immune cells that share ERAP2 eQTLs as shown by single-cell sequencing studies[47]. We selected *ERAP2* eQTLs located in active enhancer regions at *5q15* (i.e., H3K27ac peaks) that significantly interacted with the transcriptional start site of *ERAP2* for each immune cell type. This revealed diverse and cell-specific significant interactions of *ERAP2* eQTLs across the extended *ERAP2* haplotype in immune cells, indicating many regions harboring eQTLs that were physically in close proximity with the transcription start site of *ERAP2* (**Figure 5.3A**). Note that none of these SNPs showed significant interaction with the promoters of *ERAP1* or *LNPEP*. Among these, 9 common non-coding SNPs concentrated in a ~1.6 kb region downstream of *ERAP2* at the 5`end of the gene body of *LNPEP* exhibited strong interactions with the *ERAP2* promoter (**Figure 5.3A**), suggesting that these SNPs lie within a potential regulatory element (i.e., enhancer) that is active in multiple cell lineages. Consistent with these data, examination of ENCODE data of heart, lung, liver, skeletal muscle, kidney, and spleen revealed enrichment of *H3K27ac* marks spanning the 1.6 kb locus, supporting that these SNPs lie within an enhancer-like DNA sequence that is active in across tissues (**Figure 5.3A**). This also corroborates the finding that these SNPs are *ERAP2* eQTLs across tissues, as we[36] showed previously (**Figure 5.2F**). Results from a recent targeted massively parallel reporter assay (MPRA)[32] support that this region may exhibit differential regulatory effects (i.e., altered transcriptional regulation), depending in particular on the allele of SNP rs2548224 (difference in expression levels of target region; reference versus alternative allele for rs2548224, $Padj = 4.9 \times 10^{-3}$) (**Figure 5.3B**). This SNP is also a very strong (rs2248374-independent) *ERAP2* eQTL and pQTL

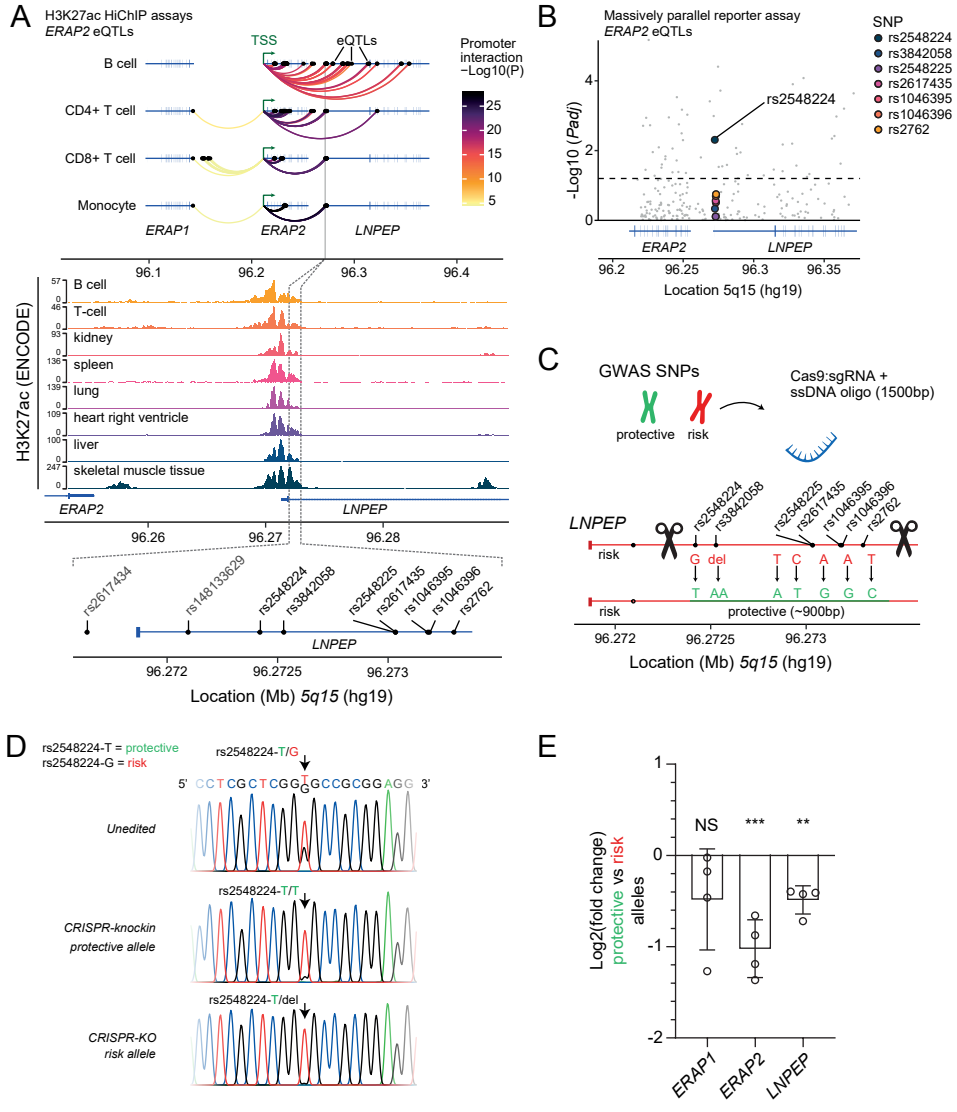

Figure 5.3: **Autoimmune disease risk SNPs tag a downstream regulatory element that regulates *ERAP2* expression.** (**a**) Chromosome conformation capture coupled with sequencing (Hi-C) data enriched by chromatin immunoprecipitation for the histone H3 lysine 27 acetylation (*H3K27ac*) in primary immune cells from Chandra *et al.*[40]. Highlighted are the *ERAP2* eQTLs (black dots) that overlap with *H3K27ac* signals that significantly interact with the transcriptional start site of *ERAP2* in four different immune cell types (B cells, CD4+ T cells, CD8+ T cells and monocytes). Nine common non-coding SNPs concentrated in a ~1.6kb region exhibited strong interactions and overlay with H3K27ac signals from ENCODE data of heart, lung, liver, skeletal muscle, kidney and spleen revealed. (**b**) The -Log10 *P* values (adjusted for multiple testing using the Benjamini-Hochberg) of the effect of 986 *ERAP2* eQTLs on differential expression (alternative versus reference allele) of their 150bp window region from a massively parallel reporter assay as reported by Abell *et al.*[32]. The 7 SNPs identified by HiChIP in *a* are color-coded (**c**) Overview of the homology-directed-repair (HDR) strategy to use CRISPR-Cas9 mediated SNP replacement in Jurkat cells to switch the alleles from disease risk SNPs (i.e., alleles associated with higher ERAP2 levels) to protective haplotype (i.e., alleles associated with lower ERAP2 expression). The region from 5' to 3' spans 879 bp. (**d**) Sanger sequencing results for the genotype of rs2548224 for Jurkat cells targeted by the CRISPR-knockin approach outlined in *c.* in

comparison to unedited Jurkat cells and Jurkat cells in which the risk haplotype was deleted by CRISPR-Cas9-mediated knock-out as shown in **Supplemental Figure 5.1**. (**e**) Expression of *ERAP2*, *LNPEP* and *ERAP1* by qPCR in Jurkat clones after allelic substitution of rs2548224. Data represents n = 4 biological replicates, Two-tailed unpaired t.test was assessed to compare WT expression to the modified clone (** P<0.01, *** P<0.001).

(**Supplemental Figure 5.5, Supplemental Table 5.1**). In light of the fact that this selected region downstream of *ERAP2* contained SNPs which are associated with ERAP2 expression independently of rs2248374, is physically in close proximity with the *ERAP2* promoter (i.e., by Hi-C), and may exert allelic-dependent effects (i.e., by MPRA), we hypothesized that the risk alleles of these SNPs associated with autoimmunity may increase the interaction with the promoters of *ERAP2*.

To investigate this, we first asked if specific introduction of the alternative alleles for these SNPs would affect the transcription of *ERAP2*. We targeted this region of the *ERAP2*-encoding chromosome in Jurkat cells using CRISPR-Cas9 and two guide RNAs in the presence of a large (1500 bp) single-stranded DNA template identical to the target region, but encoding the alternative alleles for 7 of the 9 non-coding SNPs. These SNPs were selected, because these cluster close together (~900 bp distance from 5' SNP rs2548224 to 3' SNP rs2762) and are in tight LD (r^2~1 in EUR) with each other, as well as with the GWAS lead variants at *5q15* from CD, BCR, and JIA (r^2>0.9) (**Supplemental Figure 5.6**). The introduction of the template DNA for CRISPR-knock-in by HDR did not induce other genomic changes (**Figure 5.3C** and **Supplemental Figure 5.7**). Sanger sequencing revealed targeting this intronic region by CRISPR-mediated HDR successfully altered the allele for SNPs rs2548224 in the regulatory element, but not the other targeted SNPs (**Figure 5.3D,** and **Supplemental Figure 5.8**) Regardless, altering the risk allele T to the reference allele G for rs2548224 for this SNP resulted in significant decrease in *ERAP2* mRNA (unpaired t-test, $P = 3.0 \times 10^{-4}$) (**Figure 5.3E**). In agreement with the known ability of enhancers to regulate multiple genes within the same topologically associated domain, altering the alleles of these SNPs also resulted in significant reductions in the expression of the *LNPEP* gene, (unpaired t-test, $P = 0.0018$), but not *ERAP1* (**Figure 5.3E**). Overall, these results indicate that *ERAP2* gene expression is affected by disease-associated SNPs downstream of the *ERAP2* gene.

ERAP2 promoter contact is increased by autoimmune disease risk SNPs.

RegulomeDB indicates that the SNP rs2548224 overlapped with 153 epigenetic mark peaks in various cell types (e.g., *POL2RA* in B cells). Considering its position within *LNPEP*'s promoter region, it makes it difficult to distinguish between local promoter and enhancer functions. In agreement with the inefficiency of targeting intronic regions by CRISPR *knock-in*, efforts to introduce the risk alleles of SNP in THP-1 (rs2248374-AA clone in **Figure 5.1**) cells that carry the reference alleles for these SNPs were not successful. To determine whether alleles of the SNPs in the regulatory element directly influenced contact with the *ERAP2* promoter, we used allele-specific 4C-seq[50] in B cell lines generated from blood of three BCR patients carrying both the risk and non-risk allele (i.e., heterozygous for disease risk SNPs). Using

nuclear proximity ligation, 4C-seq enables the quantification of contact frequencies between a genomic region of interest and the remainder of the genome[34]. Allele-specific 4C-seq has the advantage of measuring chromatin contacts of both alleles simultaneously and allows comparison of the risk allele versus the protective allele in the same cell population. We found that the downstream regulatory region formed specific contacts with the promoter of *ERAP2* (**Figure 5.4A**). Moreover, in two out of three patients contact frequencies with the *ERAP2* promoter were substantially higher for the risk allele than the protective allele, supporting the idea that *ERAP2* upregulation may be a consequence of a direct regulatory interaction between the autoimmune risk SNPs and the gene promoter (**Figure 5.4B**).

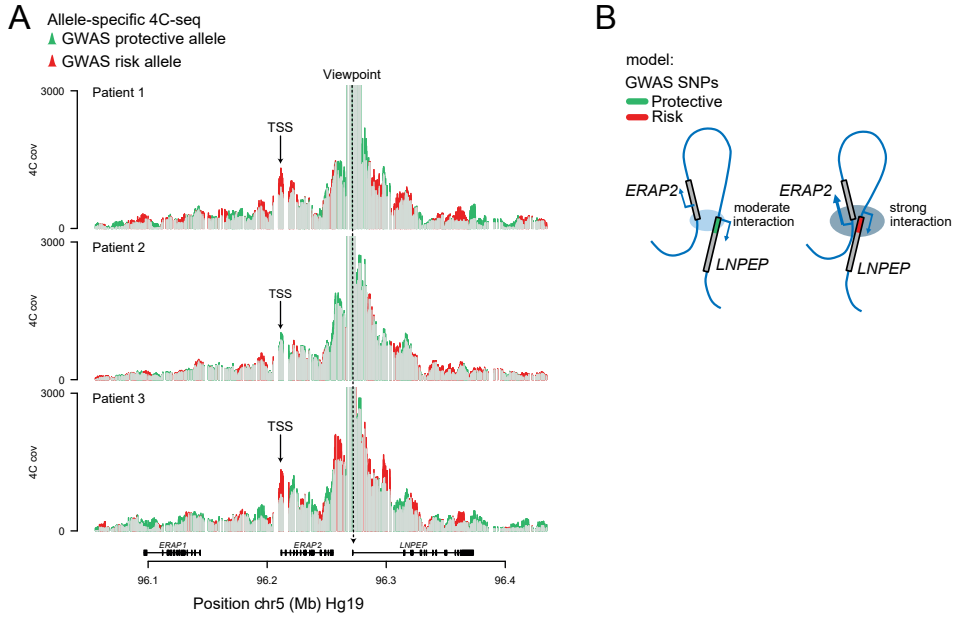

Figure 5.4: Autoimmune disease risk SNPs show high contact frequency with the *ERAP2* promoter in autoimmune patients. 4C analysis of contacts between the downstream regulatory region across the *ERAP2* locus. (**a)** 4C-seq contact profiles across the *ERAP2* locus in B cell lines from three patients with BCR that are heterozygous (e.g., rs2548224-G/T) for the *ERAP2* eQTLs located in the downstream regulatory element (the 4C viewpoint is centered on the SNP rs3842058 in the *LNPEP* promoter as depicted by the dashed line). The Y-axis represents the normalized captured sequencing reads. The red lines in each track indicate the regions where the risk alleles show more interactions compared with the reference alleles while the green lines indicate the regions where the reference alleles (i.e., protective alleles) show more interactions. TSS = transcription start site of *ERAP2*. (**b)** Schematic representation of ERAP2 regulation by autoimmune risk SNPs in the downstream regulatory element. showing the regulatory element with risk alleles (red), or reference (protective) alleles (green). The DNA region surrounding the *ERAP2* and *LNPEP* gene is shown in blue.

Discussion

In this study, we demonstrated that ERAP2 expression is initiated or abolished by the genotype of the common SNP rs2248374. Furthermore, we demonstrated that autoimmune disease risk SNPs identified by GWAS at *5q15* are statistically associated with *ERAP2* mRNA and protein expression independently of rs2248374. We show that autoimmune risk SNPs tag a gene-proximal DNA sequence that influences *ERAP2* expression and interacts with the gene's promoter more strongly if it encodes the risk alleles. Based on these findings, disease susceptibility SNPs at *5q15* likely do not confer disease susceptibility by alternative splicing, but by changing enhancer-promoter interactions of *ERAP2*.

The SNP rs2248374 is located at the 5' end of the intron downstream of exon 10 of *ERAP2* within a donor splice region and strongly correlates with alternative splicing of precursor RNA[23,26]. While the A allele of rs2248374 results in constitutive splicing, the G allele is predicted to impair recognition of the motif by the spliceosome (**Figure 5.1A**), which is conceptually supported by reporter assays outside the context of the *ERAP2* gene[26]. Through reciprocal SNP editing in genomic DNA, we here demonstrated that the genotype of rs2248374 determines the production of full-length ERAP2 transcripts and protein.

Exon 10 is extended due to the loss of the splice donor site controlled by rs2248374 and consequently includes premature termination codons (PTCs) embedded in intron 10-11[23,26]. Transcripts that contain a PTC can in principle produce truncated proteins, but if translation terminates more than 50-55 nucleotides upstream ("50-55-nucleotide rule") an exon-exon junction[51], they are generally degraded through a process called *nonsense-mediated mRNA decay* (NMD). Our data show that ERAP2 dramatically alter protein abundance proportionate to transcript levels, which is consistent with the notion that transcripts encoding the G allele of rs2248374 are subjected to NMD during steady-state[20,23]. The loss of ERAP2 is relatively unusual, given that changes in ERAP2 isoform usage manifest so dramatically at the proteome level[20,52]. However, that ERAP2 transcripts can escape NMD under inflammatory conditions, such that haplotypes that harbor the G allele of rs2248374 have been shown to produce truncated ERAP2 protein isoforms[29,53], not to be confused with "short" ERAP2 protein isoforms that are presumably generated by post-translational autocatalysis unrelated to rs2248374[54].

Most protein-coding genes express one dominant isoform[55], but since both alleles of rs2248374 are maintained at near equal frequencies (allele frequency ~50%) in the human population, this leads to high interindividual variability in ERAP2 isoform profile[23]. ERAP2 may enhance immune fitness through balanced selection, especially since recent evidence indicates that the presumed "null allele" (i.e., the G allele of rs2248374) encodes distinct protein isoforms in response to infection[29,56]. A recent and unusual natural selection pattern during the *Black Death* for the haplotypes tagged by rs2248374[25] supports this. Nowadays, these haplotypes also provide differential protection against respiratory infections[24], but they also modify the risk of modern autoimmune diseases like CD, BCR, and JIA. The SNP

rs2248374 was long assumed to be primary responsible for other disease-associated SNPs near *ERAP2*. Using conditional association analysis and mechanistic data, we challenged this assumption by showing that autoimmune disease-risk SNPs identified by GWAS influence ERAP2 expression independently of rs2248374.

These findings are significant for two main reasons: First, these results demonstrate that chromosome structure plays important roles in the transcriptional control of *ERAP2* and thus that its expression is regulated by mechanisms beyond alternative splicing. We focused on a small *cis*-regulatory sequence downstream of *ERAP2* as a proof of principle. Here, we showed that disease-risk SNPs alter physical interactions with the promoter in immortalized lymphoblast cell lines from autoimmune patients and that substitution of the allele of one common SNP (rs2548224) significantly affected the expression levels of *ERAP2*.

Another significant reason is that these findings have implications for our understanding of diseases in which ERAP2 is implicated. We recognize that the considerable LD between SNPs near *ERAP2* indicates that the effects of rs2248374 on splicing, as well as other mechanisms for regulation (i.e., chromosomal spatial organization), should often occur together. Because of their implications for the etiology of human diseases, it is still important to differentiate them functionally. In light of the fact that disease-associated SNPs affect ERAP2 expression independently of rs2248374, ERAP2 may be implicated in autoimmunity not because it is expressed in susceptible individuals but because it is expressed at higher levels[20,31]. It corresponds with the notion that pro-inflammatory cytokines, such as interferons, upregulate ERAP2 significantly, while regulatory cytokines, like TGF-β, downregulate it, or that ERAP2 is increased in lesions of autoimmune patients[56-58]. Overexpression of ERAP2 may be exploited therapeutically by lowering its concentration in conjunction with local pharmacological inhibition of the enzymatic activity[59].

We do like to stress that results from conditional eQTL and pQTL analysis in this study, supported by data from chromosome conformation capture coupled with sequencing analysis[40], as well as MPRA data[32] suggest that more SNPs may act in concert to regulate *ERAP2* expression, illustrating how intricately ERAP2 is regulated. Additional experimental work is needed to interrogate the extended ERAP2 haplotype and follow up on some of the derived associations. Mapping all the putative functional implications of these SNPs by CRISPR-knockin experiments in genomic DNA is inefficient and labor-intensive, which makes their application in primary tissue challenging. MPRA provides a high-throughput solution to interrogating SNP effects, but lacks genomic context, and can only infer local allelic-dependent effects (i.e., no long-range interactions). Due to their dependency on PAM sequences for targeting regions of interest, CRISPR/Cas9-based enhancer-targeting systems[60] may not be able to dissect functional effects at a single nucleotide (i.e., SNP) resolution. It is possible to discern allelic-dependent effects in the canonical genomic context using allele-specific 4C sequencing, but in case of high LD and closely clustered SNPs (e.g., the ~900 bp region identified in this study) functional or non-functional SNPs cannot be distinguished within the sequence window of interest. Regardless, by integrating information from all of these

available technologies, we were able to shortlist an interval suitable for interrogation by CRISPR-based knock-in techniques. A major drawback of this multi-step approach is that our study is therefore limited by sample size, and ideally we should have successfully targeted the regulatory region in a larger number of cell lines. Also, while ERAP2 also shows tissue-shared genetic regulation, there may be important cell-type specific regulatory mechanisms enforced by disease risk allele, that require study of this mechanism in lesional tissues and under inflammatory conditions. Regardless, single-cell analysis shows that the many *ERAP2* eQTLs are shared between immune cells[47,61]. This indicates that the mechanism by which the SNPs in the *cis*-regulatory region increase ERAP2 promoter interaction may be ubiquitous.
An enhancer-promoter loop increases transcriptional output through complex organization of chromatin, structural mediators, and transcription factors[62,63]. Although we narrowed down the *cis*-regulatory region to ~900bp, the identity of the structural or transcriptional regulators that juxtapose this region with the *ERAP2* promoter remains elusive. Loop-forming transcription factors such as CTCF and protein analogous (e.g., YY1, the Mediator complex) have been shown to contribute o enhancer-promoter interactions[64-68]. Given that the here identified *cis*-regulatory region is located within the *LNPEP* promoter, it is challenging to identify the factors responsible for ERAP2 expression, since promoters are highly enriched for a large variety of transcription factor footprints (i.e., high ChIP-seq signals). Further studies are required to dissect how these *ERAP2* eQTLs modify enhancer activity and transcription, and how these mechanisms are distinguished from canonical promoter activity for *LNPEP* gene.

Conclusions

In conclusion, these results show that clustered genetic association signals associated with diverse autoimmune conditions and lethal infections act in concert to control expression of *ERAP2* and demonstrate that disease-risk variants can convert a gene promoter region into a potent enhancer of a distal gene.

Acknowledgements

We thank Dr. Dennis C. Ko, Dr. Darragh Duffy, and Dr. Jimmie Ye for helpful discussions.

References

1. Rock KL, Reits E, Neefjes J. Present Yourself! By MHC Class I and MHC Class II Molecules. Trends Immunol. 2016 Nov;37(11):724–37.
2. Cresswell P, Ackerman AL, Giodini A, Peaper DR, Wearsch PA. Mechanisms of MHC class I-restricted antigen processing and cross-presentation. Immunol Rev. 2005 Oct;207:145–57.
3. Saveanu L, Carroll O, Lindo V, Del Val M, Lopez D, Lepelletier Y, et al. Concerted peptide trimming by human ERAP1 and ERAP2 aminopeptidase complexes in the endoplasmic reticulum. Nat Immunol. 2005;6(7):689–97.
4. Babaie F, Hosseinzadeh R, Ebrazeh M, Seyfizadeh N, Aslani S, Salimi S, et al. The roles of ERAP1 and ERAP2 in autoimmunity and cancer immunity: New insights and perspective. Mol Immunol. 2020 May;121:7–19.
5. Kuśnierczyk P, Stratikos E. Endoplasmic reticulum aminopeptidases as a double-faced tool to increase or decrease efficiency of antigen presentation in health and disease. Vol. 80, Human immunology. United States; 2019. p. 277–80.
6. López de Castro JA. How ERAP1 and ERAP2 Shape the Peptidomes of Disease-Associated MHC-I Proteins. Front Immunol. 2018;9(October):2463.
7. Cavers A, Kugler MC, Ozguler Y, Al-Obeidi AF, Hatemi G, Ueberheide BM, et al. Behçet's disease risk-variant HLA-B51/ERAP1-Hap10 alters human CD8 T cell immunity. Ann Rheum Dis. 2022 Nov;81(11):1603–11.
8. Kuiper JJW, Venema WJ. HLA-A29 and Birdshot Uveitis: Further Down the Rabbit Hole. Front Immunol. 2020;11:599558.
9. Robinson PC, Costello M-E, Leo P, Bradbury LA, Hollis K, Cortes A, et al. ERAP2 is associated with ankylosing spondylitis in HLA-B27-positive and HLA-B27-negative patients. Vol. 74, Annals of the rheumatic diseases. England; 2015. p. 1627–9.
10. Evans DM, Spencer CCA, Pointon JJ, Su Z, Harvey D, Kochan G, et al. Interaction between ERAP1 and HLA-B27 in ankylosing spondylitis implicates peptide handling in the mechanism for HLA-B27 in disease susceptibility. Nat Genet. 2011 Jul;43(8):761–7.
11. Franke A, McGovern DPB, Barrett JC, Wang K, Radford-Smith GL, Ahmad T, et al. Genome-wide meta-analysis increases to 71 the number of confirmed Crohn's disease susceptibility loci. Nat Genet. 2010 Dec;42(12):1118–25.
12. Hinks A, Cobb J, Marion MC, Prahalad S, Sudman M, Bowes J, et al. Dense genotyping of immune-related disease regions identifies 14 new susceptibility loci for juvenile idiopathic arthritis. Nat Genet. 2013 Jun;45(6):664–9.
13. Kuiper JJW, Van Setten J, Ripke S, Van 'T Slot R, Mulder F, Missotten T, et al. A genome-wide association study identifies a functional ERAP2 haplotype associated with birdshot chorioretinopathy. Hum Mol Genet. 2014;23(22):6081–7.
14. Gelfman S, Monnet D, Ligocki AJ, Tabary T, Moscati A, Bai X, et al. ERAP1, ERAP2, and Two Copies of HLA-Aw19 Alleles Increase the Risk for Birdshot Chorioretinopathy in HLA-A29 Carriers. Invest Ophthalmol Vis Sci. 2021 Nov;62(14):3.

15. Kirino Y, Bertsias G, Ishigatsubo Y, Mizuki N, Tugal-Tutkun I, Seyahi E, et al. Genome-wide association analysis identifies new susceptibility loci for Behcet's disease and epistasis between HLA-B*51 and ERAP1. Nat Genet. 2013 Feb;45(2):202–7.
16. Strange A, Capon F, Spencer CCA, Knight J, Weale ME, Allen MH, et al. A genome-wide association study identifies new psoriasis susceptibility loci and an interaction between HLA-C and ERAP1. Nat Genet. 2010 Nov;42(11):985–90.
17. Hutchinson JP, Temponeras I, Kuiper J, Cortes A, Korczynska J, Kitchen S, et al. Common allotypes of ER aminopeptidase 1 have substrate-dependent and highly variable enzymatic properties. J Biol Chem. 2021;296:100443.
18. Evnouchidou I, Kamal RP, Seregin SS, Goto Y, Tsujimoto M, Hattori A, et al. Cutting Edge: Coding single nucleotide polymorphisms of endoplasmic reticulum aminopeptidase 1 can affect antigenic peptide generation in vitro by influencing basic enzymatic properties of the enzyme. J Immunol. 2011 Feb;186(4):1909–13.
19. Tran TM, Colbert RA. Endoplasmic reticulum aminopeptidase 1 and rheumatic disease: functional variation. Curr Opin Rheumatol. 2015 Jul;27(4):357–63.
20. Hanson AL, Cuddihy T, Haynes K, Loo D, Morton CJ, Oppermann U, et al. Genetic Variants in ERAP1 and ERAP2 Associated With Immune-Mediated Diseases Influence Protein Expression and the Isoform Profile. Arthritis Rheumatol. 2018;70(2):255–65.
21. de Castro JAL, Stratikos E. Intracellular antigen processing by ERAP2: Molecular mechanism and roles in health and disease. Hum Immunol [Internet]. 2019;80(5):310–7. Available from: https://doi.org/10.1016/j.humimm.2018.11.001
22. Zhou Y-H, Gallins PJ, Etheridge AS, Jima D, Scholl E, Wright FA, et al. A resource for integrated genomic analysis of the human liver. Sci Rep. 2022 Sep;12(1):15151.
23. Andrés AM, Dennis MY, Kretzschmar WW, Cannons JL, Lee-Lin S-Q, Hurle B, et al. Balancing selection maintains a form of ERAP2 that undergoes nonsense-mediated decay and affects antigen presentation. PLoS Genet. 2010 Oct;6(10):e1001157.
24. Hamilton F, Mentzer A, Parks T, Baillie JK, Davey Smith G, Ghazal P, et al. Variation in ERAP2 has opposing effects on severe respiratory infection and autoimmune disease. medRxiv [Internet]. 2022 Jan 1;2022.11.04.22281942. Available from: http://medrxiv.org/content/early/2022/11/05/2022.11.04.22281942.abstract
25. Klunk J, Vilgalys TP, Demeure CE, Cheng X, Shiratori M, Madej J, et al. Evolution of immune genes is associated with the Black Death. Nature. 2022 Nov;611(7935):312–9.
26. Coulombe-Huntington J, Lam KCL, Dias C, Majewski J. Fine-scale variation and genetic determinants of alternative splicing across individuals. PLoS Genet. 2009;5(12).
27. Rotival M, Quach H, Quintana-Murci L. Defining the genetic and evolutionary architecture of alternative splicing in response to infection. Nat Commun. 2019 Apr;10(1):1671.
28. Yao Y, Liu N, Zhou Z, Shi L. Influence of ERAP1 and ERAP2 gene polymorphisms on disease susceptibility in different populations. Hum Immunol. 2019 May;80(5):325–34.

29. Ye CJ, Chen J, Villani AC, Gate RE, Subramaniam M, Bhangale T, et al. Genetic analysis of isoform usage in the human anti-viral response reveals influenza-specific regulation of ERAP2 transcripts under balancing selection. Genome Res. 2018;28(12):1812–25.
30. Bossini-Castillo L, Glinos DA, Kunowska N, Golda G, Lamikanra AA, Spitzer M, et al. Immune disease variants modulate gene expression in regulatory CD4(+) T cells. Cell genomics. 2022 Apr;2(4):None.
31. Kuiper JJW, Setten J van, Devall M, Cretu-Stancu M, Hiddingh S, Ophoff RA, et al. Functionally distinct ERAP1 and ERAP2 are a hallmark of HLA-A29-(Birdshot) Uveitis. Hum Mol Genet. 2018;27(24):4333–43.
32. Abell NS, DeGorter MK, Gloudemans MJ, Greenwald E, Smith KS, He Z, et al. Multiple causal variants underlie genetic associations in humans. Science. 2022 Mar;375(6586):1247–54.
33. Venema WJ, Hiddingh S, de Boer JH, Claas FHJ, Mulder A, den Hollander AI, et al. ERAP2 Increases the Abundance of a Peptide Submotif Highly Selective for the Birdshot Uveitis-Associated HLA-A29. Front Immunol. 2021;12:634441.
34. Krijger PHL, Geeven G, Bianchi V, Hilvering CRE, de Laat W. 4C-seq from beginning to end: A detailed protocol for sample preparation and data analysis. Methods. 2020 Jan;170:17–32.
35. Giambartolomei C, Vukcevic D, Schadt EE, Franke L, Hingorani AD, Wallace C, et al. Bayesian test for colocalisation between pairs of genetic association studies using summary statistics. PLoS Genet. 2014 May;10(5):e1004383.
36. Lu A, Thompson M, Grace Gordon M, Dahl A, Ye CJ, Zaitlen N, et al. Fast and powerful statistical method for context-specific QTL mapping in multi-context genomic studies. bioRxiv [Internet]. 2021 Jan 1;2021.06.17.448889. Available from: http://biorxiv.org/content/early/2021/06/18/2021.06.17.448889.abstract
37. Sun BB, Maranville JC, Peters JE, Stacey D, Staley JR, Blackshaw J, et al. Genomic atlas of the human plasma proteome. Nature. 2018 Jun;558(7708):73–9.
38. Jaganathan K, Kyriazopoulou Panagiotopoulou S, McRae JF, Darbandi SF, Knowles D, Li YI, et al. Predicting Splicing from Primary Sequence with Deep Learning. Cell. 2019 Jan;176(3):535-548.e24.
39. Zeng T, Li YI. Predicting RNA splicing from DNA sequence using Pangolin. Genome Biol. 2022 Apr;23(1):103.
40. Chandra V, Bhattacharyya S, Schmiedel BJ, Madrigal A, Gonzalez-Colin C, Fotsing S, et al. Promoter-interacting expression quantitative trait loci are enriched for functional genetic variants. Nat Genet. 2021 Jan;53(1):110–9.
41. Li D, Hsu S, Purushotham D, Sears RL, Wang T. WashU Epigenome Browser update 2019. Nucleic Acids Res. 2019 Jul;47(W1):W158–65.
42. Liu M, Rehman S, Tang X, Gu K, Fan Q, Chen D, et al. Methodologies for Improving HDR Efficiency. Front Genet. 2018;9:691.
43. Tian R, Pan Y, Etheridge THA, Deshmukh H, Gulick D, Gibson G, et al. Pitfalls in Single Clone CRISPR-Cas9 Mutagenesis to Fine-map Regulatory Intervals. Genes (Basel). 2020 May;11(5).

44. Odero MD, Zeleznik-Le NJ, Chinwalla V, Rowley JD. Cytogenetic and molecular analysis of the acute monocytic leukemia cell line THP-1 with an MLL-AF9 translocation. Genes Chromosomes Cancer. 2000 Dec;29(4):333–8.
45. Adati N, Huang M-C, Suzuki T, Suzuki H, Kojima T. High-resolution analysis of aberrant regions in autosomal chromosomes in human leukemia THP-1 cell line. BMC Res Notes. 2009 Jul;2:153.
46. GTEx Consortium. The Genotype-Tissue Expression (GTEx) project. Nat Genet. 2013 Jun;45(6):580–5.
47. Yazar S, Alquicira-Hernandez J, Wing K, Senabouth A, Gordon MG, Andersen S, et al. Single-cell eQTL mapping identifies cell type-specific genetic control of autoimmune disease. Science. 2022 Apr;376(6589):eabf3041.
48. Liu L, Sanderford MD, Patel R, Chandrashekar P, Gibson G, Kumar S. Biological relevance of computationally predicted pathogenicity of noncoding variants. Nat Commun. 2019 Jan;10(1):330.
49. Gasperini M, Tome JM, Shendure J. Towards a comprehensive catalogue of validated and target-linked human enhancers. Nat Rev Genet. 2020 May;21(5):292–310.
50. Holwerda SJB, van de Werken HJG, Ribeiro de Almeida C, Bergen IM, de Bruijn MJW, Verstegen MJAM, et al. Allelic exclusion of the immunoglobulin heavy chain locus is independent of its nuclear localization in mature B cells. Nucleic Acids Res. 2013 Aug;41(14):6905–16.
51. Nagy E, Maquat LE. A rule for termination-codon position within intron-containing genes: when nonsense affects RNA abundance. Trends Biochem Sci. 1998 Jun;23(6):198–9.
52. Sulakhe D, D'Souza M, Wang S, Balasubramanian S, Athri P, Xie B, et al. Exploring the functional impact of alternative splicing on human protein isoforms using available annotation sources. Brief Bioinform. 2019 Sep;20(5):1754–68.
53. Tanioka T, Hattori A, Masuda S, Nomura Y, Nakayama H, Mizutani S, et al. Human leukocyte-derived arginine aminopeptidase. The third member of the oxytocinase subfamily of aminopeptidases. J Biol Chem. 2003 Aug;278(34):32275–83.
54. Mattorre B, Caristi S, Donato S, Volpe E, Faiella M, Paiardini A, et al. A Short ERAP2 That Binds IRAP Is Expressed in Macrophages Independently of Gene Variation. Int J Mol Sci. 2022 Apr;23(9).
55. Ezkurdia I, Rodriguez JM, Carrillo-de Santa Pau E, Vázquez J, Valencia A, Tress ML. Most highly expressed protein-coding genes have a single dominant isoform. J Proteome Res. 2015 Apr;14(4):1880–7.
56. Saulle I, Vanetti C, Goglia S, Vicentini C, Tombetti E, Garziano M, et al. A New ERAP2/Iso3 Isoform Expression Is Triggered by Different Microbial Stimuli in Human Cells. Could It Play a Role in the Modulation of SARS-CoV-2 Infection? Cells. 2020;9(9):1951.
57. Berglund AK, Hinson AL, Schnabel L V. TGF-β downregulates antigen processing and presentation genes and MHC I surface expression through a Smad3-dependent mechanism. bioRxiv [Internet]. 2023 Jan 1;2023.01.30.526196. Available from: http://biorxiv.org/content/early/2023/02/01/2023.01.30.526196.abstract

58. Marusina AI, Ji-Xu A, Le ST, Toussi A, Tsoi LC, Li Q, et al. Cell-Specific, Disease-Associated and Variant-Linked Alterations In Expression Of ERAP1, ERAP2 and LNPEP Aminopeptidases. J Invest Dermatol. 2023 Jan;
59. Medve L, Gealageas R, Lam Bao V, Guillaume V, Castillo-Aguilera O, Camberlein V, et al. Modulators of hERAP2 discovered by high-throughput screening. Eur J Med Chem. 2021 Feb;211:113053.
60. Li K, Liu Y, Cao H, Zhang Y, Gu Z, Liu X, et al. Interrogation of enhancer function by enhancer-targeting CRISPR epigenetic editing. Nat Commun. 2020 Jan;11(1):485.
61. Perez RK, Gordon MG, Subramaniam M, Kim MC, Hartoularos GC, Targ S, et al. Single-cell RNA-seq reveals cell type-specific molecular and genetic associations to lupus. Science. 2022 Apr;376(6589):eabf1970.
62. Chakraborty S, Kopitchinski N, Zuo Z, Eraso A, Awasthi P, Chari R, et al. Enhancer-promoter interactions can bypass CTCF-mediated boundaries and contribute to phenotypic robustness. Nat Genet. 2023 Feb;55(2):280–90.
63. Hua P, Badat M, Hanssen LLP, Hentges LD, Crump N, Downes DJ, et al. Defining genome architecture at base-pair resolution. Nature. 2021 Jul;595(7865):125–9.
64. Nakahashi H, Kieffer Kwon K-R, Resch W, Vian L, Dose M, Stavreva D, et al. A genome-wide map of CTCF multivalency redefines the CTCF code. Cell Rep. 2013 May;3(5):1678–89.
65. Phillips JE, Corces VG. CTCF: master weaver of the genome. Cell. 2009 Jun;137(7):1194–211.
66. Weintraub AS, Li CH, Zamudio A V, Sigova AA, Hannett NM, Day DS, et al. YY1 Is a Structural Regulator of Enhancer-Promoter Loops. Cell. 2017 Dec;171(7):1573-1588.e28.
67. Luan J, Vermunt MW, Syrett CM, Coté A, Tome JM, Zhang H, et al. CTCF blocks antisense transcription initiation at divergent promoters. Nat Struct Mol Biol. 2022 Nov;29(11):1136–44.
68. Kim S, Yu N-K, Kaang B-K. CTCF as a multifunctional protein in genome regulation and gene expression. Exp Mol Med. 2015 Jun;47(6):e166.
69. Richardson CD, Ray GJ, DeWitt MA, Curie GL, Corn JE. Enhancing homology-directed genome editing by catalytically active and inactive CRISPR-Cas9 using asymmetric donor DNA. Nat Biotechnol. 2016 Mar;34(3):339–44.
70. Machiela MJ, Chanock SJ. LDlink: a web-based application for exploring population-specific haplotype structure and linking correlated alleles of possible functional variants. Bioinformatics. 2015 Nov;31(21):3555–7.
71. Hill JT, Demarest BL, Bisgrove BW, Su Y-C, Smith M, Yost HJ. Poly peak parser: Method and software for identification of unknown indels using sanger sequencing of polymerase chain reaction products. Dev Dyn an Off Publ Am Assoc Anat. 2014 Dec;243(12):1632–6.
72. Purcell S, Neale B, Todd-Brown K, Thomas L, Ferreira MAR, Bender D, et al. PLINK: a tool set for whole-genome association and population-based linkage analyses. Am J Hum Genet. 2007 Sep;81(3):559–75.
73. Auton A, Brooks LD, Durbin RM, Garrison EP, Kang HM, Korbel JO, et al. A global reference for human genetic variation. Nature. 2015 Oct;526(7571):68–74.

74. Cunningham F, Allen JE, Allen J, Alvarez-Jarreta J, Amode MR, Armean IM, et al. Ensembl 2022. Nucleic Acids Res. 2022 Jan;50(D1):D988–95.
75. Yang J, Ferreira T, Morris AP, Medland SE, Madden PAF, Heath AC, et al. Conditional and joint multiple-SNP analysis of GWAS summary statistics identifies additional variants influencing complex traits. Nat Genet. 2012 Mar;44(4):369–75, S1-3.

Supplemental figures

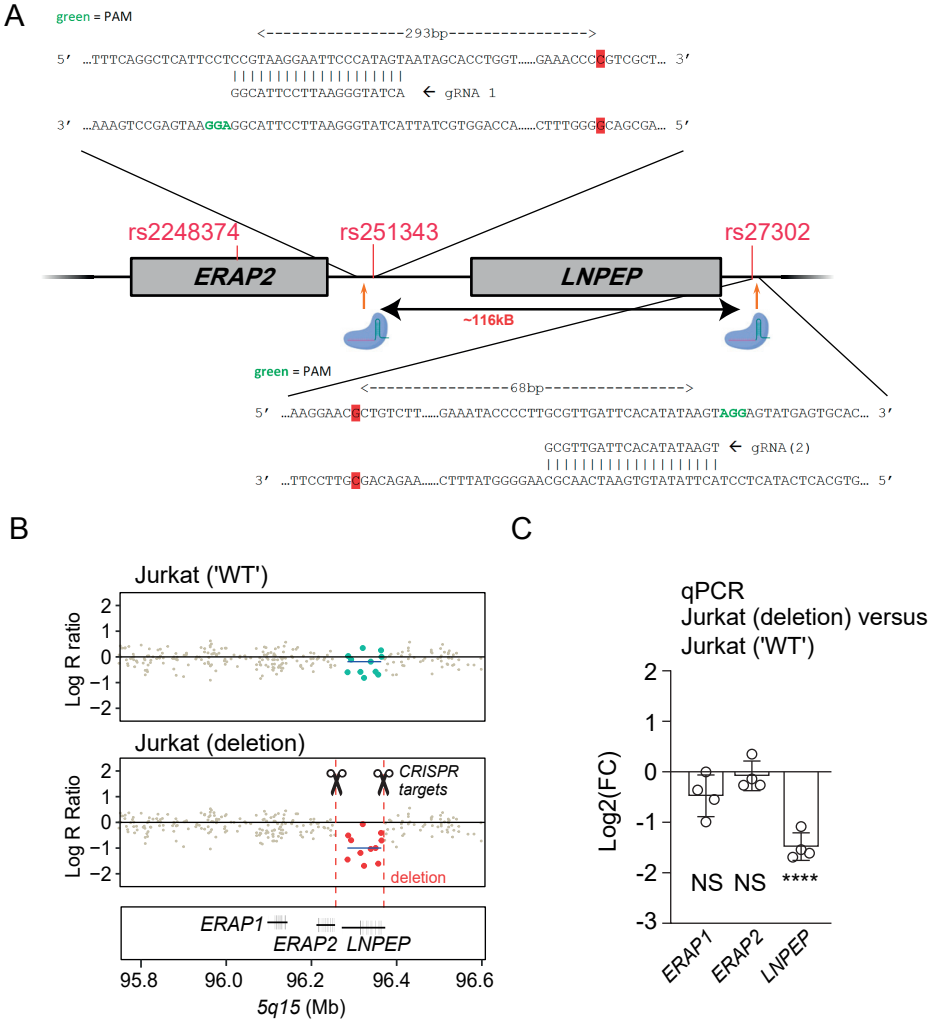

Supplemental Figure 5.1: **Deletion of downstream ERAP2 eQTLs using CRISPR Cas9.** (**a**) Overview of the guide RNA binding sites used for deletion of a 116 kb fragment that includes (from 5′ to 3′ direction) ERAP2 eQTLs from rs251343 until rs27302. Because Jurkat cells are heterozygous for rs10044354 located within the *LNPEP* gene (*P value, ERAP2 eQTL analysis* conditioned on rs2248374 = 3.2 x 10^{-120}), we screened single cell cultures for specific deletion of rs10044354 by PCR. Application of this approach to Jurkat cells resulted in an clone with evidence for deletion at *5q15*, as confirmed by sanger sequencing and (**b**) whole genome homozygosity SNP-array copy number profiling and analysis of regions of homozygosity using the Illumina CytoSNP-850K Beadchip. SNPs that reside in the region targeted by the CRISPR approach for deletion are denoted (green in unedited cells and red in the cells subjected to CRISPR-Cas9 with guide RNAs targeting this region as shown in *a*). Loss of SNP signal (in red) indicates partial deletion of ~116 kB area. Genome wide results are shown in **Supplemental Figure 5.7**. (**c**) Expression of *ERAP2, ERAP1* and *LNPEP* after CRISPR-Cas9 deletion, relative to unedited Jurkat cells (Log_2(FC))Data represents n = 4 replicates, Two-tailed unpaired t-test (NS = non-significant, **** *P*<0.0001.

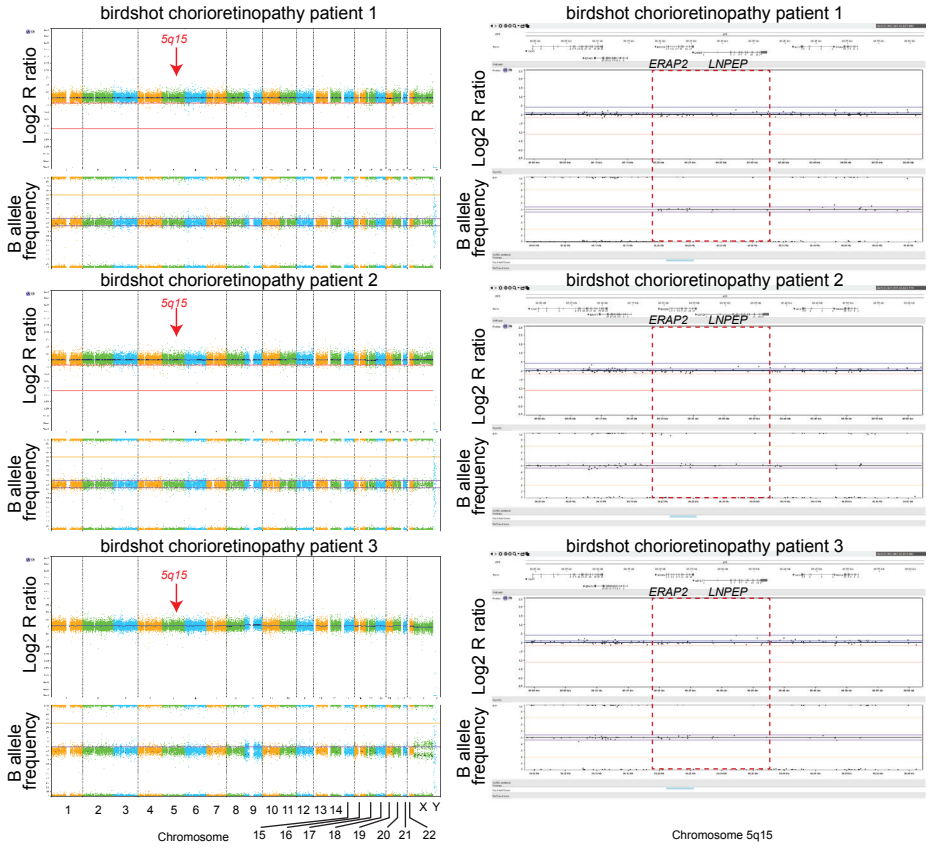

Supplemental Figure 5.2: Whole genome analysis using SNP-arrays for birdshot chorioretinopathy patient-derived lymphoblastoid cell lines used for allele-specific 4C-seq. SNP-array based copy number profiling and analysis of regions of homozygosity using the Infinium Human CytoSNP-850K v1.2 BeadChip (Illumina, San Diego, CA, USA) showed no undesired genomic abnormalities, except for LCLs derived from patient 3, which exhibited a possible low level mosaicism for trisomy 9 (~10%) and a comparable percentage of mosaicism for a monosomy of chromosome X (~10%). Zoom plots on the right of chromosome *5q15* show normal copy number for SNPs at *5q15* and B allele frequency of ~0.5 (i.e., heterozygous) for SNPs of interest in the extended ERAP2 haplotype. The panels show the array results for the whole genome. On the X-axis the chromosomes and chromosomal region are indicated. The upper Y-axis shows the Log2 R ratio and the lower Y-axis indicates the B allele frequency for each SNP.

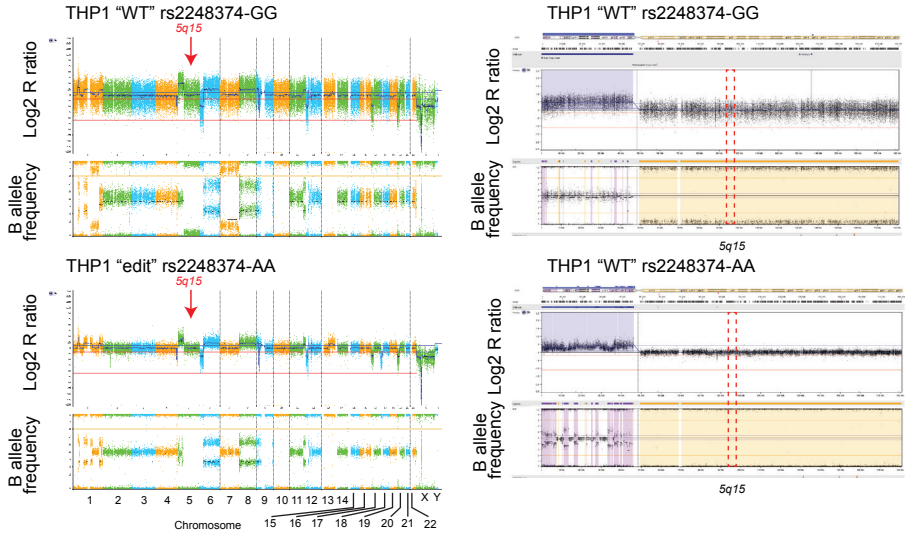

Supplemental Figure 5.3: Whole genome copy number profiling and analysis of regions of homozygosity using SNP-arrays of the THP-1 cells used in this study. SNP-array based copy number profiling and analysis of regions of homozygosity using the Infinium Human CytoSNP-850K v1.2 BeadChip (Illumina, San Diego, CA, USA) showed multiple chromosomal abnormalities in the genome, including copy number neutral loss of heterozygosity (CN-LOH) for chromosome 5q, including the *5q15* genomic region. The panels show the array results for the whole genome on the right and for chromosome 5 on the left. On the X-axis the chromosomes and chromosomal region are indicated. The upper Y-axis shows the Log2 R ratio, and the lower Y-axis indicates the B allele frequency for each SNP.

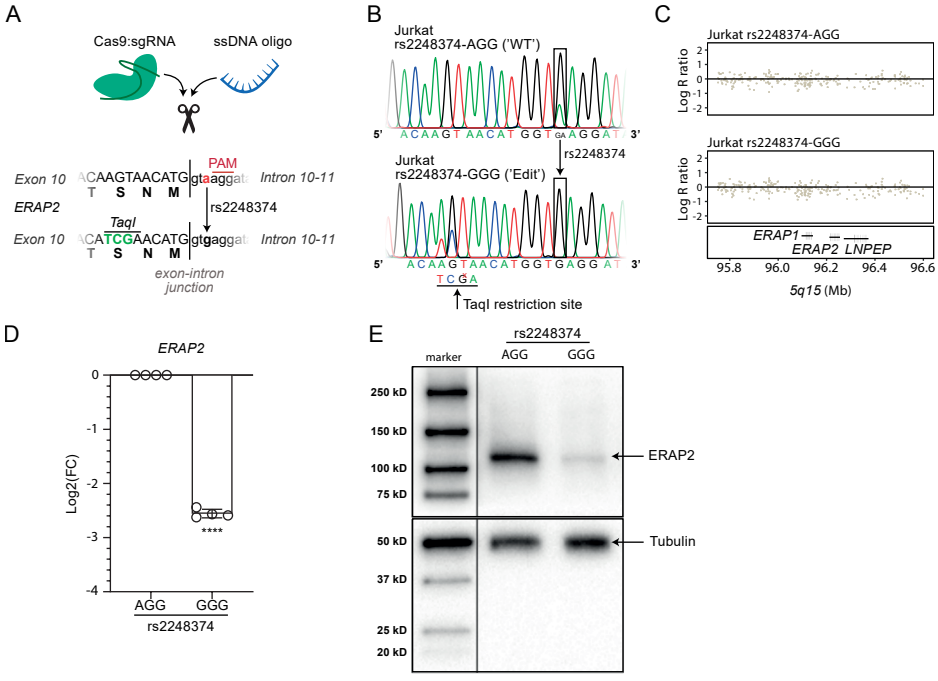

Supplemental Figure 5.4: Allelic substitution of rs2248374 A>G allele abolishes ERAP2 expression. (**a**) Overview of the homology-directed-repair (HDR) strategy to use CRISPR-Cas9 mediated SNP replacement of splice site variant rs2248374-AGG to GGG in Jurkat cells. An additional mutation was added to the ssDNA oligo template to introduce a TaqI restriction site, which was used for clone screening. (**b**) Sanger sequence data showing Jurkat 'WT' with the heterozygous rs2248374-AGG variant and the Jurkat clone with the HDR-mediated SNP modification to rs2248374-GGG. (**c**) Overview of SNP-array data, indicating no genomic abnormalities between unedited and edited clones at *5q15*. (**d**) Decreased *ERAP2* expression was detected with qPCR as a result of the mutation of A to G allele of rs2248374. (**e**) In addition, ERAP2 protein expression (determined by Western blot) was decreased in Jurkat cells that lost the A allele of rs2248374.

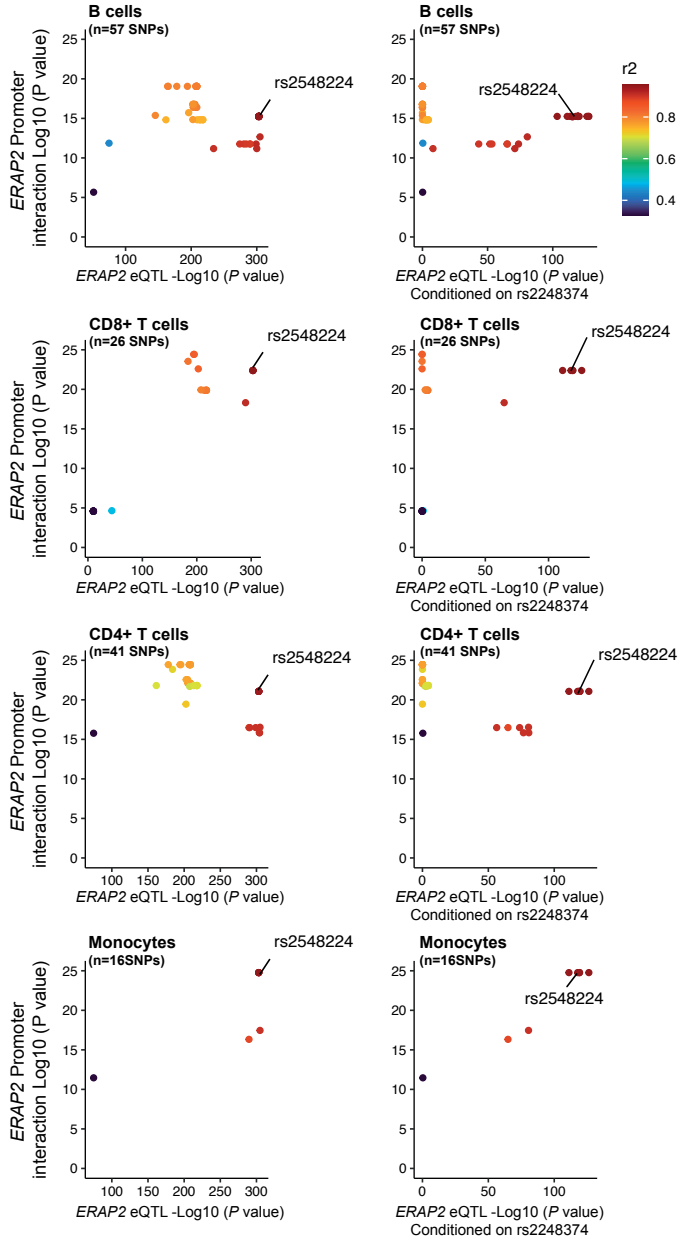

Supplemental Figure 5.5: The SNPs rs2548224 is a strong *ERAP2* eQTLs independent of rs2248374 that reside in a DNA sequence that physically interacts with the *ERAP2* promoter. Comparison of the association analysis (*P* values) from chromosome conformation capture coupled with sequencing (Hi-C) data enriched by chromatin immunoprecipitation for the activating histone H3 lysine 27 acetylation (*H3K27ac*) in primary immune cells from Chandra *et al.*[40]. SNPs with significant interaction (amount is indicated per plot) with *ERAP2* promoter in B cells, CD4+ T cells, CD8+ T cells and monocytes are shown. The color intensity of each symbol reflects the extent of LD (r^2 estimated using 1000 Genomes EUR samples) with rs2927608. The SNP rs2548224 that resides in a regulatory region is indicated.

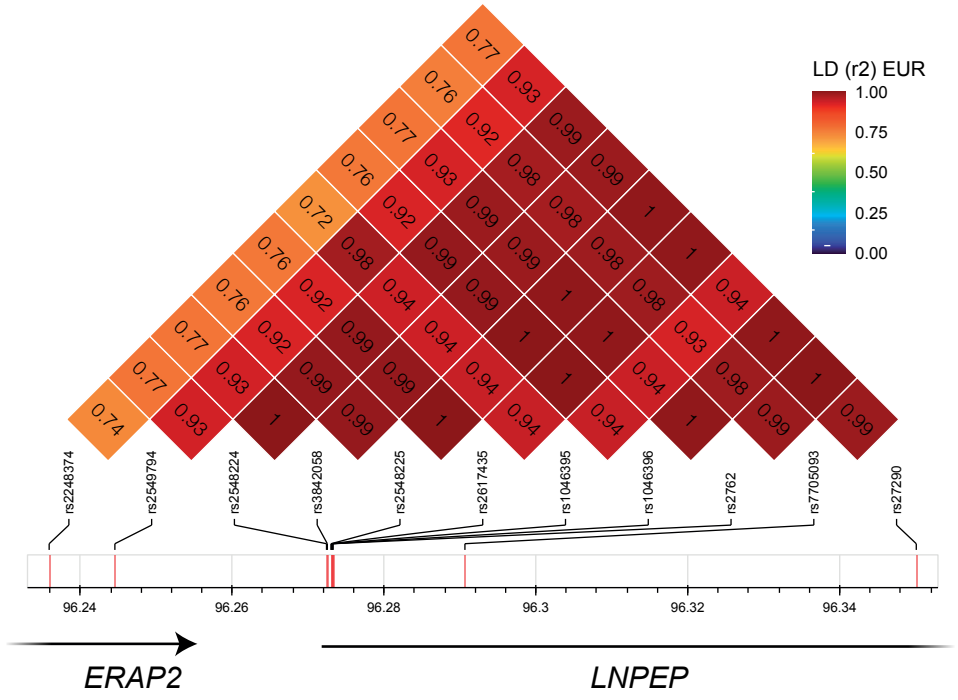

Supplemental Figure 5.6: Linkage disequilibrium (LD) plot between disease-risk SNPs, rs2248374 and SNPs identified in Figure 5.3A.

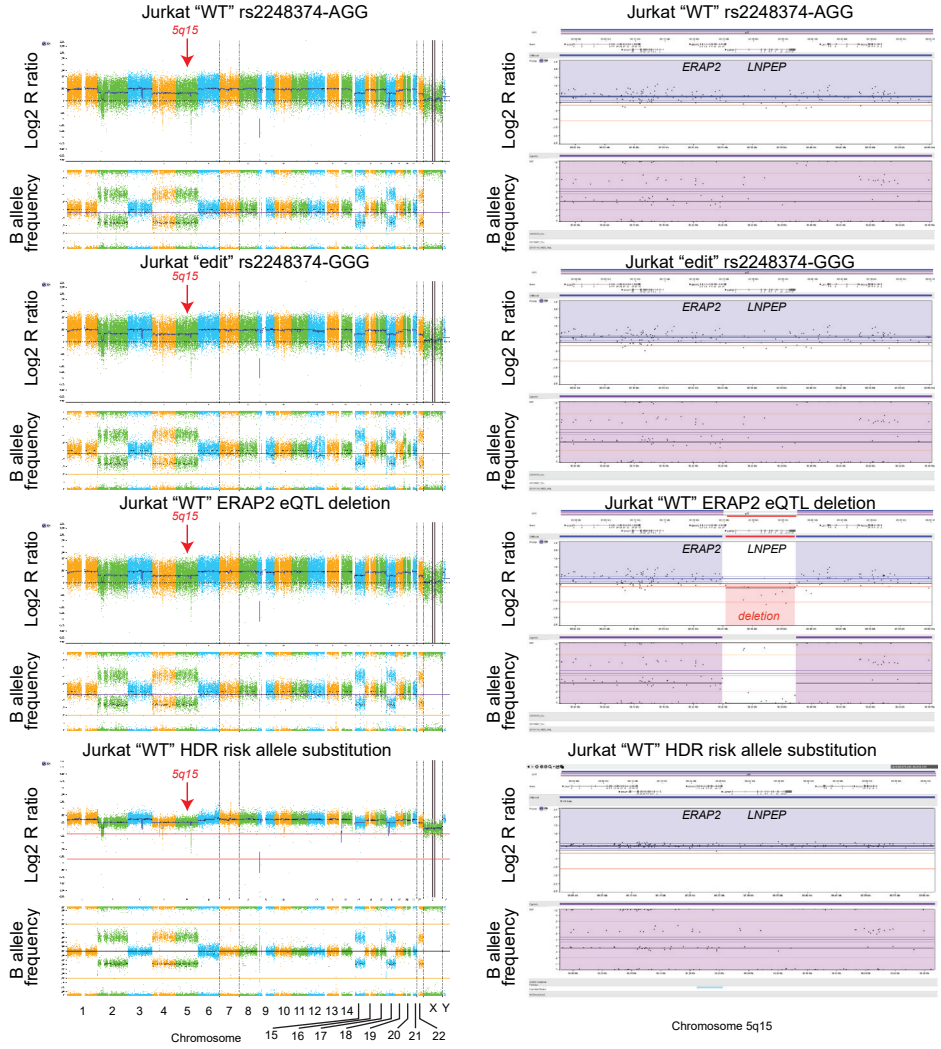

Supplemental Figure 5.7: Whole genome copy number profiling and analysis of regions of homozygosity using SNP-arrays of the genome engineered Jurkat cell lines used in this study. SNP-array based copy number profiling and analysis of regions of homozygosity using the Infinium Human CytoSNP-850K v1.2 BeadChip (Illumina, San Diego, CA, USA) showed several genomic abnormalities in the Jurkat cell lines affecting multiple chromosomes, including a trisomy of chromosome 5. The copy number of the *5q15* genomic region was comparable between each condition, except for the intended deletion of a 116 kb fragment (in Jurkat "WT" *ERAP2* eQTL deletion). Zoom plots on the right for *5q15* with highlighted *ERAP2* and *LNPEP* genes. On the X-axis the chromosomes and chromosomal region are indicated. The upper Y-axis shows the Log2 R ratio and the lower Y-axis indicates the B allele frequency for each SNP.

A

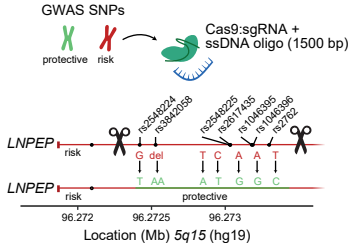

SNP #	non risk	risk
rs2548224	T	G
rs3842058	AAA	A
rs2548225	A	T
rs2617435	T	C
rs1046395	G	A
rs1046396	G	A
rs2762	C	T

B

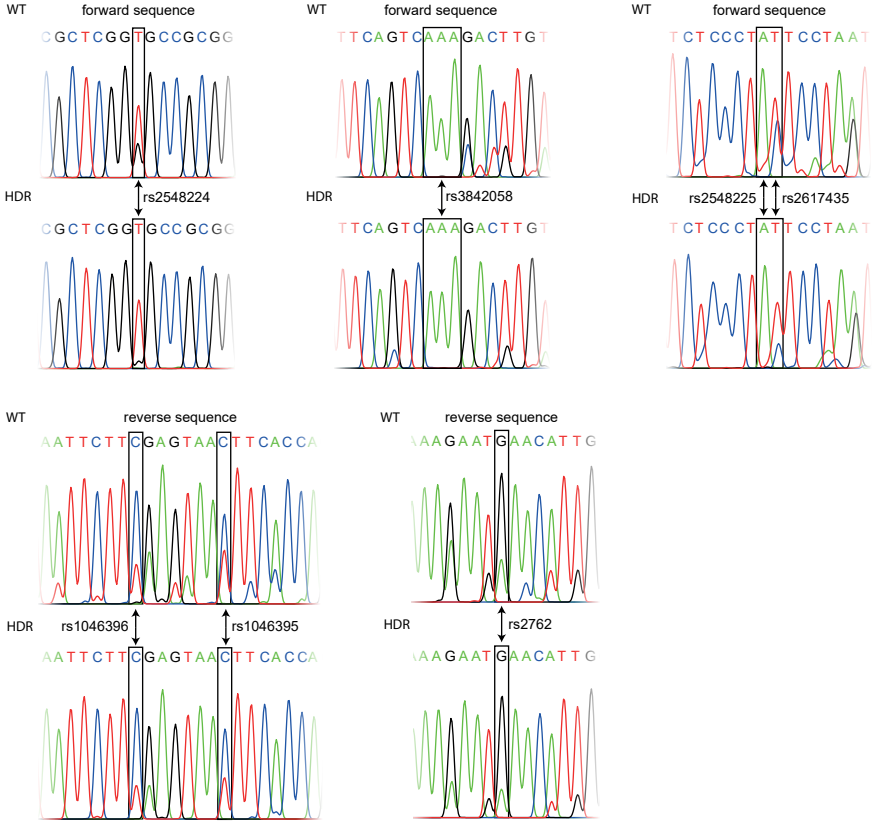

Supplemental Figure 5.8. (**a**) Overview of the homology-directed-repair (HDR) strategy to use CRISPR-Cas9 mediated SNP replacement in Jurkat cells to switch the alleles from disease risk SNPs (i.e., alleles associated with higher ERAP2 levels) to protective haplotype (i.e., alleles associated with lower ERAP2 expression). The region from 5' to 3' spans 879 bp. Note that Jurkat cells are triploid for chromosome 5 (e.g., for rs2548224 TTC > TTT would indicate a successful allelic substitution). (**b**) Sanger sequencing results for the targeted Jurkat cells confirmed that the two cutting edges were accurately joined by HDR, and precisely switched alleles for rs2548224 leaving the haplotype otherwise intact.

STAR Methods

Key resource table

REAGENT or RESOURCE	SOURCE	IDENTIFIER
Antibodies		
Goat polyclonal anti-LRAP/ERAP2 (1:2500)	R&D Systems	Cat# AF3830 RRID:AB_2099119
Sheep polyclonal anti-LNPEP (1:2500)	R&D Systems	Cat# AF6386 RRID:AB_10717574
Mouse monoclonal anti-α-Tubulin (clone DM1A) (1:5000)	Sigma-Aldrich	Cat# T9026 RRID:AB_477593
Anti-CTCF		
Chemicals, peptides, and recombinant proteins		
Alt-R® HDR Enhancer	Integrated DNA Technologies	Cat# 1081072
L-Arginine-7-amido-4-methylcoumarin hydrochloride	Sigma-Aldrich	Cat# A2027
Amersham ECL™ Prime Western Blotting	GE Healthcare	Cat# RPN2236
IGEPAL® CA-630 (NP40 substitute)	Sigma-Aldrich	Cat# I8896
cOmplete Protease Inhibitor Cocktail	Roche	Cat# 11873580001
Critical commercial assays		
AllPrep® DNA/RNA/miRNA Universal Kit	Qiagen	Cat# 80224
Infinium Human CytoSNP-850K v1.2 BeadChip	Illumina	Cat# 20025644
Deposited data		
qPCR data	This paper	Dataverse
R code for SNP-array plots	This paper	Dataverse
Experimental models: Cell lines		
Human: THP-1	ATCC	TIB-202™
Human: Jurkat	ATCC	TIB-152™
Human: Birdshot patient derived lymphoblastoid cells	This paper (see methods)	-
Oligonucleotides		
qPCR primers, see Table 2	Integrated DNA Technologies	
Alt-R crRNAs, see Table 1A	Integrated DNA Technologies	
Alt-R tracRNA	Integrated DNA Technologies	
Ultramer® DNA Oligo:	Integrated DNA Technologies	
Megamer™ ssDNA Fragment, see Table 1B	Integrated DNA Technologies	

Software and algorithms		
R Studio	R.4.2.2.	
NxClinical software v6.0	Bionano genomics	
BENCH Lab CNV	Agilent	
R package *sangerseqR*	Hill *et al*.[71]	https://www.bioconductor.org/packages/release/bioc/html/sangerseqR.html
Graphpad Prism	Graphpad Software Inc.	www.graphpad.com

Appendix 5.I

GWAS summary statistics and conditional analyses

Figure 5.2A-**5.2D** and **5.2F** use the LD (r2) between SNPs at *5q15* rs2927608. This SNP is the top *ERAP2* eQTL (n=938) in the GTEx data for tissue "whole blood" (**Supplemental Table 5.2**). LD information for rs2927608 was estimated using the EUR superpopulation of 1000 Genomes in Plink 1.09 (http://pngu.mgh.harvard.edu/~purcell/plink/)[72]. The genotype data for the EUR superpopulation[73] was extracted using the ensemble data slicer[74] with genotype file obtained via http://hgdownload.cse.ucsc.edu/gbdb/hg19/1000Genomes/ phase3/ALL.chr5.phase3_shapeit2_mvncall_integrated_v5a.20130502.genotypes.vcf.gz and region lookup parameter "5:96000000-98000000". Sample ID's from the EUR superpopulation of the 1000 Genomes were obtained by filtering using meta-data from the 1000 Genomes ftp sever url: http://ftp.1000genomes.ebi.ac.uk/vol1/ftp/release/20130502/ integrated_call_samples_v3.20130502.ALL.panel and converted into a .vcf files using the *vcfR R* package and formatted in Plink 1.09 by the "--recode" option into a BED file. We calculated the allele frequency of each SNP using the --freq function in Plink 1.09 and LD with rs2927608 using the "--r2" option (11930 variants from position 96000022-97252405 with LD information available).

In the *Data availability* section we provide a link to the repository with the full GWAS summary statistics for BCR as reported by Kuiper *et al*.[13]). The summary statistics from the BCR GWAS was filtered for variants at (Hg19) chromosome 5 (chr5) from position 96000000-97200000 (n=6307, **Supplemental Table 5.3**). For colocalization analysis, we cross referenced these BCR variants with GTEx v8 *ERAP2* eQTL from whole blood to obtain a final set of 679 SNPs. The CD GWAS summary statistics were downloaded from https://www.ibdgenetics.org/ uploads/cd-meta.txt.gz and filtered for variants at (Hg18) chr5 from position 96081460-96461460 (n=197, **Supplemental Table 5.4**) of which 195 overlapped with GTEx *ERAP2* eQTL from whole blood for colocalization analyses. Because rs2248374 is not in the summary statistics of CD, we used the association statistics for variant rs2549782 (LD (r2) = 1.0 in EUR of 1000 Genomes). We obtained the GWAS summary statistics for JIA as reported by Hinks *et al.*[12]. We filtered for variants at (Hg18) chr5 from position 95159342-98830661 (n=974, **Supplemental Table 5.5**) of which 495 variants were in common with the GTEx *ERAP2* eQTL data from whole blood and used in colocalization analysis. Note that we used the GWAS summary statistics reported by Hinks *et al*. that were calculated under a dominant genetic model.

To identify significant associations for SNPs with *ERAP2* mRNA and protein expression independent of the genotype of rs2248374, we performed approximate conditional analysis using GCTA v1.94.1 using the '--cojo-cond' option[75]. Our analysis uses the "FastGxC" tissue-shared *ERAP2* eQTL data for SNPs reported by Lu and associates, which is calculated using RNA-seq data from the GTEx Consortium GTEx v8[46]. For GCTA-COJO, we used linkage

disequilibrium (LD) information from the EUR superpopulation[73] as a reference panel (see above, n=2903 SNPs were used after cross referencing with the 11930 variants from position 96000022-97252405 Hg19 from the EUR, **Supplemental Table 5.6**). The summary statistics for *ERAP2* pQTL data from blood plasma of the INTERVAL study as reported by Sun *et al*.[37] was downloaded from https://app.box.com/s/u3flbp13zjydegrxjb2uepagp1vb6bj2. We filtered for the variants near *ERAP2*, which resulted in 6001 pQTL used in approximate conditional analysis (**Supplemental Table 5.7**).

Chapter 6

General discussion and future perspectives

Are we any closer to understanding the MHC-I pathway in birdshot uveitis?

The main objective of the work presented in this thesis was to gain a deeper understanding of the relevance of genetic risk loci within the MHC-I antigen presentation pathway of birdshot uveitis (BU). In addition to being widely accepted as a prerequisite for diagnosis, *HLA-A*29* is present in all patients, which indicates that its pathophysiology is driven by antigen presentation to $CD8^+$ T cells. In spite of this, researchers have struggled to determine the mechanism of antigen presentation that drives this severe type of eye inflammation since the early 1980s[1]. In **Chapter 3**, we exploited the fact that HLA-A*29 differs from other MHC-I alleles in the amino acid sequence that determines peptide antigen binding. By modeling this, we determined what makes HLA-A*29 functionally unique from other MHC-I alleles. By a better definition of the peptide binding capacity of HLA-A*29 we may better predict what peptides are presented by HLA-A*29 that cause T-cell mediated inflammation in the retina and choroid. While this may facilitate therapeutic approaches aimed at prevention of the presentation of such peptides, it remains to be determined if peptide presentation via HLA-A*29 is relevant during the clinical phase of disease or if this disease-defining pathway is only relevant during the onset of disease (i.e., is obsolete for therapeutic targeting). Observations from genetic association studies defined the starting point of the research questions of this thesis which identified in addition to *HLA-A*29* also the functionally closely related antigen processing aminopeptidase genes *ERAP1* and *ERAP2* located at chromosome 5[2]. The primary function of ERAP1 and ERAP2 is to trim peptides for loading and presentation by MHC-I, which makes peptide modification by ERAPs for presentation by HLA-A*29 likely to be involved in antigen presentation in BU. Since the genetic risk haplotypes for BU encode high levels of *ERAP2* and relatively low expressed and hypoactive *ERAP1,* we started our functional studies in this thesis by studying the influence of ERAP2 on the HLA-A*29 immunopeptidome. We followed this up by studies of candidate autoantigen retinal S-antigen (SAG) and T cell responses from patients and aimed to resolve the transcriptional regulation of *ERAP2* by disease risk polymorphisms. We will discuss to what extent we have obtained a novel understanding of the MHC-I pathway in birdshot uveitis in the following sections.

In **Chapter 2** we used patient-derived cell lines to measure the collection of >1000 peptides presented by HLA-A*29 at the cell surface. Unlike a similar previous study that relied on different (non-patient) cell lines that were either naturally ERAP2 competent or deficient and measured the immunopeptidome of all class I MHC alleles, the main advantage of our study was the use of isogenic cell lines from patients generated by CRISPR-Cas9 to manipulate the *ERAP2* gene. With isobaric labeling we could combine the conditions into a single mass spectrometry analysis, so that the differences in peptide abundances between the experimental conditions could be quantified more accurately. Rather than deconvoluting the entire MHC-I immunopeptidome by computation, we used a HLA-A*29-specific antibody to experimentally capture the immunopeptidome of HLA-A*29. We determined that ERAP2

has general effects on the cellular immunopeptidome, which is similar for HLA-A*29 as compared to other MHC-I alleles. For example, peptides that contain adenine (A), lysine (K), and arginine (R) at the N-terminus are preferable to trim by ERAP2, and these effects were evident across multiple MHC-I alleles' immunopeptidomes. We also identified specific effects of ERAP2 on peptides presented by HLA-A*29; ERAP2 sequesters peptides inside its enzymatic cavity for proteolytic cleavage before binding to MHC-I. Understanding the internal peptide sequence preferences for ERAP2 requires a large-scale peptide screening, extending beyond the peptides bound to MHC-I alleles (that capture only a part of all peptides trimmed by ERAP2 and ERAP1). However, dimensional reduction techniques, which consider the peptide sequence as a whole (reminiscent of our "model" where ERAP2 considers the peptides sequence as whole during proteolytic process), allowed us to shed light on relevant preference for peptide sequences presented by HLA-A*29. Our work revealed that ERAP2 disfavored peptides with bulky N-terminal residues such as tyrosine (Y) and phenylalanine (F), most likely due to potential steric hindrance[3] since the binding pocket for P2 amino acids is unfit to accommodate bulky amino acids[3,4]. According to our hypothesis, ERAP2 trims and destroys peptides with preferred N-terminal residues, allowing peptides like P2-F/Y to bind to HLA-A*29 (**Figure 6.1**). As peptides bound by HLA-A*29 most often contain a tyrosine at the C-terminus, we concluded that peptides promoted by ERAP2 carry the P2-F/Y+PΩ-Y motif. The overexpression of *ERAP2* which is often found in autoimmunity further enhances the chance that uveitogenic peptides end up on HLA-A*29. These results are significant for three reasons:

1) Peptides in the MHC-I immunopeptidome exhibit "peptide promiscuity", meaning that they can bind to multiple alleles, even when their overall binding motifs (i.e., preferences) are quite different. There are, however, some peptides that are restricted to a few or specific MHC-I alleles. As we showed **Chapter 3**, the peptides predicted to be highly specific for HLA-A*29 are those with the P2-F/Y+PΩ-Y motif and dependent on the presence of ERAP2.

2) The results from **Chapter 2** corroborated our observations in **Chapter 3** that the peptide-motif of HLA-A*29 is strongly dependent on the allele-specific amino acids residues 62 (leucine, L) and 63 (glutamine, Q). The 62L/63Q-motif is highly distinctive for HLA-A*29 compared to other common MHC-I alleles in the population and we showed that by allelic substitution that changing the amino acid residues at these positions strongly influenced predicted peptide binding capacity of HLA-A*29. Because position 62-63 directly interacts with the P2 side chains of bound peptide antigens, we hypothesize that the disease-modifying impact of ERAP2 on the immunopeptidome of HLA-A*29 should be by facilitating the binding of immunogenic peptides that contain the P2-F/Y+PΩ-Y motif (**Figure 6.1**).

3) Based on *in silico* screening, peptides with the P2-F/Y+PΩ-Y motif that have also been predicted as strongly binding ligands for HLA-A*29 are enriched in proteins expressed by melanocytes (as discussed in **Chapter 2**). This is significant, because melanocytes have been proposed as the main target cells in the choroid[5] and are also a source of autoantigens in other autoimmune conditions, such as HLA-C*06:02 associated psoriasis[6], and Vogt-Koyanagi-Harada syndrome (VKH)[7]. The use of Dextramer® technology to detect $CD8^+$ T cells that target melanocyte peptides (predicted in **Chapter 2**) would be an exciting follow up study.

What about ERAP1?

Our studies focused primarily on ERAP2's effects on HLA-A*29, but ERAP1 is also genetically associated with BU[2,8,9]. BU is also linked to polymorphisms that affect the enzymatic activity of ERAP1. Previous work suggests that HLA-A*29 combined with risk variants in both *ERAP1* and *ERAP2* showed the highest risk for BU[8]. This supports that the interaction of ERAP1 with ERAP2 and HLA-A*29 is a driving mechanism of BU. Earlier in **Chapter 3**, we demonstrated that the combination of HLA-A*29 and the key risk variants in *ERAP1* and *ERAP2* genes is only found in populations in which BU is reported (e.g. Netherlands, France, Spain, UK, but also non-European countries with a relatively large population of Western-European ancestry). Perhaps the rarity of co-occurrence of disease risk variants in both *ERAP1* and *ERAP2* may explain why BU is extremely rare in in other populations where HLA-A*29 is also prevalent, such as some Asian or African populations[10,11]. This may answers the long-standing question of why BU only affects individuals in these populations and strongly supports the role of the MHC-I pathway in this condition[12]. **Chapter 2** demonstrated that ERAP1 has non-redundant effects on HLA-A*29, and previous work showed that ERAP1 is functionally altered in BU[8], so in follow-up studies it is important to evaluate to what extent ERAP1 and ERAP2 cooperate in shaping the immunopeptidome of HLA-A*29 to better understand how this influences peptide presentation and CD8+ T cell activation in BU.

The retinal S-antigen is not a causal autoantigen in BU.

We expect that the autoantigens driving this condition are a few or maybe a single peptide antigen due to its specific impact on the peptide motif as well as the highly specific target cells that may contain the autoantigens (melanocytes), and the fact that ocular inflammation is restricted to the choroid and the retina. Moreover, our data in **Chapter 4** suggest that retinal antigens are less likely to be an autoantigen source by eliminating the retinal S-antigen (SAG) as a potential driving $CD8^+$ T cell autoantigen for BU. The HLA-A*29 peptidome from two patients was captured with extensive efforts and unbiased experiments in patient-derived cell lines. Despite demonstrating in patient-derived cell lines that SAG encodes peptides that appear natural self-derived ligands presented by HLA-A*29 (i.e., may appear in the immune-peptidome of the human body), our results differ from those of previous in vitro binding studies[13]. Such studies most likely did not consider whether the mature peptides used in binding studies

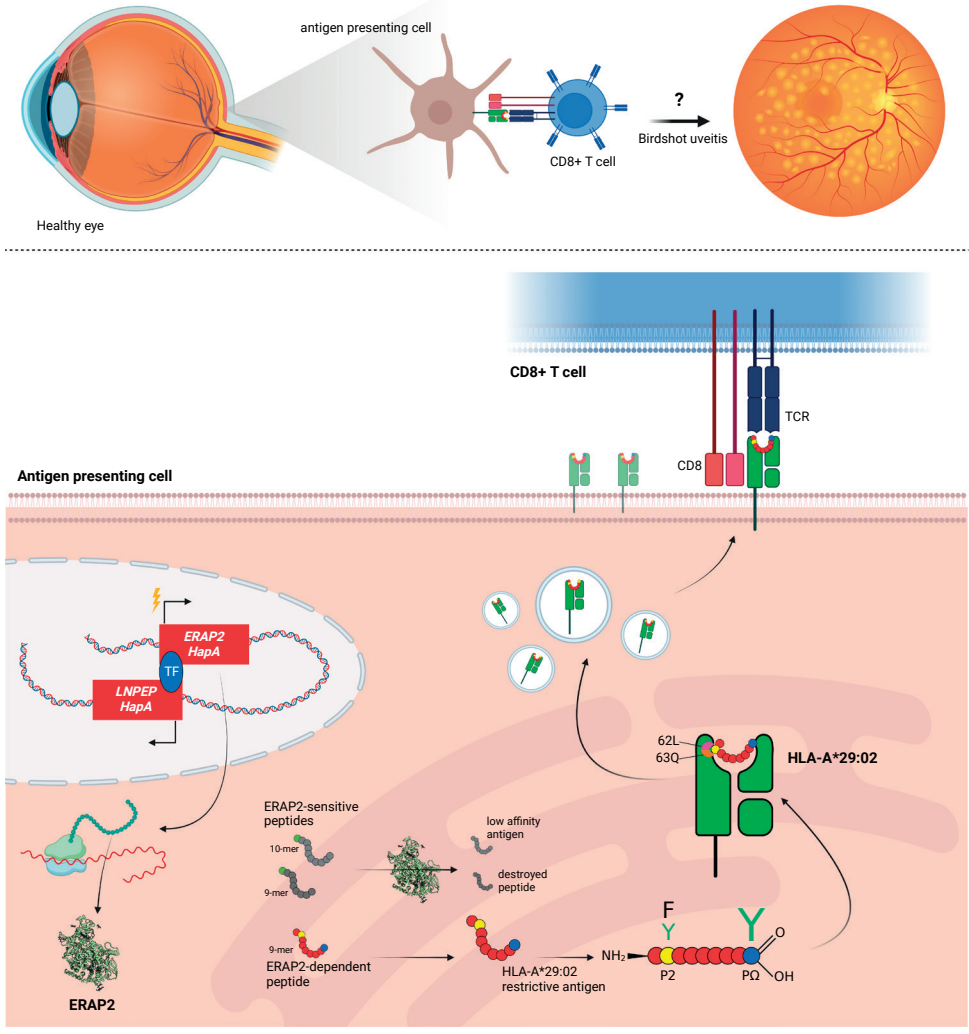

Figure 6.1: **Proposed disease mechanism based on findings in this thesis**. The disease associated *ERAP2 HapA* encodes functional ERAP2 aminopeptidase and contains SNPs in linkage disequilibrium in the downstream *LNPEP* gene that enhance transcription of ERAP2 mRNA. ERAP2 trims peptides with preferred N-terminal residues ('susceptible' peptides), which can lower their affinity for HLA-A*29. Peptides with bulky N-terminal residues are not trimmed by ERAP2, and a fraction of the peptides exhibit the HLA-A*29-specific peptide motif (P2-F/Y+PΩ-Y) that interacts with the 62L/63Q motif in the binding pocket of HLA-A*29. HLA-A*29-specific peptides presented on the cell surface initiate a $CD8^+$ T cell mediated immune response leading to sight-treating tissue damage in the eye.

would survive selection by the cellular antigen presentation machinery (e.g., proteasome, ERAPs, TAP, etc.). Regardless, in our studies, *ex vivo* culture and direct probing by peptide-HLA-A*29 multimers detected no SAG-specific $CD8^+$ T cells in ocular fluid of patients or enrichment for $CD8^+$ T cells in the circulation of patients compared to HLA-A*29^+ controls. A key insight in the pathophysiology of BU has been achieved here, ending a decades-long

debate on the role of SAG in BU as a primary autoantigen that functions via HLA-A*29. In our study, we found that peptides from SAG presented by HLA-A*29 are not immunogenic for $CD8^+$ T cells. Importantly, $CD8^+$ T cells were present in BU patient's vitreous fluid, indicating that the autoantigen source is MHC-I related. Based on in vitro SAG-stimulated T cell proliferation[14] and SAG-induced experimental autoimmune uveitis[15], which are both T helper cell-driven and mediated by MHC class II, SAG was considered as a candidate autoantigen for BU. SAG-induced cellular and humoral hyperresponsiveness in humans is not limited to BU and frequently seen in patients with other eye diseases. Accordingly, we propose that SAG is a "secondary" autoantigen involved in $CD4^+$ T helper-mediated responses following primary autoantigen-directed immunity via HLA-A*29 and $CD8^+$ T cells. Therefore, we conclude that SAG is unlikely to be relevant to the HLA-A*29-mediated pathogenic mechanisms that define the disease.

Towards autoantigen identification in BU

$CD8^+$ T-cell activation by autoantigen presentation through HLA-A*29 is likely to be a significant disease mechanism for BU. Although the disease is widely seen as a model for autoimmunity, we still don't know for sure if BU is an autoimmune disorder mediated by HLA-A*29 and $CD8^+$ T cells. The identification of the autoantigen(s) may provide powerful targets for immunomodulatory therapy for BU. It will also be possible to develop better tools for actual diagnosis, patient characterization, and pre- and post-therapy immune monitoring by gaining a more comprehensive understanding of the specificities of T cells in BU.

Due to methodological limitations, identifying $CD8^+$ T cell autoantigens is extremely labor-intensive and resource intensive. Therefore, very few autoantigens have been identified for MHC-I-associated diseases, and most epitopes are not yet rigorously verified[6]. MHC-I displays thousands of different peptides per cell, but T cells recognize only few of them. This poses a major challenge in the field. On the other hand, T-cell receptors have the potential to generate over 100 million different specificities, each with different potentials for recognizing peptides[16]. Thus, millions of putative peptides may have to be assessed in patients to discover autoantigens. Therefore, computational predictions of individual autoantigen responses have failed to produce reliable results so far[17].

Although high-multiplexed assays can be used to screen antigenic reactivities of T cells (e.g., tetramers with DNA barcodes), the number of possible peptides far surpasses the laboratory capacity and tissue accessibility. Thanks to the rapid development of single-cell technologies, it is now possible to perform high-throughput profiling of T cell receptors at the single-cell level (i.e., single-cell TCR sequencing)[18,19]. Data on the TCR amino acid sequence associated with uveitis significantly improves the chances of identifying the autoantigens that cause eye inflammation. By cloning the TCR in functional models, autoantigen reactivity can be efficiently and comprehensively screened. In particular, if the TCRs are cloned into cell lines for screening genome wide peptide libraries for autoantigens presented by risk

MHC-I alleles associated with uveitis, such as HLA-A*29. As a result of current technological advancements, the longstanding question of whether $CD8^+$ T cells recognize HLA-A*29 peptides in BU can be answered with such technologies in future studies.

From genome-wide association studies to disease mechanisms: ERAP2 in autoimmunity

A large number of SNPs are strongly associated with *ERAP2* mRNA and protein levels at the *5q15* locus where ERAP1 and ERAP2 genes are located, however due to the strong linkage disequilibrium at this locus it remains difficult to determine how these variants control the expression of *ERAP2*. Understanding their contribution to *ERAP2* regulation is critical to understanding how the genetic signatures associated with autoimmunity and other conditions result in dysregulation of ERAP2 and the MHC-I antigen pathway. SNPs in and near the *ERAP2* gene are associated with BU[2,20] and other autoimmune conditions, such as *Crohn's disease*[21], and *juvenile idiopathic arthritis*[22], as well as with protection against the *Black Death*[23-25] and severe respiratory infections[26]. In **Chapter 5**, we used population genetics, genome editing and functional genomics to identify causal variants to identify how SNPs regulate the expression of the *ERAP2* gene. Among the key observations were the demonstration that canonical *ERAP2* mRNA and protein expression is critically dependent on the genotype of the splice region variant rs2248374 located in a splice region in exon 10 of ERAP2. This answers the long-standing question whether the rs2248374 genotype is essential for ERAP2 expression (see introduction). For a long time, the SNP rs2248374 was thought to be responsible for the functional effects of other disease-associated SNPs near *ERAP2*, but we demonstrated in **Chapter 5** that this is not the case. We propose that autoimmune disease-risk SNPs, identified by GWAS, form a cis-regulatory region downstream of *ERAP2*. This region influences gene expression by interacting with the promoter of *ERAP2* if it encodes the risk alleles.

ERAP2 transcription is controlled by the chromosome structure and therefore the SNPs near *ERAP2* confer disease susceptibility by altering enhancer-promoter interactions. Therefore, these findings are significant, because they suggest that the chromosome structure plays an important role in its transcriptional control. This means that *ERAP2* may be implicated in autoimmunity not because it is expressed in susceptible individuals (those that carry at least one copy of the protein-coding haplotype A controlled by rs2248374), but because it is expressed at higher levels[8,20], such as at the site of inflammation. This also indicates that perhaps in tissues, pro-inflammatory signaling is among the leading pathways causing overexpression of ERAP2 resulting in autoimmunity. This overexpression of ERAP2 might be pharmacologically targeted to lower the level of ERAP2 and to impair the associated disease manifestations[27].

The potential role of $CD8^+$ T cells in the affected tissue has already been described for MHC Class I diseases like psoriasis (PsO), ankylosing spondylitis (AS) and acute anterior uveitis

(AAU). $CD8^+$ T cell expressing an autoreactive psoriatic TCR react against melanocytes due to presentation of the autoantigen, N-terminally trimmed by ERAP1, via risk HLA-C*06:02[6,28]. Interestingly, patients with AS and AAU have responsive $CD8^+$ T cells in eye fluid and synovial fluid respectively targeting melanocytes where the same TCRs recognize HLA-B27 bound peptides from different origin. The peptides were either derived from yeast or a self-peptide, showing that microbial-derived peptides can be similar as self-peptides. In **Chapter 4** we showed the presence of $CD8^+$ T cells within the vitreous fluid of a BU patient. Although these $CD8^+$ T cells were not targeting the high affinity SAG peptides, the fact these cells had breached the blood-retina barrier suggests the origin of the target antigen lies within the eye. This makes sense, since T cells have been found in the choroidal lesions typically seen in BU patients[29,30] and T cells in vitreous fluid from BU patients indeed do react against retinal/choroidal lysates[31].

As mentioned in **Chapter 5** the 4C-seq signal showing increased reads for ligated *ERAP2* and *LNPEP* sequences as a result of the two promoter areas being in close physical proximity. Using Hi-C-seq data from Chandra *et al*.[32] we narrowed down eQTLs overlapping *H3K27ac* enriched areas, forming the cis-regulatory region of about 900bp. In an effort to modify these *ERAP2* promoter-interacting eQTLs (pieQTLs) we managed to change rs2548224-G (*Hap A*) to rs2548224-T (*Hap B*) and we showed that allelic substitution led to reduction in *ERAP2* mRNA expression. However, the underlying molecular mechanism remains still unclear. A possibility is the presence of an enhancer-promotor loop that increases the transcriptional output, either by organization of the chromatin, the binding of transcription factors (TFs) or structural regulators[33,34]. These loop-forming TFs such as CCCTC-binding factor (CTCF), Yin Yang 1 and the Mediator complex can contribute in bringing different genomic areas in close proximity to improve transcription[35-39].

Promoters are highly enriched with a large array of potential TF binding sequences (many overlapping ChIP-seq signals), making the promoter sequence a difficult genomic area to predict and validate which TF is affected by SNPs and influence *ERAP2* expression. CRISPR-knockin to modify *HapB* to their corresponding *HapA* variant can be used in a disease model to determine differential TF binding affinity. We consider CTCF as a potential TF involved as it is a common TF present when multiple genes are entwined in expression regulation. Alternatively, an untargeted TF ChIP library approach can be used to assess many different types of TFs in order to find which TF influences *ERAP2* expression, either directly influencing the transcription of *ERAP2* or enhancing chromatin structure for improved expression.

Therapeutic targeting of ERAP2s for treatment of BU and autoimmunity

Regulating ERAPs as a method to control inflammation in autoimmune disease might be an obvious target for future pharmaceutical drug development. However, some careful consideration is needed. As we described in this thesis, ERAPs are involved in the modulation of the immunopeptidome. Based on the genetic predisposition of ERAPs in many auto-immune diseases, for example high levels of *ERAP2* are associated with BU, one might

think that downregulating ERAPs could be helpful for BU patients. However, it's important to understand that modifying the expression of ERAPs might have a harmful effect on the antigen presentation. T cell priming in the thymus is a complex arrangement of the TCR with careful screening for self-protein[40], where the level of *ERAP2* expression might be involved with the supply of (self)antigens as well[41]. Therefore, systemic inhibition of ERAP2 function might shift the peptidome towards a higher abundance of unknown self-peptides. The result might be the induction of an unwanted autoimmune reaction. Instead, local treatment to modulate ERAP2 function is a better option. For example, BU is localized inflammation in the posterior area of the eye (retina/choroid), therefore local modulation of *ERAP2* expression might be useful. This would require development of small molecules targeting ERAP2 or locally administered siRNA to knockdown *ERAP2* expression.

Since acquiring tissue samples from BU patients is difficult, a surrogate model to study the disease mechanism is required. We showed with our BU cell line model that we can study the immunopeptidome from patients' derived LCLs. The obvious way to study in vivo would be a rodent model (e.g. mouse, rat), however in contrary to humans rodents do not have a homolog for the *ERAP2* gene[42,43]. Animal studies of uveitis have so not studied the role of ERAP1. Ideally, HLA-A*29 transgenic models include humanized ERAPs, since similar to humans, the presence of HLA-A*29 itself is not sufficient to induce ocular inflammation[44].

Another approach for studying the disease mechanisms of BU would be a disease model using the tissues that are affected in BU to study the peptidome on HLA-A*29:02 and the involvement of the ERAPs. For example, HLA-A*29 positive retina pigment epithelial (RPE) cell line producing melanocyte biology proteins (predicted as potential autoantigens in **Chapter 2**) may provide a useful model. However, human ex vivo RPE cells from donors are difficult to obtain and long-term culture has limitations on RPE specific gene expression[45], such as the loss of melanosomes and pigmentation. One alternative for autoantigen discovery for HLA-A*29 could be using a melanoma cell line, expressing *HLA-A*29:02* and *ERAP2 Hap A* (including ERAP1KO or *ERAP1 Hap10*). With our developed method to determine the HLA-A*29:02 peptidome we could determine whether melanoma cells present high affinity peptides and whether these peptides are distinct for this cell type. Assessing if these peptides are ERAP2-dependent and whether they fit the peptide motif we discussed in this thesis would further support their potential role in BU. In the study by Granados *et al*. LCLs expressing HLA-A*29:02 were measured in which a high affinity HLA-A*29 peptide derived from tyrosinase was detected[46]. Tyrosinase is a well-known source of autoantigens in VKH and is functional in the melanin pathway in melanocytes. The described peptide FFISSKDLGY (10-mer) fits the ERAP2-dependent motif with bulky phenylalanine residues at P1/P2 and tyrosine at PΩ.

References

1. Nussenblatt, R. B., Mittal, K. K., Ryan, S., Richard Green, W. & Edward Maumenee, A. Birdshot Retinochoroidopathy Associated with Hla-A29 Antigen and Immune Responsiveness to Retinal S-Antigen. Am. J. Ophthalmol. 94, 147–158 (1982).
2. Kuiper, J. J. W. et al. A genome-wide association study identifies a functional ERAP2 haplotype associated with birdshot chorioretinopathy. Hum. Mol. Genet. 23, 6081–6087 (2014).
3. Mpakali, A. et al. Structural basis for antigenic peptide recognition and processing by Endoplasmic reticulum (ER) aminopeptidase 2. J. Biol. Chem. 290, 26021–26032 (2015).
4. Giastas, P. et al. Mechanism for antigenic peptide selection by endoplasmic reticulum aminopeptidase 1. Proc. Natl. Acad. Sci. 116, 26709–26716 (2019).
5. Kuiper, J., Rothova, A., de Boer, J. & Radstake, T. The immunopathogenesis of birdshot chorioretinopathy; a bird of many feathers. Prog. Retin. Eye Res. 44, 99–110 (2015).
6. Arakawa, A. et al. ERAP1 Controls the Autoimmune Response against Melanocytes in Psoriasis by Generating the Melanocyte Autoantigen and Regulating Its Amount for HLA-C*06:02 Presentation. J. Immunol. 207, 2235–2244 (2021).
7. Yamaki, K., Gocho, K., Hayakawa, K., Kondo, I. & Sakuragi, S. Tyrosinase family proteins are antigens specific to Vogt-Koyanagi-Harada disease. J. Immunol. 165, 7323–7329 (2000).
8. Kuiper, J. J. W. et al. Functionally distinct ERAP1 and ERAP2 are a hallmark of HLA-A29-(Birdshot) Uveitis. Hum. Mol. Genet. 27, 4333–4343 (2018).
9. Gelfman, S. et al. ERAP1, ERAP2, and Two Copies of HLA-Aw19 Alleles Increase the Risk for Birdshot Chorioretinopathy in HLA-A29 Carriers. Invest. Ophthalmol. Vis. Sci. 62, 3 (2021).
10. Regenold, J. et al. Birdshot chorioretinopathy in an HLA-A29 positive Asian patient. American journal of ophthalmology case reports vol. 29 101802 (2023).
11. Knezevic, A., Munk, M. R., Pappas, F., Merrill, P. T. & Goldstein, D. A. HLA-A29-POSITIVE BIRDSHOT CHORIORETINOPATHY IN AN AFRICAN AMERICAN PATIENT. Retin. Cases Brief Rep. 10, 201–204 (2016).
12. Donvito, B. et al. Different HLA class IA region complotypes for HLA-A29.2 and -A29.1 antigens, identical in birdshot retinochoroidopathy patients or healthy individuals. Invest. Ophthalmol. Vis. Sci. 46, 3227–3232 (2005).
13. Boisgerault, F. et al. Definition of the HLA-A29 peptide ligand motif allows prediction of potential T-cell epitopes from the retinal soluble antigen, a candidate autoantigen in birdshot retinopathy. Proc. Natl. Acad. Sci. U. S. A. 93, 3466—3470 (1996).
14. Whitcup, S. M., Vistica, B. P., Milam, A. H., Nussenblatt, R. B. & Gery, I. Recoverin-associated retinopathy: a clinically and immunologically distinctive disease. Am. J. Ophthalmol. 126, 230–237 (1998).
15. Mattapallil, M. J. et al. Uveitis-associated epitopes of retinal antigens are pathogenic in the humanized mouse model of uveitis and identify autoaggressive T cells. J. Immunol. 187, 1977–85 (2011).

16. Arstila, T. P. et al. A direct estimate of the human alphabeta T cell receptor diversity. Science 286, 958–961 (1999).
17. Kuiper, J. J. W. et al. EULAR study group on 'MHC-I-opathy': identifying disease-overarching mechanisms across disciplines and borders. Ann. Rheum. Dis. annrheumdis-2022-222852 (2023) doi:10.1136/ard-2022-222852.
18. De Simone, M., Rossetti, G. & Pagani, M. Single Cell T Cell Receptor Sequencing: Techniques and Future Challenges . Frontiers in Immunology vol. 9 (2018).
19. Han, A., Glanville, J., Hansmann, L. & Davis, M. M. Linking T-cell receptor sequence to functional phenotype at the single-cell level. Nat. Biotechnol. 32, 684–692 (2014).
20. Hanson, A. L. et al. Genetic Variants in ERAP1 and ERAP2 Associated With Immune-Mediated Diseases Influence Protein Expression and the Isoform Profile. Arthritis Rheumatol. 70, 255–265 (2018).
21. Franke, A. et al. Genome-wide meta-analysis increases to 71 the number of confirmed Crohn's disease susceptibility loci. Nat. Genet. 42, 1118–1125 (2010).
22. Hinks, A. et al. Dense genotyping of immune-related disease regions identifies 14 new susceptibility loci for juvenile idiopathic arthritis. Nat. Genet. 45, 664–669 (2013).
23. Klunk, J. et al. Evolution of immune genes is associated with the Black Death. Nature 611, 312–319 (2022).
24. Barton, A. R. et al. Insufficient evidence for natural selection associated with the Black Death. bioRxiv : the preprint server for biology (2023) doi:10.1101/2023.03.14.532615.
25. Vilgalys, T. P. et al. Reply to Barton et al: signatures of natural selection during the Black Death. bioRxiv : the preprint server for biology (2023) doi:10.1101/2023.04.06.535944.
26. Hamilton, F. et al. Variation in ERAP2 has opposing effects on severe respiratory infection and autoimmune disease. Am. J. Hum. Genet. (2023) doi:10.1016/j.ajhg.2023.02.008.
27. Medve, L. et al. Modulators of hERAP2 discovered by high-throughput screening. Eur. J. Med. Chem. 211, 113053 (2021).
28. Arakawa, A. et al. Melanocyte antigen triggers autoimmunity in human psoriasis. J. Exp. Med. 212, 2203–2212 (2015).
29. Gaudio, P. A., Kaye, D. B. & Crawford, J. B. Histopathology of birdshot retinochoroidopathy. Br. J. Ophthalmol. 86, 1439–1441 (2002).
30. Pulido, J. S. et al. Histological findings of birdshot chorioretinopathy in an eye with ciliochoroidal melanoma. Eye 26, 862–865 (2012).
31. Kuiper, J. J. W. et al. Detection of choroid- and retina-antigen reactive CD8+ and CD4+ T lymphocytes in the vitreous fluid of patients with birdshot chorioretinopathy. Hum. Immunol. 75, 570–577 (2014).
32. Chandra, V. et al. Promoter-interacting expression quantitative trait loci are enriched for functional genetic variants. Nat. Genet. 53, 110–119 (2021).
33. Chakraborty, S. et al. Enhancer-promoter interactions can bypass CTCF-mediated boundaries and contribute to phenotypic robustness. Nat. Genet. 55, 280–290 (2023).
34. Hua, P. et al. Defining genome architecture at base-pair resolution. Nature 595, 125–129 (2021).

35. Nakahashi, H. et al. A genome-wide map of CTCF multivalency redefines the CTCF code. Cell Rep. 3, 1678–1689 (2013).
36. Phillips, J. E. & Corces, V. G. CTCF: master weaver of the genome. Cell 137, 1194–1211 (2009).
37. Weintraub, A. S. et al. YY1 Is a Structural Regulator of Enhancer-Promoter Loops. Cell 171, 1573-1588.e28 (2017).
38. Luan, J. et al. CTCF blocks antisense transcription initiation at divergent promoters. Nat. Struct. Mol. Biol. 29, 1136–1144 (2022).
39. Kim, S., Yu, N.-K. & Kaang, B.-K. CTCF as a multifunctional protein in genome regulation and gene expression. Exp. Mol. Med. 47, e166 (2015).
40. Klein, L., Kyewski, B., Allen, P. M. & Hogquist, K. A. Positive and negative selection of the T cell repertoire: what thymocytes see (and don't see). Nat. Rev. Immunol. 14, 377–391 (2014).
41. Gabrielsen, I. S. M. et al. Autoimmune risk variants in ERAP2 are associated with gene-expression levels in thymus. Genes Immun. 17, 406–411 (2016).
42. Paladini, F., Fiorillo, M. T., Tedeschi, V., Mattorre, B. & Sorrentino, R. The Multifaceted Nature of Aminopeptidases ERAP1, ERAP2, and LNPEP: From Evolution to Disease . Frontiers in Immunology vol. 11 (2020).
43. Serwold, T., Gonzalez, F., Kim, J., Jacob, R. & Shastri, N. ERAAP customizes peptides for MHC class I molecules in the endoplasmic reticulum. Nature 419, 480–483 (2002).
44. Mattapallil, M. J. et al. The Rd8 mutation of the Crb1 gene is present in vendor lines of C57BL/6N mice and embryonic stem cells, and confounds ocular induced mutant phenotypes. Invest. Ophthalmol. Vis. Sci. 53, 2921–2927 (2012).
45. Samuel, W. et al. Appropriately differentiated ARPE-19 cells regain phenotype and gene expression profiles similar to those of native RPE cells. Mol. Vis. 23, 60–89 (2017).
46. Granados, D. P. et al. MHC I-associated peptides preferentially derive from transcripts bearing miRNA response elements. Blood 119, e181-91 (2012).

Chapter 7

Nederlandse samenvatting

Birdshot uveitis

Birdshot uveitis (BU) is een zeldzame vorm van non-infectieuze uveitis die zich laat karakteriseren door intra-oculaire inflammatie, troebel zicht, vasculaire lekkage, macula oedeem, retinale atrofie en progressief verlies van het zicht. Fundusfoto's laten BU specifieke laesies zien die waarschijnlijk ontstaan door T-cel gemedieerde ontstekingen in het choroid en de retina. Patiënten worden behandeld met systemische immunosuppressiva om de symptomen te onderdrukken.

Naast de fysieke symptomen heeft BU nog een specifieke eigenschap. Elke patiënt is drager van het *Human Leukocyte Antigen* (HLA)-A*29, een variant van het *klasse I major histocompatibility complex* (MHC-I). Tot nu toe is BU de enige aandoening waarbij alle patiënten drager zijn van tenminste één allel *HLA-A*29*. Aangezien MHC-I moleculen zorgen voor de antigenpresentatie aan CD8+ T-cellen is het hoogstwaarschijnlijk dat HLA-A*29 betrokken is bij het presenteren van antigenen die de ontsteking veroorzaken. Het HLA-A*29 komt relatief veel voor binnen de West-Europese bevolking (5-10%). Daardoor ligt de oorzaak van BU waarschijnlijk niet alleen bij het hebben van het *HLA-A*29* allel, maar spelen specifieke antigenen die via HLA-A*29 gepresenteerd worden een belangrijke rol. Vanwege de sterke associatie met HLA-A*29 maakt het BU een interessant ziektemodel om de rol van MHC-I en auto-immuniteit te onderzoeken. MHC-I gemedieerde aandoeningen zoals axiale spondylartritis (*HLA-B*27*), psoriasis (*HLA-C*06:02*) en de ziekte van Behçet (*HLA-B*51*).

Uit genetische studies waarbij BU patiënten vergeleken werden met grote controle populaties is naar voren gekomen dat naast HLA-A*29 er ook een predispositie aanwezig is voor de *ERAP* genen, *ERAP1* en *ERAP2*. Deze genen coderen voor *endoplasmic reticulum aminopepidase* 1 en 2. Beide eiwitten functioneren als aminopeptidase, waarbij precursor peptides aan de N-terminale zijde worden getrimd, voordat deze peptides op een MHC-I molecuul geladen kunnen worden. Van ERAP1 zijn er verschillende haplotypes mogelijk, afhankelijk van polymorfismen in het genoom. Deze polymorfismen hebben effect op de enzymatische activiteit van ERAP1. Haplotype 10 is bij BU patiënten sterk geassocieerd, ondanks dat dit haplotype zeer inefficiënte werking laat zien. Voor *ERAP2* zijn er twee haplotypes beschikbaar, *haplotype A* dat codeert voor een functioneel eiwit en *haplotype B* dat door incorrecte splicing een incorrect transcript geeft. Het haplotype B resulteert dan ook niet in een functioneel eiwit. Waar ziekte-geassocieerde polymorfismen in *ERAP1* te herleiden zijn naar verschillende haplotypes, zijn de BU geassocieerde polymorfismen in *ERAP2* vooral te vinden in niet-coderende delen van het gen.

ERAP2 genereert een selectief peptide motief voor HLA-A*29:02

In **hoofdstuk 2** hebben we onderzocht hoe ERAP2 betrokken is bij het trimmen van peptiden. Daarnaast hebben we antwoord gegeven of de vraag of ERAP2 in staat is om unieke peptiden voor HLA-A*29 te genereren. Hiervoor hebben we gebruik gemaakt van EBV-getransformeerde B cellen van BU patiënten om het repertoire aan peptides te bepalen op HLA-A*29:02. Daarbij hebben we ook een ERAP2 knockout (ERAP2KO) variant van deze LCLs

gebruikt om een verschil in peptide-aanbod aan te tonen tussen wild-type en ERAP2KO LCLs. Hiervoor is een HLA-A*29 specifiek antilichaam gebruikt om het immunopeptidoom van HLA-A*29 te isoleren. Door gebruik te maken van isotoop-gelabeld tyrosine/phenylalaline aminozuurisotopen konden de peptiden van wild-type LCLs direct vergeleken worden met de peptiden afkomstig van de ERAP2KO LCLs middels massaspectrometrie.
Afhankelijk van de aanwezigheid van ERAP2 konden wij verschillen aantonen in de hoeveelheid peptides die gepresenteerd worden op HLA-A*29:02 in beide condities. Gebrek van ERAP2 laat een verhoging van N-terminaal adenine/lysine/asparagine zien, wat gewenste aminozuur residuen zijn voor ERAP2 om te trimmen. Dit zagen wij ook voor de peptides op de overige HLA-klasse-I moleculen van deze LCL. Andersom konden wij ook aantonen dat in aanwezigheid van ERAP2 er een groter aanbod van peptides met grote aminozuren als phenylalanine en tyrosine aan de N-terminale zijde te vinden waren. Deze peptides worden niet door ERAP2 getrimd en krijgen in aanwezigheid van ERAP2 dus meer kans om op HLA-klasse-I moleculen terecht te komen ten opzichte van peptides met hoge affiniteit van ERAP2. Opvallend was dat ~15% van de peptides die ongevoelig voor ERAP2 zijn een uniek motief bevatten die uniek is voor HLA-A*29:02. Hieruit concluderen wij dat de combinatie van ERAP2 en HLA-A*29:02 kan leiden tot antigenpresentatie met een specifiek autoantigen dat betrokken is bij de inflammatie bij BU patiënten.

HLA-A*29:02 heeft een uniek bindingsmotief voor ERAP2-afhankelijke peptiden

In **hoofdstuk 3** zijn we verder ingegaan op de link van ERAP2 en HLA-A*29:02 en wat hun rol in de ontwikkeling van BU kan zijn. Ondanks dat HLA-A*29 relatief veel voorkomt in Europa, is de incidentie van BU zeer laag. Ook in landen buiten Europa waar BU voorkomt is de aanwezigheid van HLA-A29 te herleiden naar de herkomst van de bevolking. HLA-A*29:02 onderscheidt zich van verwante HLA-A moleculen door specifieke polymorfismen, met name door de leucine (L) op positie 62 en glutamine (Q) op positie 63. Beide aminozuren zijn onderdeel van de *peptide binding groove* en spelen een essentiële rol in de affiniteit van antigenen met HLA-A*29:02. Predictie-analyses laten zien dat elk andere aminozuurcombinatie een negatief effect heeft op de bindingscapaciteit van HLA-A*29:02. In hoofdstuk 2 hebben we beschreven dat ~15% van de ERAP2-afhankelijke peptides een specifiek hoge affiniteit hebben voor HLA-A*29. Met name de phenylalanine en tyrosine op P2 hebben een sterke affiniteit met de peptide binding groove als gevolg van 62L/63Q in HLA-A29. Hierdoor bestaat de mogelijkheid dat ERAP2 betrokken is bij het genereren van HLA-A29 specifieke antigenen, dat de genetische associatie van zowel *ERAP2* als *HLA-A29:02* zou kunnen verklaren.

CD8+ T cellen tegen het retinale S-antigen zijn niet betrokken bij birdshot uveitis

Het retinale S-antigen (S-arrestin, SAG) wordt al decennia lang beschreven als potentieel autoantigen in BU en andere oogaandoeningen. In **hoofdstuk 4** hebben wij onderzocht of SAG specifieke peptides die op HLA-A*29:02 gepresenteerd worden en of deze peptides

ook een CD8+ T cel gemedieerde immuunreactie veroorzaken. Door gebruik te maken van het BU model uit **hoofdstuk 2**, waar LCLs afkomstig van BU patiënten zijn gebruikt, hebben we twee SAG peptides (VTLTCAFRY, TVLGILVSY) met hoge affiniteit voor HLA-A29 kunnen identificeren. In vitro digestie van de precursor 10-mer peptides laat zien dat recombinant ERAP1 en ERAP2 in staat zijn om de twee antigenen te vormen. Beide SAG peptides worden vervolgens niet verder getrimd door ERAP2, wat zou betekenen dat in BU patiënten met hoge ERAP2 expressie beide peptides in hogere mate gepresenteerd kunnen worden op HLA-A*29:02.
Vervolgens hebben we gevalideerd of beide peptides in staat zijn om een immuunreactie teweeg te brengen. We hebben *Dextramers* (HLA-A*29:02 met fluorescent label), geladen met de SAG peptides, laten incuberen met *PBMCs* (*peripheral blood mononuclear cells*) van BU patiënten en HLA-A*29:02+ controles. Hierbij hebben wij geen verrijking van specifieke CD8+ T cellen gevonden, zowel in BU patiënten als in de controlegroep. Daarnaast hebben we ook uit een glasvochtpunctie van een BU patiënt SAG-specifieke CD8+ T cellen proberen te detecteren, maar ook hier vonden wij geen verrijking van reactieve CD8+ T cellen. Tenslotte hebben we PBMCs van BU patiënten en HLA-A*29:02 controles gestimuleerd met recombinant SAG peptides, maar ook hier was er geen verhoogde immuunreactie waar te nemen tussen BU patiënten en HLA-A*29:02 controles.
Al met al kunnen wij concluderen dat het retinale S-antigen geen autoantigen is voor BU, waarbij wij bewijs leveren dat tegen de jarenlange aangenomen consensus ingaat.

Een cis-regulatory element reguleert ERAP2 expressie middels auto-immuun geassocieerde polymorfismen

In **hoofdstuk 5** hebben wij beschreven hoe BU geassocieerde polymorfismen gelegen in het *ERAP2* gen en naastgelegen genoom (waaronder het nabij gelegen *LNPEP* gen) een mogelijke rol spelen in de regulatie en expressie van *ERAP2*. Deze polymorfismen zijn middels *linkage disequilibrium* (LD) aan elkaar verbonden, waarmee het mogelijk is om zogenaamde *ERAP2* haplotypes te benoemen. Één van deze polymorfismen wordt al om beschreven als drijvende kracht achter *ERAP2* expressie, namelijk *splice variant* rs2248374. Wij hebben aangetoond dat deze variant inderdaad noodzakelijk is voor een functioneel allel. Met behulp van de CRISPR-Cas9 genmodificatietechniek konden wij ERAP2 'aanzetten' of 'uitzetten'.
Als we grootschalige genoomstudies vergelijken (zoals genome wide association studies [GWAS]) zien we dat niet alleen bij BU patiënten, maar ook patiënten met de ziekte van Crohn of jeugdreuma (JIA), een grote hoeveelheid ziekte geassocieerde polymorphismen laat zien die buiten het ERAP2 gen liggen, namelijk in de promotorregio van het nabijgelegen *LNPEP* gen. Statistische correctie van het signaal van rs2248374 laat zien dat er een onafhankelijk signaal afkomstig is vanuit *LNPEP*.
Door vervolgens gebruik te maken van *chromosome confirmation capture* data, waarbij het *H3K27ac* signaal wordt overlapt met eQTL data voor de expressie van ERAP2, konden wij uit de onafhankelijke groep polymorfismen in *LNPEP* een kleine groep polymorfismen aanwijzen

die mogelijk invloed hebben op de expressie van *ERAP2*. Zo'n regio in het genoom wordt een *cis-regulatory element* genoemd. Een poging tot genmodificatie waarbij polymorfismen van het zogenaamde risico-haplotype (actief ERAP2) werden omgezet naar de alternatieve conformatie (inactief ERAP2) leidde tot reductie van de *ERAP2* expressie. Door gebruik te maken van de *4C-seq* techniek hebben we vervolgens aangetoond dat de auto-immuun geassocieerde polymorfismen waarschijnlijk een rol spelen in de chromatine structuur die daarbij ook de *ERAP2* expressie reguleert.

Met deze studie laten wij zien dat auto-immuun geassocieerde polymorfismen middels LD een functionele rol kunnen spelen in de expressie van genen. In dit geval wordt *ERAP2* waarschijnlijk gereguleerd door de aanwezigheid van een extern gelegen regulatoir element in *LNPEP*. Deze kennis kan in toekomst gebruikt worden om *ERAP2* expressie te bepalen als maat voor auto-immuniteit en als mogelijk aangrijpingspunt voor ziekte-modelerende behandelingsmethoden.

Appendices

Dankwoord

About the author

List of publications

Dankwoord

Na ruim 5 jaar zit mijn promotieonderzoek erop en natuurlijk heb ik daarvoor heel wat mensen te bedanken voor hun hulp, interesse en bijdrage om uiteindelijk dit proefschrift te kunnen schrijven. In dit dankwoord wil ik dan ook een aantal van jullie persoonlijk bedanken. Ik wil ook alle birdshot uveitis patiënten bedanken die bloedsamples hebben gedoneerd voor mijn onderzoek. Birdshot uveitis is een zeer zeldzame auto-immuunziekte in het oog dat bij het grote publiek amper bekend is. Desalniettemin verdienen ook deze patiënten een goede behandeling waar voor nu nog veel onderzoek nodig is. Ik hoop dat ons onderzoek in de toekomst zal bijdragen aan nieuwe inzichten in de behandeling van auto-immuunziekten.

Het promotieteam: beste Joke, Jonas en Annette. Bedankt voor de prettige samenwerking de afgelopen jaren. Jullie hebben mij altijd de ruimte gegeven mijzelf te kunnen ontwikkelen en zelf te laten meedenken in het verloop van mijn promotieonderzoek. Bedankt voor jullie vertrouwen en de geweldige begeleiding!

Beste Prof. Dr. de Boer, beste **Joke**. Bedankt voor je onvoorwaardelijke interesse, hulp, en betrokkenheid bij mijn onderzoek. Jij zorgde ervoor dat Jonas en ik niet te vaak afdwaalde van het doel van het onderzoek, namelijk wat er voor de patiënt belangrijk is om te weten te komen over birdshot. Bedankt dat je mij altijd gesteund hebt, ook tijdens moeilijke tijden in het begin van de coronaperiode.

Beste Dr. Kuiper, beste **Jonas**. Ik wil jou bedanken voor al je tijd en energie die je in mijn project hebt gestoken. Bedankt voor alle (soms urenlange) discussies over experimenten, de resultaten uit het lab, de nieuwste literatuur en gedachtes over hoe de ERAPs nu eigenlijk werken. Ik kan mij geen betere begeleider bedenken. Daarnaast is jouw interesse en behulpzaamheid voor iedereen die dat nodig heeft bewonderenswaardig. Niet alleen binnen de oogheelkunde, maar ook bij het CTI ben je een zeer gewaardeerd persoon die ten allen tijde bereid is om mensen te helpen met hun onderzoek. Ik wens je alle succes voor de toekomst!

Beste Dr. Ossewaarde, beste **Annette**. Waar je gedurende mijn promotieonderzoek altijd al interesse toonde in mijn projecten en ook bijgedragen hebt aan de S-antigen paper, voegde je je in het laatste jaar toe aan mijn promotieteam. Ook jou wil ik natuurlijk bedanken voor je betrokkenheid en bijdrage bij dit proefschrift.

Beste Prof. Dr. Radstake, beste **Tim**. In het begin kwam ik bij jouw groep in het lab en was je ook betrokken bij mijn promotieonderzoek. Ik ben je dankbaar dat ik heb kunnen profiteren van een leuke groep waarin ik snel mijn kennis van immunologie kon verbreden. Ook jou wil ik bedanken voor je vertrouwen en begeleiding.

Geachte leden van de beoordelingscommissie, beste **Prof. Dr. Wiertz, Prof. Dr. Hamann, Prof. Dr. van Wijk, Prof. Dr. van Hagen, Dr. Kesmir**, hartelijk dank voor jullie tijd en interesse om mijn proefschrift te beoordelen en zitting te nemen in mijn commissie.

Gedurende de corona pandemie vormde er zich een verbond genaamd *The Winchester* (aka *De Winnie*) dat in een tijd van lockdowns en verplicht thuiswerken ervoor zorgde dat we met elkaar de moed erin hielden en ervoor zorgde dat het plotselinge gat in het dagelijkse sociale contact op de werkvloer behouden bleef. Lieve **Anneline, Rianne, Nila** en **Safae**, waar moet ik beginnen. Wat heb ik genoten van onze bijna dagelijkse videocalls, onze koffiedates in de stad, jullie vriendschap in een tijd waar iedereen opeens in een sociaal isolement raakte. Gelukkig bleef dit hechte verbond ook bestaan na de periode van quarantaines, avondklokken en mondkapjes. Ik kijk terug naar mooie momenten die we samen hebben beleefd, zoals het weekendje bij Nila in Heidelberg, de bruiloft van Anneline en Ralf, de geboorte van Haroun, de geboorte van Walter. Stuk voor stuk waardevolle herinneringen en momenten die we samen hebben beleefd.
Anneline, vanaf de eerste dag dat ik in het WKZ kwam heb jij mij gelijk welkom laten voelen in het lab. Jouw aanstekelijke enthousiasme, jouw interesse in anderen en jouw gedrevenheid in het lab maakte jou vanaf het begin een dierbare collega. Door jou heb ik ook een interesse gekregen in het verzamelen van tropische kamerplanten en hielp jij mij aan allerlei stekjes waardoor mijn woonkamer snel in een jungle veranderde. Ik ben je zeer dankbaar dat je mij als paranimf wil bijstaan op de belangrijkste dag van mijn wetenschappelijke carrière.
Rianne, ik ken jou als een slimme, gedreven onderzoeker, maar bovenal een zorgzaam persoon die altijd bereid is anderen te helpen. De afgelopen jaren heb ik je zien groeien tot een volwaardige computational scientist en ik sta altijd met bewondering te kijken naar al je complexe analyses die je uitvoert. Daarnaast kijk ik terug op alle gezellige momenten die we met elkaar gehad hebben in het lab en daarbuiten. We hebben een gezamenlijke interesse in films en ik hoop dat we in de toekomst nog vaak eens een filmpje pakken. Ook jou ben ik zeer dankbaar dat je als paranimf naast mij staat.
Nila, voor jou geldt hetzelfde. Je bent een super gedreven en kundige wetenschapper, zowel in het lab als achter de pc. Je hebt mij altijd geholpen in het lab als ik een nieuw ingewikkeld experiment moest opzetten. Daarnaast ben je ook nog eens zeer geleerd in de wetenschap van bier en het brouwen daarvan. Nu je in Heidelberg zit kunnen we helaas niet meer zo makkelijk gezamenlijk naar De Molen voor een bierproeverij of blikken inslaan bij Littebeershop in Utrecht. Ondanks dat houden we elkaar goed op de hoogte van alle nieuwe bieren, brouwen we allebei zelf ons eigen bier en verzamelen we zelfs bier voor elkaar. Het wordt nodig tijd dat ik in Heidelberg eens laat zien hoe je een fatsoenlijke stout maakt 😜.
Safae, jij was goed en wel begonnen met je onderzoek toen de coronapandemie uitbrak. Gelukkig vond je je weg naar ons en ben ik blij je te mogen leren kennen. Ik heb altijd genoten van je fanatieke houding als iets je dwars zat, maar ook je liefdadigheid en zorgzaamheid

naar iedereen die je lief hebt. Je hebt ons ook veel bijgebracht van de Marokkaanse cultuur met als hoogtepunt natuurlijk de heerlijke künefe die je ons hebt laten proeven.

In het lab in het WKZ werkte ik niet alleen, maar had ik een grote groep talentvolle onderzoekers om mij heen. Ook jullie wil ik natuurlijk bedanken voor jullie bijdrage, interesse, en gezelligheid! Op de eerste plaats wil ik jou, **Sanne**, bedanken voor al je hulp, gezelligheid en inzet in het onderzoek rondom de ERAPs en birdshot. Jij en Jonas waren de grondleggers voor het onderzoek waar ik in september 2018 instapte. Jij had o.a. met veel tijd en moeite de basis gelegd voor het gebruik van CRISPR-Cas9. Daarmee heb je de birdshot LCLs met ERAP2KO kunnen maken, waarmee we de functie van ERAP2 hebben kunnen beschrijven. Samen hebben we gedurende het overgrote deel van mijn promotieonderzoek gewerkt aan het verder ontwikkelen van complexe CRISPR methodes, heb je mij geholpen met het S-antigen project en stond je altijd klaar om mij te helpen als mijn western blots weer eens geen bandjes hadden. Ik weet zeker dat ze bij Genmab ook een geweldige collega aan jou hebben.
Daarnaast wil ik ook de rest van de vroegere Radstake groep bedanken die mij altijd geholpen hebben en interesse hebben getoond. **Rina, Sarita, Michel, Cornelis** en **Ralph**, bedankt voor de hulp en gezelligheid in het lab. Op jullie kon ik altijd rekenen! Natuurlijk wil ik ook de rest van de voormalig Radstake groep bedanken voor de gezelligheid bij de labuitjes, jullie mening over data/theorieën tijdens de labmeetings en jullie hulp op het lab.

Lieve roomies, bedankt voor alle gezelligheid de afgelopen jaren. Van gezellig met elkaar lunchen en koffiedrinken tot etentjes in Utrecht en zelfs daarbuiten op mijn aanraden bij De Molen. Samen hebben we elkaars successen gevierd, elkaar een hart onder de riem gestoken als het een keertje niet mee zat, maar bovenal ook een vriendschap opgebouwd die we hopelijk in de toekomst blijven koesteren. **Tim**, aan jou de eervolle taak om het gezag over de kamer te houden. Ik wens jou en natuurlijk ook **Shiva, Xiaolin, Femke, Saskia, Rowie, Greta** en **Jelleke** veel succes en plezier met jullie onderzoek. **Akashdip**, wij zijn tegelijk begonnen en ook voor jou zit het er nu op. Veel succes met de afronding van jouw proefschrift. Ook mijn oud-kamergenoten wil ik bedanken voor de gezellige tijd. **Matevž**, met jou was het altijd lachen, konden we heerlijk klagen over dingen in het lab, maar ook genieten van elkaars successen. **Juliette**, jouw doorzettingsvermogen om het beste resultaat te krijgen was bewonderens-waardig. Ondanks jouw gedrevenheid in je onderzoek had je altijd tijd voor een praatje bij de koffie, moesten wij altijd het Formule 1 weekend uitvoerig bespreken en stond je klaar om anderen te helpen. Veel succes met je opleiding tot reumatoloog, je gaat vast een fantastische arts worden. Dear **Ana** (and **Tiago** of course), I want to thank you for the great time I had with you as my colleagues. I always liked our discussions about science, sports, the mess in the lab… Thank you for your interest and support whenever I needed a second opinion about a challenging experiment. I'm sure your colleagues in the PMC are lucky to have you around. **Lotte**, van leuke gesprekken bij de koffieautomaat tot

leuke gesprekken bij ons in de kamer toen je onze roomie werd. Heel veel succes met het afronden van je proefschrift naast je baan als kinderarts. Dear **Aroosha**, although you were our roomie for a brief moment, we still count you as part of our group. When you arrived in Utrecht you thought you would work as a computational PhD student, but suddenly you were in the lab with me and Sanne. I hope you still like the lab, luckily Aafke is there for you to support you. Apart from our mutual interest in science we also share the love for heavy metal. Where most people would run away from this kind of music, I was surprised to find you in the mosh pit when we went to a concert together. I wish you all the best with your research and hopefully we can meet up at a metal concert again in the future. Dear **Uxía**, you quickly became a well-loved colleague in our room during your stay in Utrecht. I really enjoyed your presence in the lab, I hope the CRISPR-Cas9 protocols I taught you will help your research to achieve great results. Apart from work you have become a dear friend to me. You inviting me to Santiago de Compostella to meet your friends and family, showing me the city and the beautiful landscape of Galicia will be an experience I will never forget. Hopefully I can come back soon, I still have plenty to see in Galicia!

Aafke, jij kwam tijdens mijn laatste maanden op het lab onze groep versterken. Ik ben blij voor jou dat je in een leuke groep terecht bent gekomen en dat het ook goed klikt met de andere onderzoekers binnen het CTI. Jij hebt de eervolle taak mijn werkzaamheden voort te zetten en van wat ik gezien heb doe je dat uitstekend! Uiteraard blijft ik graag op de hoogte van alle ontwikkelingen in het lab, blijf ik je af en toe muziek sturen in de hoop dat je metal ooit gaat leren waarderen en zie ik je graag nog eens terug bij De Molen voor een lekker biertje.

Tenslotte wil ik iedereen binnen het **CTI** bedanken die ik tussendoor op het lab, bij de koffieautomaat, in het restaurant, in de gang op weg naar de theme meeting, bij de gezellige retreats, tijdens de coffee & catch ups en tijdens de mooie feestjes ben tegengekomen. Bedankt voor de mooie tijd samen!

Naast het lab heb ik ook veel mensen te bedanken in het AZU. Beste **collega's van de oogheelkunde**, ook jullie wil ik natuurlijk van harte bedanken voor jullie interesse en bijdrage in mijn onderzoek. Hopelijk hebben jullie iets kunnen leren van mijn presentaties over onderzoek in het lab tijdens het klinisch rapport. Andersom heb ik veel geleerd van jullie praatjes, lezingen en voordrachten tijdens congressen over de klinische kant van het onderzoek en de patiëntenzorg.

Beste **oog-onderzoekers**, bedankt voor de gezellige tijd de afgelopen jaren. Ook al was ik maar af en toe in het AZU, zag ik jullie vooral bij meetings en bijeenkomsten, ook jullie zijn waardevol voor de fijne tijd die ik heb gehad tijdens mijn promotieonderzoek. In het begin namen jullie mij gelijk op in de groep, hielpen jullie mij wegwijs te maken in het doolhof

dat het AZU is en lieten jullie mij gelijk thuis voelen bij oogheelkunde. Ik wil jullie bedanken voor alle vele koffietjes, gezellige etentjes, feestjes bij DOPS, jullie interesse in mijn labwerk en hulp als ik een klinische vraag had. **Kamil, Sara, Anna, Fleurieke, Anne-Mieke, Roos, Nienke, Bas, Myrthe, Brendan, Evianne, Lude, Carlyn, Els, Deniz, Jytte, Cansu, Janneau** en **Casper**, dank jullie wel!

Ninette, jij hebt mij in het voorjaar van 2018 geïntroduceerd bij Jonas voor een mogelijk promotieonderzoek. Ik was toen al een tijdje aan het zoeken, maar gelukkig was Jonas net bezig een project op te zetten waar een nieuwe PhD student voor nodig was. Ook tijdens mijn onderzoek heb je mij vaak geholpen, vooral met de inclusies van birdshot patiënten. Dankzij jou konden we een cohort opbouwen van nieuwe (onbehandelde) patiënten waar we voor mijn onderzoek nieuwe inzichten mee hebben kunnen beschrijven. Hopelijk helpt dit cohort ook in de toekomst voor nieuwe ontwikkelingen in het begrijpen van birdshot uveitis.

Beste **Suzan** en **Petra**, bedankt voor jullie hulp en inzet bij alle administratieve zaken en planningen.

Graag wil ik ook **Prof. Dr. Ronald Bleys, Dr. Cindy Cleypool** en **Marco Rondhuis** van de afdeling Anatomie bedanken voor hun hulp en bijdrage bij mijn onderzoek. Onderzoek doen op oogweefsel is niet iets wat zomaar kan, maar met jullie hulp hebben we onze theorieën toch kunnen toetsen op donorweefsel.

Ook wil ik graag mijn **medeauteurs** bedanken voor hun tijd, bijdrage en kennis die mij geholpen hebben om het onderzoek te kunnen verwerken tot mooie publicaties. Binnen het UMC wil ik graag **Lars van der Veken** (Genetica) en **Jorg van Loosdregt** (CTI) bedanken voor jullie bijdrage en ondersteuning. Daarnaast wil ik graag **Peter van Veelen** en **George Janssen** (CPM, LUMC) bedanken voor de samenwerking. Dankzij jullie konden we middels massaspectrometrie de peptiden op HLA-A*29 identificeren en hebben jullie daarmee bijgedragen aan nieuwe inzichten rondom de functie van de ERAPs op antigenpresentatie. I want to thank **Efstratios Stratikos** (National and Kapodistrian University of Athens) for your knowledge and input about the chemical properties of the ERAPs. Tenslotte wil ik ook **Wouter de Laat** en **Peter Krijger** (Hubrecht Institute) bedanken voor jullie hulp met de 4C-seq waarmee we een nieuwe invalshoek voor de ERAP2 eQTLs hebben beschreven.

Buiten het UMC Utrecht kon ik ook veel steun en interesse vinden bij mijn familie en vrienden. Allereerst wil ik mijn dierbare vrienden **Bram, Joyce, Alex, Laura, Casper, Matthijs** en **Linda** bedanken voor alle gezelligheid, gekkigheid, onzinnigheid die we dagelijks met elkaar delen, maar ook jullie bijdrage en interesse in mijn onderzoek. **Wijb** en **Daan**, ik ken jullie sinds mijn poging LST wat jullie wel met succes hebben afgerond. Bedankt voor jullie vriendschap die

is blijven bestaan en jullie interesse en hulp tijdens mijn onderzoeksperiode. Opdat we nog vaak op Bierrr!! excursie gaan!

Beste **Cor**, ik ben geregeld bij jou in de winkel geweest voor de nieuwste bieren en lekkerste whisky's. Meestal op de vrijdag op weg naar huis kwam ik even bij je buurten. Je had mij dan al getipt dat er weer wat moois was binnengekomen (lees Springbank). Daarnaast was je ook altijd geïnteresseerd in wat ik nou precies deed daar in het UMC. Hopelijk kan ik in de toekomst nog regelmatig bij je langskomen in de winkel, al moet ik er misschien voor omrijden.

Lieve **familie**, ik wil jullie bedanken voor jullie welgemeende interesse om nieuwe dingen te leren over wetenschappelijk onderzoek. Ik heb genoten van onze gesprekken en jullie vragen over mijn werk wanneer we elkaar zagen tijdens de verjaardagsfeestjes. Hopelijk kunnen jullie met dit proefschrift een concreter beeld krijgen wat ik de afgelopen jaren heb gedaan in Utrecht 😉.

Lieve **Tess** en **Ellen**, ook jullie bedankt voor jullie interesse en steun de afgelopen jaren. Ik heb genoten van onze gezamenlijke uitjes, avondjes bier drinken in Leiden, met elkaar naar concerten gaan, de spontane bezoekjes. Ik hoop dat we dit in de toekomst nog vaak zullen herhalen.

Lieve **pap** en **mam**, jullie onvoorwaardelijke steun is mij bijzonder dierbaar. Er ging geen dag voorbij of jullie wilden weten hoe het ging op werk, of mijn experiment goed was gegaan, of mijn paper al geaccepteerd was, of ik niet te lang in de file stond op weg naar huis, of ik vervolgens nog eten thuis had liggen, of ik mij verveelde in een moment dat ik eindelijk even rust had voor mijzelf. Mam, jij wilde altijd alle details weten over mijn experimenten, of het nog een beetje vergelijkbaar was met jouw tijd bij Unilever. Pap, voor jou was het lab wat abstracter, maar je was altijd nieuwsgierig naar mijn werk. Dit resulteerde in lange gesprekken over wetenschap die soms in de kleine uurtjes nog doorgingen. Ik wil jullie bedanken voor alle steun, interesse en vertrouwen tijdens mijn studie en tijdens mijn promotieonderzoek.

Lieve **oma Joke**, bedankt voor je onuitputtelijke interesse, steun, liefde en trots die je mij hebt gegeven. Je wilde altijd alles weten over de nieuwste ontwikkelingen in de wetenschap en wat ik op het lab deed. Helaas kan ik je dit proefschrift niet persoonlijk overhandigen, maar heb je mijn reis op afstand kunnen volgen waar dat ook moge zijn.

About the author

Wouter Venema was born on the 26th of February 1993 in Gouda. In 2011 he completed his high school at the Coenecoop College in Waddinxveen. He completed his bachelor Bio-Pharmaceutical Sciences at the University of Leiden in 2015, which included a short internship at the department of Biopharmaceutics within the Leiden Academic Center for Drug Research (LACDR). Wouter continued his Master's degree in Bio-Pharmaceutical Sciences in Leiden, which consisted of a nine month internship at the department of Biopharmaceutics (LACDR) and a six month internship at Genmab B.V. in Utrecht. During his first master internship he studied the role of macrophages and dendritic cells in the onset and progression of atherosclerosis, including the role of the NLRP3 inflammasome. In his second master internship he validated new potential antibody targets for immune therapy as well as setting up a new bioassay to validate antibody target response. In February 2018 Wouter received his Master's degree, followed by the start of his PhD in September 2018 in the group of Prof. Dr. Joke de Boer and Dr. Jonas Kuiper within the ophthalmology department of the UMC Utrecht. During his PhD Wouter studied the role of ERAPs and HLA-A29 in birdshot uveitis, a very rare form of auto-immune uveitis.

List of publications

This thesis

J.J.W. Kuiper, **W.J. Venema**. HLA-A29 and Birdshot Uveitis: Further Down the Rabbit Hole. *Front Immunol*. 2020;11:599558.

W.J. Venema, S. Hiddingh, J.H. de Boer, F.H.J. Claas, A Mulder, A.I. Den Hollander, E. Stratikos, S. Sarkizova, L.T. van der Veken, G.M.C. Janssen, P.A. van Veelen, J.J.W. Kuiper. ERAP2 increases the abundance of a peptide submotif highly selective for the Birdshot Uveitis-associated HLA-A29. *Front Immunol*. 2021;12:634441.

W.J. Venema, S. Hiddingh, G.M.C. Janssen, J. Ossewaarde-van Norel, N. Dam van Loon, J.H. de Boer, P.A. van Veelen, J.J.W. Kuiper. Retina-arrestin specific CD8+ T cells are not implicated in HLA-A29-positive birdshot chorioretinitis. *Clin Immunol*. 2023;247:109219.

W.J. Venema, S. Hiddingh, J. van Loosdregt, J. Bowes, B. Balliu, J.H. de Boer, J. Ossewaarde-van Norel, S.D. Thompson, C.D. Langefeld, L.T. van der Veken, P.H.L. Krijger, W. de Laat, J.J.W. Kuiper. A cis-regulatory element regulates ERAP2 expression through autoimmune disease risk SNPs. *bioRxiv*. 2023;2023.03.03.530973.